DISSERTATION

CHARACTERIZATION OF OSSEOINTEGRATIVE PHOSPHATIDYLSERINE AND CHOLESTEROL ORTHOPAEDIC IMPLANT COATINGS

Submitted by

William Paul Rodgers III

Graduate Degree Program in Bioengineering

In partial fulfillment of the requirements

For the Degree of Doctor of Philosophy

Colorado State University

Fort Collins, Colorado

Spring 2013

Doctoral Committee:

Advisor: Susan James

Ketul Popat
Nicole Ehrhart
Susan De Long

ABSTRACT

CHARACTERIZATION OF OSSEOINTEGRATIVE PHOSPHATIDYLSERINE AND CHOLESTEROL ORTHOPAEDIC IMPLANT COATINGS

Total joint arthroplasties/replacements are one of the most successful surgeries available today for improving patients' quality of life. By 2030 in the US, demand for primary total hip and knee arthroplasties are expected to grow by 174% and 673% respectively to a combined total of over 4 million procedures performed annually, driven largely by an ageing population and an increased occurrence of obesity. Current patient options for load-bearing bone integrating implants have significant shortcomings. Nearly a third of patients require a revision surgery before the implant is 15 years old, and those who have revision surgeries are at an increased risk of requiring additional reoperations.

A recent implant technology that has shown to be effective at improving bone to implant integration is the use of phosphatidylserine (DOPS) coatings. These coatings are challenging to analyze and measure due to their highly dynamic, soft, rough, thick, and optically diffractive properties. Previous work had difficulty investigating pertinent parameters for these coating's development due in large part to a lack of available analytical techniques and a dearth of understanding of the micro- and nano-structural configuration of the coatings.

This work addresses the lack of techniques available for use with DOPS coatings through the development of original methods of measurement, including the use of scanning white light interferometry and nanoindentation. These techniques were then applied for the characterization of DOPS coatings and the study of effects from several factors: 1. the influence of adding

calcium and cholesterol to the coatings, 2. the effect of composition and roughness on aqueous contact angles, and 3. the impact of ageing and storage environment on the coatings.

This project lays a foundation for the continued development and improvement of DOPS coatings, which have the promise of significantly improving current patient options for bone integrating implants. Using these newly developed and highly repeatable quantitative analysis methods, this study sheds light on the microstructural configuration of the DOPS coatings and elucidates previously unexplained phenomena of the coatings. Cholesterol was found to supersaturate in the coatings at high concentration and phase separate into an anhydrous crystalline form, while lower concentrations were found to significantly harden the coatings. Morphological and microstructural changes were detected in the coatings over the course of as little as two weeks that were dependent on the storage environment. The results and understanding gained pave the path for focused future research effort. Additionally, the methods and techniques developed for the analysis of DOPS coatings have a broader application for the measurement and analysis of other problematic biological materials and surfaces.

ACKNOWLEDGMENTS

This work would not have been possible, or even attempted, without the incredible advice, support and encouragement from numerous people. My incredible advisor, Dr. Susan James, is the primary reason I started the project, and has been fundamental to my progression throughout the project, and to me personally as a developing researcher. Sue, I owe you a debt of gratitude for all your guidance and advice. I have highly appreciated and valued your technical expertise, and your communication and advising skills. It has been an absolute pleasure working with you for the last 5+ years. From the bottom of my heart, thank you!

I also want to thank my committee members, past and present. Thank you Dr. Erick Egger and Dr. Stewart Ryan, for all your advice and direction. To Dr. Ketul Popat, thank you for being the reason I know how to harvest, culture, and assay cells, and for your technical advice and the mentoring role you've had in my research career. And also a large thanks to Dr. Nicole Ehrhart and Dr. Susan De Long, who were willing to take the time to step in at the end and help me finish this project. A huge sum of gratitude goes to Jack Clark, without whom the SWLI methods would never have happened.

Next I want to thank the many colleagues I've had the pleasure of working with. The list of people who have greatly aided my research is too long to for me to do proper justice towards, but I am extremely thankful to you all. In particular, I want to thank my direct lab colleagues, Dr. David Prawel, Jason Marini, Dustin Williams, Tom Triffo, Nicole Lewis and others for all your help and assistance. I would not have been able to finish this project without the extraordinary help of our undergraduate research assistants, especially Justin Gangwish, Ashley Beckwith and Josh Krokowski. Thanks go to Dr. Chung-Souk Han and Farid Alisafaei, as well as Dr. Virginia

Ferguson and Mosood Hasheminiasari, for all your invaluable help with nanoindentation. Thank you to Dr. Matt Kipper, Dr. Don Heyse and Dr. Brian Newell in CIF, and to Dr. Barb Smith and Dr. Tim Ruckh who helped me learn tissue engineering techniques. There are many more that I have regretfully not listed here and I truly thank you for all your help!

To my family and friends, thank you thank you! I would not have been able to get through this without all the support, patience and babysitting you have provided. I have been so blessed to have your love and encouragement. I would not be here without you.

I also have an inexpressible quantity of gratitude for my beautiful wife and companion, Heather. You have been incredibly supportive of my endeavors, and it is obvious to me that this would never have happened without you. I love you with all of my heart, and I look forward to the next stages in our lives together.

And finally I want to acknowledge and thank my best friend and Lord, Jesus Christ. It has ultimately been his strength, companionship, encouragement, peace, and rest that are the reason I am where I am today. You love me more than I can possibly know. Thank you, and I honor you!

Thank you everyone!

TABLE OF CONTENTS

LIST OF TABLES

LIST OF FIGURES

Chapter 1: Motivation for Research

1.1 Motivation

Total joint replacements are one of the most successful surgeries available today for improving patients' quality of life [1]. With an estimated 1.5 million total joint replacements performed annually worldwide [2], orthopaedics is quickly becoming one of the largest medical industries in the United States. By 2030 in the US, demand for primary total hip and knee arthroplasties are expected to grow by 174% and 673% respectively to a combined total of over 4 million procedures performed annually [3], driven largely by an ageing population and increased occurrence of obesity. By 2030, revision surgeries for total hip and total knee replacements are projected to grow by 137% and 601% respectively [3].

In order to improve implant integration with the surrounding bone and the ultimate success of the procedures, several advances in the field of implants that interface with bone have been explored and developed. Among these are improvements in surgical techniques, advances in implant materials, the incorporation of porosity to the implant surface, and the addition of bioactive surface coatings to further promote osseointegration [4]. The exploration of bioactive coatings is of particular interest. While many different bioactive coatings have been used with varying levels of effectiveness, a prominent new category of coating materials is phospholipids. Previous studies have demonstrated an increased osseointegrative response to titanium (Ti) surfaces coated with phospholipids [5]–[7]. In particular, phosphatidylserine (PS) was found to be effective at increasing the rate of bone formation and ingrowth [5], [6].

An additional benefit of using phospholipids as a bioactive implant coating material is that they can also be used as a drug delivery medium. Using lipids as a drug carrier is a well-

researched and documented field [8]–[12]. Phospholipids have been used as a carrier for the systemic delivery of specific drugs such as platinum based chemotherapeutics [8]–[10], as well as for more general drugs such as antibiotics [13]. While the percentage of infections in total joint arthroplasties is relatively small, the sheer number of these operations performed annually leads to many complications due to infection [14]–[16]. Drugs can easily be incorporated into phospholipid implant coatings, and their incorporation would prove useful for the treatment of osteosarcomas (bone cancer), and for decreasing the rate of post-operative infections.

The previously mentioned studies [5]–[7] that have explored the use of phospholipids as an osseointegrative implant coating have been limited to the use of drip and dip coating methodologies [5], [6], leaving room for improved application methods that aid control and scalability. Implants with complex or custom geometries may prove difficult to coat evenly using a drip or dip process. Recently developed atomizing nozzle spray and electrospray deposition methods (Appendix B and [17]) allow efficient application and customizable properties of surface coatings. Very little characterization has been performed on the coatings produced by these newly developed spray deposition methods. This project will help researchers improve current patient options for implants through the further development and characterization of spray deposited phosphatidylserine coatings on titanium implants.

1.2 Long Term Goal

The long term goal of this work is to aid the development and implementation of phospholipid implant coatings for improved osseointegration. The bioactive and osseointegrative nature of the phospholipid coating addresses the issue of incomplete integration of the bone to the implant surface, by helping to prevent fibrous encapsulation of the implant (and subsequent

implant loosening). The use of these phospholipid coatings will also promote better patient outcomes by enabling local, targeted drug delivery from the implant surface. The benefit this work provides is improved techniques for the study, characterization and optimization of phospholipid coatings, increased knowledge of the coatings' morphology, mechanical properties and microstructure, and knowledge of the effects of storage environment and ageing on the coatings.

Chapter 2: Background and Literature Review

2.1 Bone Integrating Implants

Osseointegrating implants have a significant impact in the lives of millions of Americans. Common examples include dental applications [18], reconstructive surgeries [19] and total joint arthroplasties [20]. Of these, total joint arthroplasties are one of the most challenging applications due to the high mechanical requirements, difficulty of the procedure and recovery, high level of consequence in the case of failure and limited options for reparation. However, total joint arthroplasties are also one of the most successful surgeries available today for improving patients' quality of life [1]. By the year 2030 in the US, demand for primary total hip and knee arthroplasties alone is expected to grow by 174% and 673% respectively, to a combined total of over 4 million procedures performed annually [3]. This increase is driven largely by an ageing population and an increased occurrence of obesity [21], [22].

Current patient options for load-bearing bone integrating implants have significant shortcomings. Despite the fact that current clinical options are largely successful in the short term, the long term results remain largely inadequate. Total joint replacements have a limited life, with nearly a third of patients requiring a costly and painful revision surgery before the implant is 15 years old [23] in order to maintain the limb. Patients who require revision surgeries are at a considerable risk of encountering subsequent problems that result in additional reoperations [23]. A revision surgery necessitates the removal of more native tissue, limiting the number of revisions that can take place. With longer life expectancies and younger patients needing joint repair, the need for better technologies is clear. The primary weakness of current metallic implants lies in their inability to maintain a long term intimate bone-implant interface,

with more than 50% of the failures occurring due to loosening of the implant [23]. While structurally stable, metallic implants create stress shielding in bone due to their higher modulus (where bone resorbs due to decreases in perceived normal stress) [24]–[26], they can also release toxic ions locally and systemically [27]–[29], and they fail to integrate chemically at the atomic level with native tissue [30].

2.1.1 Materials Used for Bone Interfacing Implants

Numerous materials have been used for bone interfacing implants over the years, with varying success. The structural materials that commonly contact bone can be categorized into three main groups; metals, polymers and ceramics. For metals, the most frequently used currently are titanium and cobalt-chrome-molybdenum alloys. [31], [32] Among the polymers, polytetrafluoroethylene (PTFE) and polymethylmethacrylate (PMMA) are common, [33], [34] and among ceramics, alumina and zirconia are a couple of common examples.

Metals utilized as implant materials historically include FE, Cr, Co, Ni, Ti, Ta, Mo and W. Most of these metals can be tolerated (and some can even be beneficial) when dissolved in very small amounts in the body. However, they are harmful or toxic in large quantities [4]. This is of particular concern due to the fact that the caustic *in vivo* environment corrodes many metals. Titanium and cobalt-chrome-molybdenum alloys are two that have performed particularly well *in vivo* and are widely used today. The Ti can be used in its pure form or as an alloy (alloying elements are usually Al and V) [4]. Ti alloys are particularly attractive due to their high strength to density ratio. *In vivo*, a thin, stable Ti oxide layer forms at the surface of the metal and quickly passivates the implant from further corrosion [4].

2.1.2 Implant Surface Strategies Used to Promote Osseointegration

Obtaining an excellent bone to implant interface is critical for long term implant survival [35], but current options are limited. At this time there are two predominately used options for bone integrating implants; a titanium implant with a porous surface [36], [37], or a titanium implant with a smooth surface that is coated in a layer of hydroxyapatite [38]–[42]. The porous titanium implants usually employ a sintered micron-scale ball surface [36]. While structurally stable, these metallic implants create stress shielding at the bone interface due to their high modulus, release toxic ions locally and systemically, and have very little ability to bond at the atomic level directly to bone tissue [30].

Hydroxyapatite (HA) is a ceramic similar to that found naturally in bone and is used as an implant coating because of its ability to help bone mineralize and chemically attach directly to the implant surface shortly after implantation [38]–[41]. While HA coated implants are better able to bond with bone [43], the HA coating's ability to adhere (and not delaminate) from the implant surface is problematic due to limitations of coating deposition technologies, the different properties of the materials being bonded together (a metal vs. a ceramic), and the high modulus mismatch that exists between the metallic titanium substrate and the ceramic hydroxyapatite [44].

Though metal is used as a direct interface for bone apposition, different materials may be coated on the implant to improve osseointegration. Nonetheless, a metal component remains standard for structural support in the implant. Using coatings on the metal substrates to improve integration can introduce problems due to different material properties. A common example of a bone-implant interposing material is PMMA bone cement, which is used in about 60% of total joint replacements [45]. Traditionally, PMMA bone cements have been the 'gold standard' for

implants, with survival rates in excess of ten years [45]. 30% of the long term failures in PMMA bone cement can be attributed to osteolysis at the interface of the bone and implant [46].

An ideal implant coating would have both the mechanical advantage of a porous metallic implant surface (for bone ingrowth), along with the ability for bone to bind to, and integrate directly with, the implant surface through the use of a bioactive coating on the implant surface. Some examples of other bioactive coatings which are currently being developed to induce bone formation include bioglasses and synthetic calcium phosphates [47], however, these technologies have not been widely applied or approved by regulatory agencies at this time. Also, another class of bioactive coating materials that have been explored recently is phospholipids.

2.2 Phospholipids

2.2.1 Background and Biological Function

Phospholipids are a specific type of lipid. Lipids in general are an expansive category of molecules that include many naturally occurring substances such as fatty acids, sterols, waxes, fats, fat soluble vitamins, monoglycerides, diglycerides, and triglycerides, among other examples [48]. Broadly, the term lipid usually refers to small amphiphilic molecules, i.e., molecules that have both hydrophobic and hydrophilic properties.

Phospholipids are lipids that typically contain a diglyceride, a phosphate group, and an organic molecule (e.g., choline) [49]. Phospholipids have two primary parts, a hydrophilic (polar) phosphate ‘head’ and a hydrophobic (non-polar) acyl chain ‘tail’ [50]. A diagram of the basic structure of a phospholipid can be seen in Figure 2-1.

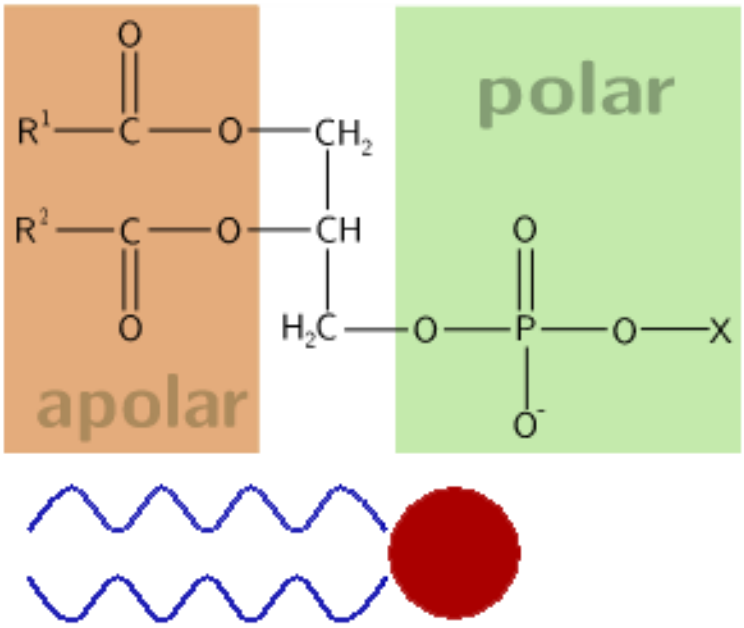

Figure 2-1 Top: General structure of a phospholipid (tan: two apolar fatty acid chains represented by repeating hydrogen and carbon 'R' group, and green: the polar headgroup). Bottom: cartoon representation of the entire phospholipid molecule, with two acyl chains (blue lines) and the phosphate headgroup (red circle) [51], [52].

Phospholipids are ubiquitous and have been extensively studied. In a given cell type, there may be more than a thousand molecular varieties of phospholipids [53]. To date, more than 600,000 scientific articles reference phospholipids. In addition to being a critical component of all eukaryotic biological membranes, it is well acknowledged that phospholipids play a critical role in a vast variety of biological processes [54]. Phospholipids have direct interactions with proteins (e.g., in blood coagulation [55]), and are active participants in membrane mediated events [56]. In an active role, phospholipids can exhibit a phosphoinositide effect, where the lipid becomes a substrate during membrane signaling [57]. A second active role is demonstrated in the phosphoinositide effect, where the phospholipid is involved as a direct chemical mediator in cell membrane signaling events [58]. In addition to being key structural molecules, phospholipids are important constituents for cell function [56].

Phosphatidylserine

A specific biological phospholipid is 1,2-dioleoyl-sn-glycero-3-phospho-L-serine, also referred to as DOPS. It has a chemical formula of $C_{42}H_{77}NO_{10}PNa$ and a molecular weight of 810.025 [grams/mole] [59]. Phosphatidylserine (DOPS) has two unsaturated acyl chains, with each acyl tail containing one mid-chain double bond. Each acyl chain has 18 carbons [59]. The structure of phosphatidylserine can be seen in Figure 2-2. While the term phosphatidylserine refers to phospholipids that contain the head group configuration seen in the top of Figure 2-2, phosphatidylserines with the 18 carbon acyl chains seen in the middle and lower parts of Figure 2-2 indicate the specific variety of phosphatidylserine named DOPS.

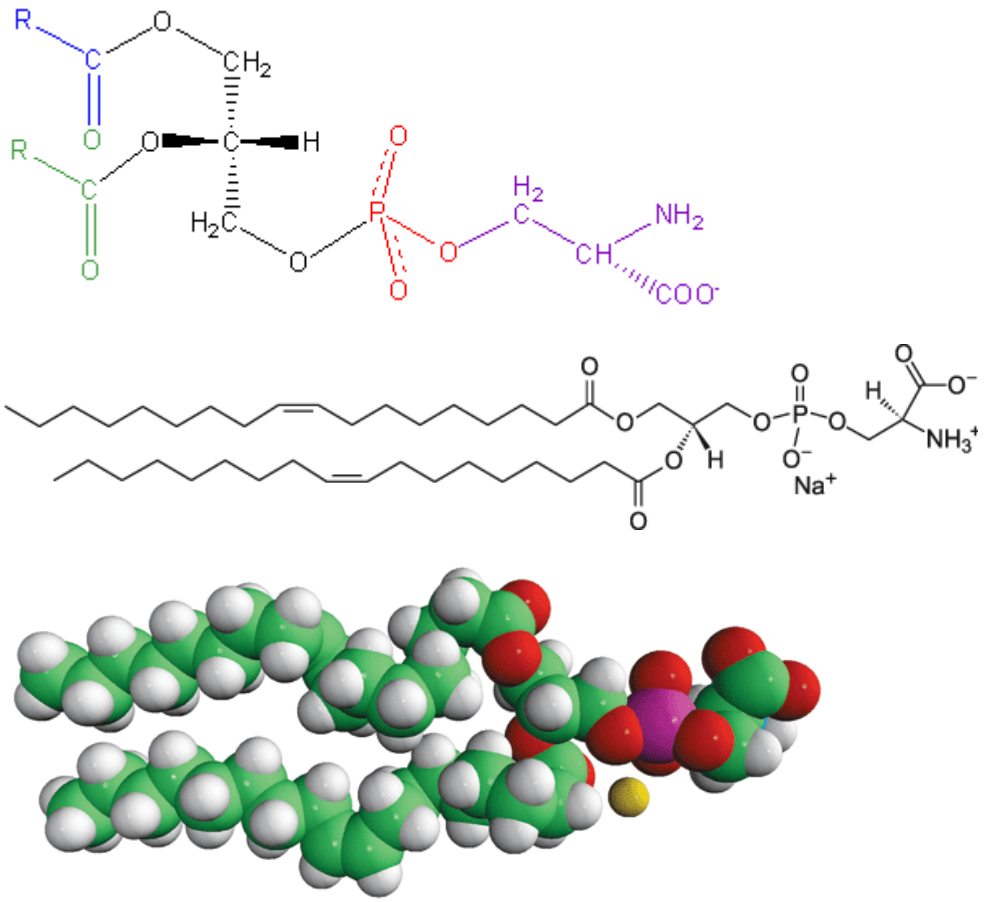

Figure 2-2 Top: structural formula of Phosphatidylserine (blue/green: fatty acid tails, black: glycerol backbone, red: phosphate, purple: serine) [60]. Middle: chemical structure of the entire Phosphatidylserine molecule [59]. Bottom: Space filling model of a phosphatidylcholine molecule.

Phosphatidylserines constitute between 4-14% of the membrane lipid content in a mammalian cell [61]. Phosphatidylserine has been found to improve cognitive functions in humans and other animals when taken as a oral supplement [62]. Phosphatidylserine plays an important role in the membranes of neurons, it is involved in intracellular maintenance, signal transduction, secretory vesicle release, cell growth regulation and cell to cell communication [63]–[67]. Phosphatidylserine is a unique phospholipid in that it is the only lipid in the phosphoglyceride family that contains an amino acid (serine) [61].

A biological characteristic of phosphatidylserine is that it normally resides on the cytosolic side of a cell membrane due to the flippase enzyme. When a cell undergoes apoptosis, this characteristic is lost and the phosphatidylserine is expressed on both sides of the membrane [60]. This attribute allows for the early detection of cell death [68].

2.2.2 Organizational Structure

Phospholipids are dynamic molecules; they self-assemble and reassemble to form a variety of nano- and micro-structures. The structures formed by phospholipids are dependent on their environment. Variables that influence their structure include a sensitivity to the type of fluid (air or liquid, polar or non-polar) they reside in, amount of any nearby water, ionic strength of the media, availability of crosslinking molecules (such as divalent cations), proteins, other varieties of lipids present, and the proximity of other biomolecules [69].

The amphiphilic nature of phospholipids is the foundation for their ability to spontaneously assemble. These assemblies can be bilayer in nature, as found in a cell's cytoplasmic membrane. A typical cytoplasmic membrane (which is made primarily of phospholipids) is on the order of 7-10 nm in thickness [50]. A diagram showing some common structures of phospholipids in an aqueous solution is shown in Figure 2-3.

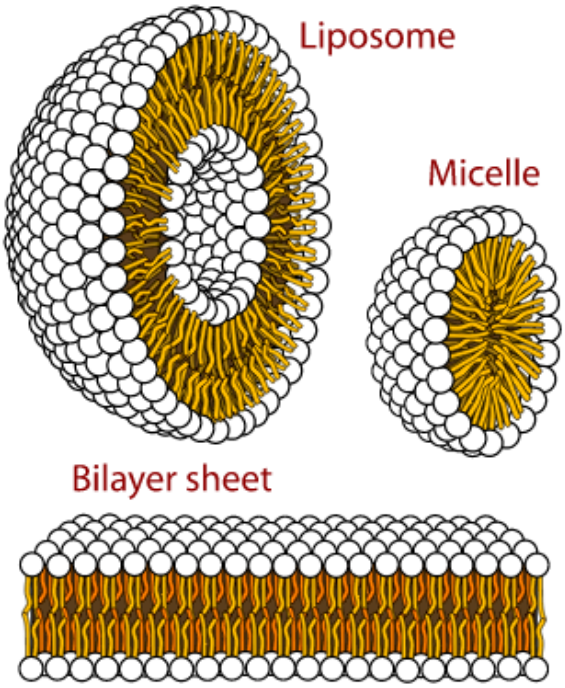

Figure 2-3 Cross-sections of common phospholipid structures in an aqueous solution. Spheres represent hydrophilic head groups and wavy lines represent the apolar acyl tails [70].

These self-assembling phospholipids will align their hydrophilic heads to the outside, aqueous environment, while grouping their hydrophobic fatty acid tails together. This allows for the formation of liposomes, micelles and bilayers, and multilamellar structures [69].

Additional phospholipid structures are possible with the modification of their molecular environment. Examples include changing the fluid (to apolar or gaseous mediums), or adding other molecules (such as calcium or cholesterol). These changes can result in the phospholipids assuming the form of long tubes, hexagonal packing, reverse micelles, monolayered and multilayered structures [71], [72]. These supramolecular structures can be polymer-like, with 3 dimensional networks of cylindrical micelles that overlap, entangle and interpenetrate [73].

Liquid Crystals

A liquid crystal is a material structural state that has properties similar to both a liquid and a crystalline solid. The general hallmark of a liquid crystal is a regular, repeating order within the material, along with the ability for flow and movement within the material. Liquid crystal states can take place in a variety of materials, and have a variety of specific phase types, including the nematic, smectic, chiral, blue, and discotic phases [74]. Just because a material may be able to take on a liquid crystal structure, does not mean that it will always be in that phase.

An important property of many liquid crystals is birefringence, where the materials optical properties are dependent on the incidence light's direction and polarization states. Birefringence is the fundamental functional property that makes liquid crystal display (LCD) panels work. Incoming lights of a particular polarization state will see a different refractive index in the material than concomitant light at a different polarization state, resulting in a phase lag in the transmitted light between the two polarization states. This can results in a split image when observing an object through a mostly transparent birefringence material.

When in a lamellar configuration, phospholipids can be in a solid (gel) state, or in a liquid (crystal) state. The ease in which they make the transition from a gel to liquid state depends on the following: the type of polar head group in the lipid, the ionic strength of their surrounding medium, the length of the lipid's acyl chain, and the degree of saturation of the acyl chain [69]. In a given phase, the structure of the lipid bilayers is primarily driven by Van der Waals interactions between the molecules [75]. The gel to liquid transition temperature is decreased with increased saturation of the acyl chains, due to the kinks in the chains allowing greater mobility between the lipid tails. Fully saturated acyl chains are able to pack closer and tighter

together, allowing for much higher transition temperatures. DOPS (which has one unsaturated bond in each acyl chain) has a gel to liquid phase transition temperature of -7° C (in 0.15 M NaCl; buffer, pH 9.5; EDTA) [76], while DPPS (which is fully saturated) has a transition temperature of 53° C (in 0.1 M NaC1 buffer, pH 7.0, EDTA) [77].

2.2.3 Applications of Phospholipids

Given their unique properties and diverse roles, phospholipids have been widely studied in application. Medically, this has ranged the gamut from injecting phosphatidylcholine subcutaneously to dissolve fat [78], [79], taking phosphatidylserine as an oral dietary supplement for cognitive enhancement [80], use in both topical [71], [81] and intravenous drug delivery [82], and as a cell culture scaffold [83], [84].

Phospholipids as a Carrier for Drug Delivery

Lipids have been extensively studied for use as a drug carrier. They are ideal candidates for transporting both polar and non-polar molecules *in vivo*, as well as increasing circulation times and effectiveness for many drugs [8]–[12]. The typical configuration for the lipids is to take on a micellar form for apolar drugs and liposomal forms for water soluble drugs, so as to orient their polar and non-polar regions appropriately [85].

2.2.4 Phospholipids for use as an Osseointegrative Implant Coating

Phosphatidylserine is used by osteoblasts to form bone, and has recently been shown to increase osseointegrative response when used as an implant surface coating [5]–[7]. Of the phospholipids, the DOPS variety of phosphatidylserine was found to be the most effective at increasing osteoblast's response. It was found that DOPS increased mineralization *in vitro* [5],

and improved osseointegration *in vivo* [6]. These results are largely due to the net negative charge of the phosphate headgroup on the DOPS molecule. The charged headgroup of phosphatidylserine allows it to bind strongly to divalent cations, especially Ca^{2+}. This property is used by osteoblasts during the manufacture of bone. Osteoblasts release matrix vesicles rich in phosphatidylserine [86], [87] and calcium channels (Annexin V), through which the influx of calcium ions eventually reaches saturated levels and forms an amorphous mineral phase. The cacium then acumulates and ruptures the vesicle to form the nucleation sites for the mineral phase of bone [88]. When used as an implant coating *in vivo* in a rabbit model, phosphatidylserine provided significantly higher apposition values in the short term when compared to plain Ti or hydroxyapatite coated implants [6].

In the work by Merolli *et al* [5], [6], [89]–[91] that demonstrated increased mineralization and osteoblast activity on phospholipid coated surfaces, various combinations of phosphatidylcholine, phosphatidylinositol, phosphatidylserine and cholesterol were used to coat Ti in the studies. These studies consistently concluded that coatings of phosphatidylserine alone were the best at increasing osteoblast response, mineralization and *in vivo* osseointegration in a canine model [5], [89]. A challenge associated with these previous studies included excessively thick coatings, likely due in part to the coatings being applied via a drip or dip coating methodology. As reported by the authors, the coatings were ‘relatively thick’, leading to a lack of intimate conformational contact with the newly formed bone during the course of the *in vivo* study. This was attributed to the *in vivo* environment not being able to resorb the coatings quickly enough [6].

Another characteristic of phosphatidylserine, is its role in reducing innate inflammatory responses [92]. As macrophages ingest apoptotic cells expressing phosphatidylserine on their

surface, the macrophages secrete TGF-β1, resulting in an anti-inflammatory effect [92]. The anti-inflammatory nature of PS has been confirmed *in vitro* when used as a surface coating on Ti [89]. This fact points to the additional benefit of using phosphatidylserine as an osseointegrative coating, since a protracted inflammatory response to an implant leads to the formation of a fibrotic capsule surrounding the implant [93]. This fibrotic capsule interposes between the bone and implant, negating the ability for osseointegration.

2.3 Molecules that Bind with Phosphatidylserine

There are many molecules that phosphatidylserine interacts with; among them are cholesterol and calcium. These two are of particular interest in the presented work and will be discussed further. Charged phospholipids have the ability to bind to ions. DOPS has two negative charges and one positive, resulting in a net negative charge. The positive charge is located at the amine, while the negative charges are located at the phosphate head group and at the carboxylic acid (see Figure 2-2) [59].

2.3.1 Calcium

Calcium is a key ion in biology. It is used throughout the body in a variety of physiological processes and is of particular relevance in bone biology. Phosphatidylserine is known specifically as a calcium binding phospholipid. Calcium is well characterized in its ability to crosslink DOPS molecules together. In its as-received form, DOPS is shipped with a Na^{+} salt [59]. Phosphatidylserine's negative charge at the phosphate group binds readily to divalent cations such as Li^{2+} and Ca^{2+} [5], [91], [94]. The bonding between DOPS and Ca^{2+} is fairly insensitive to the degree of saturation in the acyl chains, and causes a significant change in

conformation of the phosphodiester group. Specifically, the P-O group changes into an antiplanar-antiplanar conformation after binding to Ca^{2+} [94]. These changes can be detected through the use of vibrational spectroscopy techniques (e.g., fourier transform infrared spectroscopy) [95], [96].

The binding of Ca^{2+} with DOPS has the effect of dehydrating lipid systems, and is critical to the membrane fusion processes [97]. The phosphate group on DOPS has a higher affinity for Ca^{2+} than water. Due to Ca^{2+}'s double positive charge, it acts to draw together and bridge two DOPS molecules (each of which have a single negative charge), resulting in decreased inter-membrane distances and the expulsion of any interstitial water molecules [97]. In the absence of Ca^{2+} and in the presence of water, DOPS readily hydrates [94].

2.3.2 Cholesterol

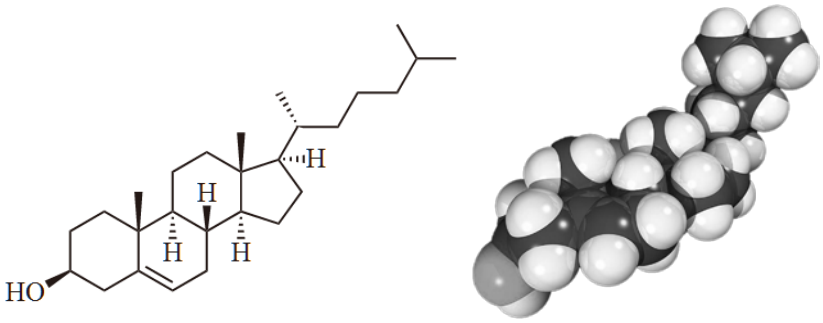

Figure 2-4 Chemical formula of cholesterol (left), and space filling model of

Cholesterol is an important biomolecule and has a variety of roles in the body. Systemically, cholesterol serves a role as a precursor in the synthesis of hormones [98], and is carried through the blood stream as a part of lipoprotein complexes [99]. Cholesterol plays both a structural and regulatory role within biomembranes [100]. It preferentially resides within cell membranes and plays a crucial role in the regulation of membrane rigidity [101], [102]. Lipid membranes are highly sensitive to both the amount of, and the configuration of, different sterols [101]. Changes

in membrane stiffness can have a profound impact on cellular function and the regulation of cholesterol is a tightly controlled biological process [103]. Please see Figure 2-4 for the chemical formula of cholesterol.

Cholesterol-Phospholipid Interactions

Conformationally, cholesterol preferentially resides within lipid bilayers and associates with the apolar acyl chains of the phospholipids [104], [105]. Cholesterol prefers fully saturated acyl chains (as found in phosphatidylcholine), due to cholesterols ability to more fully interact with the less kinked acyl chains [53], and often congregates within lipid rafts (glycolipoprotein microdomains within cell plasma membranes) [106], [107]. Dependent on the local microenvironment, cholesterol can either increase or decrease the mobility of phospholipid systems. In the presence of cholesterol, fluid phospholipid monolayers condense. Cholesterol can also act to liquefy solid phospholipid systems [108].

Cholesterol Crystallites

Pure cholesterol is able to assemble into three-dimensional crystals that can further undergo crystalline polymorphic phase changes [109]. Cholesterol crystals can also phase change from an anhydrous to a monohydrate form when in the presence of water [109]. In addition to cholesterol's ability to diffuse into membranes, it can crystalize when it surpasses saturated levels [100]. These cholesterol crystals are tertiary in nature [53]. Cholesterol can phase separate within the membrane [110], as well as bridge across membranes in multi-lamellar vesicles [100]. The primary factors that affect cholesterol crystallization in biological membranes is the concentration of cholesterol in the system, the degree of acyl chain saturation in the lipid, the presence of charges on the phospholipid head groups, and any inter-headgroup bonds [100].

Several polymorphic phase transitions for cholesterol take place. The monohydrate crystalline form of cholesterol has a triclinic structure. A shift in this triclinic crystal form takes place during heating at about 37º C. This polymorphic phase shift doubles the unit cell of the cholesterol crystal from one of 8 molecules to one of 16. This transition also doubles the length of the α-axis of the unit cell [100]. and has an associated enthalpy of transition of 0.81 ±0.21 kcal/mol (or 3.39 ±0.88 kJ/mol) [76]. Upon cooling, a large hysteresis takes place in this transition, with the transformation back to the 8 unit cell happening at around 20-25º C [100]. Cholesterol crystals dehydrate from the monohydrate form into an anhydrous form at around 86º C [100]. There is also a second, less studied transition at 95º C that is also associated with a monohydrate dehydration [109]. Complete melting of the cholesterol crystal occurs between 150-157º C [100].

It should be noted that cholesterol usually has a higher solubility in fully saturated phospholipids versus unsaturated phospholipids before it phase separates into a crystalline form. In DOPS, which has two unsaturated bonds in its acyl chains, cholesterol crystallites are formed at relatively low molar ratios [109]. Cholesterol is able to form crystals that are intimately associated with their lipid microenvironment, and certain types of phospholipids are able to push the cholesterol crystals into phases that are not otherwise independently stable [111].

2.4 Coating Deposition Methods

There are a variety of methods for coating lipids onto substrates. The majority of these methods are borrowed from the paint industry. Examples include aerosol spray deposition (e.g., spray painting) and electroplating/spraying (e.g., as used in automotive manufacturing). In the

medical field, little has been done to transfer these industrial coating methodologies for the purpose of coating implants with phospholipids.

2.4.1 Techniques Used Previously to Coat Implants with Phospholipids

Previous works that looked at the *in vitro* and *in vivo* effects of phospholipid coatings on Ti used dip or drip coating methodologies [5], [6], [89]. In both the dip and drip coating cases, the phospholipids were first dissolved in chloroform. In the drip coating method, the phospholipid solution was pipetted in a known amount onto the titanium samples surface [5], [89]. For the dip coating method, the metallic implant was partially submerged and rotated in a bath of the phospholipid solution [6]. The surfaces were then allowed to air dry. The phospholipid(s):chloroform concentration used for dip coating was 222 mM [5], [89], while the concentration for drip coating was 62.5 mM [6]. While effective, the dip and drip coating methods are not readily scalable for commercial application and tend to produce excessively thick coatings.

2.4.2 Atomizing Nozzle Spray Deposition

Atomizing spray deposition utilizes the venturi effect to produce a fine spray from a liquid. This process works by using an air source that flows over a nozzle that feeds from the liquid medium being sprayed. The low pressure created at the nozzle tip by the high velocity airflow draws the fluid into the air flow where it subsequently boils/evaporates in the low pressure. This process forms thousands of atomized droplets which are propelled forward in the airstream. Common applications of this technology include painting and carburetors. The author has developed the atomizing spray method for the novel use of depositing phospholipid coatings onto titanium substrates. Further details of how the atomizing spray method was developed and

characterized can be found in Appendix B: Atomizing Nozzle Spray Deposition Methodology Development. Briefly, a small air compressor was employed in conjunction with a modified artist's airbrush to spray a phospholipid in chloroform solution onto metallic substrates. The air compressor was used for the high pressure air source and a digital airflow regulator was used to finely control the air flow to an airbrush. The airbrush was then used to spray the phospholipid solutions onto titanium sheet metal squares. The benefit of the aerosol coating method is that it can be easily used for further commercial development of the coatings, and can deposit coatings of any desired thickness.

2.4.3 Electrospray Deposition Method

Electrohydrodynamic atomization (also referred to as electrospray or e-spray) is a commonly employed method that utilizes a voltage differential to atomize materials carried in a liquid solvent. An e-spray setup includes a syringe pump filled with the medium to be sprayed, connected to a needle which is kept at high voltage during the spray process. The conductive substrate to be coated is then placed a fixed distance from the needle and kept at electrical ground potential. A basic diagram of an e-spray setup can be found in Figure 2-5.

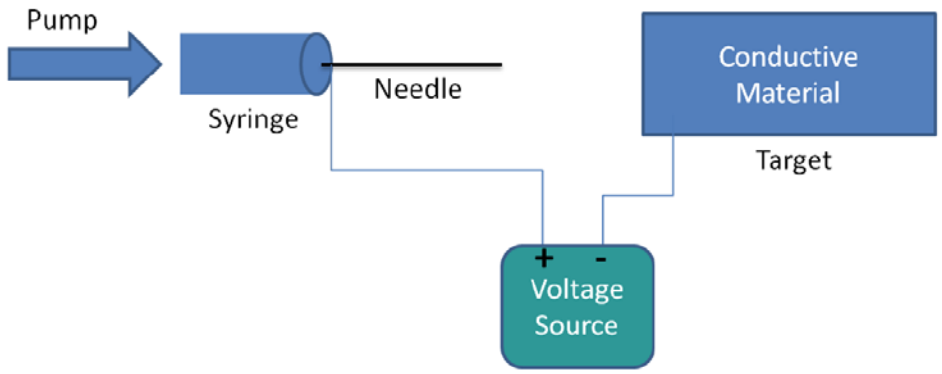

Figure 2-5 Diagram of E-spray equipment layout [17].

While simple in concept, the e-spray process is fundamentally sensitive to an array of parameters. There are at least 13 of these parameters that are recognized [112], includeing the voltage differential used, the spray distance, pump rate, solvent properties, and concentration of the medium, among others. Figure 2-6 shows the variables involved in one of these parameters, the electrical potential path.

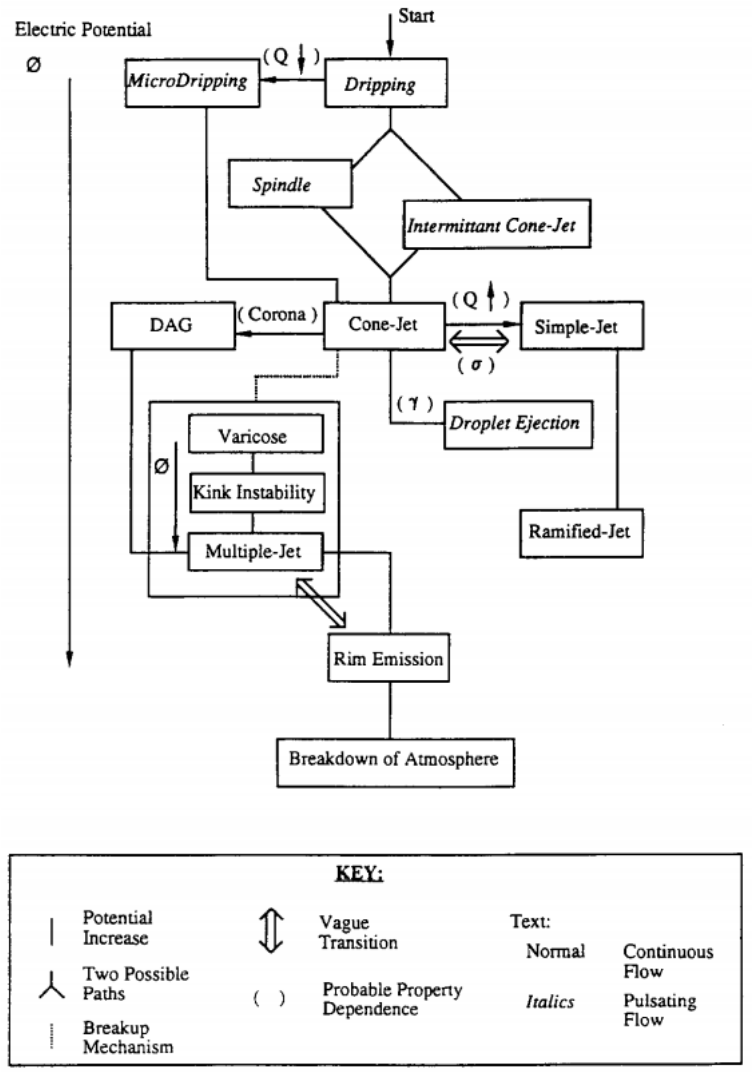

Figure 2-6 Diagram of the E-spray modes in electrical potential space [113].

The electrical path in the e-spray process is sensitive to several spray modes that go through distinct changes at different spray parrameters. Each spray condition is referred to as a

spray mode, though transitions between modes are often ill-defined. Two primary categories for spray modes include a continuous flow from the meniscus (simple-jet, cone-jet, and ramified-jet), and non-continuous flow (dripping, micro-dripping, spindle, and intermittent cone-jet modes) [113]. Each of these modes have distinct properties that include variations in droplet size, homogeneity, and Taylor cone properties [113].

Previous work [17] was done to develop a parameter set for utilizing the e-spray method to coat DOPS onto Ti substrates. This method utilized a 1.3% (vol%) DOPS (in chloroform) solution that was deposited onto cleaned and passivated samples cut from commercially pure Ti sheets. A 12 kV voltage differential was used with a pump rate of 14 mL/min with an 8 cm working distance between the needle and the samples [17].

2.5 Differential Scanning Calorimetry

2.5.1 Development and Theory

In basic terms, simple calorimetry is the measurement of heat, and in particular, the exchange of heat [114]. Ice calorimeters have been used since the 1780's [115]. Newer instruments (e.g., a differential scanning calorimeter, or DSC) have added the ability to precisely measure heat flow rates as a function of temperature and heating/cooling rates in order to measure enthalpy changes in a specimen [114]. This allows for the accurate determination of the characteristic temperature of material transitions and reactions. In addition to assessing the total heat of a reaction, a DSC is able to measure the "partial heats" within a given temperature interval, which in turn allows for the analysis of crystallinity, purity and kinetic studies of materials [114].

2.5.2 Applications

DSC has been used in many fields, including polymer research [116], [117], the food industry [118]–[120], and for the study of biological membranes [121]–[123]. Within the lipid research realm, it is useful for studying the thermotropic phase behavior of lipids, without the need for probe molecules [121]. While this is useful for the study of crystalline and phase transitions in lipid systems, it should be noted that the enthalpy changes associated with these transitions are non-specific, and adjunct methods may be required in order to fully elucidate the physical phenomena being perceived [120].

2.6 Scanning White Light Interferometry

Scanning white light interferometry (SWLI) is a type of interferometer that uses vertical scanning to map 3 dimensional surfaces. SWLI offers high lateral density, and extremely high vertical precision (less than 1 angstrom in the Z direction). A diagram of a typical configuration for SWLI can be found in Figure 2-7.

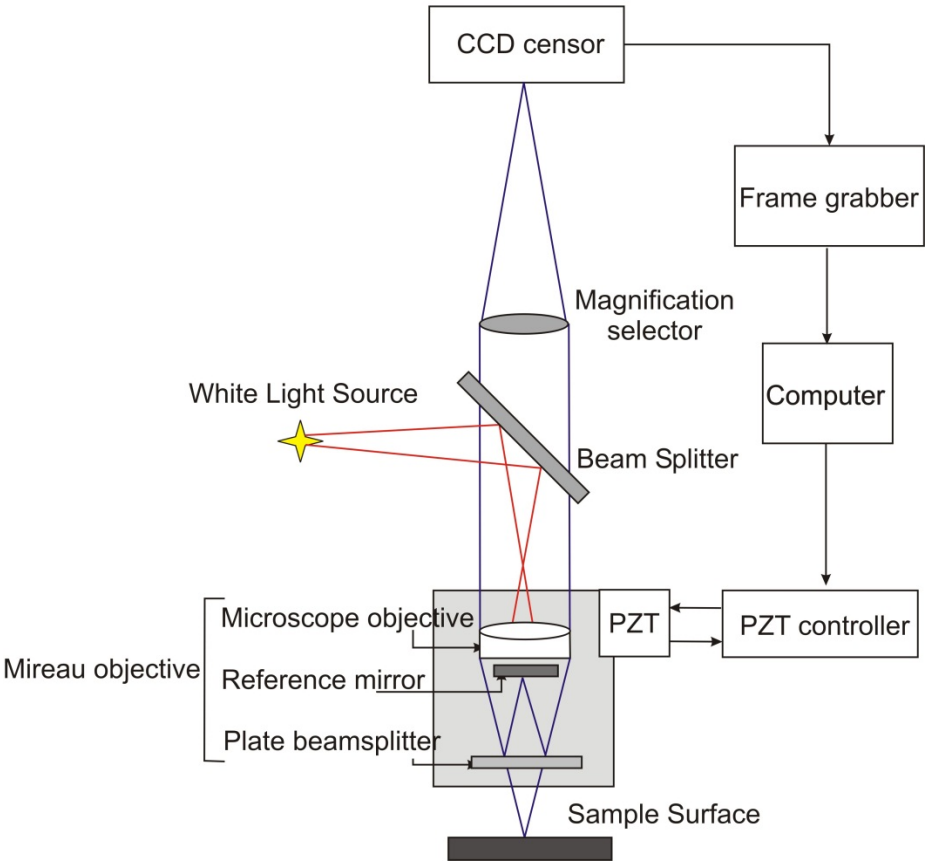

Figure 2-7 Schematic diagram of vertical scanning interferometer (as used in SWLI) [124].

The primary method of action in a vertical scanning interferometer is the utilization of wave interferences developed from a reference mirror located within the microscope objective. As seen in Figure 2-7, the white light source is directed through the microscope objective where it is partially reflected by a beamsplitter to a calibrated reference mirror. This reference light is then reflected back to the CCD sensor along with the reflected light from the sample surface. At the distance where the surface is the same path length as the light from the reference mirror, interference patterns form due to the light actively interfering with itself. Through the use of a high resolution vertical piezoelectric (PZT) actuator, the CCD then capture a series of vertical

images of the surface and uses the resulting interference patterns to locate the height of the sample's surface at each pixel.

SWLI's primary advantages lie in its ability to quickly, non-destructively analyze surfaces without contacting them. Unlike time consuming atomic force microscopy (AFM), SWLI takes a full surface measurement in seconds or less. Surfaces do not need to be coated or prepped prior to measurement with SWLI, and can be analyzed in atmospheric conditions. Being a non-contact technique, SWLI is ideal for use with samples that could be easily damaged from other techniques (e.g., contact profilometers), or when the surface may significantly interact/interfere with the measurement device (as with tip induced imaging artifacts from AFM on soft materials [125]).

SWLI has primarily been applied as a metrology instrument with application to relatively hard surfaces. SWLI has been applied to a variety of industrial applications, but the technique has not been generally applied to the study of biological materials and systems. Optical coherence tomography (OCT), a technique similar to SWLI [126], has been used to image unstained epithelial cells [127], as well as a beating Xenopus laevis (African frog) heart. While OCT is valuable for 3d permeative measurements (similar to an ultrasound), it has a lower resolution than SWLI (on the order of several microns) [128].

2.7 X-ray Diffraction

X-ray diffraction (XRD) techniques utilize the principle of Bragg's law to explore the crystalline structure of solid materials [129]. Diffraction patterns can form when incident X-rays satisfy Bragg's law. This takes place when an X-ray passes through a material that has a regular, repeating structure on the same order of length scale to that of the traversing wave.

2.7.1 Development and Theory

The general concept of diffraction has been used for over 200 hundred years, and for the last 100 years, it has been used to explore the crystal structures of materials. Diffraction was first used with light in the early 1800s by Thomas Young in the double slit experiment, where he showed that light constructively and destructively interferes with itself when shone through two adjacent slits [130]. Young died in 1829 and was likely unaware of the later application of his technique in the yet-to-be-discovered X-ray region of the electromagnetic spectrum.

In 1912, Max von Laue grasped the concept that X-rays had a similar wavelength to the spacing of atomic planes in crystalline materials. Max von Laue went on to use this property to perform the first X-ray diffraction experiments, confirming his suspicion that X-rays had similar wave properties to that of light [131]. Von Laue's findings came to be the foundation of modern X-ray spectroscopy. Since then, X-ray spectroscopy has developed into a variety of techniques.

2.7.2 Experimental Configurations

There is a large subset of applications of X-ray diffraction for the analysis of specific material properties. Among these are techniques for solids, powders, and films [132]. Experimental setups include the traditional XRD (also referred to as the θ-2θ or Bragg-Brentano) technique, parallel beam geometries, crystal monochromators, double and triple axis diffractometers, and point source geometries [133]. A few X-ray setups of interest can be found in Figure 2-8.

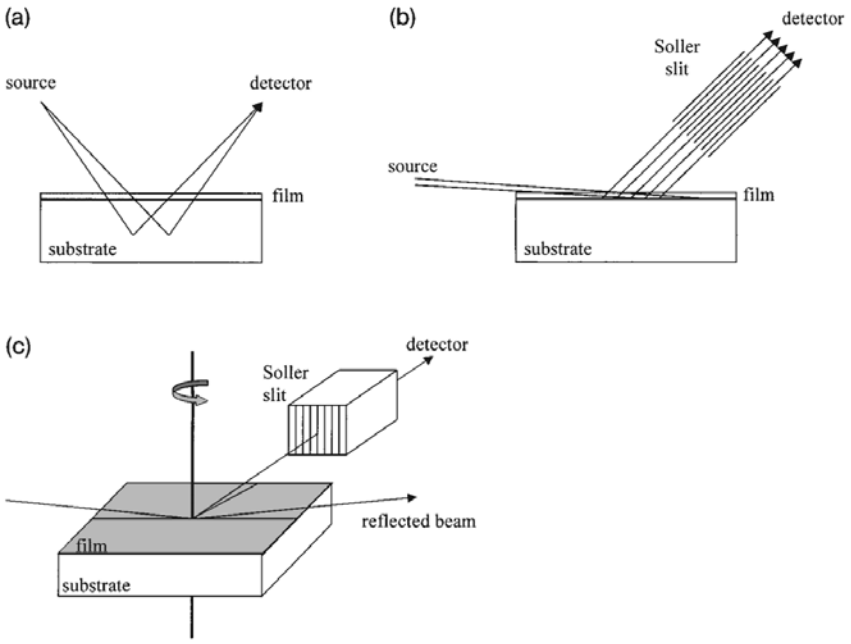

Figure 2-8 Diagrams of different X-ray diffraction techniques. Standard XRD goemetry (a), Glancing Angle geometry (GAXRD) (b), and Grazin Incidence X-ray Scattering (GIXS) geometry (C) [129].

Figure 2-8 shows schematic setups for the traditional XRD setup (a), as well as two common glancing angle configurations (b and c). As diagrammed in Figure 2-8 part (a), a traditional XRD (θ-2θ) experiment maintains a consistent incident and detector angle, that is, the detector changes angle to the same degree as the incoming X-rays such that any detected crystals in the sample will be parallel to the surface of the sample. Of the two common glancing angle configurations diagrammed in Figure 2-8, the first (b) is for detecting diffraction in plane to the incident glancing X-ray beam, the second (c) is for detecting diffracted X-rays out of plane of the incident X-ray beam. The second, asymmetric glancing angle configuration is widely employed and is more suited for polycrystalline surfaces than it is for single crystal surfaces [129].

2.8 Nano Indentation

Nanoindentation (NI), also known as instrumented or depth-sensing indentation, is a mechanical testing method that probes the micro- and nano-scale mechanical properties of materials. The NI technique is able to bridge the gap between molecular level properties (e.g. those measured using AFM) and results from macroscale mechanical testing. Using known material property models and contact mechanics, uniaxial material properties can often be extracted from the load-displacement results of a nanoindentation test. While this process works especially well for hard, linear-elastic materials, it can become considerably more difficult with soft, viscous materials due to the inability to directly measure the contact area between the NI probe tip and the material's surface.

In the case of hard, linear-elastic materials, stiffness and reduced modulus are calculated from the unloading curve using the following equations.

Equation 2-1

$$S = \frac{2\sqrt{A}}{\sqrt{\pi}} E_r$$

In Equation 2-1; S is the stiffness and A is the area of contact between the tip and the surface.

Equation 2-2

$$\frac{1}{E_r} = \frac{1 - \nu_i^2}{E_i} + \frac{1 - \nu_s^2}{E_s}$$

In Equation 2-2; E_r is the reduced modulus, ν is the Poissons ratio, and the subscripts i and s refer to the indenter and sample material respectively.

Doerner and Nix first assumed a linear relation between loading and displacement [134], however, later developments by Oliver and Pharr improved on this by using a tip shape function from a separate calibration to determine the contact area [135]. This addition by Oliver and Pharr made it possible to account for the non-linearity in the unloading section.

Universal Hardness

The universal hardness (or Martens Hardness *HM*) can be calculated when using sharp indenter tips and incorporates the elastic properties of the tested surface, including soft polymers (though it does not differentiate plastic effects). This methods advantage is that it does not rely on imaging techniques to determine the contact area under the indenter tip (with associated uncertainties) [136]. It is computed using the maximum peak load and the nominal displacement from the load displacement curve to evaluate the hardness as seen in Equation 6-1.

Equation 2-3 Universal Hardness for Nanoindentation [137]

$$H_U = \frac{P}{A_p(h_c)}$$

In Equation 6-1, H_U is the universal hardness (Pa), P is the maximum indentation load applied to the sample (mm), and the denominator is an area function, where, A_p is a tip function constant, and h_c is the maximum indentation depth (m). In the case of the standard Berkovich tip, A_p = 26.43 [137]–[139].

2.9 Motivation for Dissertation Research

This work will further the understanding and technology needed to improve clinical options for implants through the development and characterization of DOPS and cholesterol implant coatings. Through the understanding of coating morphology and microstructure gained

in the following study, an optimized solution to osseointegrative implant coatings will be able to be pursued.

The focus of the James research group is on the research, development and characterization of bio-inspired implant technologies. While the discoveries encountered in the presented work have broader implications than just for medical implants, the focus of discussion and analysis will be for the use of DOPS and cholesterol coatings in the field of bioengineering.

Chapter 3: Research Overview

3.1 Goals and Objectives

This chapter's purpose is to give an overview of the hypotheses and specific aims that directed the presented work, and will outline the goals used in the subsequent chapters.

3.1.1 Chapter 4 Objectives

Understanding coating roughness and morphology is critical to implant surface stability, release kinetics, and the understanding of biological interactions. The work presented in chapter 4 was towards the development of new methods to analyze DOPS and DOPS-cholesterol coatings for the purpose of elucidating structure function relationships of the coatings.

The purpose of Chapter 4 is to develop methods to use scanning white light interferometry (SWLI) for the characterization of DOPS coatings in order to be able to later elucidate structure function relationships of the coatings. The method development goals for Chapter 4 are as follows:

Method Development Goal 4.1: Develop methods to use scanning white light interferometry to observe surface morphology and measure nano- and micron-scale surface roughness of DOPS and DOPS-cholesterol coatings.

Method Development Goal 4.2: Develop methods to Develop methods to use scanning white light Interferometry to measure the thickness of E-sprayed DOPS and DOPS-cholesterol coatings.

3.1.2 Chapter 5 Objectives

The purpose of the work described in Chapter 5 wa to use the SWLI measurement methods developed in Chapter 4 for the measurement and characterization of DOPS and cholesterol coatings. Additionally, contact angle measurements were used to study the effects of roughness and surface chemistry on the DOPS and cholesterol coatings. The hypotheses and specific aims for Chapter 5 are as follows:

Hypothesis 5.1: Coating contact angle measurements will negatively correlate with coating roughness due to an increase in surface roughness in DOPS only coatings.

Specific Aim 5.1-1: Measure coating surface roughness using SWLI.

Specific Aim 5.1-2: Measure the aqueous contact angle of coating surface with a goniometer, and look for possible correlations between these and the roughness measurements.

Hypothesis 5.2: Coating morphology (specifically surface roughness) will be the primary reason for contact angle changes between coating compositions. That is, increased roughness resulting from the addition of cholesterol in the coatings will result in decreasing contact angle of the DOPS:cholesterol coatings, even though cholesterol is hydrophobic and results in high contact angles when used by itself.

Specific Aim 5.2-1: Compare coating roughness (as measured using SWLI) with aqueous contact angles for coatings with various concentrations of cholesterol in the coatings.

Hypothesis 5.3: The coating roughness and morphology measured by SWLI will be more consistent on polished Ti_6Al_4V substrates compared to as-machined substrates, and will increase the statistical power for studies of DOPS and cholesterol coatings.

Specific Aim 5.3-1: Measure the coating surface roughness of samples that were polished prior to coating, and compare the variance and power to un-polished samples.

3.1.3 Chapter 6 Objectives

The purpose of the work described in Chapter 6 is to analyze and characterize the effects of adding a calcium pretreatment to the coating substrate, and the effects of the addition of cholesterol to the coating on the coatings' thickness, roughness, hardness, and microstructural states. The hypotheses and specific aims for Chapter 6 are as follows:

Hypothesis 6.1: Adding a calcium solution pretreatment to the substrate will not have a significant impact on the coatings' thickness or surface roughness due to the localized effects of the calcium near the substrate surface.

Specific Aim 6.1-1: Use SWLI to measure the thickness of DOPS coatings with and without a calcium pretreatment.

Specific Aim 6.1-2: Use SWLI to measure roughness of DOPS coatings with and without a calcium pretreatment.

Hypothesis 6.2: Adding a calcium pretreatment will harden the DOPS coatings due to a binding of the phospholipid headgroup in the presence of calcium.

Specific Aim 6.2-1: Use nanoindentation to measure the universal hardness of DOPS coatings with and without inclusion of a calcium substrate pretreatment.

Hypothesis 6.3: DOPS coatings will increase in roughness with increasing cholesterol content due to a higher surface energy from the binding and entanglement of cholesterol in the DOPS.

Specific Aim 6.3-1: Use SWLI to measure the roughness of DOPS coatings with varying concentrations of cholesterol added to the coating.

Hypothesis 6.4: Increasing the amount of cholesterol in the coatings will harden the DOPS coatings due to cholesterol dispersing in the lipid system and stiffening the lamellar DOPS structure.

Specific Aim 6.4-1: Use nanoindentation to measure universal hardness of DOPS coatings with varying concentrations of cholesterol added to the coating.

Specific Aim 6.4-2: Use differential scanning calorimetry to measure the heat flow of DOPS coatings with varying concentrations of cholesterol added to the coating.

Specific Aim 6.4-3: Use glancing angle X-ray diffraction to measure the diffraction patterns of DOPS coatings with varying concentrations of cholesterol added to the coating.

3.1.4 Chapter 7 Objectives

The purpose of Chapter 7 is to analyze effects that storage (i.e., ageing) may have on the coatings, and whether there is a change in the effects between storage locations (in a vacuum desiccator versus an ambient location). Coatings will be analyzed for changing surface morphology (SWLI), crystalline microstructure (GAXRD), and thermal phase transitions (DSC). The hypotheses and specific aims for Chapter 7 are as follows:

Research Question 7.1: DOPS and cholesterol samples stored in a vacuum desiccator will maintain a stable surface roughness and coating thickness over time.

Specific Aims 7.1-1: Use SWLI to measure the coating roughness and thickness of DOPS and cholesterol coatings immediately following their manufacture, and after 4 and 12 weeks of storage in a vacuum desiccator.

Research Question 7.2: DOPS and cholesterol samples stored in ambient conditions will change in surface roughness and microstructure over time due to changes that enhance molecular mobility and reconfiguration.

Specific Aim 7.2-1: Use SWLI to measure the coating roughness of DOPS and cholesterol coatings immediately following their manufacture, and after 4 and 12 weeks of storage in ambient conditions.

Specific Aim 7.2-2: Use differential scanning calorimetry to measure phase transitions of DOPS and cholesterol coatings immediately following their manufacture, and after 4 and 12 weeks of storage in ambient conditions.

Specific Aim 7.2-3: Use glancing angle X-ray diffraction to characterize any crystalline microstructure of DOPS and cholesterol coatings after long term storage in ambient conditions.

Chapter 4: Characterization of E-Sprayed DOPS Coatings Using Scanning White Light Interferometry

4.1 Purpose and Chapter Overview

Understanding coating roughness and morphology is critical to implant surface stability, release kinetics, and the understanding of biological interactions. The work presented in this chapter developed new methods to analyze DOPS and DOPS-cholesterol coatings for the purpose of elucidating structure function relationships of the coatings.

Despite the *in vitro* [5], [17], [89] and *in vivo* [6], [140] studies that have been completed with DOPS coatings, there is still relatively little known about the coatings and many limitations arise when trying to study DOPS coatings with previously attempted analytic techniques. DOPS coatings are much softer and thicker compared to typically studied thin films. This makes the DOPS coatings difficult to characterize with the techniques available currently.

4.1.1 Limitations of Traditional Microscopy Techniques

Typical biological coating characterization methods include light microscopy, scanning electron microscopy (SEM), atomic force microscopy (AFM), contact angle measurements, thin film analysis techniques, *in vitro* cell studies and *in vivo* animal studies [141]. Many thin film analysis techniques do not work with DOPS coatings on metallic implants due to the coatings relatively thick and rough nature (coatings are on the order of 5-20 μm in thickness).

Typical light microscopy techniques have limited utility for the analysis of DOPS coatings given their shallow depth of field and the transparent nature of the DOPS coatings. Please see Figure 4-1 for an example of a traditional microscope image of a DOPS coating.

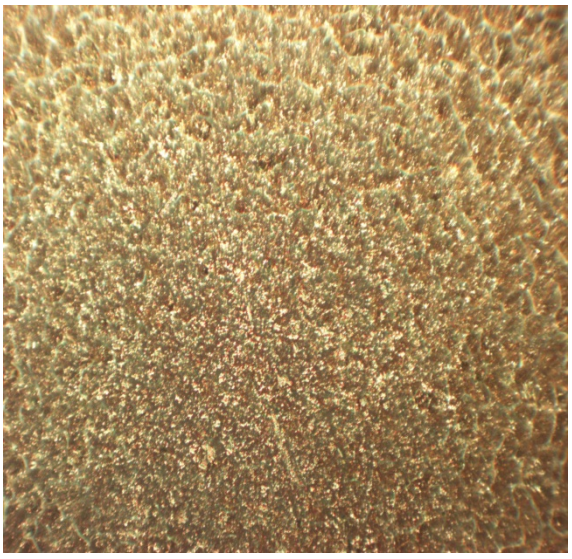

Figure 4-1 Traditional light microscope image of a DOPS coating at 20X.

As seen in Figure 4-1, traditional light microscope images have difficulty distinguishing the coating from the metallic substrate due to coating transparency. The majority of the texture seen in Figure 4-1 is from the substrate, despite the fact that the microscope's focus was on the coating surface. One can easily focus through the coating to the substrate during inspection, making the qualitative and quantitative analysis of the coating surface difficult.

SEM is disadvantageous in that it requires a vacuum to take an image and is often a terminal measurement. Ideally for SEM, the coatings need to be coated with a conductive material in order to be imaged effectively. SEM is also largely qualitative by nature.

AFM can provide useful information, but is time and resource intensive. It is also limited to a relatively narrow size scale of useful information that can be measured (e.g., techniques focus on returning quantifiable information in only the nano or in the micro sized scale range) [142]. AFM also suffers from tip induced imaging artifacts with the relatively soft and sticky DOPS coatings [125].

In vitro and *in vivo* methods are inherently difficult and expensive. It is often difficult to isolate causal relationships, and there has been limited ability to show statistical differences between groups of DOPS coatings due to gross variance in the results [6], [17].

Due to the limitations of the currently employed analysis techniques, effort was undertaken in the present work to develop alternative methods of analysis for DOPS coatings. These efforts were primarily focused on using a scanning white light interferometer to measure both qualitative and quantitative attributes in order to aid the development and understanding of DOPS and DOPS-cholesterol implant coatings.

4.2 Chapter Goals and Objectives

Method Development Goal 4.1: Develop methods to use scanning white light interferometry to observe surface morphology and measure nano- and micron-scale surface roughness of DOPS and DOPS-cholesterol coatings.

Method Development Goal 4.2: Develop methods to use scanning white light Interferometry to measure the thickness of E-sprayed DOPS and DOPS-cholesterol coatings.

4.3 Preparation of DOPS and DOPS-Cholesterol Coated Samples

In order to develop a measurement method using scanning white light interferometry (SWLI), test specimens coated with DOPS and DOPS-cholesterol were prepared. The samples were prepared and coated via an E-Spray deposition process as outlined in the following sections.

4.3.1 Materials

7.5x7.5 mm Ti_6Al_4V sheet metal samples were used for all samples. The stock Ti_6Al_4V sheeting was purchased from Titanium Joe, Inc. (Kingston, Ontario, Canada) [143]. The Ti_6Al_4V sheet metal was then prepared at CSU by shearing the sheets into 7.5x7.5 mm squares using a foot actuated sheet metal shearing table.

Phosphatidylserine (DOPS) was purchased in lyophilized form from Avanti Polar Lipids, Inc. (Alabaster, Alabama) [59]. The DOPS was stored in as-received form in a -20º C freezer and mixed with Chloroform prior to e-spraying. Cholesterol (CAS# 57-88-5) was obtained from Alfa-Aesar (Ward Hill, MA) [144], and mixed with DOPS along with the chloroform prior to e-spraying.

4.3.2 Methods

Cleaning

Samples were thoroughly cleaned prior to coating according to the protocol found in Appendix A: Protocol A - Titanium Square Sample Preparation. Briefly, the square Ti_6Al_4V samples were sonicated sequentially in Acetone, Chloroform, 5% Liquinox, rinsed three times and sonicated in Di water. Samples were then rinsed in ethanol, blow dried with nitrogen and stored in a vacuum desiccator.

Passivation

After cleaning, samples were passivated according to the protocol found in Appendix A: Protocol D - Titanium Passivation. Briefly, samples were immersed in 30% nitric acid solution for 40 minutes, then rinse with DI water, and blow dried with lab air. Samples were then stored in a vacuum desiccator prior to coating.

Electro-Spray Coating Process

Coatings were applied to the cleaned and passivated 7.5x7.5 mm square Ti_6Al_4V samples using an electro-spray process (see Section 2.4.3). Briefly, a 1.3% (vol%) DOPS in chloroform solution was e-sprayed onto cleaned and passivated 7.5x7.5 mm Ti_6Al_4V samples. A 12 kV voltage differential was used with a pump rate of 14 mL/min and an 8 cm working distance.

Drying Samples

After e-spraying, the coated samples were dried under a vacuum in a desiccator for at least 48 hours. Samples were stored similarly until utilized for analysis.

4.4 Method Development for Using Scanning White Light Interferometry to Analyze DOPS Coatings

4.4.1 Initial Measurements Using SWLI

In order to determine whether scanning white light interferometry (SWLI) could be used to look at the morphology of DOPS coatings, a series of tests were conducted to explore its efficacy. The initial methods used with the SWLI on DOPS coatings and their results are outlined in the following section.

4.4.2 Initial Methods for Scanning White Light Interferometry

SWLI Settings

A NewView 7300 scanning white light interferometer (Zygo Corporation, Connecticut, USA) was used to measure pure DOPS coated samples. Instrument control, data acquisition and

analysis were performed using the instrument software (MetroPro 9.0.2). Samples were prepared and coated with DOPS as outlined previously in Section 0.

The initial microscope objectives that were utilized included the 10X, 20X and 50X magnifications. The NewView instrument was in a standard configuration and isolated from vibration on an air table. All samples were evaluated in atmospheric conditions in an as-sprayed condition (i.e. no surface preparation such as gold coating was done prior to analysis). Standard data fill and filtering techniques were utilized during SWLI measurements. The camera within the NewView 7300 used to measure samples had a 640 x 480 resolution. The light level of the SWLI was adjusted to maximize data capture. The standard protocol used was to remove 4^{th} order surface form from the SWLI measurements.

Results

As seen in Figure 4-2, an uncoated Ti_6Al_4V sample was measured using SWLI.

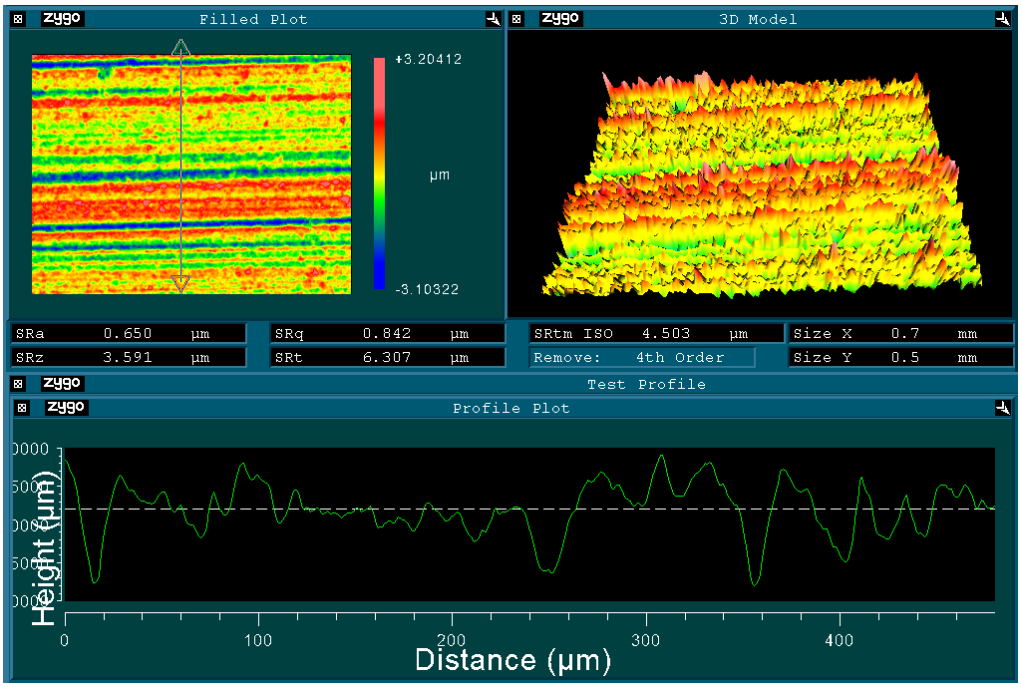

Figure 4-2 SWLI measurement of an uncoated Ti_6Al_4V sample. Top left: aerial view of the surface. Top right: 3D model of the surface. Bottom: cross section of the surface as located by the vertical trace located in the aerial view.

In Figure 4-2, a representative SWLI measurement of an uncoated Ti_6Al_4V sample can be seen. The field of view of the entire measurement was 0.7 x 0.5 mm. The top left aerial view of the surface contains a vertical trace marker, which corresponds to the 2-dimensional trace found in the bottom of the figure. Note that the vertical scale is arbitrary and highly exaggerated in all three views (in the 2D trace, the maximum peak to valley distance (SRt) is 6.31 µm over the 500 µm trace. The arithmetic average height of the surface (SRa) is 0.650 µm, and the SRz (an average peak to valley measurement) is 3.56 µm. The material machining marks are clearly visible across the surface of the sample, showing as horizontal ridges and valleys.

A SWLI measurement of a representative DOPS coated Ti_6Al_4V sample can be found in Figure 4-3.

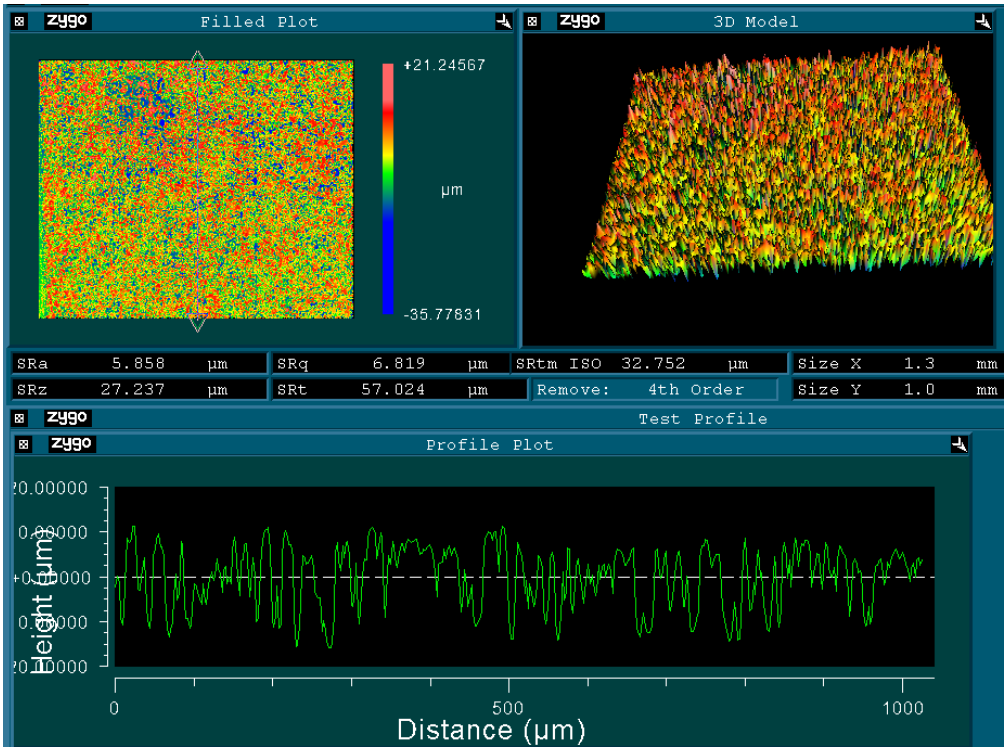

Figure 4-3 SWLI measurement of DOPS coated Ti_6Al_4V sample. Top left: aerial view of the surface. Top right: 3D model of the surface. Bottom: cross section of the surface as located by the vertical trace located in the aerial view.

As seen in Figure 4-3, the SWLI measurement of the coating has two distinct heights throughout the measurement. This is most clearly seen in the 2D trace profile (bottom of Figure 4-3). The height of the profile jumps sporadically between the +10 µm and the -10 µm regions.

While the substrate machining marks can still be seen across the surface of the sample, there is a larger discrepancy between the two height levels seen in this measurement than what was found from just the substrate. The substrate roughness was on the order of several microns, while the coated sample measurement jumps between 10 and -10 microns.

Discussion

Surface measurement of the uncoated Ti_6Al_4V sample proceeded as expected. There were no particular issues or reasons to question the measured interpretation of the data. Of note, there was evidence of the substrate's machining marks on the sample. The machining marks were visible on the coating surface. The average roughness (SRa) was on the order of less than 1 µm for all measured uncoated Ti_6Al_4V samples.

For the DOPS coated samples, there was an apparent duality to the interpreted surface height. This is explained by the interferometers ability to 'see' through the coating and produce interference patterns at both the surface of the coating as well as the surface of the metallic (Ti_6Al_4V) substrate. This was similar to the results found when using a regular microscope (see Figure 4-1).

An important part of a SWLI measurement is the precise marking of the peak of the interference pattern in the raw SWLI trace. In an ideal measurement, this Gaussian modulation envelope will be easily distinguishable and have a high signal to noise ratio. Two example traces can be found in Figure 4-4.

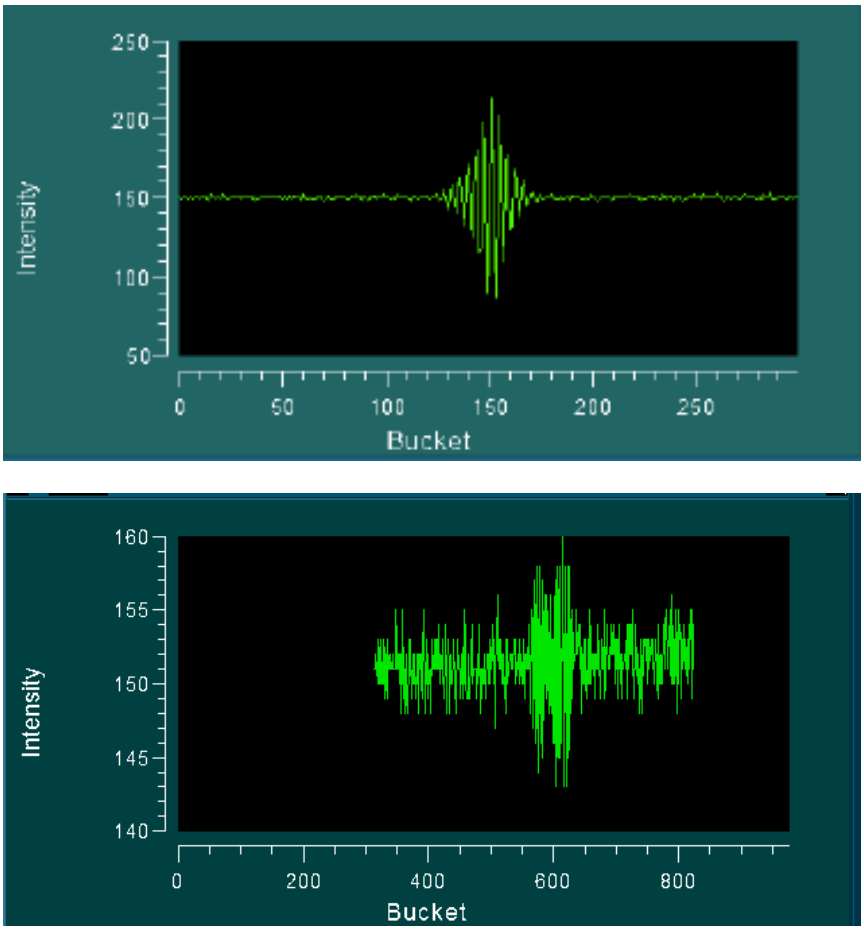

Figure 4-4 SWLI raw measurement traces showing interference pattern modulations. Top: a typical SWLI trace [145]. Bottom: a trace from a DOPS coated sample.

As seen in Figure 4-4, the top trace has a high signal to noise ratio and provides easy location of the peak of the interference modulation. The lower trace is from a DOPS coated surface and illustrates the difficulty the instrument encounters while measuring the transparent and diffractive coating. The modulation signal is only marginally stronger than the background noise. Additionally, one can see that there are two interference patterns that partially overlap. These two patterns come from the two primary interfaces, the coating surface (the larger modulation towards the right), and from the metallic substrate (the slightly smaller modulation towards the left). This duality in the trace is the reason that the heights in the 3D map in Figure 4-3 jump between the interfaces.

Conclusions

Given the SWLI measurement results from the DOPS coated samples, it was concluded that the instrument parameters and/or capture methods needed to be changed in order to isolate the top surface of the coating from the substrate. Without some means of isolating the coating surface from the substrate, the SWLI measurement returned height information from both the coating surface and from the substrate. That is, some of those the heights measured were from the coating surface, and some were from the substrate. Since the software in the SWLI is only looking for one surface, it picks the predominant interference pattern, and assigns that as the height of the sample at a given pixel. As is apparent in Figure 4-3, the predominant interference pattern at a given pixel alternated between the coating surface and the substrate.

4.4.3 Interim Methods for Scanning White Light Interferometry

SWLI Settings

Two methods were next implemented to try to isolate the coating surface from the substrate in the SWLI measurements. The first was to use a still-in-development films application within the MetroPro software. The second was to manually ‘clip’ the coatings during scanning.

The films app in MetroPro was first used to try to isolate the coating surface from the substrate. The films app allows the MetroPro software to look for two predominate interference patterns in the SWLI data, as opposed to looking for only one height at each pixel. The methods used for capture were similar to the methods used in the previous section (Section 4.6.2), with small adjustments made to the light level in order to minimize data dropout (i.e., places where no height information was interpreted for given sections of the sample).

The second method used to try and minimize substrate intrusion within the SWLI measurements was to manually 'clip' the surface during scanning. Each SWLI measurement requires an input setting for how long a scan should be in the z direction. This was typically set anywhere from 5-20 µm for the DOPS coatings. The scan length uses the current z-position as the middle point of the scan. For example, if focus on a sample was at an absolute height of 50 µm above the stage and the scan length in the z-direction was set to 20 µm, the stage would move down 10 µm (increasing the distance between the sample and the objective by 10 µm), and the instrument would then collect the measurement while moving the stage upwards 20 µm (ending with the stage 10 µm higher than its initial starting position). After measurement, the stage would then be returned to the original, in focus, position (where the focal plane is 50 µm above the stage height).

During the manual clipping method, an attempt was made to raise the scan floor (i.e., the lowest level at which SWLI captured height information on the sample) above the level of the substrate, while remaining below the height of the coating surface. This was typically done by focusing on the coating surface and then using a custom script to lower the stage 5-15 µm away from the objective and then using either a 10 or 20 µm scan distance.

Results

MetroPro Films App

A SWLI measurement of a representative DOPS coated Ti_6Al_4V sample taken using the films app can be found in Figure 4-5.

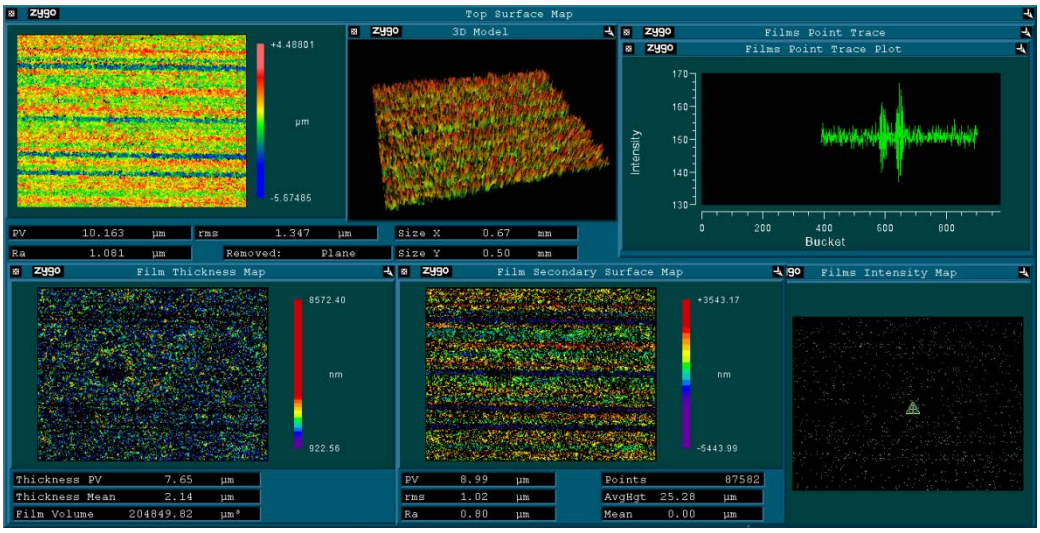

Figure 4-5 Films app measurement of a DOPS coated sample. Note; the data fill option was disabled for this analysis.

As seen in Figure 4-5, there is clear evidence in the trace (top right) for two surfaces, one at the coating, and one at the substrate. Given a default index refraction value of 1, the films app interpreted the coating thickness to have an average thickness of 2.14 µm, with a peak to valley height of 7.65 µm in thickness. It should be noted that the data fill option was disabled in the analysis shown in Figure 4-5 in order to show the level of completeness of the data. For reference, disabling the data fill option in measurements from previous sections had negligible visual impact on the final image.

A SWLI measurement of a representative 1:1 DOPS:cholesterol coated Ti_6Al_4V sample taken using the films app can be found in Figure 4-6.

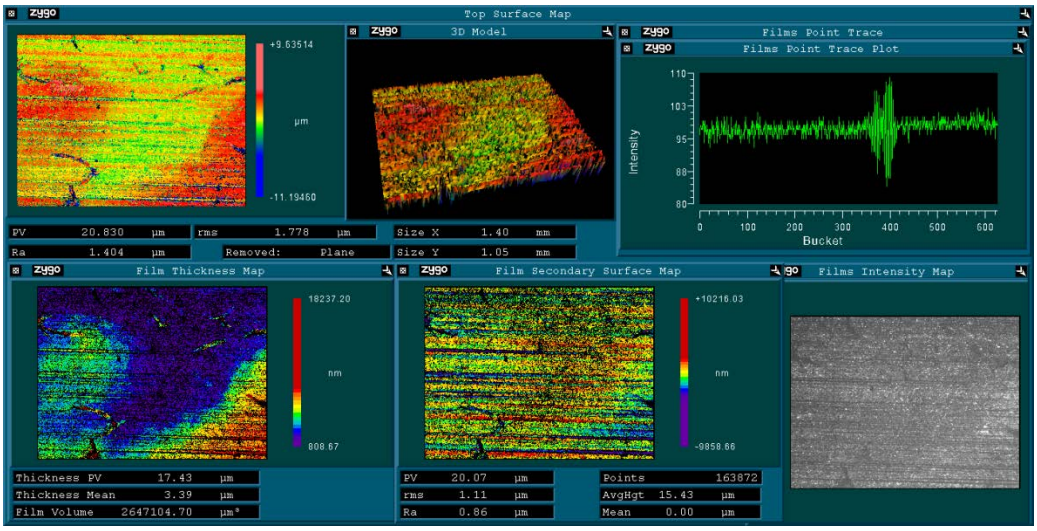

Figure 4-6 Films app measurement of a 1:1 DOPS:cholesterol coated sample. The data fill option was disabled for this analysis.

As seen in Figure 4-6, there was still evidence for two interfaces in the SWLI trace. In general, the addition of cholesterol to the coatings impeded the ability of the MetroPro films app to accurately distinguish both the coating and substrate surfaces. There was still height information at both interfaces, but there was also evidence of additional mid-coating interpretations of sample height due to increased diffraction within the coating.

Manual Scan Clipping Method

A SWLI measurement of a representative DOPS coated Ti_6Al_4V sample taken using the manual clipping method can be found in Figure 4-7.

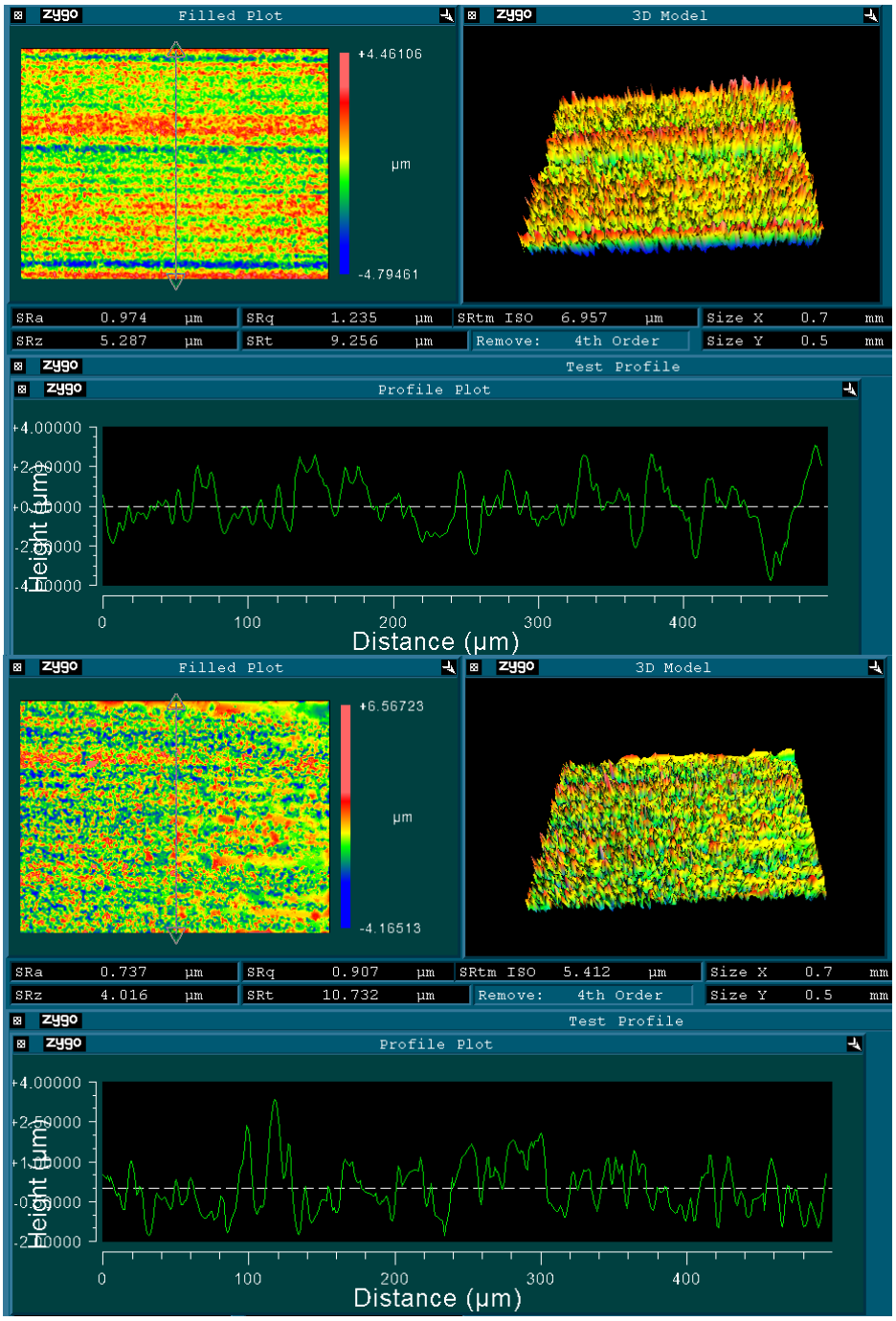

Figure 4-7 SWLI measurement of a DOPS coated sample captured before and after implementation of the manual clipping method. The top screenshot was scanned normally; the bottom screen shot was manually clipped in order to attempt to exclude the substrate.

As seen in Figure 4-7, the manual clipping method was able to remove much of the substrate contribution to the measurement, and consequently decreased the reported roughness.

However, the veracity of the data was sometimes questionable, due to the substrate topography being on the same height scale as the lowest parts of the coating.

Discussion

MetroPro Films App

The films app successfully detected two surfaces during SWLI measurements, but had two drawbacks. First, it suffered from severe data dropout, especially when measuring the DOPS:cholesterol coatings, and secondly it requires one to know the index of refraction. Data dropout was severe using the films app due to poor signal to noise ratios in the raw data (as seen in Figure 4-5). This is a difficult limitation to overcome with DOPS coatings due to the inherently thick, diffractive, and inhomogeneous nature of the DOPS coatings.

The index of refraction of bulk DOPS and DOPS:cholesterol coatings is not available for input into the films app. Even if it were known, the index of refraction is coating composition specific and varies from sample to sample. Coating inhomogeneities would also change the index of refraction locally within the coating and adversely affect measurement interpretation. A point worth noting for the films application is that it requires you to input the optical index of refraction for the coating being measured. While this is easily done for homogenous films with known optical properties, it is more difficult with DOPS and cholesterol coatings given their largely unknown optical properties.

Additionally, it was observed that using the films app became increasingly difficult with increasing concentrations of cholesterol in the coatings. This indicates that the cholesterol coatings were more diffractive and inhomogeneous in comparison to the plain DOPS coatings.

In order for a SWLI films app measurement to be highly repeatable, the signal to noise ratio needs to be high. Example SWLI traces can be found in Figure 4-8.

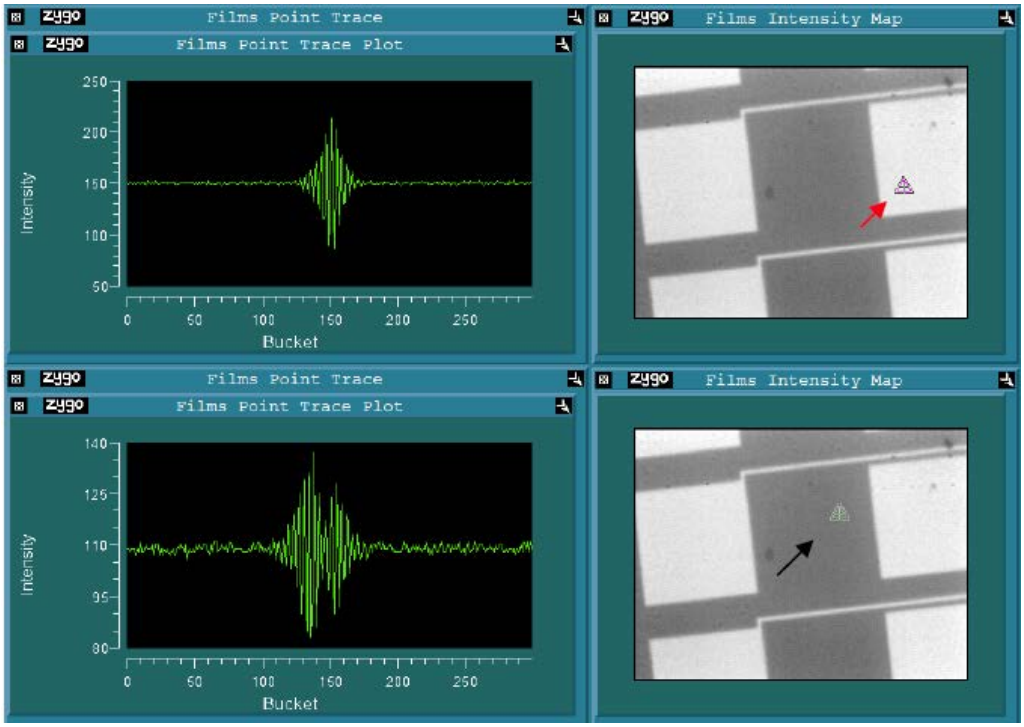

Figure 4-8 Example of a SWLI trace containing a single (top), and multiple Gaussian modulation envelopes (bottom). Top left and right; a SWLI trace with a single modulation from a point on the sample that has one interface (red arrow). Bottom left and right: a trace with multiple modulations representing the detection of two interfaces on the sample (black arrow) [145].

In Figure 4-8, there are two SWLI traces, the top SWLI trace shows a single Gaussian modulation envelope from a point on the sample that has one interface, i.e., no coating (red arrow). The bottom trace exhibits multiple modulations, representing the detection of two interfaces on the sample, i.e., a coating (black arrow). These signals are from the silicone industry [145], and demonstrate a much stronger signal to noise ratio as those measured for the DOPS coatings (Figure 4-5, Figure 4-6).

Manual Scan Clipping Method

During implementation of the manual clipping method, the set points used for the scan range start point and scan length were usually iteratively discovered based on the apparent coating thickness and the resulting SWLI measurements. If there was significant data dropout, it was concluded that the scan floor was set too high and did not include the coating surface. If there was significant duality in the sample height (i.e., apparent addition of substrate height along with that of the coating surface, as found in Section 4.4.2), it was concluded that the scan floor was not set high enough (was including the substrate in the scan).

The manual clipping method worked best with very thick coatings. The coatings measured in this work generally ranged from 3-20 μm in thickness. For the thicker coatings, it was relatively easy to exclude the substrate in the scan range. However, for the thinner coatings, it was difficult or impossible to do this, as the transition between the substrate surface and top of the coating was often indistinct. There were many times that the substrate was higher in areas than low points in the coating surface. This made it impossible to select a scan range floor that was above the metallic substrate while remaining below the coating surface.

As with the films app, it was found that the manual clipping method was significantly less successful when measuring coatings that included cholesterol. This was primarily attributed to the fact that the cholesterol coatings were more diffractive than the plain DOPS coatings.

Conclusions

Neither the MetroPro films app nor the manual clipping method was fully deemed acceptable for analysis of the DOPS coatings. While both methods improved results over those found in Section 4.4.1 and showed promise, they each had limitations. The MetroPro films app

worked for plain DOPS coatings, but had significant signal to noise issues (that were especially apparent when analyzing the DOPS:cholesterol coatings), resulting in severe data dropout and limited utility for the presented work. The manual clipping method worked for thick coatings, but was difficult or impossible to implement effectively with thin coatings where the substrate roughness was on the same size scale as the coating thickness. This was primarily due to substrate roughness that was on the same order of scale as the coating thickness.

It was concluded that better isolation of the coating surface was still needed. The primary difficulty encountered during measurements in this section was still related to the interferometer 'seeing through' the coating and reading surface height values below the surface of the coating.

4.4.4 Final SWLI Measurement Methodology

Given the limitations found above while using the 5X, 10X and 50X objectives, the next strategy employed was to take advantage of the reflectance changes associated with changing the numerical aperture of the objective. Each objective has a fixed numerical aperture, which generally increases with increasing magnification. The previously engaged measurement techniques suffered from the consequence of the SWLI seeing through the coating surface. Given the observation of slight, but noted, changes in coating reflectance between objectives, the highest numerical aperture lens available (100X) was chosen to limit sub-surface SWLI measurements.

A 100X objective was used in combination with a multi-frame composite stitching strategy in order to isolate the coating surface and increase the field of view for the analyzed area. The 100X objective was used because of its high numerical aperture, and consequent ability

to help exclude the substrate during measurement. A multi-frame composite stitch strategy was then used, increasing the field of view for the analyzed area.

Methods

The following changes were implemented to the methods outlined in Sections 4.4.2 and 4.4.3. A 100X objective and 0.5X zoom were used to capture each frame. A custom frame stitching script was then used within MetroPro to produce a 35 frame composite image (i.e., each analyzed area was a composite comprising of 35 individual capture frames). The composite pattern was 5 columns by 7 rows, with each frame having 25% overlap with adjacent frames in the final composite. Each individual frame had a field of view of 138 x 103.5 µm and 640 x 480 pixels and underwent a 40 µm vertical scan. This resulted in a lateral pixel resolution of 0.22 µm. The final composite had a field of view of 500 x 500 µm and 2319 x 2319 pixels. A 0.0025 µm low pass noise filter was used to filter out high frequency optical noise. As used before, the data fill option within MetroPro was enabled to fill-in occasional data dropout.

The zoom setting was set to 0.5X for the SWLI measurements in this section. In addition to the objective used (and its associated fixed magnification), there is an additional optical zoom setting on the New View 7400 that can be set to 1X, 2X, or 0.5X. The SWLI measurements in the previous sections utilized the 1X zoom setting.

Results

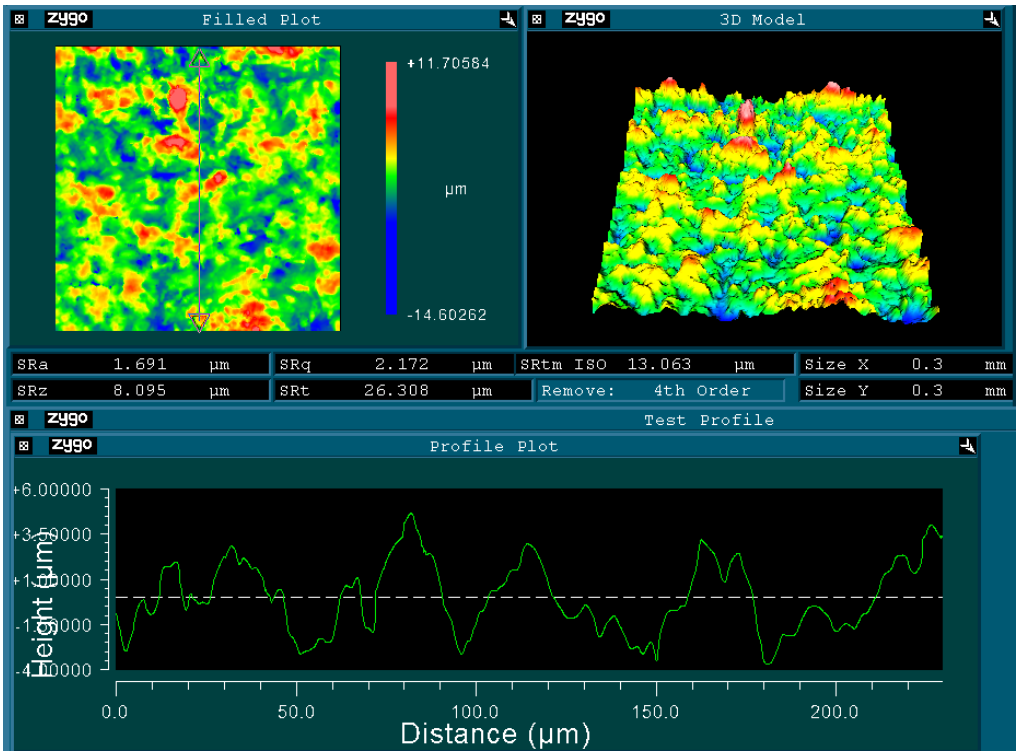

Figure 4-9 SWLI composite stitch comprised of 35 individual 100X capture frames of a DOPS coating surface.

A representative composite SWLI capture can be seen in Figure 4-9. The final mapped coating surface does not jump between the substrate and coatings surfaces as with prior measurements (as was seen in Figure 4-3and Figure 4-5).

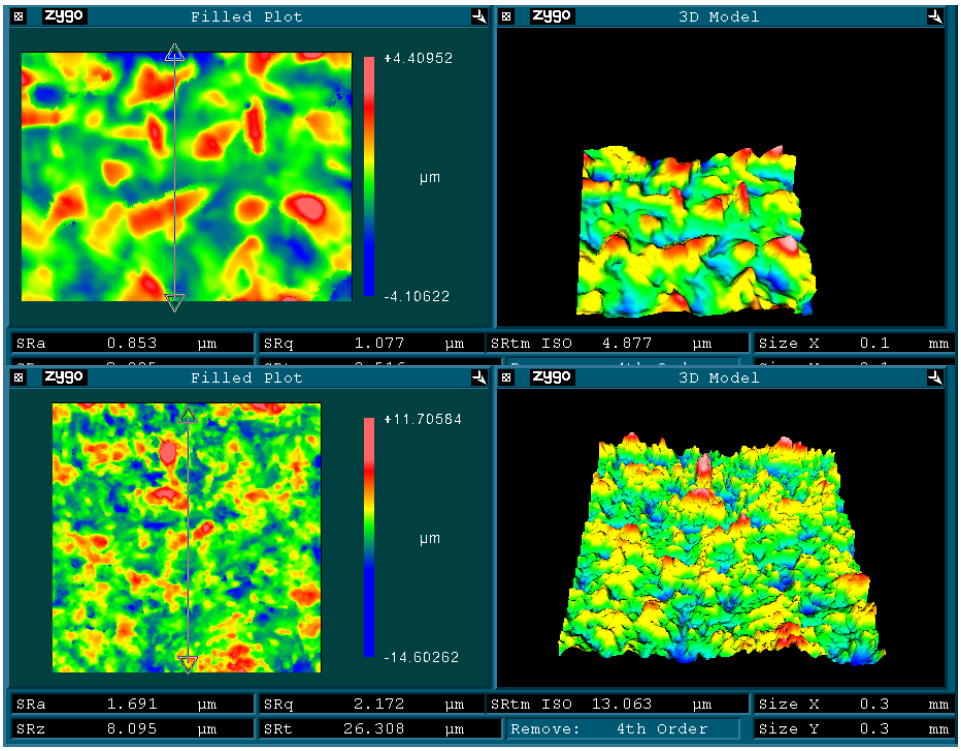

Figure 4-10 SWLI 3D maps of 1 frame (top), and 35 frames (bottom) from a DOPS coated sample. Frames were captured using the 100X objective.

A representative composite capture of a DOPS coated sample can be seen in Figure 4-10. Similar to the SWLI measurement shows good isolation of the coating surface, with no evidence of substrate height measurements.

Discussion

The 100X objective showed great improvement in selecting only the top surface of the coating, there was little evidence for substrate interference in the measurements. This was also seen in the raw SWLI traces, with the 100X objective, the substrate did not contribute a significant Gaussian modulation envelope compared to the surface interface.

A significant benefit of using the 100X objective frame stitching strategy is increased lateral pixel density. The 10X objective (with a 697 x 522 µm field of view) has a 1.09 µm pixel

pitch, whereas the 35 frame 100X composite analysis area (with its 0.5 x 0.5 µm field of view) has a 0.22 µm pixel pitch. This is a fivefold improvement over using the 10X objective, and allows for increased high frequency surface information to be captured.

A downside of the composite strategy is that it takes longer to measure the surface. A typical SWLI scan takes less than 2 seconds, so the added time is comparatively minimal. A 35 frame stitched are takes about 2 minutes to capture, combine and process.

The stitch strategy was necessary to capture enough repeating form and surface features so as to have an accurate representation of the surface. The 0.5 x 0.5 mm area was shown to provide a large enough analysis area to provide a good representation of the surface. If the area was much smaller, size features may have been missed, and larger areas were found to be generally unnecessary. This can be illustrated by the roughness measurements changing dramatically between the individual capture frame (SRa = 0.85 µm and SRz = 2.905 µm as seen in the top of Figure 4-10), and the final composite analysis area (SRa = 1.691 µm and SRz = 8.095 µm as seen in the top of Figure 4-10).

Conclusions

The high magnification objective and composite stitch strategy successfully allowed the use of SWLI for measurement of DOPS coatings. By taking advantage of the high numerical aperture of the 100X lens, the SWLI measurements excluded the substrate. There was little evidence for substrate surface interference in the final SWLI measurements. This strategy allowed better imaging of the DOPS and DOPS:cholesterol coating surfaces. The interference pattern for the coating surface became the predominant interference pattern, allowing the

effective measurement of DOPS coatings. The stitching then allowed sufficient analysis area for effective visualization of the coating morphology.

4.4.5 SWLI Method Development Discussion

Numerical Aperture Effects

The numerical aperture (NA) of a lens is an important property for the measurement of DOPS coatings using SWLI. The NA of a lens is a measure of how much detail can be resolved and light gathered from a surface by an objective at a fixed distance [146].

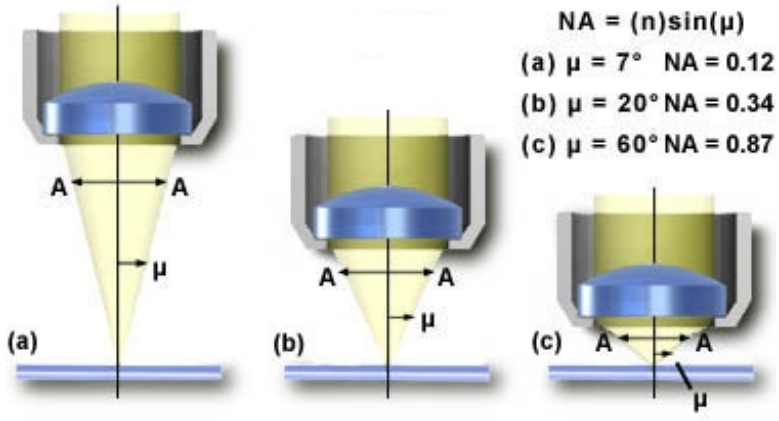

Figure 4-11 Examples of different objectives and their associated changes in numerical apertures [146].

As seen in Figure 4-11, the numerical (or angular) aperture is calculated the following equation: NA = (n)sin(μ), where n is the refractive index of the imaging medium (in our case n = 1.0 for air), and μ is the angle of the imaging cone (and has a maximum angle of 90 degrees). In air, the maximum NA that can be achieved is 1.0. However, in practice, building a dry (i.e., air) objective with a NA over 0.95 is not practical. In Figure 4-11, the first objective (a) has an angle (μ) of 7º, and a NA of 0.12. The last objective (c) has an angle (μ) of 60º, and a NA of 0.87. All

other things being equal, increasing the numerical aperture decreases the working distance and increases the resolving power of the objective.

An advantage of an increased NA is the ability to capture surface information at higher slopes. The NA determines the maximum slope angle that can be measured on a surface, with low NA apertures being unable to capture high slope regions [147]. The theoretical maximum angle that is half of the angle μ (as seen in Figure 4-11). Thought of simply, the reflected light from the surface must be within the acceptance cone of the objective, otherwise the microscope is unable to record the surface feature. With high slope angle features, it is possible for the reflected light to be outside the numerical apertures acceptance cone [148].

Common objective attributes including the numerical apertures of the different objectives available on the utilized NewView 7300 can be found in Table 4-1.

Table 4-1 Common attributes of the NewView 7300 objectives utilized.

Objective Magnification	Numerical Aperture (NA)	Lateral Resolution	Depth of Field	Working Distance
5 X	0.13	2.7 μm	± 17 μm	9.3 mm
10 X	0.30	1.2 μm	± 3.17 μm	7.4 mm
20 X	0.40	0.9 μm	± 1.78 μm	4.7 mm
50 X	0.55	0.6 μm	± 0.94 μm	3.4 mm
100 X	0.80	0.4 μm	± 0.45 μm	0.55 mm

As seen in Table 4-1, the 100X objective has a significantly higher numerical aperture (0.80) than the other available objectives. In addition to being able to increase captured resolution of the surfaces, an important attribute was discovered while developing SWLI methods with DOPS coatings. It was noted during SWLI measurements with the 5X, 10X and 50X objectives that the SWLI seemed more easily able to see the substrate at lower magnifications.

The higher numerical aperture objectives have the ability to decrease interference from the substrate in readings. That is, the lower numerical apertures are more likely to capture unwanted height information at the metallic substrate. This is likely due to the shallow approach angle of the incident light in low numerical objectives. In contrast, the high numerical aperture lenses light has a significantly longer and more convoluted path to reach the substrate, thereby decreasing the strength of the interference pattern associated with the substrate. This led to the realization and association of coating reflectance to numerical aperture of the lens. This in turn led to the development of the final SLWI measurement methodology of using the high numerical aperture 100X objective and multi-frame stitch strategy.

Difficulty in Using SWLI for DOPS Coatings with Cholesterol

Measuring DOPS coatings was easier than measuring coatings that contained cholesterol. It was noted that once cholesterol was added to the coatings that the coating surfaces became more diffuse and diffractive. This was overcome with the use of dual light level stitching. When utilizing a dual light level capture the SWLI first collects at a low light intensity, and then again at a higher light intensity and combines the height information from the two measurements. The two light levels were manually set to maximize data capture, with one level being much brighter than used with pure DOPS coatings.

Small Working Distance of 100X Objective

It is worth noting is that the 100X objective only has a 550 µm working distance (see Table 4-1) between the sample surface and the glass of the objective. This small working distance warrants the need for particular care while manually controlling the stage. An additional instrument use protocol was consequently developed to help prevent a stage collision. Instead of

manually setting the z-stop on the manual stage controller, protocol was developed to first focus on the sample surface with a lower magnification objective (either the 10X or 20X magnification), and then change to the 100X objective. After changing to the 100X objective, focus is confirmed, and then a custom MetroPro script is used to raise the sample 50 μm closer to the 100X objective. The Z-Stop on the manual stage controller is then set in order to prevent an accidental stage collision with the objective. After setting the Z-stop at 50 μm below the focal plane of the coating, another custom script is used to raise the objective 50 μm back into focus.

SWLI Measurement Automation

The SWLI measurement and stitch process and the dual light level capture are automated via the use of MetroPro scripting. In the stitching mode, the input variables can be customized for the final size of grid to capture (or for the number of rows and columns of frames), and for the percentage of overlap between frames. The dual light level script asks for the two desired light level settings and then automatically captures and combines the scan measurements.

SWLI measurement automation could be implemented further with custom patterns for the stitch routine for sampling across one sample, and/or multiple samples. In the presented work, this was not necessary as the samples were done in smaller batches and required enough supervision of light level settings so as to negate the advantage of full automation. In the future, full automation could be a significant advantage dependent on the application.

4.4.6 SWLI Method Development Conclusions

DOPS and cholesterol coatings are semi-transparent and tend to scatter light in such a way as to make measurements of only the top (or bottom) surface of the coating difficult. The use of lower magnification objectives in the SWLI (and their associated lower numerical

apertures) was found to collect unwanted height information at the metallic substrate and at anomalies within the coating, in addition to the coating surface.

This led to the use of manual control of the scan range in order to physically exclude the substrate surface in the SWLI scan, effectively ‘clipping’ the lower coating surface. However, this manual ‘clipping’ technique was impractical for thinner coatings due to roughness of the Ti6Al4V substrate being on the same size scale as the thickness of the coatings. Also, manual clipping did not help avoid mid-coating refraction of light or help with coatings that had regions of highly sloped surfaces. The films app in MetroPro showed promise, but suffered from a large amount of data dropout due to very low signal to noise ratios.

These discoveries led to the final SWLI method of using the 100X objective in order to take advantage of its higher numerical aperture, and its inherent ability to increase the prominence of the interference pattern at the coating surface. The 0.5X zoom and composite frame stitching strategy were then utilized in order to increase the effective field of view and analysis area of the coating surface for SRa and SRz measurements. Using these methods, all of the stitched capture areas generally had much greater than 80% height information before data fill, and any missing data was usually only in the highest slope regions of the coating, which had little impact on roughness measurements.

These methods are extensible for the quantitative measurement and analysis of other rough, thick, and optically diffractive coatings of biological materials. Traditional applications for the SWLI instrument have been nearly exclusively applied towards the optics and manufacturing industries. The modification and further development of the basic principles of these methods could prove very beneficial for other biological applications given the limited prior application of this technology in the realm biological systems research.

4.5 Quantitative Measurement of Coating Roughness Using Scanning White Light Interferometry

4.5.1 Purpose and Overview

The next step in using SWLI to analyze DOPS coatings is to be able to quantitatively analyze the surfaces. Building on the previous sections progress, effort was undertaken to determine a SWLI parameter set to numerically measure the roughness of the coating surfaces. This will allow quantitative evaluation of coating properties and better understanding and control of the deposition process.

This section's purpose is to address the chapter's **2nd Technology Development Goal:** Develop methods to use Scanning white light Interferometry to measure the surface roughness of DOPS and DOPS-cholesterol coatings.

4.5.2 Materials and Methods

Samples were prepared as previously outlined in Section 0. Briefly, DOPS coatings were applied to cleaned and passivated 7.5 x 7.5 mm Ti_6Al_4V samples. A 1.3% (vol%) DOPS in chloroform solution was e-sprayed onto cleaned and passivated 7.5x7.5mm Ti_6Al_4V samples. The voltage differential used was 12 kV with a pump rate of 14 mL/min and an 8 cm working distance.

Three treatment groups were prepared: (1) a pure DOPS groups, (2) a 1:1 DOPS:cholesterol group, and (3) a pure cholesterol group. Prior to coating with DOPS and cholesterol, the Ti_6Al_4V samples were pretreated in a calcium salt solution as outlined in Appendix A, Protocol C.

SWLI Methods

SWLI measurements were made as outlined in Section 4.4.4. Briefly, a 100X objective and 0.5X zoom was used to capture a 140 x 110 µm field of view frame. A composite stitch of 35 of these capture frames was used to analyze the roughness in an area of 0.5 x 0.5 mm. Spike removal was used (xRMS = 2.00) to remove pixel level noise. Data fill was used to fill in infrequent data dropout. A 2.50 µm low pass noise filter was used to remove higher frequency optical noise and 2π errors. The low pass noise filter was selected using iterative application and visual analysis of the mapped surface.

In order to check coating consistency across a given sample each sample was analyzed at seven locations on the coating surface. The underlying manufacturing marks were oriented East to West, and the seven composite capture areas were taken at the following locations: in the center of the sample, 2 mm East of center, 2 mm North of the East location, 2 mm North of the center, 2 mm East of center, 2 mm North of the West location, and 2mm South of the center. Or, stated in clockwise order, these locations were at the East, North-East, North, North-West, West, South, and Center of the samples.

Six non coated Ti_6Al_4V samples were also measured for reference. These samples also underwent the calcium pretreatment process as outlined in Appendix A, Protocol C. The six uncoated sample blanks were measured at the center of the sample, 2mm North of center, and 2mm South of the center.

4.5.3 Results

SRa=1.94 SRz=9.68	SRa=1.26 SRz=6.99	SRa=1.24 SRz=7.08
SRa=1.11 SRz=5.30	SRa=0.92 SRz=4.95	SRa=1.34 SRz=8.15
	SRa=1.40 SRz=8.08	

Figure 4-12 SRa and SRz measurements at different locations across a 1-1 DOPS:cholesterol coated sample. The top left of the diagram represents the top left of the sample (or North-West corner), the center of the diagram represents the measurement taken at the center of the sample, etc.

A representative measurement set from different points on a single 1:1 DOPS:cholesterol sample can be found in Figure 4-12. Each measurement on the sample is shown on the diagram by its location, as if viewed on a map. Similar measurements were made on a single DOPS and a single 12:1 sample. An additinoal five samples from each of the three groups (DOPS, cholesterol, and 1:1 treatments) were then measured in the center of the sample, and the results tabulated in Figure 4-13.

	Sample #	Location on the sample: Center	W	NW	N	NE	E	S	*Average*	*StDev.*
100% DOPS coating	1	2.157	2.491	2.788	2.034	2.147	2.119	4.11	***2.549***	***0.737***
	2	1.056								
	3	0.861								
	4	1.613								
	5	0.816								
	6	2.73								
	Average	***1.539***								
	StDev.	***0.777***								
1:1 DOPS:cholesterol	1	0.922	1.109	1.935	1.256	1.237	1.341	1.395	***1.314***	***0.316***
	2	1.398								
	3	1.235								
	4	1.759								
	5	0.637								
	6	1.677								
	Average	***1.271***								
	StDev.	***0.435***								
100% cholesterol	1	3.614	6.104	4.576	3.048	2.555	3.032	2.092	***3.574***	***1.367***
	2	1.04								
	3	1.284								
	4	3.129								
	5	1.2								
	6	4.179								
	Average	***2.166***								
	StDev.	***1.411***								

Figure 4-13 SRa roughness measurements from SWLI of DOPS, 1:1, and cholesterol groups by sample number and location within a sample. All values are in µm.

As seen in Figure 4-13, SRa measurements from the 7 locations measured on the first sample are compared with the centers of the additional five unique samples. The standard deviation in each treatment group was larger across samples than it was within a given sample. Results for the SRz parameter were similar to the SRa measurements, as seen in Figure 4-14 below.

		Location on the sample								
	Sample #	Center	W	NW	N	NE	E	S	*Average*	*StDev.*
100% DOPS coating	1	11.702	13.373	14.206	11.206	11.221	10.455	10.118	***11.754***	***1.505***
	2	5.095								
	3	4.205								
	4	8.423								
	5	4.552								
	6	15.119								
	Average	***8.183***								
	StDev.	***4.452***								
1:1 DOPS:cholesterol	1	4.947	5.302	9.677	6.992	7.081	8.152	8.083	***7.176***	***1.661***
	2	6.611								
	3	8.762								
	4	11.324								
	5	3.678								
	6	7.243								
	Average	***7.094***								
	StDev.	***2.728***								
100% cholesterol	1	19.018	28.716	21.576	15.621	13.584	15.556	21.432	***19.358***	***5.142***
	2	6.545								
	3	7.118								
	4	16.835								
	5	7.524								
	6	22.347								
	Average	***12.074***								
	StDev.	***7.142***								

Figure 4-14 SRz roughness measurements from SWLI of DOPS, 1:1, and cholesterol groups by sample number and location within a sample. All values are in µm.

In Figure 4-14, the seven locations measured on the first sample are compared with the centers of six unique samples. As with the SRa measurements in Figure 4-13, the standard deviation in each treatment group was larger across samples than it was within a given sample.

SRa		Location on the sample				
	Sample #	Center	N	S	*Average*	*StDev.*
Uncoated Ti6Al4V	1	0.571	0.722	0.556	***0.616***	***0.092***
	2	0.644	0.667	0.585	0.632	0.042
	3	0.739	0.747	0.718	0.735	0.015
	4	0.615	0.740	0.698	0.684	0.064
	5	0.890	0.674	0.604	0.723	0.149
	6	0.807	0.711	0.866	0.795	0.078
	Average	***0.711***	***0.710***	***0.671***	***0.697***	
	StDev.	***0.123***	***0.033***	***0.115***		***0.095***

SRz		Location on the sample				
	Sample #	Center	N	S	*Average*	*StDev.*
Uncoated Ti6Al4V	1	3.364	3.832	2.877	***3.358***	***0.478***
	2	3.209	3.232	3.093	3.178	0.075
	3	3.310	3.662	3.498	3.490	0.176
	4	3.078	3.794	3.302	3.391	0.366
	5	4.933	3.274	3.342	3.850	0.939
	6	3.959	3.583	4.148	3.897	0.288
	Average	***3.642***	***3.563***	***3.377***	***3.527***	
	StDev.	***0.701***	***0.257***	***0.435***		***0.483***

Figure 4-15 SRa and SRz SWLI measurements of uncoated Ti_6Al_4V. All values are in µm.

The results for the uncoated Ti_6Al_4V samples can be found in Figure 4-15. The average SRa and SRz roughness across all eighteen measurement points was 0.697 ±0.095 µm and 3.527 ±0.438 µm, respectively.

4.5.4 Discussion

Ultimately, the SWLI measurement results need to be critically evaluated for credibility in the context of the surface being measured. It is easy to get a measurement using SWLI, but the results should be confirmed (as possible) and questioned for the presence of measurement artifacts. These artifacts can be optical, as well as morphological. In the case of the DOPS and

cholesterol coatings, the translucent and diffractive nature of the coatings made the SWLI measurement method development process an iterative event. It was only after confidence was gained in the measurement process (as outlined in section 4.4) that the quantitative results measured in this section could be relied upon. The process for filtering involved looking at 2D measurement traces and selecting the smallest low pass filter size that adequately removed high frequency optical noise. The low pass filter size used was chosen based on commonly utilized 2D profilometer tip sizes in order to support comparison with other techniques. The low pass filter was then paired with the use of a standard pixel level spike filter that removed height jumps 2-pixels in diameter or less that represented measurement artifacts.

Some difficulties interpreting and filtering SWLI measurements of the DOPS coatings still exist, but these have minimal effect on the measurement parameters chosen (SRa and SRz). While there was still some data dropout in SWLI measurements at very high slope regions on the DOPS and cholesterol coatings, its absence has negligible effects on the SRa and SRz roughness parameters. This is due to the way that SRa and SRz are calculated. In a plateaued surface, both SRa and SRz are minimally affected from changing the slope of the cliffs in the data from a steep to a 90º angle. The issue of high slope data dropout would become more of a concern if one were to look at topological properties that dealt with slopes and slope angle distributions.

A significant amount of roughness was found on the uncoated Ti_6Al_4V samples (as seen in Figure 4-15). The roughness values of the uncoated Ti_6Al_4V were generally one half to one third of values of the coated samples. The underlying machining marks were clearly visible on the surface of the coated samples during SWLI measurements. These machining marks clearly affected the measured roughness (SRa and SRz) at different locations within a single sample. As seen in Figure 4-12, the roughness values were similar in a given row, corresponding to the East

to West orientation of the machining marks prior to measurement (i.e., the ridges in the Ti_6Al_4V samples were oriented East to West prior to measurement).

4.5.5 Conclusions

The method developed for measuring roughens with SWLI works well, is repeatable, much faster than profilometer, able to measure without contacting the surface, and allows for a much larger amount of surface information to be gathered than with other 1D and 2D measurement techniques. After the iterative confirmation of an appropriate low pass filter size (2.5µm), optical artifacts were satisfactorily removed without significantly affecting the measured roughness values. The high lateral pixel density gained from using the 100X objective (0.22 µm per pixel) combined with the frame stitching strategy allows for excellent high frequency information gathering and valuable quantitative surface insights.

Given the higher variance between coated samples compared within a single sample, it was determined that one SWLI composite stitch measurement per sample with a higher number of samples tested was a suitable testing strategy. This strategy allows for an increased understanding of process variations and is a more true representation of treatment affects than using smaller sample numbers and multiple measurements per sample.

It was also concluded from the results that the underlying machining marks of the Ti_6Al_4V samples were decreasing the statistical power of the treatment groups. This conclusion led to the development and use of a polishing procedure (as outlined in Appendix A, Protocol E). The polishing procedure was found to further confirm the need to only measure each sample once at the center of the sample due to decreased variation across the sample as caused be anisotropic machining marks.

4.6 Measurement of Coating Thickness with Scanning White Light Interferometry

4.6.1 Purpose and Overview

This section's purpose is to address this chapter's **3rd Technology Development Goal:** Develop methods to use scanning white light Interferometry to measure the thickness of E-sprayed DOPS and DOPS-cholesterol coatings. This will allow further qualitative evaluation of coating properties and better understanding and control of the deposition process.

4.6.2 Material and Methods

Samples were prepared as previously outlined in Section 0. Briefly, DOPS coatings were applied to cleaned and passivated 7.5 x 7.5 mm Ti6Al4V samples. A 1.3% (vol%) DOPS in chloroform solution was e-sprayed onto cleaned and passivated 7.5x7.5mm Ti6Al4V samples. The voltage differential used was 12 kV with a pump rate of 14 mL/min and an 8 cm working distance. Prior to coating with DOPS, Ti6Al4V samples were mirror polished on a histology grinder as outlined in Appendix A, Protocol E.

SWLI Methods

SWLI measurements were made as outlined in Section 4.4.4. Briefly, a 100X objective and 0.5X zoom was used to capture frame with a 140 x 110 μm field of view. A composite stitch of 35 of these capture frames was used then used to analyze the roughness in a final area of 0.5 x 0.5 mm. Spike removal was used (xRMS = 2.00) to remove pixel level noise. Data fill was used to fill in infrequent data dropout. A 2.50 μm low pass noise filter was used to remove high frequency optical noise.

Sample Scratching Method

Prior to measuring with the SWLI, a small metal pick/awl was used to create a scratch through the sample coating. This was done manually, using relatively little force, and at an angle of approximately 20 degrees from the vertical. The tip of the awl had an 100 µm tip radius.

Film Thickness Measurement Script Automation

In order to automate the scratch depth measurement process, a custom mask was used to level the 2D profiles. This mask only included the two side regions of the coated sample, with the scratch running from south to north in the center of the sample. A measurement window was then set to fit five 2D profile traces to the mean height of the masked regions (forcing the profile lines zero point to the mean of the non-scratched region of the coating). The lowest point of each trace (the bottom of the trough) was then set to display for each line, and averaged across the lines.

4.6.3 Results

The coating scratched easily and consistently using the metal awl and manual method. A full thickness scratch can be seen in the SWLI scan shown in Figure 4-16.

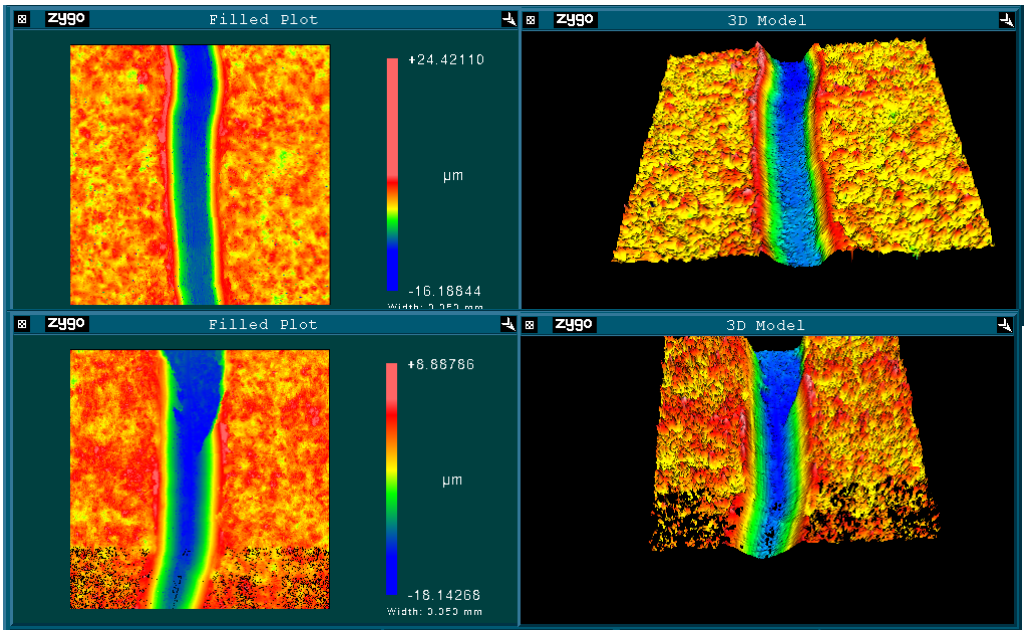

Figure 4-16 SWLI measurements of two DOPS coated samples (with Ca pretreatment) with a full thickness scratches.

As seen in Figure 4-16 with the exaggerated z axis height scale, it is apparent that the coating is soft enough to be pushed aside by the scratching process. There was clear evidence of the scratch reaching completely to the substrate when examining the bottom of the scratch trough. An example of this is illustrated in the lower half of Figure 4-16, where the coating partially delaminated near the top of the scan area from the scratching process. The bottom of the delaminated section is constant to the bottom of the trough. Additional evidence for the scratch reaching the substrate surface was the observation of Ti6Al4V surface morphology at the bottom of the trough that was clearly visible at higher magnifications.

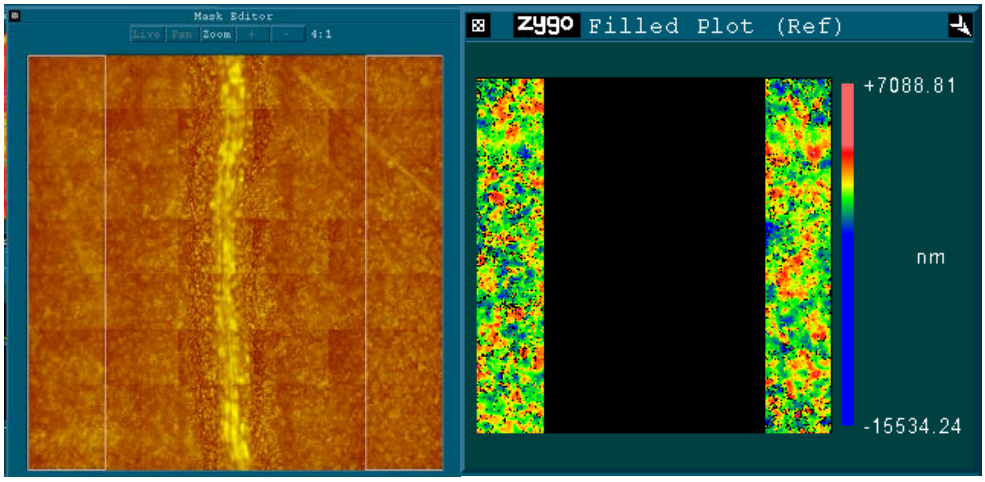

Figure 4-17 SWLI mask selections for leveling the profile data in the unscratched

The masked region chosen and implemented in the mask editor of MetroPro can be seen in Figure 4-17. The left hand side of the Figure shows the rectangles input to the mask editor, and the right hand side show a representative coating surface with only the masked regions visible. These masked regions were then used to level the 2D profiles as seen in Figure 4-18, that is, the side regions of the surface were used to level the entire surface for the following analysis.

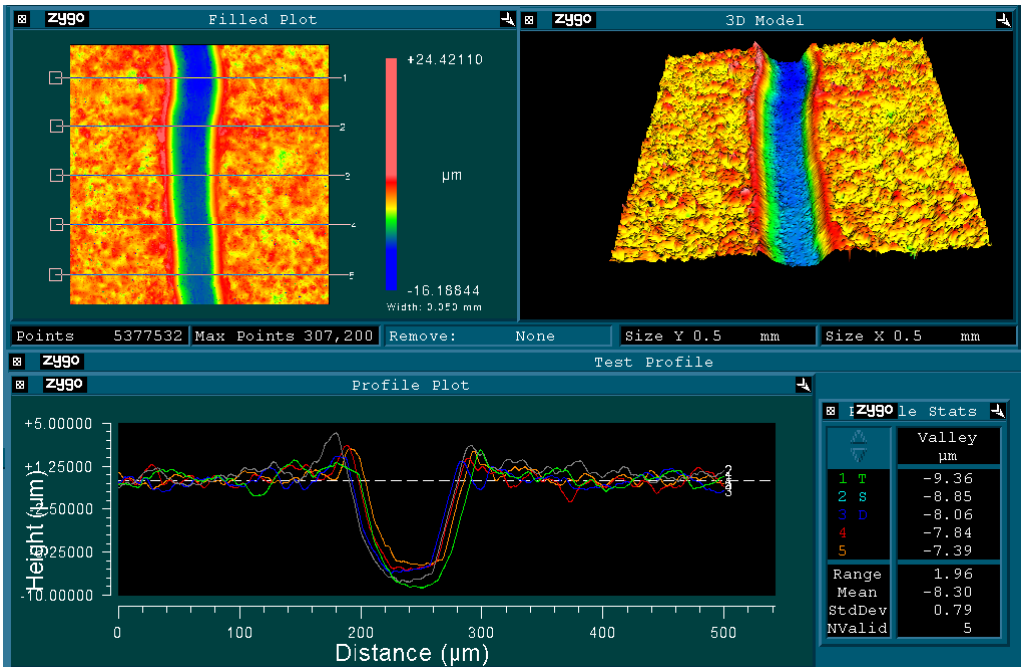

Figure 4-18 2D profiles used to automatically measure the scratch trough depth of coated DOPS and cholesterol samples.

Figure 4-18 shows the 2D profiles set at repeating distances across the sample from West to East (as would be mapped aerially), with the scratch going from South to North. Each 2D profile is set to use the mean height of the masked region (Figure 4-17) as the zero height. The lowest point of each profile is then tabulated, averaged, and displayed in the lower right hand corner of the instrument control window (as seen in the lower right of Figure 4-18). In the case of the pure DOPS coating seen in Figure 4-18, the scratch trough depth ranged from 7.39 to 9.36 µm, with and average depth of 8.30 µm.

4.6.4 Discussion and Conclusion

For the sake of method consistency, the same 100X objective and thirty five frame stitch strategy was used to measure the scratch depth. It could be that a longer section of the scratch

would be desirable to measure (longer than 0.5 mm), and a different stitch shape/size could easily be implemented.

4.6.5 Conclusion

The scratch thickness measurement method worked consistently and accurately. The automation process allows quick, non-biased trough depth measurements. The method is easily implemented on a small section of the sample, without damaging the rest of the coating. This method could also be used to check coating height consistency across the same sample, in addition to across multiple samples.

4.7 Chapter Conclusions

SWLI was found to be an excellent surface analysis technique for characterizing these biomimetic DOPS implant coatings, and these methods can easily be translated for the use with other difficult biological surface applications. Using the methods developed above, SWLI proved useful for the quantitative measurement of coatings roughness and thickness properties. Previously, there were no practical and effective techniques for accomplishing these tasks due to the coating's rough, soft, and diffractive nature. Using SWLI for future studies will allow for the further understanding and optimization of DOPS coating parameters, as well as for use with similarly difficult surfaces and coatings in other fields of research.

Use of SWLI to capture surface morphology and roughness information of these implant coatings is uniquely beneficial in several ways. It allows for non-destructive measurement of the coatings. Unlike SEM, which requires a conductive gold (or similar) coating on the surface and decreased atmospheric pressure for imaging, SWLI can be used to measure these coatings before

or after other testing is performed. Prior to development of the SWLI methods, it was assumed that SEM images were fully representative of the DOPS coating morphology. It is now known (from comparisons with SWLI data) that the gold coating process and high vacuum environment of the SEM chamber tends to alter the coating surface structure, and SWLI allows for the analysis of coatings without damaging the surfaces.

SWLI measurements have also been found to be a more repeatable and consistent way to analyze these implant coatings compared to traditional *in vitro* techniques such as contact angle measurements. Contact angle tests have a high amount of inherent variance. Due to a significant correlation between the SWLI measured SRa and contact angle (as shown in the next chapter), SWLI was used to help understand similar aspects of the coating's properties with higher repeatability and precision.

Thirdly, SWLI allows for higher throughput and is less resource intensive than many *in vitro* techniques. This allows for a greater sampling ability and a resulting better understanding of developmental issues in the manufacture of the coatings. Process control issues that were not apparent previously from small sample size testing in SEM analysis of these coatings were elucidated in the investigations with the SWLI instrument.

SWLI is a useful tool for the characterization and ongoing development DOPS implant coatings. SWLI was particularly practical for these many-micron thick and rough biomimetic implant coatings in comparison to traditional thin film techniques that are limited to sub-micron coating thicknesses. SWLI measurements offer the ability to test in series with other *in vitro* measurements as it is non-destructive to the coating. It is a quick, highly repeatable method for use with environmentally sensitive and optically diffractive biological coatings.

4.7.1 Future Work

There are many opportunities for the future application of the SWLI measurement methods developed and presented herein. Being able to quickly and non-destructively measure and quantitate surface morphology opens up many possibilities for future studies to further elucidate structural and functional properties of these biological coatings. Some of these possibly studies of particular interest could include the characterization and optimization of spray parameter effects on coating morphology, increasing coating deposition consistency, and SWLI measurements in concert with *in-vitro* and *in-vivo* studies. For example, it would be valuable to track the roughness and thickness changes of DOPS coatings over time while the coatings are subjected to different relevant conditions (such as a high humidity environment).

One of the particularly insightful discoveries that was found after using SWLI to analyze the coatings was the relatively high level of variation that exists between e-sprayed samples within the same batch, and of variance between e-spray batches. Prior to this, the coating's qualitative appearance from SEM was the primary measurement point to ensure consistency between samples and batches. With the new knowledge of SEM's tendency to alter/damage the coating surface, and with the increased ability of SWLI to differentiate the coatings quantitatively, coating variations were discovered and are now better able to be studied. It is suggested that the effects of environmental variables during the e-spray process be further characterized now that the SWLI measurement technique is available to better characterize coatings non-destructively.

Dependent on the scope and scale of future studies, it may also prove beneficial to more fully automate the SWLI measurement process. While further automation was not found to be necessarily beneficial in the presented work, future studies may want to take further advantage of

the powerful scripting options within the MetroPro software. This would include the ability to fully automate the measurement process into a measurement pattern that spans across multiple samples. The script could be set up to drive the stage to a preset location (e.g., the center of the next sample), autofocus, measure a 35 frame composite stitch, go to the next sample, and repeat. This would be advantageous in freeing the operator from constant supervision in what could otherwise be a time intensive process in a large study.

Information related to the coatings' mechanical properties can be gleaned from the qualitative analysis of the scratch cross section. These relatively soft DOPS and cholesterol coatings tend to push and mound up at the edges of the scratch. Stiffer coatings may delaminate. These observations may be able to be expanded into additional quantitative analysis with further development [149]. It may be useful to ensure the application of a more repeatable scratch angle and force in order to achieve a uniform response in the coating.

There may be some interesting insights of the DOPS coatings that could easily be gained using the films app in combination with the other methods developed in this chapter. For instance, using the films app in conjunction with the manual scratch depth method developed herein to determine the bulk index of refraction of the coatings. This would be done using the scratch depth (using the methods presented in Section 4.6), and a lower magnification films app scan near the scratch, and then changing the index of refraction setting in the films app until the reported coating depths match.

Chapter 5: Roughness and Contact Angle Study

5.1 Purpose and Chapter Overview

Understanding implant roughness and its relation to implant surface hydrophobicity are key implant design criteria. Aqueous contact angle measurements are a useful way to measure surface hydrophilicity. However, effects of surface composition on contact angle are often confounded by concomitant changes in surface roughness. It is therefore desirable to be able to non-destructively measure roughness of samples prior to performing contact angle tests.

Using the measurement methods developed in the previous chapter, effort was taken to elucidate possible correlations between surface roughness and contact angle. Scanning white light interferometry (SWLI) was used to measure the surface roughness of DOPS coatings on Ti_6Al_4V samples with varying concentrations of cholesterol. The roughness measurements of the DOPS coatings were then compared to aqueous contact angle measurements.

5.2 Chapter Goals and Objectives

The purpose of this chapter is to characterize the roughness of e-sprayed DOPS and DOPS-cholesterol coatings using SWLI, measure the aqueous contact angle of the same coatings, and then compare the results in order to elucidate effects from composition and/or roughness on coating hydrophilicity.

A secondary goal is to determine whether it is helpful or necessary to polish Ti_6Al_4V substrates prior to coating in order to increase the statistical power. The chapter hypotheses and specific aims are listed below.

Hypothesis 5.1: Coating contact angle measurements will negatively correlate with coating roughness due to an increase in surface roughness in DOPS only coatings.

Specific Aim 5.1-1: Measure coating surface roughness using SWLI.

Specific Aim 5.1-2: Measure the aqueous contact angle of coating surface with a goniometer, and look for possible correlations between these and the roughness measurements.

Hypothesis 5.2: Coating morphology (specifically surface roughness) will be the primary reason for contact angle changes between coating compositions. That is, increased roughness resulting from the addition of cholesterol in the coatings will result in decreasing contact angle of the DOPS:cholesterol coatings, even though cholesterol is hydrophobic and results in high contact angles when used by itself.

Specific Aim 5.2-1: Compare coating roughness (as measured using SWLI) with aqueous contact angles for coatings with various concentrations of cholesterol in the coatings.

Hypothesis 5.3: The coating roughness and morphology measured by SWLI will be more consistent on polished Ti_6Al_4V substrates compared to as-machined substrates, and will increase the statistical power for studies of DOPS and cholesterol coatings.

Specific Aim 5.3-1: Measure the coating surface roughness of samples that were polished prior to coating, and compare the variance and power to un-polished samples.

5.3 Roughness and Contact Angle Study

Building on the methods developed in the previous chapter, work was then done to look at the surface roughness and aqueous contact angle of the coatings. The purpose of this study was to elucidate possible correlations and interactions between the coating roughness and measured contact angles. Particular interest was paid to the elucidation of the cause of changes in

contact angle, whether it be from differences in the chemical nature of the coating (i.e. hydrophobic vs. hydrophilic characteristics) versus morphology based changes (i.e. from increased roughness and surface energy of the coatings).

5.3.1 Materials and Methods

Sample Preparation

As outlined previously in Section 4.3, samples were prepared, cleaned, calcium treated, and passivated as detailed in Appendix A, Protocol A through Protocol D. DOPS coatings were applied to as-machined, cleaned, and passivated Ti_6Al_4V samples using the e-spray deposition method. Briefly, a 1.3% (vol%) DOPS in chloroform solution was e-sprayed onto cleaned and passivated 7.5x7.5mm Ti_6Al_4V samples. The voltage differential used was 12 kV with a pump rate of 14 mL/hr and with an 8 cm working distance. These parameters were chosen to provide a final coating density of 1 mg of DOPS per cm^2 of sample.

The DOPS coated samples were prepared with varying concentrations of cholesterol incorporated into the coating. Molecular ratios of DOPS to cholesterol used for the coating groups were as follows; 100% DOPS, 24:1 (DOPS:cholesterol), 12:1, 6:1, and 1:1.

Table 5-1 Sample treatment groups and the percentage of DOPS contained within each group.

Treatment Groups	Percentage of DOPS molecules	Percentage of DOPS weight
100% DOPS	100.0	100
24:1 DOPS:chol	96.0	98.0
12:1 DOPS:chol	92.3	96.2
6:1 DOPS:chol	85.7	92.6
1:1 DOPS:chol	50.0	67.7
100% Cholesterol	0.0	0.0

As seen in Table 5-1, the sample groups prepared ranged from a pure DOPS coating, to a pure cholesterol coating. Treatment groups with a combination of DOPS and cholesterol were in the following molecular ratios of DOPS to cholesterol (DOPS:cholesterol); 24:1, 12:1, 6:1, and 1:1. The molecular weight of DOPS is 810.025 g/mol, and the molecular weight of cholesterol is 386.65 g/mol. The middle column in Table 5-1 lists the percentage of DOPS molecules to the total number of molecules in the coating, and the right column lists the percentage of weight that the DOPS contributes to the total weight of the coating.

Prior to coating with DOPS and cholesterol, the Ti6Al4V samples were pretreated in a calcium (Ca) salt solution as outlined in Appendix A, Protocol C. As controls, some of the groups were repeated without the calcium pretreatment. These non-calcium controls included a DOPS, 12:1, and 1:1 treatment groups.

Statistical Analysis

Statistical analysis was performed using a one-way ANOVA and a natural log transform. An all pairwise multiple comparison procedure was used (Holm-Sidak method), with a significance threshold of $p \leq 0.05$. The log transformed data passed normality tests (Shapiro–Wilk test), but had unequal variances between treatment groups (due to differences in the types of variance between coating compositions).

Contact Angle Measurements

Aqueous contact angle measurements were used to determine coating hydrophilicity. Contact angle results were taken with a Krüss DSA 10 goniometer (KRŰSS GmbH, Hamburg) using 2 µL droplets of de-ionized water. The contact angle of the droplet was measured 5 seconds after initial contact with the coating. Six samples per treatment group were measured, with one contact angle measurement taken per sample.

Statistical Analysis

Statistical analysis was performed using a one-way ANOVA and a natural log transform of the data. An all pairwise multiple comparison procedure was used (Holm-Sidak method), with a significance threshold of $p \leq 0.05$. The log transformed data passed both normality (Shapiro–Wilk test) and equal variance tests. For the Pearson correlation test, the contact angle

measurements were averaged for each treatment group, and then correlated to the each group's average roughness measurement. This was repeated for both the SRa and SRz roughness parameters.

Roughness Measurements Using SWLI

Roughness was measured using the methods outlined previously in Section 4.5.2. Briefly, a 100X objective and 0.5X zoom was used in the SWLI to measure the SRa and SRz surface roughness parameters. A 100X objective was used to capture a 140x110 µm field of view with a lateral pixel resolution of 0.22 µm. A composite stitch of 35 of these capture frames was used to analyze SRa and SRz in an area of 0.5x0.5 mm. A low pass noise filter was used along with data fill in the analysis of the composite stitch area.

On each coated sample, three 0.5x0.5 mm composite stitched SWLI capture areas were analyzed. Six samples per treatment group were measured. The underlying manufacturing marks were oriented East to West, and the composite capture areas were taken in the center of the sample, 2 mm north of center, and 2 mm south of the center.

5.3.2 Results

Roughness Results from SWLI

See Figure 5-1 for SWLI measured roughness results.

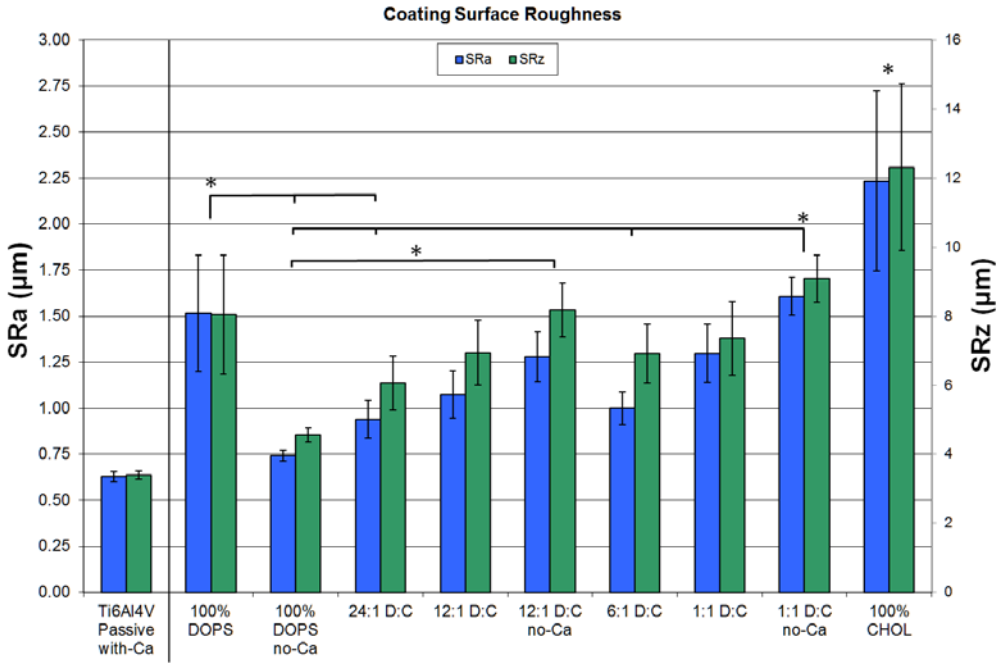

Figure 5-1 SWLI measured coating roughness of DOPS and cholesterol coatings. Error bars represent the standard error of the mean. Statistical significance between groups for SRa is indicated with horizontal bars and asterisks. N = 6 for all groups, and each coated sample was tested in 3 locations.

As seen in Figure 5-1, the cholesterol group (SRa mean = 2.23 µm and SRz mean = 12.32 µm) was significantly rougher for SRa than all of the other groups, and SRz roughness was significant compared to all but the 1:1 (no Ca) and 12:1 (no Ca) treatment groups.

The roughest DOPS containing treatment group was the 1:1 DOPS:cholesterol group (SRa mean = 1.607 µm and SRz mean = 9.08 µm), which was significantly rougher than the DOPS (no Ca), 24:1, and 6:1 treatment groups.

The least rough treatment was the plain DOPS without calcium group (SRa mean = 0.743 µm, SRz mean = 4.56 µm), which was significantly less rough than the 12:1 (no Ca) group in

both SRa and SRz, and was significantly less rough than the 12:1, 6:1, and 1:1 groups in SRz. The DOPS (with Ca) group was significantly more rough than the DOPS (no Ca) and 24:1 groups.

The overall observed trend was an increase in surface roughness (both SRa and SRz) with increasing concentration of cholesterol. Results indicate that excluding the calcium pretreatment tended to increase the surface roughness in the DOPS and cholesterol coatings (the 12:1 and 1:1 groups), while decreasing the roughness in the DOPS-only coating. However, the changes due to the addition of the calcium treatment were only significant in the DOPS group.

Contact Angle Results

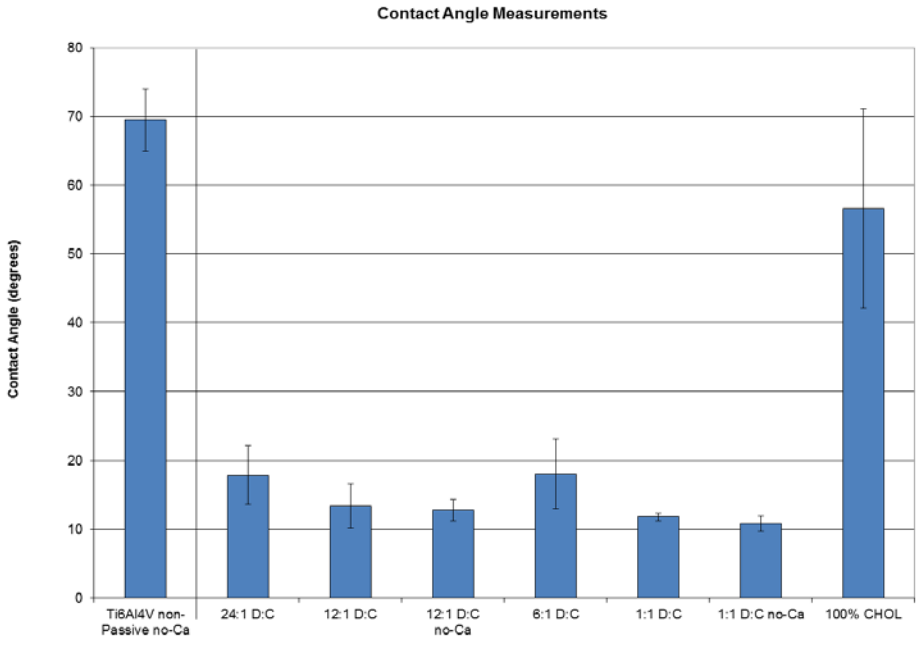

Figure 5-2 Contact angle measurements for the DOPS coated samples. Error bars represent the standard error of the mean. N = 6 for all groups (except for uncoated titanium where N = 2).

The contact angle measurement results can be found in Figure 5-2. The cholesterol group had a significantly higher contact angle than all of the DOPS and cholesterol treatment groups with the exception of the 24:1 group. All of the DOPS containing samples exhibited relatively

low contact angles, below about 20 degrees. For reference, two contact angle measurements were taken on uncoated Ti_6Al_4V (far left column in Figure 5-2, mean = 69.5 degrees).

The contact angles were lowest (i.e., the surfaces were most hydrophilic) in the 1:1 DOPS-cholesterol group (mean = 10.8 degrees). The observed trend was decreasing contact angle with increasing amount of cholesterol in the coatings, though this decrease was not statistically significant.

Correlation Between Coating Roughness And Contact Angle

The contact angle and roughness results for just the DOPS:cholesterol coatings can be found in Figure 5-3 and Figure 5-4, respectively.

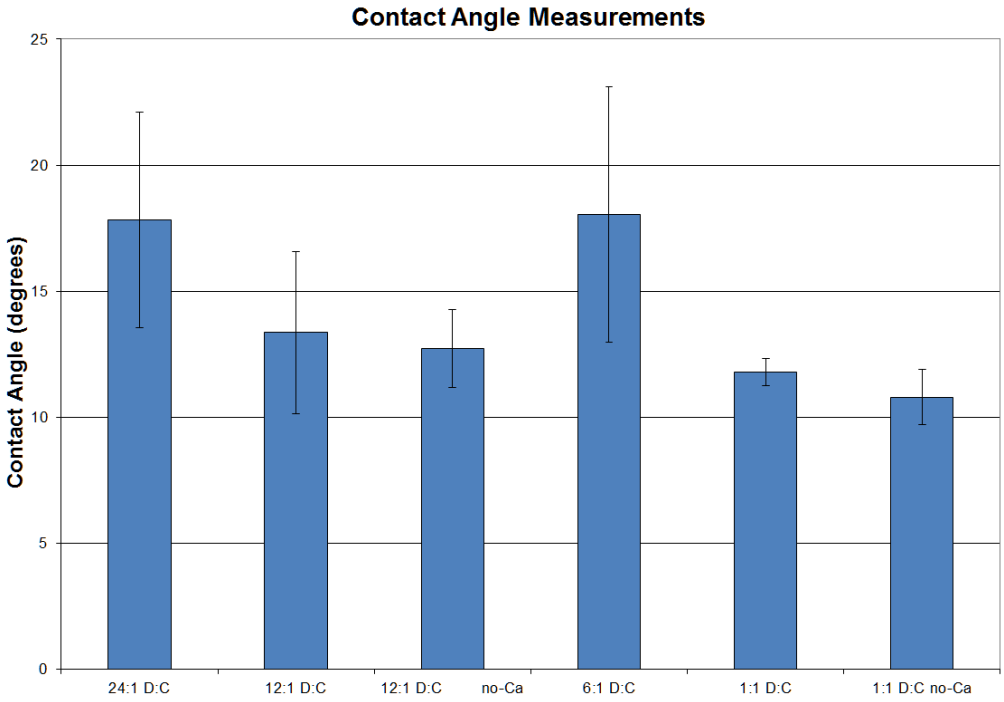

Figure 5-3 Contact angle measurements for the DOPS coated samples. Error bars represent the standard error of the mean, N = 6 for all groups.

As seen in Figure 5-3, there were no statistically significant differences between the DOPS:cholesterol treatment groups for contact angle.

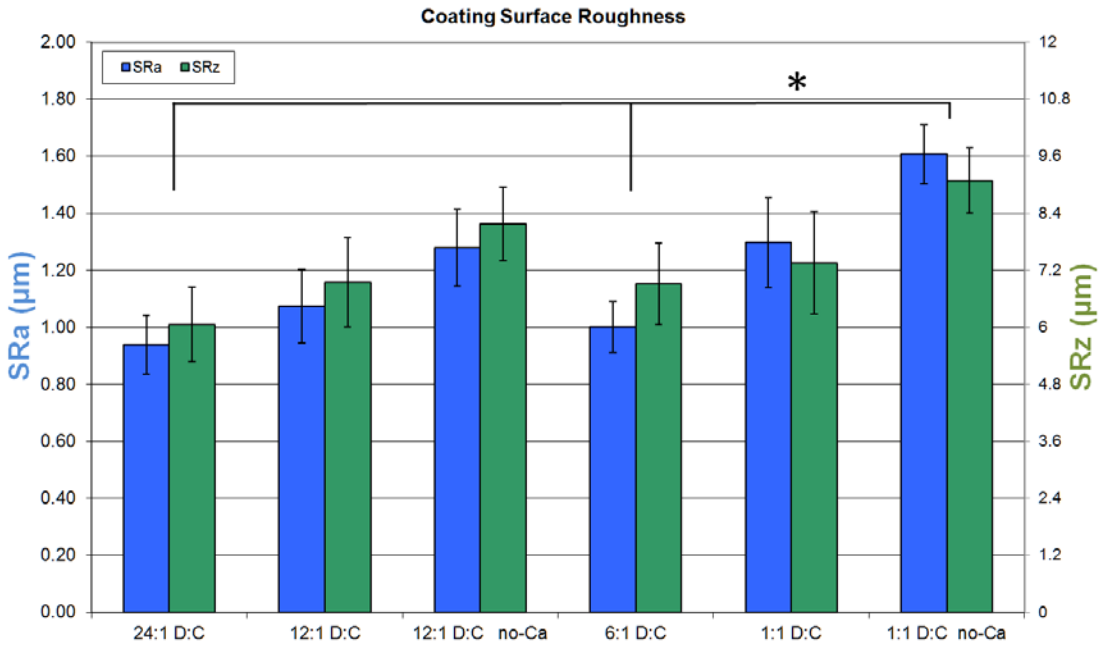

Figure 5-4 SWLI measured coating roughness of DOPS and cholesterol coatings. Error bars represent the standard error of the mean. Statistical significance between groups is indicated with horizontal bars and asterisks. N = 6 for all groups, each sample was tested in 3 locations.

As seen in Figure 5-4 and discussed prior (above in Section 5.3.2), the 1:1 (no Ca) group was significantly more rough in SRa and SRz than the 24:1 and 6:1 groups.

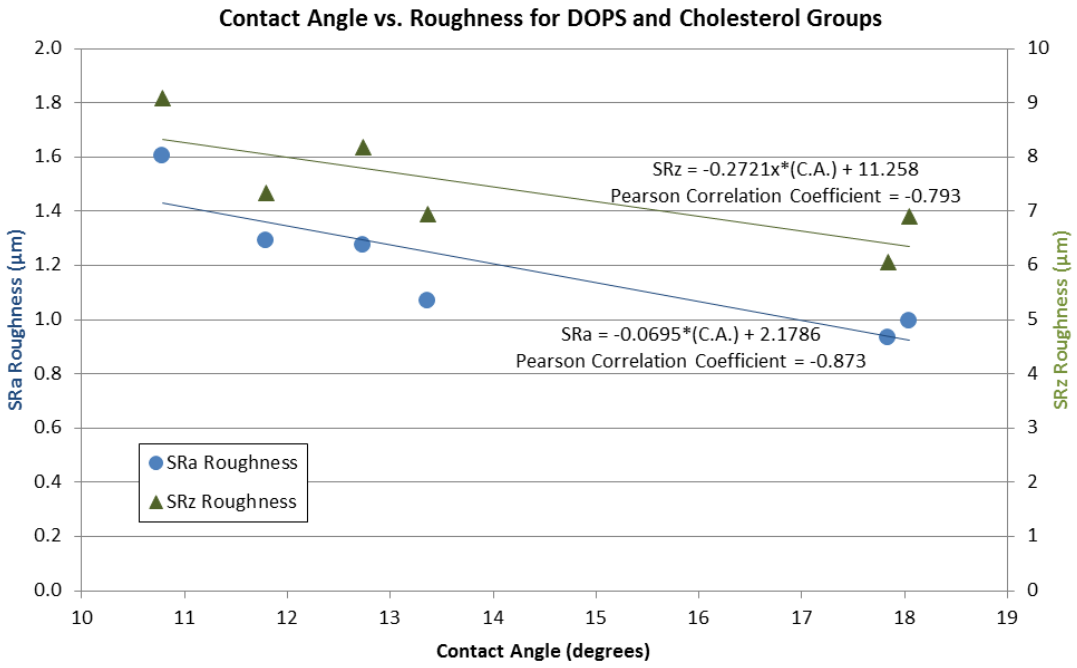

Figure 5-5 Scatter plot of the roughness values vs. contact angle for DOPS and cholesterol groups (the 24:1, 12:1, 12:1 no-Ca, 6:1, 1:1 and 1:1 no-Ca compositions).

A graph of the SRa and SRz roughness (see Figure 5-4) and contact angles (see Figure 5-3) are plotted against each other in Figure 5-5, with roughness on the y axis, and contact angle on the x axis.

A Pearson correlation of the means was significant for the SRa roughness parameter and the contact angle (correlation coefficient = -0.873 with p = 0.0231). As coating roughness decreased, contact angle also decreased (hydrophilicity increased). For the SRz roughness vs. contact angle, the Pearson correlation of the means was a trend, but not significant (correlation coefficient = -0.793 with p = 0.060).

5.3.3 Discussion

Biological responses to surfaces are sensitive to many traits, and surface hydrophilicity is an important characteristic. Contact angle is a useful measure of overall hydrophilicity, and

adding the measurement of surface roughness is essential in order to decouple hydrophilic/hydrophobic effects from chemical composition and/or surface morphology.

Within the DOPS containing coatings, the roughness increased with increasing cholesterol. The contact angle decreased with increasing cholesterol. Given observed decreases in contact angle with increasing surface roughness [150], this suggests that the coating hydrophilicity was primarily a function of coating roughness in these DOPS coatings, as opposed to being primarily driven by aqueous exposure to differing chemical moieties at the surface.

Both the contact angle and the roughness measurements were greatest in the pure cholesterol group, suggesting a different fundamental structure and mode of action for contact angle compared to the DOPS containing groups. The pure cholesterol group had a markedly increased contact angle, with much lower hydrophilicity than the next closest compositional groups (the 1:1 DOPS:cholesterol groups). This drastic change indicates that at some concentration, the hydrophilicity of the surface changes to a chemically driven property. That is, at a high enough concentration of cholesterol, the coating becomes hydrophobic (as seen in the 100% cholesterol case). Given the apolar nature of the cholesterol compared to DOPS, it was reasonable to expect that the contact angle would increase in coatings of only cholesterol. As the polar DOPS molecule is added to the coatings, it is then able to attract water molecules. While important to note, this contact angle-to-cholesterol content trend reversal in the pure cholesterol case is not principally pertinent, as the DOPS containing coatings are the functionally relevant coatings in the presented work.

The roughness and contact angle measurement averages for each treatment group were used for the Pearson correlation test. This strategy was employed due to the large amount of heterogeneity within the individual treatment groups (for both contact angle and roughness

measurements), and because of the fact that one of the primary points of the test was to find out whether contact angle changes happened over increasing concentrations of cholesterol.

The addition of calcium in the 12:1 and 1:1 groups did not have a statistically significant effect on the roughness or contact angle measurements. This is likely due to the fact that the calcium was added only as a substrate pretreatment, and did not have time or ability to significantly alter the roughness or hydrophilicity of the coatings. Calcium has been shown in previous work to increase coating retention and durability [17], and was therefore included as an additional treatment parameter for three of the groups.

It is interesting that the 1:1 DOPS:cholesterol coating was significantly rougher than several of the other compositions. It is likely that this is due to a microstructural change in the coating, and may be due to a cholesterol crystalline phase separation that is taking place in the coating. That is, the cholesterol may be supersaturating and dissociating from the DOPS molecules and then forming a separate crystalline phase.

Substrate Roughness

As seen in Figure 5-1, the uncoated Ti_6Al_4V (far left columns) have a large amount of inherent roughness. Some of the coated groups were only marginally rougher than the uncoated substrates. This leads to the thought that removing substrate roughness may help isolate coating deposition and composition effects.

5.3.4 Conclusion

These results point out that surface roughness, as measured by SWLI, is strongly correlated (correlation coefficient = -0.873 with $p = 0.0231$) with contact angle and indicates that surface roughness appears to have more of an effect on contact angle than did coating

composition within the range of DOPS and cholesterol coating compositions studied herein (24:1 to 1:1). Furthermore, SWLI was confirmed to be a helpful method for measuring surface morphology and roughness, and proved useful for investigating effects from coating composition on these DOPS implant coatings.

Additionally, it was concluded that higher statistical power may be achieved by polishing the Ti_6Al_4V substrates prior to coating. Polishing is expected to reduce the contribution and interference of the substrate on the coating's morphology measurements.

5.4 Substrate Morphology Effects on SWLI Measurements of DOPS Coatings

Prompted by the significant substrate roughness and high variance that was observed within treatment groups in Section 5.3, an investigation into the possible benefits of polishing the substrates prior to coating with DOPS and cholesterol was explored. This section addresses the following Hypothesis.

Hypothesis 5.3: The coating roughness and morphology measured by SWLI will be more consistent on polished Ti_6Al_4V substrates compared to as-machined substrates, and will increase the statistical power for studies of DOPS and cholesterol coatings.

Specific Aim 5.3-1: Measure the coating surface roughness of samples that were polished prior to coating, and compare the variance and power to un-polished samples.

5.4.1 Methods

Materials

Samples were prepared as outlined previously in Sections 4.3 and 5.3.1. Briefly, DOPS coatings were applied to as-machined Ti_6Al_4V samples using the e-spray deposition method. Coating treatment groups were as follows: 100% DOPS, 24:1 (DOPS:cholesterol), 12:1, 6:1, and 1:1. A calcium salt solution pretreatment was applied to uncoated Ti_6Al_4V samples as outlined in Appendix A: Protocol C.

Polished Ti6Al4V substrates

A second group of samples were polished prior to the other surface treatments (cleaning and passivation) and coating deposition. A commercial histology grinder was used to mirror polish [151] the Ti_6Al_4V samples. The detailed polishing procedure developed for the samples can be found in Appendix A: Protocol E. The Ti_6Al_4V samples were mounted on a polymer histology slide via the use of 3M double sided tape in a grid of 25-60 samples per sample and then polished with progressively finer grit sandpapers. A 240 (or 320) grit paper was used first to level all of the samples (5-60 minutes), then an 800 grit was used (until all 240 grit scratches are removed, usually 10-30 minutes), then a 1,000 grit paper for 7 minutes, a 1200 grit for 7 minutes, a 2500 grit for 7 minutes, and lastly a final polishing paper step for 8 minutes. Samples were checked between each step to check that the deepest scratches from the prior step were removed.

SWLI

Measured SRa and SRz using methods outlined previously in Sections 4.5.2 and 5.3.1. Briefly, a 100X objective with 0.5X zoom was used to measure the SRa and SRz surface roughness parameters in a 35 frame composite stitch area of 0.5x0.5 mm size. On each coated

sample, three composite stitch areas were analyzed, and six samples per treatment group were measured.

5.4.2 Results

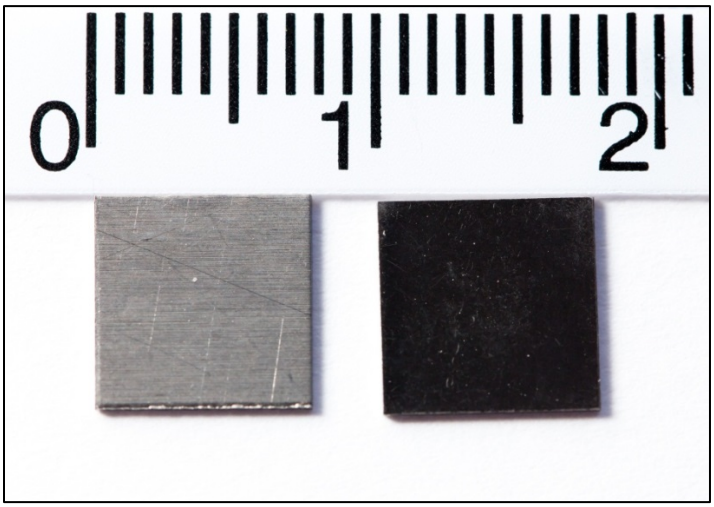

Figure 5-6 Photograph of uncoated Ti_6Al_4V samples; an as-machined unmodified sample (left) and a polished, non-passivated sample (right).

A picture of an as-machined 7.5 x 7.5 mm Ti_6Al_4V substrate and a polished substrate can be seen in Figure 5-6. The machining marks are clearly visible in the as machined sample, along with random larger handling scratches. The polished sample exhibits a mirror finish that is free of visible defects.

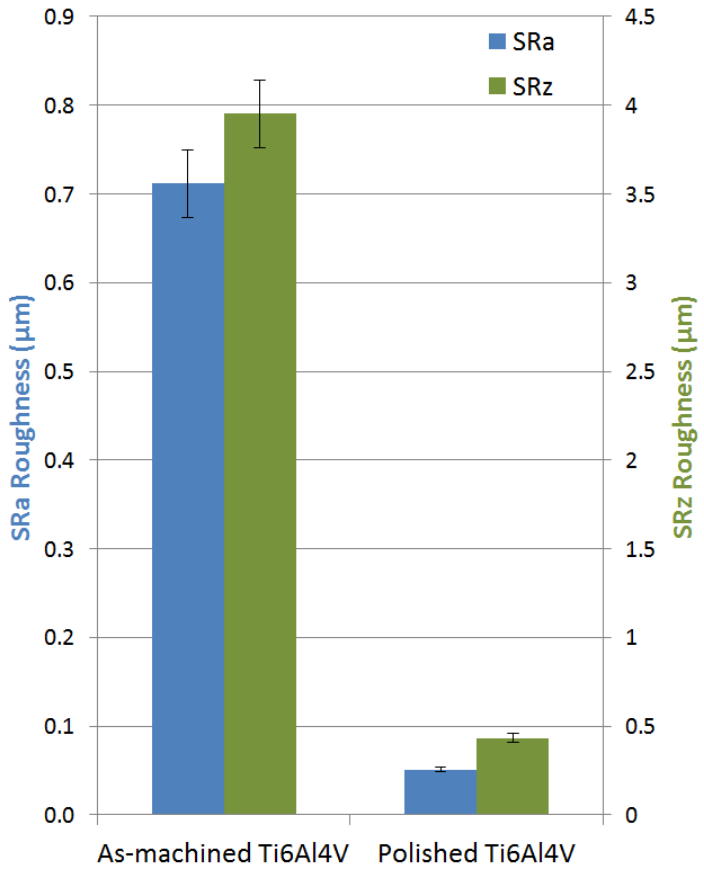

Figure 5-7 Roughness of as-machined and polished Ti_6Al_4V samples. Error bars represent the standard error of the mean. N = 6 for all groups.

As seen in Figure 5-7, the SRa roughness of uncoated Ti_6Al_4V substrates can be found in an as machined state, and after the polishing procedure described in Section 5.4.1.The average roughness decreased to about 10% of the its initial value in the un-polished state. The SRa decreased from 0.712 µm to 0.0513 µm, and the SRz decreased from 3.95 µm to 0.432 µm. Also of importance, the variance decreased dramatically, from 38.4 nm to 2 nm for SRa and from 189.7 nm to 25.4 nm for SRz.

Table 5-2 Measured SRa roughness means, standard deviations, and statistical power of coatings on as-machined vs. polished Ti_6Al_4V substrates.

		As-machined			Polished		
		Mean	Standard Deviation	Power for 10% change	Mean	Standard Deviation	Power for 10% change
100% DOPS	no Ca	**1.539**	*0.777*	12.3	**0.930**	*0.276*	20.4
	with Ca	**0.713**	*0.035*	100	**0.844**	*0.066*	93.0
12:1 DOPS:Chol	no Ca	**1.088**	*0.290*	23.4	**1.086**	*0.142*	58.6
	with Ca	**1.276**	*0.291*	29.9	**1.057**	*0.135*	60.3
1:1 DOPS:Chol	no Ca	**1.271**	*0.435*	17.6	**0.943**	*0.088*	83.4
	with Ca	**1.603**	*0.141*	87.2	**0.972**	*0.181*	37.0
Average Value		**1.248**	*0.328*	45.1	**0.972**	*0.148*	58.8

As seen in Table 4-1, the treatment group average roughnesses are listed along with the group standard deviations and statistical power. The statistical power (π) listed is for a desired detection ($p \leq 0.05$) and for an expected 10% change in the mean of a group. The power was calculated from only the center measurement point on each group (i.e., an N = 6 for the six samples in a treatment, one measurement per sample).

All but two of the groups (the DOPS with Ca and 1:1 with Ca groups) had large increases in power after the addition of the polishing step. If these two groups are excluded, the average power per group increased from 20.8% to 55.7%, or a 268% increase. Averaged across all groups, the power still increased from 45.1% to 58.8%. If a cutoff of 58% power is used, the unpolished groups had two out of six groups pass, while the polished groups had four of six groups pass.

5.4.3 Discussion

The nature of the DOPS and cholesterol e-sprayed coatings results in changing variance across treatment groups (i.e., the variance of roughness measurements within a treatment group was not consistent between groups). This is due to different compositions having differing morphological structures and resultant differences in measured roughness variances. With the

addition of a random substrate roughness, this made it difficult to deduce statistically significant changes in coating roughness and morphology.

Due to the variance in treatment measurements, the statistical power of the e-sprayed samples was deficient. As a rule of thumb, the statistical power in a study should aim to be 80%. In the case of the DOPS coated samples, this was not met in the unpolished groups, with statistical power below 30% for all but two groups. After polishing the Ti_6Al_4V substrates, the coated samples decreased in variance and increased in power to around 60% for most of the groups. Two of the groups had lower power (20% and 37%), and two of the groups had higher power (83% and 93%). These resulting, post-polished, levels of power were deemed adequate for the following work, and the polishing procedure was implemented henceforward.

It should be noted that while helpful for the subsequent study and optimization of coating characterizations, the polishing process can be avoided once coating parameters have been optimized. It is useful to have a controlled system for the exploration of microstructures and surface morphology of the coatings, and the regular, repeating substrate machining marks contributed significantly to the SWLI measurements due to their being on the same size scale as the coating thickness and surface features. Once the machining marks and substrate roughness were removed, it made differentiating compositions and treatments of DOPS and cholesterol coating much easier. After optimizing the coatings with the knowledge gained in this controlled system, it may then it may be desirable to purposefully include and/or induce substrate roughness in order to further improve biological response and integration with the implant surface.

5.4.4 Conclusion

A satisfactory solution for the problem of high sample to sample variance was found by mirror polishing the Ti_6Al_4V substrates. The intrinsic variance of the coatings combined with the conflicting substrate roughness led to the development and implementation of a polishing treatment for the Ti_6Al_4V substrates. Polishing the substrate prior to coating with DOPS and cholesterol decreased the standard deviation in the majority of the coated groups by half, which consequently increased the statistical power to an average of 58.8% per treatment group.

5.5 Chapter Conclusions

Aqueous contact angles of e-sprayed DOPS and cholesterol coatings were found to significantly correlate to the SWLI measured roughness. This leads to the conclusion that DOPS coatings hydrophilic properties are largely morphologically driven, and that the addition of the more apolar cholesterol is not playing a significant role in contact angles for the concentrations used herein.

Low statistical power in the treatment groups and interference from substrate roughness was addressed via the development and utilization of a polishing protocol. The polishing procedure reduced surface roughness and associated variance. Mirror polishing the Ti_6Al_4V substrates was found to dramatically increase the statistical power of the coated samples. Polishing of the samples was therefore implemented from this point forward in the presented work.

5.5.1 Future Work

Future effort may be directed towards a further understanding of contact angle and surface hydrophilicity in the presence of biologically relevant ionic and molecular species. Aqueous contact angle measurements are a standard technique for gaining information about surface energy and fluid interactions, however, the primary use for these coatings will be in biological environments and it would therefore be useful to gain an increased knowledge of coating surface interactions with biological fluids.

After understanding is expanded about the coating compositions and structures, it may be useful to transition to rough and/or porous substrates. While it is helpful to polish substrates in order to isolate and analyze coating morphology and microstructural differences, future effort may take place on purposefully roughened and or porous substrates after the coating optimization has taken place on smooth substrates.

Chapter 6: Analysis of Effects from the Addition of Calcium and Cholesterol to the DOPS Coatings

6.1 Purpose

The purpose of this chapter is to study changes to the properties and/or structure of DOPS coatings when adding a calcium pretreatment or incorporating cholesterol into the coatings. In particular, attention will be paid to the effects that adding calcium and cholesterol may have on the hardness and roughness of the coatings. DOPS is a well-known calcium binding molecule, calcium binds the negatively charged DOPS head groups [152], [153] and often acts to dehydrate DOPS structures [97]. Cholesterol is an important biomolecule that plays both a structural and regulatory role in biomembranes [100]. Cholesterol preferentially resides within cell membranes and plays a vital role in the regulation of membrane rigidity [101], [102].

Previous work has used both calcium and cholesterol to enhance the durability of the DOPS coatings, as well as for the modification of drug release rates from the coating [17]. Adding calcium to phospholipid (DOPS) systems has been shown to bind the lipid head groups of DOPS molecules [5], [96] and previous work has already shown its utility in controlling elution rates for use in implant coatings [17]. However, it remains to be seen if the addition of a calcium substrate pretreatment has a significant effect on the surface morphology, thickness or hardness of DOPS coatings.

Cholesterol has been used for similar purposes as calcium in previous work, but instead of being used as a substrate pretreatment, the cholesterol was mixed directly into the coatings in order to provide further structural reinforcement of the implant coatings [17]. Little has been done to understand the specific effects that cholesterol has on the microstructural and

morphological nature of the DOPS implant coatings. This work aims to elucidate effects from adding cholesterol through the use of scanning white light interferometry, differential scanning calorimetry, and nanoindentation.

Hypothesis 6.1: Adding a calcium solution pretreatment to the substrate will not have a significant impact on the coatings' thickness or surface roughness due to the localized effects of the calcium near the substrate surface.

Specific Aim 6.1-1: Use SWLI to measure the thickness of DOPS coatings with and without a calcium pretreatment.

Specific Aim 6.1-2: Use SWLI to measure roughness of DOPS coatings with and without a calcium pretreatment.

Hypothesis 6.2: Adding a calcium pretreatment will harden the DOPS coatings due to a binding of the phospholipid headgroup in the presence of calcium.

Specific Aim 6.2-1: Use nanoindentation to measure the universal hardness of DOPS coatings with and without inclusion of a calcium substrate pretreatment.

Hypothesis 6.3: DOPS coatings will increase in roughness with increasing cholesterol content due to a higher surface energy from the binding and entanglement of cholesterol in the DOPS.

Specific Aim 6.3-1: Use SWLI to measure the roughness of DOPS coatings with varying concentrations of cholesterol added to the coating.

Hypothesis 6.4: Increasing the amount of cholesterol in the coatings will harden the DOPS coatings due to cholesterol dispersing in the lipid system and stiffening the lamellar DOPS structure.

Specific Aim 6.4-1: Use nanoindentation to measure universal hardness of DOPS coatings with varying concentrations of cholesterol added to the coating.

Specific Aim 6.4-2: Use differential scanning calorimetry to measure the heat flow of DOPS coatings with varying concentrations of cholesterol added to the coating.

Specific Aim 6.4-3: Use glancing angle X-ray diffraction to measure the diffraction patterns of DOPS coatings with varying concentrations of cholesterol added to the coating.

6.2 Experimental Methods

6.2.1 Materials

Samples were polished, cleaned, passivated and prepared as described previously in Sections 4.3 and 5.4.1. Briefly, 7.5x7.5 mm Ti_6Al_4V sheet metal samples were coated with phosphatidylserine (DOPS) purchased from Avanti Polar Lipids, Inc. (Alabaster, Alabama) [59] and Cholesterol (CAS# 57-88-5) obtained from Alfa-Aesar (Ward Hill, MA) [144], and mixed with with chloroform prior to e-spraying.

6.2.2 Sample Preparation

Samples were thoroughly cleaned and passivated as described previously in Section 4.3 and according to Appendix A: Protocol A - Titanium Square Sample Preparation and Protocol D - Titanium Passivation. Prior to coating with DOPS and cholesterol, some of the Ti6Al4V samples were pretreated in a calcium (Ca) salt solution as outlined in Appendix A: Protocol C.

Electro-Spray Coating Process

Coatings were applied to the Ti_6Al_4V samples using an electro-spray process (see Sections 2.4.3 and 4.3). A 1.3% (vol%) DOPS in chloroform solution was e-sprayed onto

cleaned and passivated 7.5x7.5mm Ti_6Al_4V samples. The voltage differential used was 12 kV with a pump rate of 14 mL/hr (or 3.89 uL/sec) and with an 8 cm working distance. Ten Ti_6Al_4V substrates were E-sprayed at a time, with a spray time of 44.6 seconds per coat, with two coats applied with a short pause (about 2 minutes) between coats. These parameters were chosen to provide a final coating density of 1 mg of DOPS per cm^2 of sample. This equated to a total of 347 µL of solution per sample, or 0.563 mg of DOPS on each sample. Some DOPS and cholesterol groups were sprayed eight samples at a time with all spray parameters kept the same except that the time of spray was varied such that the total amount sprayed per samples remained constant.

Incorporation of Cholesterol in the Coatings

Coatings that included cholesterol were e-sprayed similar to the DOPS samples, but with the addition of cholesterol into the 20mM DOPS-chloroform solution. The resulting DOPS-cholesterol-chloroform solution was then e-sprayed onto the Ti_6Al_4V substrates as outlined above.

The DOPS:cholesterol coated samples were prepared with varying concentrations of cholesterol at the following molecular ratios of DOPS to cholesterol: 100% DOPS, 12:1 (DOPS:cholesterol), and 1:1. This resulted in solutions that maintained a 20mM DOPS concentration, and added a 0.0mM, 1.667mM, and 20mM cholesterol concentration (for the 100% DOPS, 12:1, and 1:1 groups respectively). See Table 5-1 for the amount of DOPS and cholesterol contained within the sample treatment groups on a percentage basis of the total mass in the coating.

Drying DOPS and Cholesterol Samples

After e-spraying, the coated samples were dried under a vacuum in a desiccator for at least 48 hours prior to analysis.

Preparation of DOPS:cholesterol DSC samples

Differential Scanning Calorimetry (DSC) sample pans were coated using an aerosol spray deposition method. An overview of the aerosol spray deposition method can be found in Appendix B: Atomizing Nozzle Spray Deposition Methodology Development. Two DOPS:cholesterol treatment groups were tested. A 20mM DOPS in chloroform solution was used for both groups, with cholesterol being added at a 12:1 (DOPS:cholesterol) and 1:1 molecular ratio (resulting in 1.667 mM and 20 mM cholesterol concentrations, respectively). 2mL of solution was sprayed onto 3 DSC pans for the 1:1 group, and 2.66 mL of solution sprayed onto 2 pans for the 12:1 treatment group. The coated pans were then left to dry under vacuum in a desiccator for at least 72 hours prior to testing with the DSC.

6.2.3 Scanning White Light Interferometry

Quantitative Measurement of Coating Morphology

Scanning White Light Interferometry (SWLI) was used to measure SRa and SRz as outlined previously in Sections 4.5.2 and 5.3.1. Briefly, a 100X objective with 0.5X zoom was used to measure the SRa and SRz surface roughness parameters in a 35 frame composite stitch area of 0.5x0.5 mm size. Each sample was tested once in the center of the sample. A custom script that allowed the capture and combination of a dual light level scan was utilized as needed.

Measurement of Film Thickness

Each sample's coating was scratched and measured for thickness using SWLI as outlined in Section 4.6.2. Briefly, prior to measuring with SWLI, a metal pick/awl was used to create a scratch through the sample coating and a custom mask and set of scripts in the MetroPro software was then used measure the lowest point in the scratch at 5 cross sectional areas within the composite stitch's field of view. These five depths were then averaged to determine the thickness of that particular sample.

Statistical Analysis

All data measured by SWLI was analyzed using the Proc Mixed procedure in SAS and was modeled as a 2 way factorial ANOVA model unless noted otherwise. The 2 fixed effects modeled were the composition (DOPS, 12:1 or 1:1) and the presence of calcium (yes or no). Up to 2 way interactions were allowed in the first pass of the model. All treatments had non-significant 2 way interactions (at a $p = 0.05$ threshold) and were subsequently analyzed by dropping interaction effects from the model. This left an analysis of the main effects only (composition and calcium).

6.2.4 Nano Indentation

The XP head on a Nanoindenter G200 (Agilent Technologies, Inc., Santa Clara, CA) was used for indentation. A standard Berkovich tip was utilized to indent the coated samples to a maximum load of 20 μN with a ramp time of 5 seconds, followed by a 120 second hold at the 20 μN force, followed with an unload over 5 seconds. Surface detection prior to indents was performed using the very sensitive approach parameter (50 N/m stiffness). Samples were tested at room temperature and in atmospheric conditions.

Prior to indentation, the sample coating thicknesses were measured with SWLI using the methods previously detailed in Section 4.6.2. All sample coatings were at least 3 μm in thickness. This knowledge led to the use of the 20 μN max force during indentation. In order to avoid the material properties of the substrate contributing to the indentation measurements, the maximum indent depth needs to be 10% or less of the coating thickness [154]. The 20 μN force was found to indent to a depth of approximately 250 μm or less into the coatings, and was therefore used as the maximum indent load for subsequent testing.

Four treatment groups were prepared, a pure DOPS e-sprayed coating (Section 6.2.2), and a DOPS coating where the substrate was first calcium pretreated (Appendix A: Protocol C), a 12:1 (DOPS:cholesterol) group without the calcium treatment, and a 1:1 (DOPS:cholesterol) group also without the calcium treatment. Four samples for each group were sprayed, both of the DOPS groups were sprayed at one time (eight samples), and the cholesterol groups were sprayed separately in groups of four. Nanoindentation tests were performed on 4 samples at a time (one from each treatment group). The testing was performed overnight and the testing order for the 4 samples was randomized. 20 indents were performed on each sample, for a total of 80 indents (across 4 samples) for each treatment group.

Due to sample roughness, some of the indents failed within the 20-indent arrays. Any indents that failed to record data or were obviously misshapen (e.g. that visibly broke through local surface asperities or high points on the surface) were removed from the data set (8.1% of the indents). Some of the indents were much harder than the other indents and were removed from the data set if they were more than 5 standard deviations from the rest of the indents (1.9% of the indents). These were likely due to indents performed at deep local surface depressions, or from contaminants on the surface.

Universal Hardness

The universal hardness was computed for each nanoindentation curve. Universal hardness is a function of the maximum indentation depth and the applied load and is computed as seen in Equation 6-1.

Equation 6-1 Universal Hardness for Nanoindentation

$$H_U = \frac{P}{A_p(h_c)}$$

In Equation 6-1, H_U is the universal hardness (Pa), P is the maximum indentation load applied to the sample (N), and the denominator is an area function, where, A_p is a tip function constant, and h_c is the maximum indentation depth (m). In the case of the standard Berkovich tip, A_p = 26.43 [137]–[139].

Statistical Analysis

Statistical analysis was performed using SAS. Studentized residuals were plotted for each of the treatment groups, and a log transform was selected as it provided the best approximation of normal data with equal variances. The raw, non-transformed data did not pass an equal variance test. The statistical model included the treatment group and testing order as fixed effects, and the day the test was performed on as a random (block) effect.

6.2.5 Differential Scanning Calorimetry (DSC)

Differential Scanning Calorimetry (DSC) sample pans were coated using an aerosol spray deposition method. An overview of the aerosol spray deposition method can be found in Appendix B: Atomizing Nozzle Spray Deposition Methodology Development. Two DOPS:cholesterol treatment groups were tested. A 20mM DOPS in chloroform solution was

used for both groups, with cholesterol being added at a 12:1 (DOPS:cholesterol) and 1:1 molecular ratio (resulting in 1.667 mM and 20 mM cholesterol concentrations, respectively). 2mL of solution was sprayed onto 3 DSC pans for the 1:1 group, and 2.66 mL of solution sprayed onto 2 pans for the 12:1 treatment group. The coated pans were then left to dry under vacuum in a desiccator for at least 72 hours prior to testing with the DSC.

A DSC 2920 Modulated DSC (TA Instruments, New Castle, DE) was used to analyze the phase transition of the DOPS and cholesterol coatings between 0 and 100C. A 2º C/min ramp rate was used to cycle the DSC sample from room temperature (24º C) to 100º C and back twice (i.e., two heating and two cooling ramps). The sample was then cooled all the way to 0º C, after which it was cycled up to 100º C and down to 0º C twice (for a complete total of 4 heating cycles, and 4 cooling cycles). 1 sample was tested for each treatment group at each time point.

The reason for choosing 8 heating and cooling cycles is due to the possible dehydration of the monohydrate cholesterol phase into the anhydrous phase. It has been noted that at least two high temperature heating cycles (above 86º C) needs to be performed in order to ensure that all monohydrate cholesterol crystals have dehydrated to the anhydrous form [100]. The anhydrous crystalline form is then measureable by DSC from its polymorphic phase transitions at approximately 37º C and 20º C (during heating and cooling, respectively).

6.3 Addition of a Calcium Pretreatment

6.3.1 Results

The results for the studies on DOPS coatings that either included or did not include a calcium pretreatment to the Ti_6Al_4V substrate are presented in the following sections.

Scanning White Light Interferometry

Coating Surface Morphology

The roughness of DOPS coatings with and without a calcium substrate pretreatment can be seen in Figure 6-1. The blue bars represent the SRa surface roughness, and the green bars represent the SRz roughness. 12 samples were measured for each treatment group.

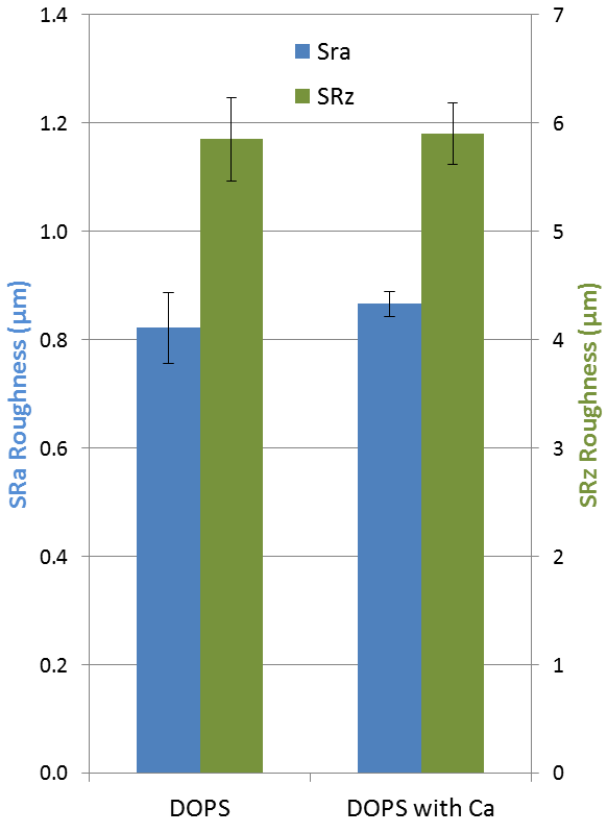

Figure 6-1 SWLI measured SRa and SRz surface roughness of DOPS coatings with and without the addition of a calcium pretreatment to the substrate. Error bars represent the standard error of the mean. N = 12 for all groups.

As seen in Figure 6-1, there was little difference in surface roughness between the DOPS (no calcium) and DOPS with calcium groups. Both SRa and SRz roughness measurements were not statistically significantly different ($p = 0.305$ and $p = 0.511$ for SRa and SRz respectively).

Coating Thickness

The thickness of DOPS coatings with or without the addition of calcium substrate pretreatment can be found in Figure 6-2. 12 samples were measured for each treatment group.

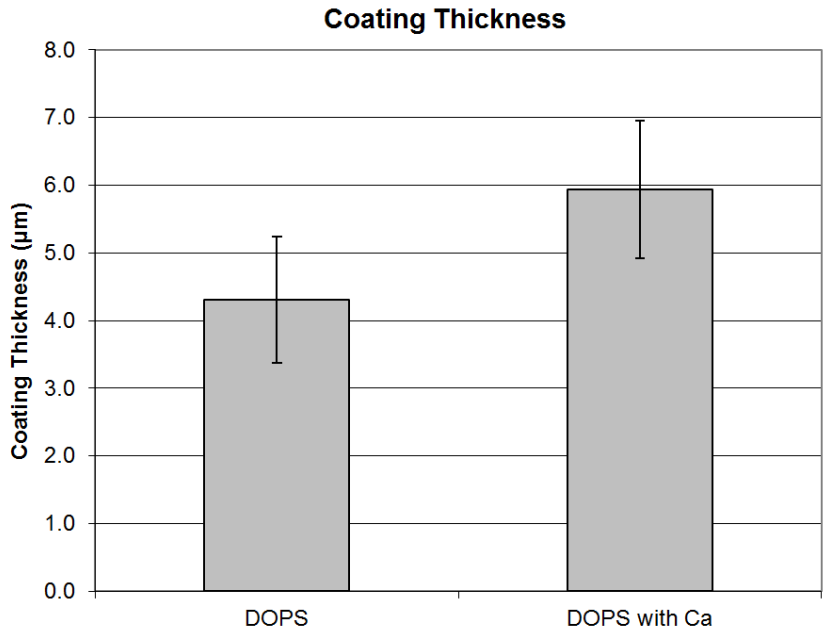

Figure 6-2 Coating thickness as measured by SWLI of DOPS coatings with and without the addition of a calcium pretreatment to the substrate. Error bars represent the standard error of the mean. N = 12 for both groups.

As seen in Figure 6-2, the coating thickness was similar in both groups; with the average thickness of the non-calcium treated group being 4.31 ±0.933 µm and the calcium treatment group was 5.94 ±1.016 µm. There was not a statistically significant difference between the groups ($p = 0.237$). Due to a non-normal distribution of data, statistical analysis was done as a Mann-Whitney rank sum test.

Nanoindentation

A representative nanoindentation load displacement curve can be found in Figure 6-3. This particular nanoindentation curve was for a plain DOPS sample.

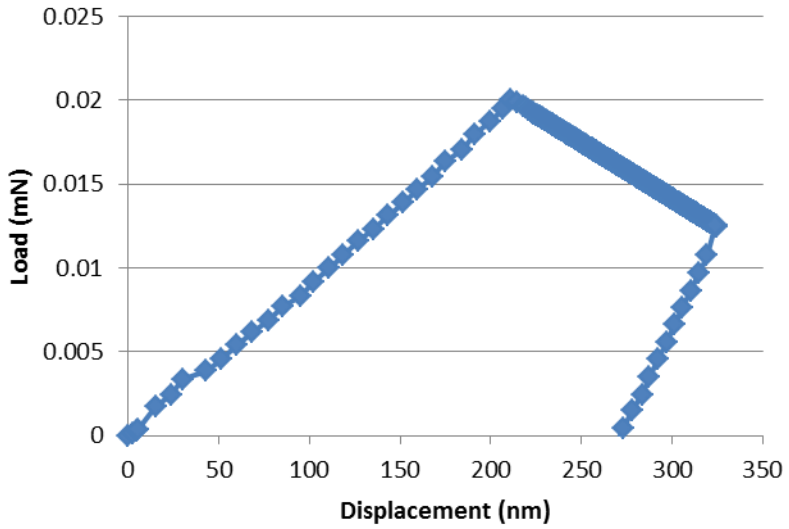

Figure 6-3 Representative nanoindentation load displacement curve for DOPS (no calcium) coated titanium sample.

Nanoindentation curves for all treatment groups had a similar shape to the load displacement curve in Figure 6-3. As can be seen in Figure 6-3, the nanoindenter had difficulty keeping the small holding load of 20 μN constant, as indicated by the downward drift in the hold region. The universal hardness results for the DOPS coatings were then compiled as found in Figure 6-4. Four samples were measured for each treatment group, with 20 indents performed on each sample.

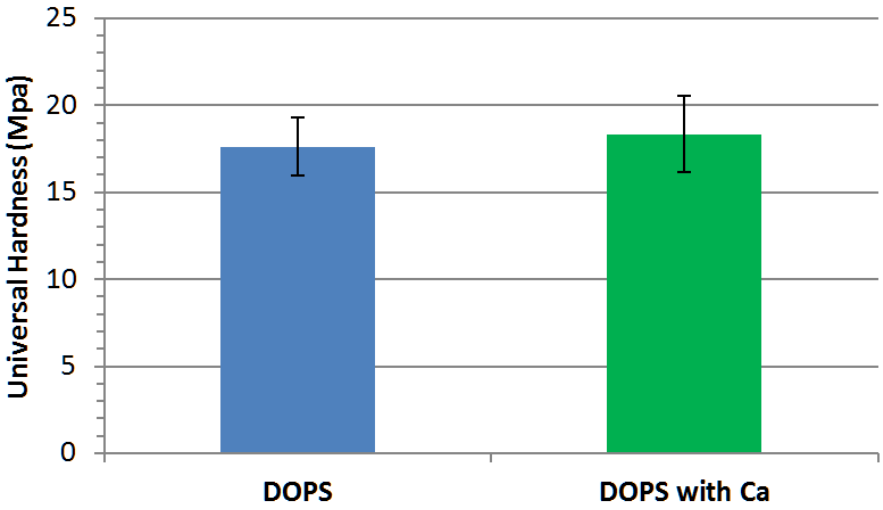

Figure 6-4 Universal hardness results from nanoindentation for E-Sprayed DOPS coatings without and with the calcium substrate pre-treatment. Error bars represent the standard error of the mean. N = 4 for both groups, with 20 indents per sample.

As seen in Figure 6-4, universal hardness results were similar for the two treatment groups. There was no significant ($p = 0.1787$) difference between the treatment groups. The average hardness of the groups was as follows: 17.63 ±1.646 MPa for DOPS, 18.33 ±2.19 MPa for the non-calcium containing DOPS group.

6.3.2 Discussion

Scanning White Light Interferometry

The methods developed in the prior chapters for measuring surface morphology and roughness of the DOPS coatings using SWLI worked well. The DOPS and DOPS with calcium coatings were of similar roughness, both in the SRa and SRz roughness parameters.

Significant differences for surface roughness were not evident between the plain DOPS and DOPS with calcium pretreatment. The lack of detectible differences in roughness is likely due to the calcium treatments effects being localized to the substrate, as the calcium solution was

applied only to the substrate (and prior to coating with DOPS). It is possible that there are changes in the order and microstructure near the substrate surface within the coating in the calcium treated samples, but these effects were not propagated to the surface in a measurable way, likely due in part to the high roughness (> 0.8 for both SRa and SRz) and variability of the native coatings.

Nanoindentation

Nanoindentation effectively measured the average surface hardness of the coatings. There was not a significant difference in hardness in the DOPS vs. DOPS with calcium samples. As with the surface roughness, this is most likely due to any calcium effects on the hardness being localized to near the Ti_6Al_4V substrate. The fact that there were no significant differences in hardness in the DOPS coatings with calcium indicates that there may be a negligible long range change in coating morphology that would significantly affect the stiffness of the coatings and/or that the calcium has not diffused into the bulk of the coating given the short time frames of measurement here. Given the nanoindentation test primarily tests the mechanical properties at and near the top surface of the coating, it minimizes the tests ability to detect any changes in the bulk coating hardness that may be present.

It is probable that the calcium pretreatment does indeed act to increase the DOPS structure's hardness (as initially hypothesized). However, it is also likely that it would only be measureable in the very near vicinity of the substrate's surface due to limited diffusion of the calcium molecules into the coating. Measuring these slight and near-substrate stiffening effects would most likely prove to be very difficult using current technologies without significantly disrupting the coating or changing their microstructural state in the process. As a reference, the

measured hardness of these DOPS and cholesterol coatings (18 MPa) is on the same order of other soft polymers like UHMWPE (34 MPa) [155], while orders of magnitude softer than materials like PMMA (0.40 GPa) [136] and the enamel of bone (4 GPa) [156].

6.3.3 Conclusions

Scanning white light interferometry was an efficient way to measure the coating roughness, and SWLI measurements did not detect significant changes in roughness in the DOPS coatings with the addition of the calcium pretreatment. This may be explained by the limited diffusion of calcium through the coating over the short manufacture to measurement timeframe.

Nanoindentation with a Berkovich tip and a high number of tests per group is an effective way to test the hardness of these DOPS coatings, and the method outlined in this chapter provided useful insights into the mechanical properties of the DOPS and cholesterol coatings. Little to no mechanical characterization of bulk systems of pure DOPS systems have been done before, and the coating's universal hardness for both of the tested DOPS groups found here was approximately 18 MPa. This compares similarly to other soft materials (such as UHMWPE at 34 MPa [155]), and is a useful reference for future efforts. There were no significant differences in universal hardness from nanoindentation of the DOPS vs. the DOPS with calcium treatment. This may be because the calcium has a negligible effect on the coatings, or it may be attributed to the limited amount of diffusion of the calcium from the Ti_6Al_4V substrate, and the fact that the nanoindentation test primarily measures the mechanical properties near the surface of the coating. Even though it was not measured here, it is suspected that the calcium does indeed have an effect, due to the positive role it played in coating retention in previous work (which had longer time frames for diffusion) [17].

The hypothesis (6.1) sought to find out whether the calcium pretreatment process has an effect on coating thicknesses within a given treatment. This was not found to be the case, but the SWLI thickness measurement method was able to detect thickness changes due to increasing amounts of coating material (between the DOPS and DOPS+cholesterol groups). This confirms that the thickness measurement method was effective at detecting changes, and that it did not detect a change due to the calcium pretreatment process.

The lack of significant differences in the roughness results between the calcium and non-calcium treated samples was as expected. This confirms our original hypotheses (6.1), that any effect would be negligible. The fact that the hardness of the coatings (as measured by nanoindentation) did not increase significantly with the inclusion of a calcium substrate pretreatment is not surprising for the same reason. While the lack of increased hardness with the inclusion of calcium was contrary to our initial hypothesis (6.2), it is explained via the same argument derived from the roughness results, that any hardening effect is only measureable near the substrate's surface due to limited diffusion of the calcium molecules into the coating. Regardless, the fact that the addition of the calcium pretreatment had no negative effects on roughness and hardness confirms its continued value as a coating treatment given it has already demonstrated its utility in controlling elution rates [17].

6.4 Incorporation of Cholesterol into the Coatings

6.4.1 Results

Scanning White Light Interferometry

Coating Surface Morphology

The roughness of DOPS coatings with varying concentrations of cholesterol in the coating is presented in Figure 6-5. The blue bars represent the SRa surface roughness, and the green bars represent the SRz roughness. Twelve samples were measured for each treatment group.

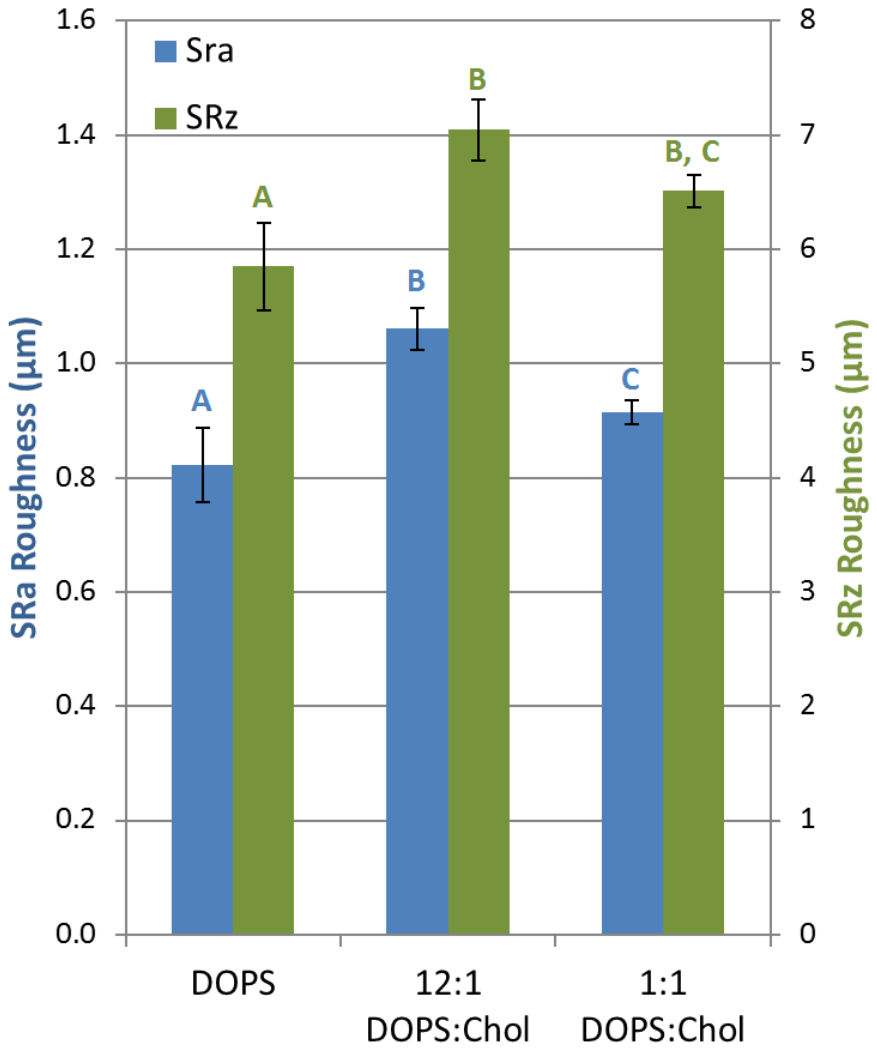

Figure 6-5 SWLI measured SRa and SRz surface roughness of DOPS and DOPS:cholesterol coatings. Error bars represent the standard error of the mean. Significance is indicated by letter groups; if bars share a letter, they are not significantly different. N = 12 for all groups.

As seen in Figure 6-5, the roughness between groups peaked for each parameter in the 12:1 (DOPS:cholesterol) group. For the SRa roughness parameter, all groups were significantly different. The 12:1 group was significantly higher than both the DOPS and 1:1 groups ($p < 0.0001$ and $p = 0.0423$ respectively). The 1:1 group was significantly rougher than the DOPS group ($p = 0.0071$).

For SRz, both the 12:1 and 1:1 groups were significantly rougher than the plain DOPS group ($p < 0.0001$ and $p = 0.0072$ respectively). The 12:1 group was not significantly rougher than the 1:1 group ($p = 0.0639$).

Coating Thickness

The coating thickness of DOPS coatings with varying concentrations of cholesterol in the coating is presented Figure 6-6. Twelve samples were measured for each treatment group.

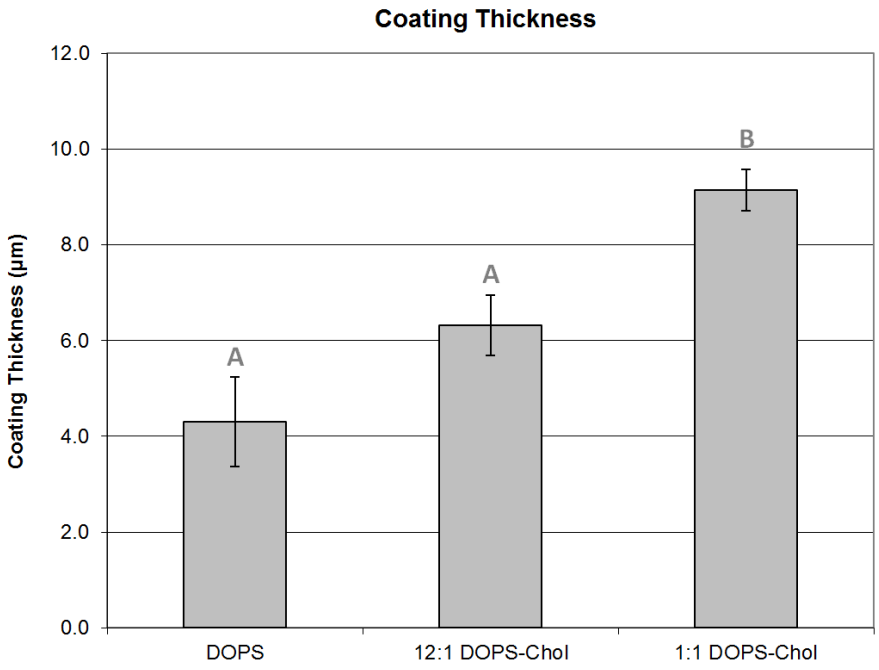

Figure 6-6 SWLI measured coating thickness of DOPS and DOPS:cholesterol coatings. Error bars represent the standard error of the mean. Significance is indicated by letter groups; if bars share a letter, they are not significantly different. N = 12 for all groups.

As seen in Figure 6-6, the coating thickness steadily increased with increasing concentration of cholesterol in the coating. The group averages were 4.31 ±0.933 µm (DOPS), 6.315 ±0.631 µm (12:1), and 9.15 ±0.433 µm (1:1) for the different groups. Both the DOPS and 12:1 groups were significantly thinner than the 1:1 group ($p < 0.0001$ and $p = 0.0001$ respectively). The 12:1 group was not significantly thicker than the DOPS group ($p = 0.1237$).

Nanoindentation

Nanoindentation curves for all treatment groups had a similar shape to the load displacement curve in Figure 6-3. The universal hardness was computed for each nanoindentation curve as outlined in Equation 6-1 and Section 6.3.1. The universal hardness results for the DOPS and DOPS:cholesterol coatings were then compiled as found in Figure 6-7.

Four samples were measured for each treatment group, with 20 indents performed on each sample.

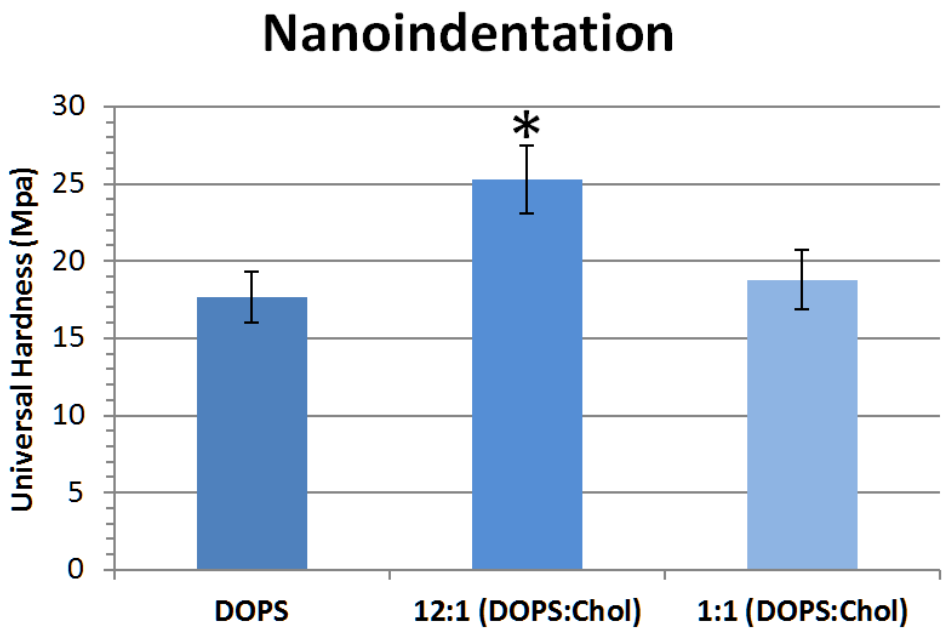

Figure 6-7 Universal hardness results from nanoindentation for DOPS and cholesterol coatings. Asterisk indicates significance at p=0.05 level, error bars represent the standard error of the mean. Asterisk represents a significant difference compared to groups without an asterisk. N = 4 for all groups, with 20 indents per sample.

As seen in Figure 6-7, the universal hardness was significantly higher in the 12:1 treatment group ($p = 0.0473$ against the DOPS group, and $p = 0.0070$ against the 1:1 group). There was no significant difference between the DOPS treatment and the 1:1 group ($p = 0.6168$). The average hardness of the groups was as follows: 17.63 ±1.646 MPa for DOPS, 25.3 ±1.921 MPa for 12:1, and 18.78 ±1.773 MPa for the 1:1 group. Statistical analysis was performed on the log transformed data, as the raw data was not normally distributed.

Statistical analysis using other transformations of the raw data yielded similar results, with the 12:1 group also being significantly harder than the other treatment groups. There was no statistically significant difference in the variance between different treatment groups.

Additionally, when analyzed as a separate factor, the testing order within a given overnight nanoindentation session did not contribute a statistically significant effect to the universal hardness results. That is, the treatment group tested first in the evening was not significantly harder or softer than the treatments tested last in a given indentation session, across all of the evenings tested.

Differential Scanning Calorimetry (DSC)

An example set of measured DSC curves can be found in Figure 6-8.

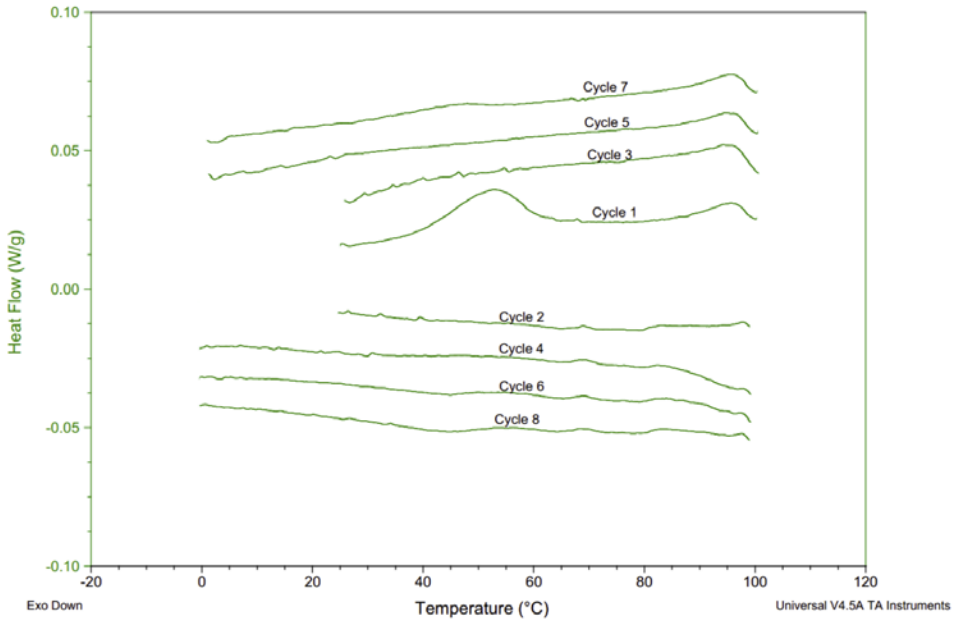

Figure 6-8 DSC of 12:1 group. The top 4 curves are heating scans, and the bottom 4 are cooling scans. Curves are displaced along the y axis for presentation. Scan rate was 2º C/min, exothermic peaks point downward.

As seen in Figure 6-8, there were a total of 8 thermal scans that were run on each sample. The first 3 cycles were between 24º C and 100º C, and the last 5 cycles were between 0º C and 100º C. The top 4 curves are heating scans, and the bottom 4 are cooling scans.

A full compilation of the printouts for the individual DSC scans for both compositions and time points can be found in Appendix C: Differential Scanning Calorimetry Measurements for DOPS and cholesterol coatings. The results of the 12:1 and 1:1 treatment group DSC scans are compiled in Table 6-1.

Table 6-1 Summary of temperatures and heat of enthalpies associated with specific peaks from DSC scans of the 12:1 and 1:1 DOPS:cholesterol groups. Heating scans are indicated by a light red background, and cooling scans with a light blue background. Exothermic peaks have a negative sign preceding the measurement.

		12:1 Composition		1:1 Composition
		Peak 1	Peak 2	Peak 1
Cycle 1 (24-100°C)	Peak Temp (°C)	52.76	95.79	38.06
	Onset Temp (°C)	40.26	87.8	36.03
	Enthalpy (J/g)	5.362	0.9478	0.3798
Cycle 2 (100-24°C)	Peak Temp (°C)	NA		NA
	Onset Temp (°C)	NA		NA
	Enthalpy (J/g)	NA		NA
Cycle 3 (24-100°C)	Peak Temp (°C)	96.36		94.98
	Onset Temp (°C)	92.66		92.2
	Enthalpy (J/g)	0.3152		0.167
Cycle 4 (100-0°C)	Peak Temp (°C)	NA		NA
	Onset Temp (°C)	NA		NA
	Enthalpy (J/g)	NA		NA
Cycle 5 (0-100°C)	Peak Temp (°C)	96.29		33.73
	Onset Temp (°C)	89.77		29.66
	Enthalpy (J/g)	0.7671		1.033
Cycle 6 (100-0°C)	Peak Temp (°C)	NA		-19.01
	Onset Temp (°C)	NA		-23.4
	Enthalpy (J/g)	NA		-0.9037
Cycle 7 (0-100°C)	Peak Temp (°C)	96.26		33.43
	Onset Temp (°C)	90.47		29.18
	Enthalpy (J/g)	0.6867		1.109
Cycle 8 (100-0°C)	Peak Temp (°C)	NA		-20.1
	Onset Temp (°C)	NA		-24.15
	Enthalpy (J/g)	NA		-0.9746

As seen in Table 6-1, none of the cooling scans had any significant peaks in the 12:1 group, and the first heating scan had a large, broad endothermic peak at 52.8º C. All of the heating cycles had small endothermic peaks at 96º C.

In the 1:1 group, all of the peaks were at one of two primary locations, around 33º C during the heating cycles, and at 20º C during the cooling cycles. During the heating cycles there were endothermic peaks at 38º C (in cycle 1), and then at 33º C in cycles 5 and 6. During the 100-0º C cooling cycles (cycles 6 and 8) there were exothermic peaks at 20º C. There was also a very sharp exothermic peak in the 2nd heating scan (cycle 3) at 98º C (data not tabulated) that was interpreted as noise from the instrument's liquid nitrogen controller (see Appendix C: Differential Scanning Calorimetry Measurements for DOPS and cholesterol coatings).

6.4.2 Discussion

Scanning White Light Interferometry

Scanning white light interferometry worked well for the DOPS and cholesterol coatings in this chapter, but it should be noted that the SWLI capture protocol was modified slightly as needed for the cholesterol coated samples. The cholesterol samples tended to absorb and/or diffract more light than the plain DOPS samples, leading to the use of dual light level scanning with SWLI in order to maximize data fill in the scans.

Overall, the cholesterol samples were notably rougher than the non-cholesterol containing samples. This roughness was evident by visual inspection as a more matte appearance, during SWLI measurements as it often required a dual light level scan, and in the resulting SRa and SRz measurements. In particular, the 1:1 samples were the most likely to require a dual light level stitch.

The thickness of the coatings increased for the samples that had cholesterol, as expected due to the increased amount of material sprayed onto the substrates in these cholesterol containing groups. Interestingly, the increase in thickness was not proportional to the increase in mass of the coatings. The thickness of the cholesterol coatings were increased by a higher percentage than the weight gain would have led one to expect. In the 1:1 case, the mass of the coatings increased by 48% (from average of 0.563 mg per plain DOPS coating to 0.831 mg for the 1:1 coating). And in the 12:1 case, the mass of the coatings increased by 3.98% (from average of 0.563 mg per plain DOPS coating to 0.585 mg for the 12:1 coating). This is contrasted with the coating thickness changes, which increased by 112% for the 1:1 coating and 46.6% for the 12:1 coating. This is interpreted as a result of a decreased density of the coatings that included cholesterol, or due to an increased porosity of the coatings, both scenarios of which confirm that cholesterol may be acting to disrupt, bind and/or entangle the intermolecular DOPS bonding.

Nanoindentation

Nanoindentation Method development

Initial effort was taken to use a conical spherical shaped tip in order to better test the viscous nature of the coatings, as the spherical tip reduces plastic deformation near the tip [157], [158]. However, after further testing and method development, it was found that the surface roughness of the coatings made testing with a spherical tip problematic. This was primarily attributed to the very high level of surface roughness on the DOPS coatings. As a rule of thumb, the maximum RMS surface roughness that is allowable for a nanoindentation test specimen should be 10% or less of the indentation depth [154]. In the coatings tested herein, the maximum

nanoindentation depths averaged a few hundred nanometers, and the coating roughness for the coated samples were over 1 µm RMS. A typical DOPS and cholesterol coating had even higher levels of roughness. Drastically deeper indent depths were not possible, as the coatings were only on the order of several microns in depth, and the maximum allowable testing depth is 20% of the coating thickness in order to avoid substrate effects [154]. A 2D trace of the surface roughness on a representative DOPS coating (as measured by SWLI) can be found in Figure 6-9.

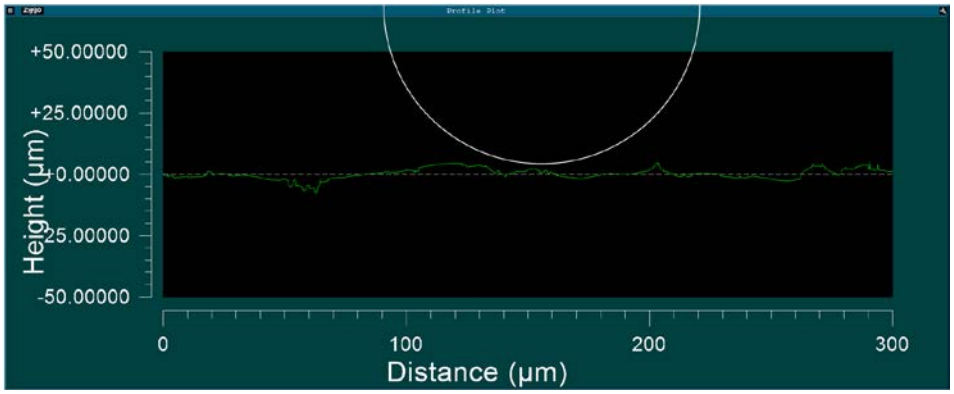

Figure 6-9 A 2D Surface profile of a DOPS coating, with a superimposed profile representing a 65µm spherical tip indenter.

As seen in Figure 6-9, the coating surface presents a significant inconstant for tip-surface contact area for indent depths of several hundred nanometers or less. In order to overcome this problem of high surface roughness, a sharp indenter tip was used to reduce the effect of local surface asperities, and a large number of indents were performed in order to average the measured hardness response of the surface.

The coatings proved to be soft and highly viscous, consequently limiting the amount of analysis that the nanoindentation instrument was able to perform. The unload region of the indentation curve is often used to measure the properties of the material [135]. However, the DOPS and cholesterol coatings proved to be viscoplastic and rough enough to make analysis of the unload region of the load displacement curve problematic. Additionally, the machine was not

able to the constant low loads required for the nanoindentation test on the DOPS and cholesterol coatings, as evidenced by the non-level hold region seen in Figure 6-3. Inspection of the coatings with light microscopy post-indentation revealed that even the surface detection indent approaches produced significant permanent plastic deformation in the coatings. This is notable, as the indenter approached the surface slowly and at a very sensitive detection setting (the setting was for surfaces of 50 N/m stiffness or less). Because of these coating qualities, a quick load time was used in conjunction with analysis of only the loading region of the load displacement curve.

Discussion of results for DOPS and Cholesterol Coatings

The nanoindentation universal hardness results were significantly higher for the 12:1 (DOPS:cholesterol) group. This is attributed to the ability of cholesterol to increase intermolecular binding in lipid structures [159], similar to the mechanism that the body uses to regulate membrane stiffness *in vivo* [53]. The 12:1 DOPS:cholesterol samples therefore stiffened with the additional cholesterol that fully dispersed within the lipid structure.

It is also known that cholesterol has a limited solubility in phospholipid systems, after which it supersaturates into a crystalline form, thereby interrupting the larger scale lamellar microstructure of lipid bilayers [100]. This phenomena explains why the 1:1 group begins to lose stiffness after a high level of cholesterol is added to the system. As the cholesterol supersaturates and forms crystals, the microstructure of the lipid system is compromised, resulting in an overall decrease in hardness as observed in the nanoindentation testing. In the 12:1 group, the bulk mechanical properties appear to be driven primarily by dispersed cholesterol within the lipid microstructure (that stiffens the system), while the 1:1 group's cholesterol is supersaturated,

forming membrane-interrupting crystals that soften the matrix. Any hardening that may have taken place at the molecular scale in the 1:1 group's lipid-cholesterol matrix due to dispersed cholesterol is presumably offset by the overall weakening of the matrix that results from phase separated cholesterol crystallites.

Differential Scanning Calorimetry

Differential scanning calorimetry is useful for determining the presence and quantity of highly ordered regions of crystalline or crystalline like molecules. It was used here to determine if there were peaks associated with phase separated cholesterol crystals in the DOPS coatings. There was not an expectation of seeing peaks associated with the plain DOPS composition, as its gel to liquid transition temperature (-11º C) and its complete melting temperature (150-157º C) were outside the measured range [76].

While useful for determining the occurrence of cholesterol crystals, XRD techniques are best combined with DSC in order to confirm the presence and type of crystalline cholesterol. DSC is a valuable tool for detecting cholesterol crystallites within phospholipid systems [100], [109] (and as discussed prior in Section While useful for determining the occurrence of cholesterol crystals, XRD techniques are best combined with DSC in order to confirm the presence and type of crystalline cholesterol. DSC is a valuable tool for detecting cholesterol crystallites within phospholipid systems [100], [109] (and as discussed prior in Section 2.3.2). DSC experiments at biologically relevant temperatures can detect a number of polymorphic phase transitions for cholesterol. Of particular interest is the triclinic crystal form shift that occurs while heating at about 37º C, from an 8 to a 16 molecule unit cell (see Section 2.3.2 for more detail). This polymorphic phase shift also doubles the length of the α-axis of the unit cell

[100], and has an associated enthalpy of transition of 0.81 ±0.21 kcal/mol (or 3.39 ±0.88 kJ/mol) [76]. Upon cooling, a large hysteresis takes place, with the transformation back to the 8 unit cell occurring at around 20-25º C [100]). DSC experiments at biologically relevant temperatures can detect a number of polymorphic phase transitions for cholesterol. Of particular interest is the triclinic crystal form shift that occurs while heating at about 37º C. This polymorphic phase shift also doubles the length of the α-axis of the unit cell [100], and has an associated enthalpy of transition of 0.81 ±0.21 kcal/mol (or 3.39 ±0.88 kJ/mol) [76]. Upon cooling, a large hysteresis takes place, with the transformation back to the 8 unit cell occurring at around 20-25º C [100].

Also of interest are the dehydration transitions of the monohydrate form of cholesterol at approximately 86º C and 95º C [100], [109]. Due to these high temperature dehydration peaks, it is useful to cycle the temperature to 100º C twice before cooling below 20º C in order to convert and monohydrate crystal that may be present into the anhydrous form. The anhydrous form is much more stable than the monohydrate form, and any converted monohydrate crystal usually takes days to weeks to reform into the monohydrate form [109]. Therefore, any peaks associated with the dehydration of the monohydrate crystal above 80º C will only appear during the first one or two heating cycles, after which it will be converted to the more stable anhydrous form.Also of interest are the dehydration transitions of the monohydrate form of cholesterol at approximately 86º C and 95º C [100], [109]. Due to these high temperature dehydration peaks, it is useful to cycle the temperature to 100º C twice before cooling below 20º C in order to convert and monohydrate crystal that may be present into the anhydrous form. The anhydrous form is much more stable than the monohydrate form, and any converted monohydrate crystal takes days to weeks to reform into the monohydrate form [109]. Therefore, any peaks associated with the

dehydration of the monohydrate crystal above 80º C will only appear during the first one or two heating cycles, after which it will be converted to the more stable anhydrous form.

12:1 Composition Group

For the 12:1 group, there were very few discernible peaks in any of the heating and cooling scans. There was a relatively large and broad peak occurring only in the first heating scan at 52.8º C (with an enthalpy of 5.36 J/g), and smaller endothermic peaks at about 96º C (enthalpies of 0.315-0.948 J/g) in all of the heating scans. The 96º C endothermic transitions are interpreted as being possibly associated with a water phase transition in the sample, as it would also be an endothermic peak. Additionally, this is proposed as it appears in each of the heating cycles, unlike the 96º C peak associated with a monohydrate cholesterol crystal dehydration which would only appear in the first 1 or 2 cycles [109]. Furthermore, the peaks reported in the literature associated with the monohydrate cholesterol crystal dehydration that are in the 96º C region have sharp, narrow profiles, unlike the ones seen in the 12:1 group [109]. For the 12:1 group, there were very few discernible peaks in any of the heating and cooling scans. There was a relatively large and broad peak occurring only in the first heating scan at 52.8º C (with an enthalpy of 5.36 J/g), and smaller peaks at about 96º C (enthalpies of 0.315-0.948 J/g) in all of the heating scans. The 96º C transitions are interpreted as being possibly associated with a water phase transition in the sample. This is proposed as it appears in each of the heating cycles, unlike the 96º C peak associated with a monohydrate cholesterol crystal dehydration which would only appear in the first 1 or 2 cycles [109]. Furthermore, the peaks reported in the literature associated with the monohydrate cholesterol crystal dehydration have sharp, narrow profiles, unlike the ones seen in the 12:1 group [109].

The large endothermic phase transition peak at 52º C is interpreted as being associated with an intimate association of DOPS and cholesterol molecules that form a mesophase that includes only dispersed cholesterol within the DOPS matrix (as opposed to phase separated cholesterol crystals). This phase likely is (or includes) a hexagonally packed lipid structure, as cholesterol is known to promote a stable formation of hexagonal packing in phospholipid systems [69]. This interpretation is further aided by the knowledge that previous studies have shown that cholesterol has a modest ability to increase the mobility and lateral diffusion of phospholipid molecules in bilayer lipid systems [160], [161], and can work to lower the gel to liquid transition temperature at higher concentrations (at greater than 20% mole percent cholesterol) [160].

In other words the cholesterol is acting as a type of plasticizer to the DOPS molecules, that is, in its dispersed state the cholesterol is intimately associating with both the lipid acyl chains and the head groups, thereby changing the conformational preferences of the molecule. This cholesterol induced change in preferred chain/molecule shape may be pushing the energy of the system towards a hexagonally packed form, as previously seen in other lipid and cholesterol systems [69]. It is likely that the 52º C peak results from a highly structured DOPS: cholesterol mesophase, due to the fact that the gel-liquid transition temperature the DOPS is much lower (-11º C), while the melting temperature of DOPS is much higher (150º C), and there are no repeating peaks that are associated with any form of cholesterol crystallites (at ~35º C, 86º C or 96º C).

1:1 Composition Group

In the 1:1 group, there was an endothermic peak at 38.1º C (enthalpy of 0.380 J/g) during the first heating scan, but not in the second high temperature heating scan (cycle 3). The initial peak at 38.1º C is interpreted as the anhydrous cholesterol crystal within the coating undergoing the polymorphic transition from an 8 to 16 unit cell. The second heating cycle (cycle 3) did not have this transition due to the fact that cycle 2 only cooled to 24º C, which is above the temperature required to convert the 16 unit cell back into the 8 unit cell. Cycling twice above 100º C converted any monohydrate cholesterol crystal to an anhydrous form [100]. After cooling to 0º C (and the associated phase change back to the 8 unit cell), the last two 0-100º C heating scans had peaks at about 33º C (with enthalpies of about 1.1 J/g).

According to the measured heat of enthalpy of 0.380 J/g in the initial 38º C peak, and from the known 0.81 ±0.21 kcal/mol anhydrous cholesterol polymorphic phase transition enthalpy, we can determine that there was approximately 13.4% [10.6-18.1% accounting for error] of the cholesterol in the anhydrous crystalline form at the initial state (or 0.321 g of the total 2.39 g of cholesterol in that sample's coating).

Subsequent high temperature cycles and the assumed conversion of any other crystalline forms into the anhydrous phase, the 33º C transition peaks from the last cycles can be used to determine the total initial percentage of cholesterol crystals in any form in the coating. Using the measured heat of enthalpies of 1.1 J/g in the 33º C peaks, and from the 0.81 ±0.21 kcal/mol transition enthalpy it is determined that there was approximately 39.2% [31.1-52.9%] of the cholesterol in crystalline form after conversion to the anhydrous state. Subtracting from the initial anhydrous state phase (13.4%), we can assume that approximately 25% [20.5-34.8%] of the initial cholesterol in the coating was converted into an anhydrous form after the initial two high temperature heating cycles. It is likely that the cholesterol that was converted to an

anhydrous form was in one of two states initially; a monohydrous crystalline phase or in an oligomeric phase (that is, a conglomeration of nearby cholesterol molecules that are not in a full crystalline state). It is most likely that it was initially in the monohydrate form. If it was in a separate oligomeric phase (that was possibly associated in or with the DOPS), it would have needed to be easily convertible to an anhydrous crystalline form in order to be measured in the DSC scans.

6.4.3 Conclusions

Scanning White Light Interferometry

The SWLI measurements statistically differentiated the coatings, and showed that adding cholesterol at both 12:1 and 1:1 molar ratios increased the SRa and SRz roughness of the coatings. Additionally, the coatings increased in thickness for the treatment groups with more cholesterol, as expected from the increased amount of coating being sprayed onto the cholesterol containing samples.

While both cholesterol containing groups were rougher than the DOPS group, their increases are attributed to different morphological phenomena. The 12:1 group had the highest roughness of all the groups (both SRa and SRz), and this is ascribed to the unique DOPS:cholesterol mesophase that formed (as indicated by DSC measurements). The 1:1 group was also significantly rougher than the DOPS group, and this is attributed to the apparent phase separation of cholesterol crystals in the coatings due to supersaturated levels of cholesterol in the coating. The strictly dispersed cholesterol in the 12:1 group caused a large amount (or all) of the DOPS structure to be converted into a secondary mesophase, while the 1:1 group had a large quantity of crystalline cholesterol that phase separated within the coating.

Nanoindentation

Nanoindentation methods developed above proved to be useful in the measurement of DOPS and cholesterol coatings, and provided mechanical properties for this particularly difficult to measure coating. The 12:1 group was found to have a significantly higher universal hardness, with an increase of over 70% compared to the pure DOPS case (from 17.6 MPa for the DOPS group to 25.3 MPa for the 12:1 group). This increase is attributed to a mechanically stiffer mesophase that formed through the addition of dispersed cholesterol in the lipid matrix. The 1:1 group was more similar in hardness to the DOPS group, and 1:1 groups decrease in hardness (compared to the 12:1 group) is attributed to widespread disruption of the DOPS microstructure due to phase separated cholesterol crystals. This is contrasted to the original hypothesis (6.4), that proposed that increasing cholesterol content would continue to increase coating hardness. It is now known that the dispersed cholesterol acts to harden the coating (as in the 12:1 group), but that the phase separated cholesterol crystallites act to soften the coatings (as in the 1:1 group).

Differential Scanning Calorimetry (DSC)

DSC was valuable for determining thermotropic behavior of the DOPS and cholesterol groups, and was able to detect the presence of phase separated cholesterol crystals within the coatings. In the 1:1 group, there were distinct endothermic peaks associated with the anhydrous form of crystalline cholesterol (at 38º C) in the first heating scan that correlated to an initial amount of 13.4% [10.6-18.1%] of phase separated anhydrous cholesterol crystals in the coating. After heating twice to 100º C from room temperature, any easily consolidated cholesterol and/or monohydrate crystalline cholesterol was converted to the anhydrous crystalline form and further full temperature cycles revealed that the total crystalline content of the coatings after conversion

was 39.2% [31.1-52.9%] of the original amount of cholesterol within the 1:1 group's coating. This suggests that future efforts should look to avoid concentrations of cholesterol greater than approximately 2:1 (DOPS:cholesterol) in order to avoid phase separated cholesterol crystallites and associated decreases in coating hardness.

For 12:1 composition, there was a large and broad primary peak at 52.8º C (enthalpy of 5.36 J/g), that is attributed to a DOPS and cholesterol mesostructure. There were no peaks associated with any crystalline form of cholesterol in the 12:1 group, indicating that the cholesterol remained in a dispersed state in the lipid matrix. It is notable that large 52º C peak only appeared during the first heating cycle (and not during subsequent cycles). It is suggested that this mesophase is not at a lowest energy state configuration due to its non-reversibility in the temperature range tested with DSC.

6.5 Chapter Summary

Prior work has shown that the addition of a calcium pretreatment was useful for controlling and extending coating elution times [17]. This work proposed to determine if the additional calcium pretreatment made a significant difference in the roughness or hardness of the coatings. It was found that neither parameter significantly changed by the addition of the calcium pretreatment, thus encouraging the calcium pretreatment's continued use. This is explained by the calcium pretreatment's localized effects near the substrate, and due to its limited ability to diffuse and affect the bulk properties of the coatings. The addition of calcium has already been shown to be a beneficial coating additive for controlling elution rates, [17] and may be continued for use as a surface pretreatment without negatively altering the coating's surface morphology or hardness.

Both the SWLI and Nanoindentation methods proved to be useful in the measurement of DOPS and cholesterol coatings. The nanoindentation method allowed the characterization of the hardness of DOPS and cholesterol coatings, of which the coating stiffness was found to be about 18 MPa for the DOPS composition and about 25 MPa for the 12:1 DOPS:cholesterol group. This work is the first time that the mechanical properties and surface morphology has been quantified for phospholipid implant coatings, and there has been little to no mechanical characterization of bulk systems of pure DOPS performed before. The nanoindentation method developed herein overcame the high surface roughness and highly plastic nature of the coatings by using a sharp Berkovich tip, a rapid loading rate, and a large number of indents in order to average the results and gain an accurate representation of the average coating hardness.

Cholesterol incorporation into DOPS coatings changes the microstructure of the coatings, and in the dispersed form, dramatically increases coating stiffness. Previous work has demonstrated the effectiveness of cholesterol in controlling the elution of DOPS and gentamycin coatings, but had little explanation for the cause of this phenomenon [17]. Additionally, it was not previously known that there was a threshold event after which increasing the cholesterol concentration acts to soften the coatings. It was assumed (as stated in Hypothesis 6.4) that increasing the cholesterol would lead to continued increases in coating hardness. This work has shown that cholesterol does indeed stiffen the matrix at lower concentrations (12:1), but then softens the coatings at high concentrations (1:1). Previous work [17] primarily used a concentration of 6:1 DOPS, which according to the results above, was likely maintaining a dispersed state of cholesterol (the upper limit for dispersed cholesterol appears to be at about a 2:1 ratio). The concentrations chosen in this work were 12:1 and 1:1, in order to bracket any phenomena in the previously used 6:1 concentration. With the discoveries presented above, it is

proposed that further development of DOPS and cholesterol coatings should seek to maximize the formation of this mesostructure of DOPS and dispersed cholesterol. This would prevent the formation of a phase separated crystalline cholesterol form to appear, given its negative effects on coating hardness and its phase transition peaks near body temperature.

Increasing cholesterol in order to improve mechanical properties of the coatings worked only to a point, after which additional cholesterol diminished coating properties. This work has elucidated the underlying mechanisms of these traits. The coating hardness and elution rate changes can be explained by the role cholesterol plays in stiffening the lipid systems by likely reordering its mesostructure while the cholesterol is in a dispersed state. The cholesterol has the greatest effect in hardening the lipid matrix at the 12:1 concentration, where it is below the saturation point that forms cholesterol crystallites. However, at high concentrations (the 1:1 group), the cholesterol mechanically weakens the DOPS:cholesterol matrix due to structurally disruptive cholesterol crystallites and because of increased mobility of the lipids due to the added cholesterol. While at the 12:1 concentrations, the cholesterol acts to stiffen the lipid matrix due to its ability to increase binding between the phospholipid head groups (while in a strictly dispersed state), and at higher concentrations, the cholesterol supersaturates into a crystalline form which disrupts the mechanical stability of the lipid structure.

These interpretations are reflected in the SWLI, DSC, and nanoindentation results from this chapter. The SWLI results show an increased roughness in the cholesterol containing coatings due to changed mesophases and phase separated cholesterol crystals (in the 12:1 and 1:1 groups respectively). The DSC results indicate the formation of phase separated cholesterol crystallites in the 1:1 group, while their presence is absent in the lower cholesterol concentration coating (the 12:1 group). Likewise, nanoindentation hardness results were significantly higher in

only the 12:1 group, strongly indicating a threshold event that the 1:1 group passes, resulting in a decreased matrix coherence and hardness.

6.6 Limitations

A disadvantage of e-spraying in atmospheric conditions is the lack of control of environmental conditions between e-spray sessions. Consequently, it is noted that batch to batch variance may have been exacerbated by spray sessions being conducted on different days. This was controlled for as much as was possible by spraying all samples for a given study at once if possible and by removing excess humidity from the e-spray room as needed (with a household de-humidifier).

Some of the nanoindentation samples were not able to be measured immediately after vacuum drying due to the length of time required for testing (1 week). It is possible that any ageing process may have affected some of the treatment groups more than others, though this effect was blocked for (randomized across treatments) in the study design, and was not found to be a statistically significant effect in the statistical model.

Due to variations between coatings within a given e-spray set, and from variations between e-spray sessions, there was limited ability to detect significant differences between groups. It was observed that some of the DOPS and cholesterol coatings had slightly uneven appearances, and this could have led to non-representative thickness and roughness measurements within a given sample. Due to this phenomenon, coating parameters were measured across a large number of samples. It is possible that a larger sample size may have helped further.

The DSC sample pans were prepared via an aerosol-sprayed deposition technique due to limitations in the e-spray process for coating DSC sample pans. The DSC instrument requires special hermetically sealed sample pans to be used for measurements, and the standard Ti_6Al_4V samples could not be used. E-spraying of the DSC pans was attempted, but it was not possible to deposit enough coating onto the pans in order to effectively measure phase transitions with DSC. The DSC measurement technique and instrument requires 5-10 mg of material in the DSC pan in order to take an effective measurement, and the e-spray process yielded less than 0.1 mg of coating on the pans while using approximately triple the amount of material normally e-sprayed per unit area. That is, even when e-spraying three times as much as normally deposited on a sample of similar size, the DSC pans were coated with less than 1% of the necessary amount of coating for an effective DSC measurement. It is possible that the e-spray deposition process produces a different microstructure and cholesterol crystal composition compared with aerosol-sprayed coatings. It is also conceivable that e-spraying the Aluminum DSC pan (that has cupped sides), even if it were possible, would produce an inherently different microstructure. Therefore, characterizing this difference would be useful in order to more accurately compare treatment composition changes for e-sprayed samples.

6.7 Future Work

Effort should be taken to reduce variability in samples from the e-spray process. It is likely that environmental changes (such as temperature and humidity in the chamber) during the e-spray process are a cause for variance and inhomogeneity in the coated samples. Gaining greater consistency in the manufacture process through tighter environmental control (possibly

through the use of a controlled environmental chamber) will aid further characterization, study and optimization of the coatings.

The non-significant results in coating hardness found here may be different after hydration of the coatings. Given the diffusion limited process of calcium on the Ti_6Al_4V substrate dispersing into the coating, it is likely that the tested samples (which were never hydrated), would be more prone to indicating significant differences in coating adhesion and mechanical properties after coming into contact with an aqueous environment. Changes in mechanical properties would also be more likely evident after hydration of the coatings, when the calcium ions are able to disperse through the coatings, and cause inter-headgroup binding of the DOPS [5], [91], [94]. The non-significant results in coating hardness found here may be different after hydration of the coatings. Given the diffusion limited process of calcium on the Ti_6Al_4V substrate dispersing into the coating, it is likely that the tested samples (which were never hydrated), would be more prone to indicating significant differences in coating adhesion and mechanical properties after coming into contact with an aqueous environment. Changes in mechanical properties would also by more likely evident after hydration of the coatings, when the calcium ions are able to diffuse through the coatings, and cause inter-headgroup binding of the DOPS [5], [91], [94]. This phenomena of diffused calcium under hydrated conditions may prove very difficult to test mechanically, but would prove useful if testing were successful, as it would allow further optimization of the coatings in and the coatings changes after immersion in biologically relevant media.

Only coatings with 12:1 and 1:1 DOPS to cholesterol concentrations were studied in this chapter, further work could continue these studies with other cholesterol concentrations. Due to the exploratory nature of this study, only a limited number of sample compositional groups could

be tested. With the knowledge gained herein about cholesterol crystal states and their cholesterol's limited diffusion into DOPS, it would be desirable to optimize the amount of cholesterol to DOPS, while avoiding excess cholesterol and resulting phase separation. The fact that the anhydrous cholesterol crystals in the 1:1 treatment group changed form at 37º C adds further reason to avoid concentrations above the phase separation point for cholesterol, as the coatings would possibly lose stability when implanted in the body. Future studies should therefore be undertaken to adjust the concentration of cholesterol to lipid ratio, relative to the mechanical, chemical, and biological environmental variables of consequence for the system to be designed.

It is suggested that future work prioritizes the minimization of cholesterol crystallite formation, as it has was found to decrease the mechanical properties of the coating, and its presence is generally associated with pathological states in biological systems [162]–[165]. Using the knowledge gained of the presence of cholesterol crystallites at high concentrations, effort should be taken to optimize the amount of, and type of, dispersed cholesterol in the lipid microstructures. It is likely that a solubility limit for cholesterol within e-sprayed DOPS coatings exists near a 2:1 ratio of DOPS to cholesterol given the results found above, and finding this critical concentration may prove valuable in maximizing coating hardness and retention. Additionally, it may be that certain DOPS:cholesterol superstructures (such as a hexagonal lipid structure) are only reproducible within narrow molar ratio ranges, or that they may be combined with other mesostructures. It would be helpful to pursue increased knowledge in this area and it may be useful to combine XRD and DSC techniques with NMR studies in order to gain further insights into the spacing and configuration of any repeating structures.

Along with cholesterol concentration optimization studies, further effort could be taken to characterize the elution profile of the DOPS and cholesterol coatings in biologically relevant media and environmental conditions. Since cholesterol undergoes crystalline phase transitions near body temperature [100], it would be useful to characterize and optimize coating parameters with this in mind (while noting that the saturation point changes with increasing temperature). Given the fact that cholesterol suppresses the gel to liquid transition temperature of many phospholipid systems [166], it may also be useful to look into mixtures of DOPS with other phospholipids that have a higher affinity to cholesterol (and are fully saturated) in order to develop a lipid system that is more easily able to form stable mesostructures (such as a hexagonal packed configuration).

An additional strategy that could be employed in future explorations is the use of layered cholesterol concentrations, that is, cholesterol could be sprayed at higher or lower concentrations near the substrate surface in order to further fine tune and control elution rates of the DOPS coating. As an example, this could allow for an initial bolus of coating and/or drug release that would be programmed into the coatings, with a gradual release thereafter. The near substrate layer of the coating could have a particularly tuned mesostructure, and the top layer(s) of the coating could have another, allowing for precise tuning of elution rates.

Chapter 7: Stability of Stored Phosphatidylserine Coatings

7.1 Purpose and Overview

One of the large practical concerns with research on these DOPS and cholesterol coatings is whether they change or degrade over time. Previous assumptions were that they were stable when stored in a clean, low humidity environment (a lab desiccator). Prior work generally assumed their stability and did not appear to pay careful attention to the exact age of the samples before performing analytical tests on the samples, as evident by a lack of precise sample history reporting [5], [17], [140].

It is not only pertinent to have further information about any changes that may take places in the coatings for research purposes, but also for the eventual development and commercialization of these coatings for use on medical implants. Due to a few coincidental discoveries, it was suspected that the coatings may indeed be unstable in ambient (atmospheric) conditions. This discovery was primarily prompted by the observation that coated samples changed in appearance (to the naked eye) over time after being left in ambient conditions.

Thus, the powerful quantitative SWLI measurement techniques recently developed (in Chapter 4) were used to explore any possible effects of ageing on the roughness of the samples, and to see if the desiccator storage condition was indeed a stable storage condition. DSC and XRD were then used to probe the microstructural changes associated with the roughness changes. The purpose of Chapter 7 was to analyze effects that storage (i.e., ageing) may have on the coatings, and whether there was constancy of the coatings in a vacuum desiccator, and whether they were unstable when left in ambient conditions. The hypotheses and specific aims for Chapter 7 are as follows:

Research Question 7.1: DOPS and cholesterol samples stored in a vacuum desiccator will maintain a stable surface roughness and coating thickness over time.

Specific Aims 7.1-1: Use SWLI to measure the coating roughness and thickness of DOPS and cholesterol coatings immediately following their manufacture, and again after 4 and 12 weeks of storage in a vacuum desiccator.

Hypothesis 7.2: DOPS and cholesterol samples stored in ambient conditions will change in surface roughness and microstructure over time due to changes that enhance molecular mobility and reconfiguration.

Specific Aim 7.2-1: Use SWLI to measure the coating roughness of DOPS and cholesterol coatings immediately following their manufacture, and after 4 and 12 weeks of storage in ambient conditions.

Specific Aim 7.2-2: Use differential scanning calorimetry to measure phase transitions of DOPS and cholesterol coatings immediately following their manufacture, and after 4 and 12 weeks of storage in ambient conditions.

Specific Aim 7.2-3: Use X-ray diffraction to characterize the crystalline microstructure of DOPS and cholesterol coatings immediately following their manufacture, and after storage in ambient conditions.

7.2 Experimental Methods

7.2.1 Sample Preparation

Samples were polished, cleaned, passivated and prepared as described previously in Sections 4.3, 5.4.1, 6.2.1 and 6.2.2 and according to Appendix A: Protocol A - Titanium Square

Sample Preparation and Protocol D - Titanium Passivation. Prior to coating with DOPS and cholesterol, some of the Ti6Al4V samples were pretreated in a calcium (Ca) salt solution as outlined in Appendix A: Protocol C.

7.2.2 Electro-Spray Coating Process

DOPS and cholesterol coatings were deposited on the cleaned and passivated 7.5x7.5 mm square Ti_6Al_4V samples using an electro-spray process (see Sections 2.4.3 and 6.2.2). Briefly, a 1.3% (vol%) DOPS in chloroform solution was e-sprayed onto Ti_6Al_4V samples using 12 kV, a pump rate of 14 mL/hr, and an 8 cm working distance. Ten Ti_6Al_4V substrates were E-sprayed at a time, with a spray time of 44.6 seconds per coat, with two coats applied with a short pause (about 2 minutes) between coats. These parameters were chosen to provide a final coating density of 1 mg of DOPS per cm^2 of sample. Some of the DOPS and cholesterol groups were sprayed eight samples at a time, with all spray parameters were kept the same, except the time of spray was varied such that the total amount of material sprayed on each sample remained the same.

After e-spraying, the coated samples were dried under a vacuum in a desiccator for at least 48 hours. Samples were stored similarly until utilized for analysis.

7.2.3 Incorporation of Cholesterol in the Coatings

Coatings that included cholesterol were e-sprayed with the same spray parameters of the DOPS only samples. Cholesterol was added into the 20mM DOPS-chloroform solution prior to e-spraying at concentrations of 12:1 and 1:1 DOPS:cholesterol. The resulting DOPS-cholesterol-chloroform solution was then e-sprayed onto the Ti_6Al_4V substrates as previously outlined (Section 6.2.2).

7.2.4 Scanning White Light Interferometry

Quantitative Measurement of Coating Morphology

Scanning White Light Interferometry (SWLI) was used to measure SRa and SRz as outlined previously in Sections 4.5.2 and 5.3.1. Briefly, a 100X objective with 0.5X zoom was used to measure the SRa and SRz surface roughness parameters in a 35 frame composite stitch area of 0.5x0.5 mm size. Each sample was tested once in the center of the sample. A custom script that allowed the capture and combination of a dual light level scan was utilized as needed.

Measurement of Film Thickness

Each sample's coating was scratched and measured for thickness using SWLI as outlined in Section 4.6.2. Briefly, prior to measuring with SWLI, a metal pick/awl was used to create a scratch through the sample coating and a custom mask and set of scripts in the MetroPro software was then used measure the lowest point in the scratch at 5 cross sectional areas within the composite stitch's field of view. These five depths were then averaged to determine the thickness of that particular sample.

Sample Groups and Test Time Points

Three compositions of coatings were used for the thickness, SRa and SRz measurements. The treatments were plain DOPS, 12:1 and 1:1(DOPS:cholesterol molecular ratios). Each of the treatments was repeated with the addition of a calcium substrate pretreatment (i.e., there were 6 treatment groups, half with a calcium treatment, and half without). In each treatment group, 6 samples were stored in a vacuum desiccator, and 6 samples were stored on a shelf in a 48 well plate in atmospheric conditions. This resulted in a total of 24 samples within each of the three coating composition categories (e.g., the 12:1 composition), 12 for the desiccator, and 12 for the

shelf storage locations. Of those 12, half had a calcium treatment, and half did not receive the calcium treatment.

All of the samples were tested immediately after drying for 48 hours in a vacuum desiccator, and then 4 weeks later, and again at 12 weeks from the first measurement time point. Given the time required to manufacture and test the thickness, SRa and SRz properties of the coatings, the three coating compositions were tested separately and in succession. That is, the DOPS treatment group samples were manufactured and tested the first week; the next week the 12:1 group was manufactured and tested, followed by the 1:1 group. The following week was the 4 week time point for the DOPS group, followed by the 4 week time point for the 12:1 group, and so on. A historical record of local atmospheric weather conditions during the time of the study can be found in Appendix D: Scanning White Light Interferometry Ageing Study: Measurement Time Points Schedule and Weather Almanac Tables.

Statistical Analysis

All data measured by SWLI was analyzed using the Proc Mixed procedure in SAS and was modeled as a 3 way factorial ANOVA model, separated by storage condition (i.e., modeled for the desiccator location, and again for the shelf location).

The 3 fixed effects modeled were the composition (DOPS, 12:1 or 1:1), the presence of calcium (yes or no), and the time at measurement (day-1, week-4, or week-12). A random effect was used to account for repeated measurements across time on the same samples. Up to 3-way interactions were allowed in the model. All groups had non-significant 3-way interactions and were next studied at their 2-way interactions if they existed, or else by dropping interaction effects from the model if none of the interactions were significant (at a $p = 0.05$ threshold). If

there were no significant interactions in the model between factors, this left an analysis of the main effects only (composition, calcium and time effects).

7.2.5 Differential Scanning Calorimetry (DSC)

Differential Scanning Calorimetry (DSC) sample pans were coated using an aerosol spray deposition method. An overview of the aerosol spray deposition method can be found in Appendix B: Atomizing Nozzle Spray Deposition Methodology Development. Two DOPS:cholesterol treatment groups were tested. A 20mM DOPS in chloroform solution was used for both groups, with cholesterol being added at a 12:1 (DOPS:cholesterol) and 1:1 molecular ratio (resulting in 1.667 mM and 20 mM cholesterol concentrations, respectively). Two mL of solution was sprayed onto three DSC pans for the 1:1 group, and 2.66 mL of solution sprayed onto two pans for the 12:1 treatment group. The coated pans were then left to dry under vacuum in a desiccator for at least 72 hours prior to testing with the DSC. One sample was tested immediately following removal from the desiccator, and a second sample was testing after being left in atmospheric conditions for two weeks.

A DSC 2920 Modulated DSC (TA Instruments, New Castle, DE) was used to analyze the phase transition of the DOPS and cholesterol coatings between 0 and 100C. A 2º C/min ramp rate was used to cycle the DSC sample from room temperature (24º C) to 100º C and back twice (i.e., two heating and two cooling ramps). The sample was then cooled all the way to 0º C, after which it was cycled up to 100º C and down to 0º C twice (for a complete total of 4 heating cycles, and 4 cooling cycles). One sample was tested for each treatment group at each time point.

The reason for choosing 8 heating and cooling cycles is due to the possible dehydration of the monohydrate cholesterol phase into the anhydrous phase. It has been noted that at least

two high temperature heating cycles (above 86º C) needs to be performed in order to ensure that all monohydrate cholesterol crystals have dehydrated to the anhydrous form [100]. The anhydrous crystalline form is then measureable by DSC from its polymorphic phase transitions at approximately 37º C and 20º C (during heating and cooling, respectively).

7.2.6 Glancing Angle X-ray Diffraction

A D8 Discover by Bruker AXS Inc. (Madison, WI) was used to measure the glancing angle X-ray diffraction patterns of DOPS coatings. An incident angle of 1º was used. A small angle (SAXS) scan range of 0.1º to 5º was performed in conjunction with a wide angle scan range of 5º to 80º. The step size used was 0.003º, and the time per step was 0.5 seconds. The samples tested were the same samples used for the SWLI thickness and roughness measurements. They were prepared as detailed in Section 6.2.2. Samples tested with XRD were allowed to age in atmospheric conditions for 9 months prior to testing. All samples were aligned prior to collecting, and a background spectrum was collected of an uncoated, cleaned, polished, and passivated Ti_6Al_4V sample substrate in order to compare with XRD results from the coated Ti_6Al_4V samples.

7.3 Ageing Study in Vacuum Desiccator

7.3.1 Purpose

The purpose of this section is to use SWLI to study coating surface morphology stability over time when the coatings are stored in a vacuum desiccator. Any changes will be tracked using the SRa and SRz roughness parameters, as well as by measuring the thickness of the coating. This section addresses the following research question:

Research Question 7.1: DOPS and cholesterol samples stored in a vacuum desiccator will maintain a stable surface roughness and coating thickness over time.

Specific Aims 7.1-1: Use SWLI to measure the coating roughness and thickness of DOPS and cholesterol coatings immediately following their manufacture, and after 4 and 12 weeks of storage in a vacuum desiccator.

7.3.2 Results

Coating Thickness

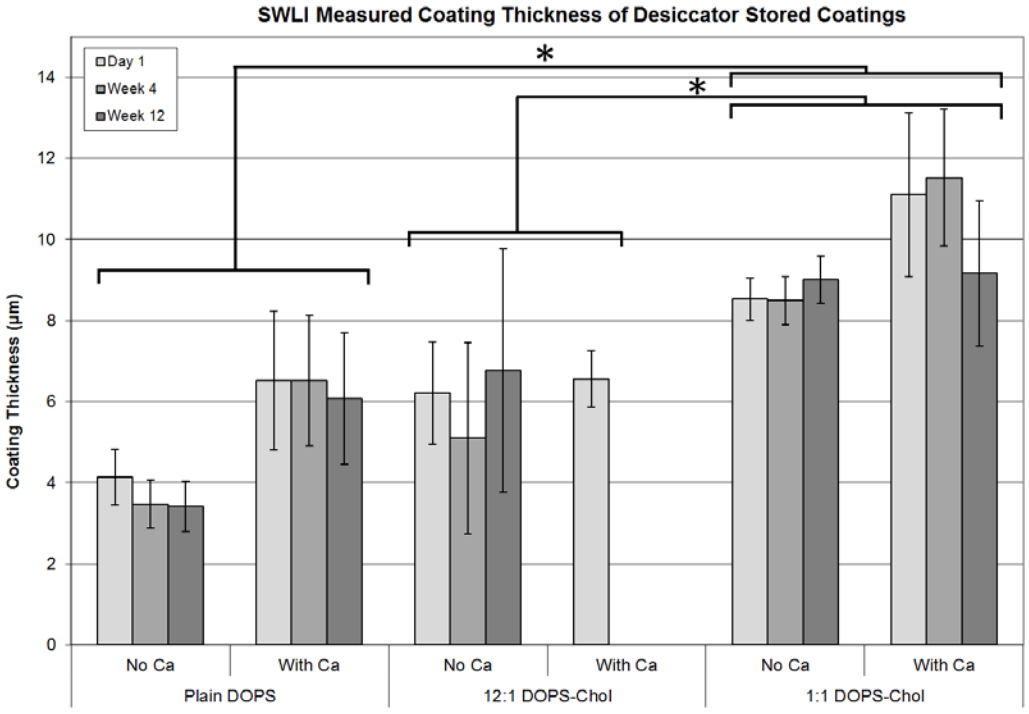

Figure 7-1 Thickness measurements from SWLI over time of DOPS and cholesterol coatings stored in a vacuum desiccator. N = 6 in each group and error bars represent the standard error of the mean. Significance between treatment groups is indicated by brackets and an asterisk.

The thicknesses of the various DOPS and cholesterol groups are shown in Figure 7-1. Light gray bars represent measurements taken on Day-1, and the bars in the graph darken as time

progresses to the darkest gray at the week-12 measurement. In the 3-way factorial ANOVA model (see Section 7.2.4: Statistical Analysis for more detail), only the treatment composition effect was significant (at $p = 0.0006$), the calcium and time effects were statistically insignificant at $p = 0.0640$ and $p = 0.3140$ respectively. With regard to the composition effect, both the DOPS and 12:1 treatments were significantly thinner than the 1:1 group ($p = 0.0003$ and $p = 0.0039$ respectively).

It should be noted that all but two of the 12:1 treatment group samples were lost after the day-1 measurement time point due to a lab incident. This resulted in increased standard errors or null measurements for the thickness, SRa and SRz at the following time points (weeks 4 and 12) within the 12:1 treatment group samples.

Coating Roughness

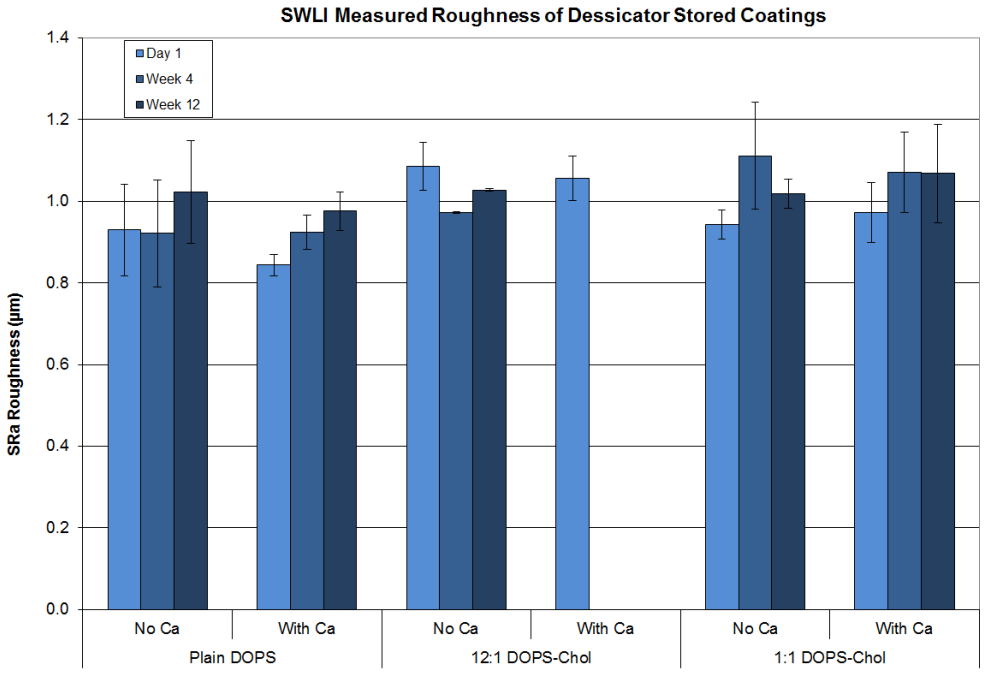

Figure 7-2 SRa roughness measurements from SWLI over time of DOPS and cholesterol coatings stored in a vacuum desiccator. N= 6 in each group and error bars represent the standard error of the mean and statistical significance is noted in Figure 7-3.

All of the SWLI measured SRa results can be seen in Figure 7-2. In the 3-way factorial ANOVA model (reference Section 7.2.4: Statistical Analysis for details), there were no-3 way interactions, but there was a significant composition by time interaction. When the data was examined further with an analysis of simple effects, the DOPS and 1:1 treatment groups had significant differences in SRa at various time points. These results are graphically represented in Figure 7-3.

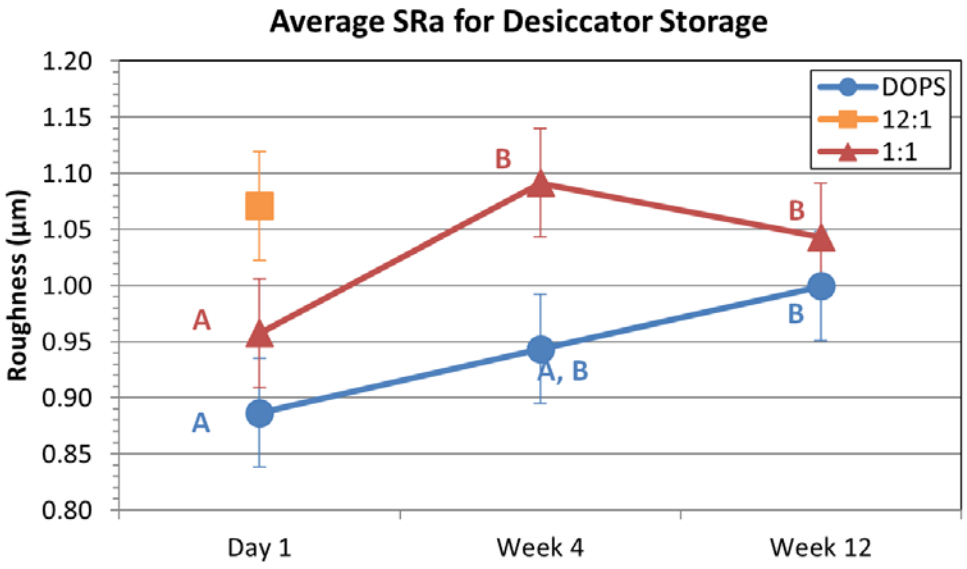

Figure 7-3 Average SRa roughness (µm) of DOPS and cholesterol coatings stored over time in a vacuum desiccator. Significance is indicated by letter groups; if bars share a letter, they are not significantly different.

In Figure 7-3, the mean SRa roughness for each time point is graphed by treatment group. Statistically, only a composition by time interaction was significant ($p = 0.0391$). When averaged across the other non-significant factors, the roughness at the individual time points differed significantly as represented by the letter groups in Figure 7-3. The Week-4 and 12 time points were significantly higher compared to the day-1 measurement in the 1:1 group ($p = 0.0009$ and $p = 0.0283$ respectively). For the DOPS group, the day-1 point was significantly lower than the week-12 time point ($p = 0.0046$).

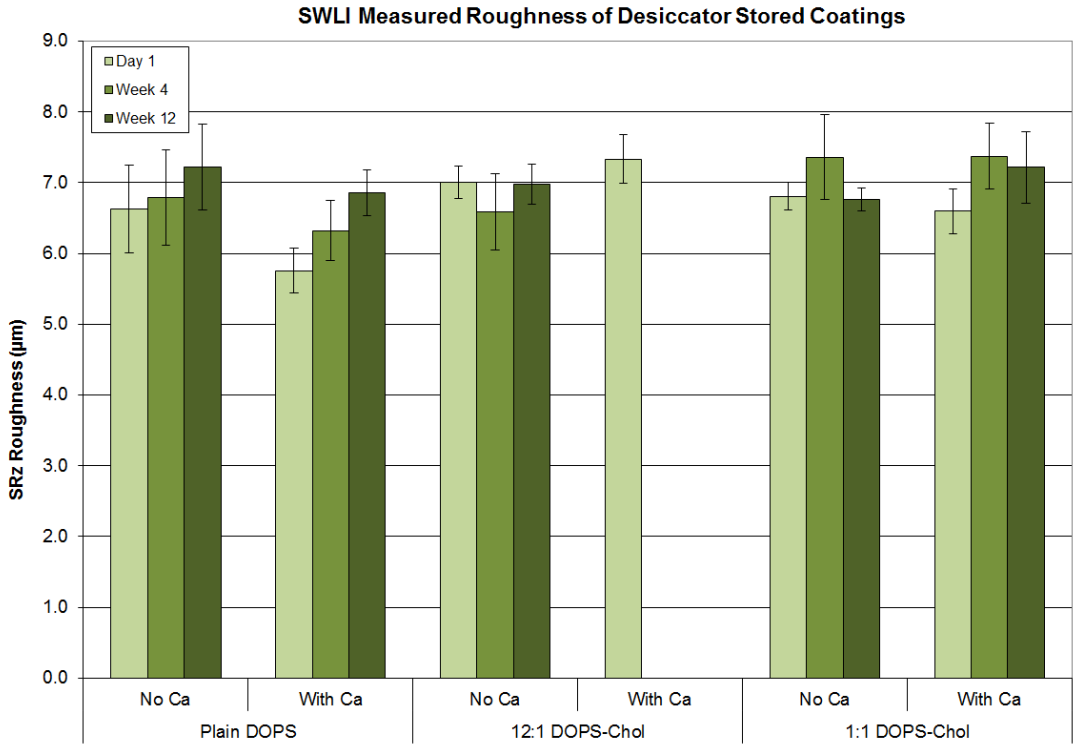

Figure 7-4 SRz roughness measurements from SWLI over time of DOPS and cholesterol coatings stored in a vacuum desiccator. N= 6 in each group and error bars represent the standard error of the mean and statistical significance is noted in Figure 7-5.

The SWLI measured SRz results can be seen in Figure 7-4. In the 3-way factorial ANOVA model, there were no 3-way interactions. There was a significant composition by time interaction, as well as a significant time effect. When the data was examined further with an analysis of simple effects from each of the compositions across time points, the DOPS and 1:1 treatment groups had significantly differing time points. These results are graphically represented in Figure 7-5.

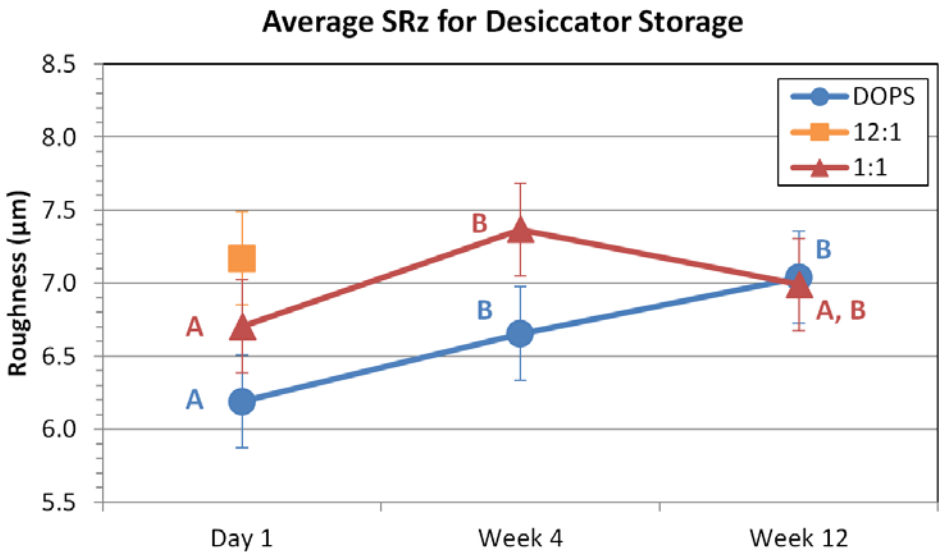

Figure 7-5 Average SRz roughness of DOPS and cholesterol coatings stored over time in a vacuum desiccator. Significance is indicated by letter groups; if bars share a letter, they are not significantly different.

As seen in Figure 7-5, the mean SRz roughness for each time point is graphed by treatment group. Statistically, the composition by time interaction was significant, as well as the time effect ($p = 0.0380$ and $p = 0.0447$ respectively). When averaged across the other factors, the roughness at the individual time points differed significantly as represented by the letter groups in Figure 7-5. In the 1:1 group, the Week-4 time point was significantly higher compared to the day-1 measurement ($p = 0.0014$). For the DOPS group, the day-1 point was significantly lower than the week-4 and 12 time points ($p = 0.0262$ and $p < 0.0001$ respectively).

7.3.3 Discussion

Coating Thickness

The coating thicknesses were not significantly influenced by the age of the samples in the desiccator storage condition. Significant differences did exist between compositions groups, as expected from the additional amount of material sprayed onto the substrates in the cholesterol containing groups. In particular, the 1:1 group was significantly thicker than the DOPS and 12:1

groups. This is explained by the fact that the 1:1 group had 48% more coating mass (0.831 mg, compared with 0.563mg for the DOPS group).

Coating Roughness

The coating roughness did have significant changes that were attributable to the passing of time for both the SRa and SRz roughness parameters. In the SRa measurements, there was a significant interaction between the composition and time. That is, time did not have a similar effect across all of the treatment groups. As seen in Figure 7-3 and Figure 7-5, the DOPS group steadily increased in roughness over time while the 1:1 quickly increased, and then stayed similar (or slightly decreased) in roughness at later time points. The SRz roughness showed a similar trend, with significant changes between time points for each treatment group. The fact that the treatment composition influenced the effect of time, indicates that the underlying phenomena that is causing change in the coatings is likely different for the DOPS vs 1:1 groups over the time period studied. The DOPS group seems to be undergoing a slow, but consistent change over time, while the 1:1 group seems to react quickly, and then stabilize after passing an equilibrium point.

It is worth noting that these significant changes happened across repeated measures on the samples, that is, each individual sample was keyed and re-measured in the same location at each time point. This combined with the high number of measured samples (24 within each treatment group) and the substrate surface polishing procedure developed in Section 5.4 allowed for a large ability to detect significant changes.

7.3.4 Conclusions

Contrary to Hypothesis 7.1, the coatings were found to change surface roughness over time, even when stored in a vacuum desiccator. The high statistical power of the study design, combined with the sensitive ability of the SWLI measurements to quantitate changes in coating surface morphology allowed for this discovery. Due to the significant interaction of the time and treatment effects in the SRa results, it is furthermore observed that the ageing effect was not constant across treatment groups. That is, the compositions reacted differently to the ageing process, indicating that there are likely separate microstructural reasons for the changes within each treatment group over time.

7.4 Ageing Study in Ambient Conditions

7.4.1 Purpose

The purpose of this section is to study any possible morphological changes to the coatings over time using SWLI. Any changes will be tracked using the SRa and SRz roughness parameters, as well as by measuring the thickness of the coating. Additionally, given the suspected changes in the ambient storage condition, studies will be undertaken of any thermal transitions in the coatings (using DSC), as well as any endpoint differences in glancing angle X-ray diffraction patterns (GAXRD). This section addresses the following research question:

Hypothesis 7.2: DOPS and cholesterol samples stored in ambient conditions will change in surface roughness and microstructure over time due to changes that enhance molecular mobility and reconfiguration.

Specific Aim 7.2-1: Use SWLI to measure the coating roughness of DOPS and cholesterol coatings immediately following their manufacture, and after 4 and 12 weeks of storage in ambient conditions.

Specific Aim 7.2-2: Use differential scanning calorimetry to measure phase transitions of DOPS and cholesterol coatings immediately following their manufacture, and after 4 and 12 weeks of storage in ambient conditions.

Specific Aim 7.2-3: Use glancing angle X-ray diffraction to characterize any crystalline microstructure of DOPS and cholesterol coatings after long-term storage in ambient conditions.

7.4.2 Results

Scanning White Light Interferometry (SWLI)

Coating Thickness

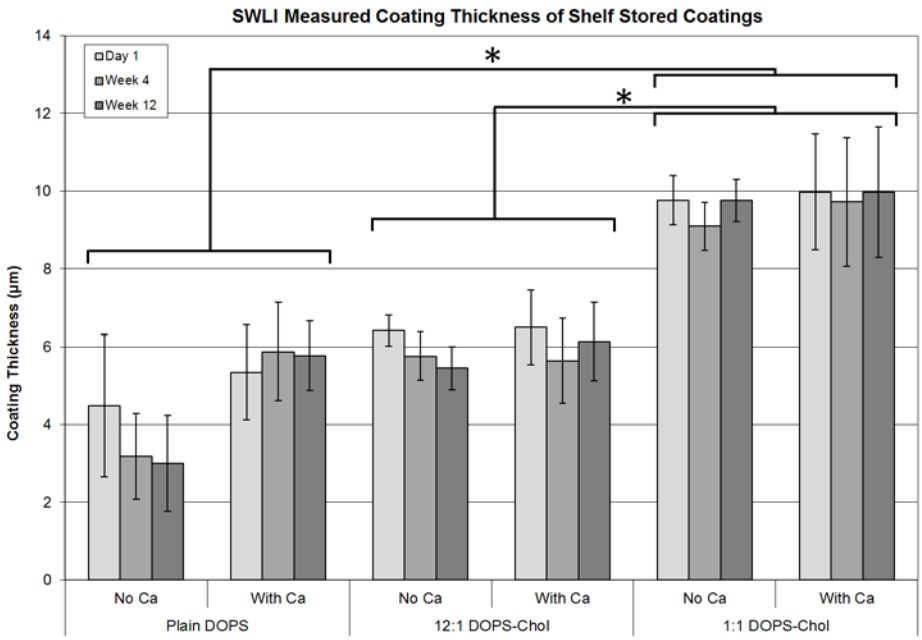

Figure 7-6 Thickness measurements from SWLI over time of DOPS and cholesterol coatings stored in a vacuum desiccator. N= 6 in each group and error bars represent the standard error of the mean.

As seen in Figure 7-6, the thicknesses of the various DOPS and cholesterol groups are listed for samples stored in ambient conditions. Light gray bars represent measurements taking on Day-1, and the graph bars darken as time progresses to the darkest gray at the week-12 measurement. In the 3-way factorial ANOVA model (see Section 7.2.4: Statistical Analysis for more detail), only the treatment composition effect was significant (at $p < 0.0001$), the calcium and time effects were statistically insignificant at $p = 0.2874$ and $p = 0.2905$, respectively. With regard to the composition effect, both the DOPS and 12:1 treatments were significantly thinner than the 1:1 group ($p < 0.0001$ and $p = 0.0007$ respectively).

Coating Roughness

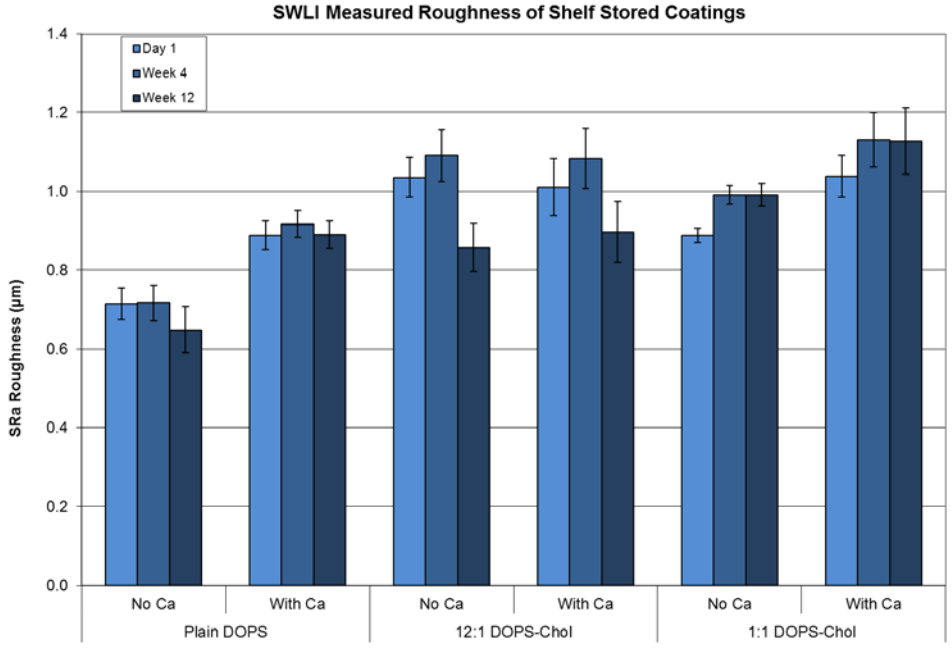

Figure 7-7 SRa roughness measurements from SWLI over time of DOPS and cholesterol coatings stored in a vacuum desiccator. N= 6 in each group and error bars represent the standard error of the mean and statistical significance is noted in Figure 7-8.

The SWLI SRa results can be seen in Figure 7-7. In the 3-way factorial ANOVA model (please see Section 7.2.4: Statistical Analysis for details), there were no 3-way interactions. However, there was a significant composition by time interaction, and all of the individual model effects were significant. The addition of calcium acted to increase the roughness across all treatments and time points ($p = 0.0115$). When the data was examined further with an analysis of simple effects for each of the treatments across each time point, all three treatment compositions had significantly differing time point measurements. These results are graphically represented in Figure 7-8.

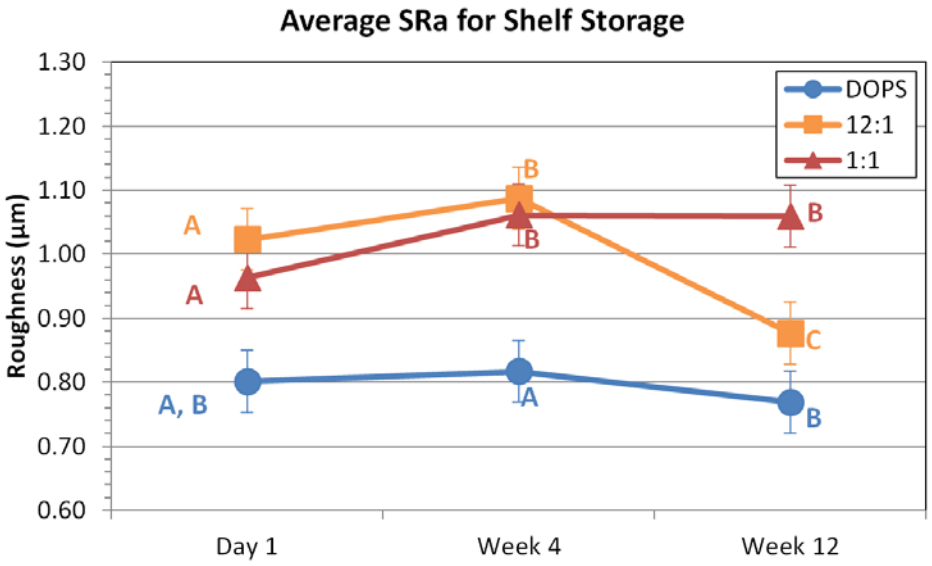

Figure 7-8 Average SRa roughness of DOPS and cholesterol coatings stored over time in ambient conditions. Significance is indicated by letter groups; if bars share a letter, they are not significantly different.

In Figure 7-8, the mean SRa roughness for each time point is graphed by treatment group. The composition by time interaction was statistically significant ($p < 0.0001$). Additionally, all of the individual factors were significant; composition ($p = 0.0002$), time ($p < 0.0001$), and calcium ($p = 0.0115$) effects. When averaged across the other factors, the roughness at the individual time points significantly differed as represented by the letter groups in Figure 7-8.

For the DOPS group, the Week-4 point was significantly higher than the week-12 time point ($p = 0.0141$). In the 12:1 group, the Week-4 time point was significantly higher than both the the day-1 and week-12 measurements ($p = 0.0012$ and $p < 0.0001$ respectively). The week-12 point was also significantly lower than the day-1 time point in the 12:1 group ($p < 0.0001$). Within the 1:1 group, the day-1 measurement was significantly lower than the week-4 and 12 time points (both at $p < 0.0001$).

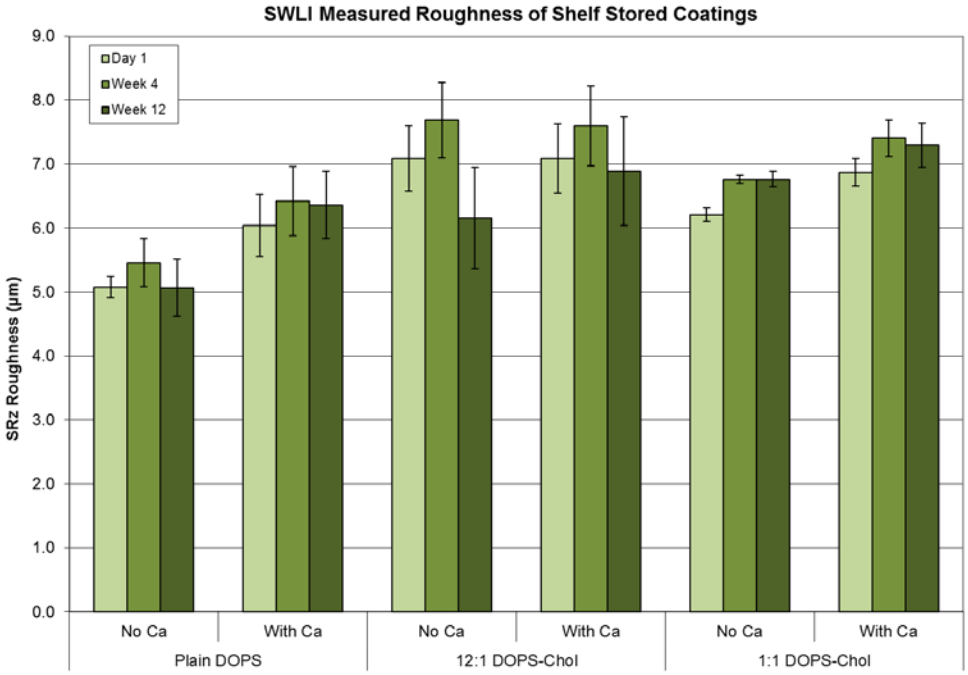

Figure 7-9 SRz roughness measurements from SWLI over time of DOPS and cholesterol coatings stored in a vacuum desiccator. Error bars represent the standard error of the mean and statistical significance is noted in Figure 7-10.

The SWLI SRz results can be seen in Figure 7-9. In the 3-way factorial ANOVA model, there were no 3-way interactions. There was a significant composition by time interaction, as well as a significant composition and time effect. When the data was examined further with an analysis of simple effects from each of the compositions across time points, all three treatment compositions had significantly differing time point measurements. These results are graphically represented in Figure 7-10.

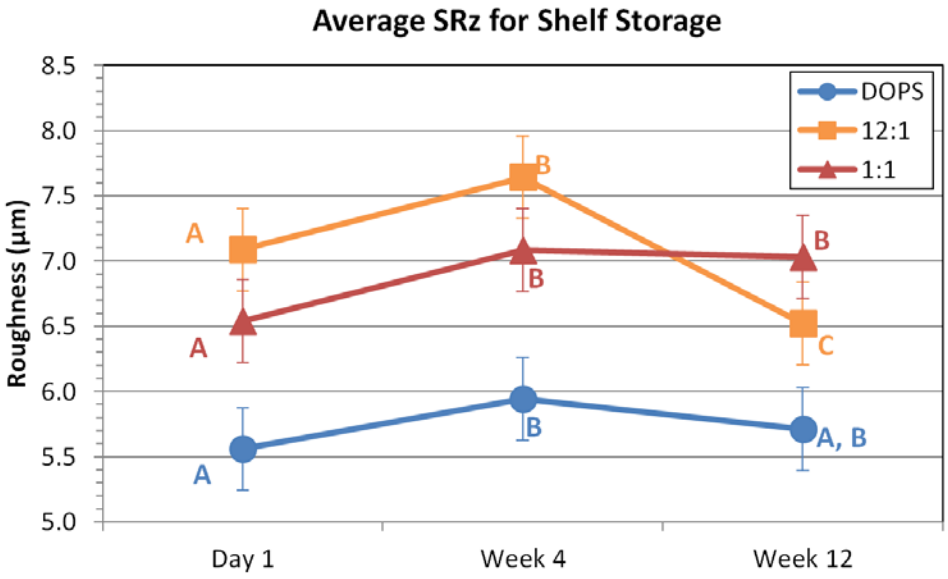

Figure 7-10 Average SRz roughness of DOPS and cholesterol coatings stored over time in ambient conditions. Significance is indicated by letter groups; if bars share a letter, they are not significantly different.

The mean SRz roughness for each time point is graphed by treatment group in Figure 7-10. Statistically, the composition by time interaction was significant ($p = 0.0004$), as were both the time and composition effects ($p < 0.0001$ and $p = 0.0117$ respectively). When averaged across the other factors, the roughness at the individual time points differed significantly as represented by the letter groups in Figure 7-10.

For the DOPS group, the day-1 point was marginally significantly lower than the week-4 time point ($p = 0.0451$). In the 12:1 group, the Week-4 time point was significantly higher than both the the day-1 and week-12 measurements ($p = 0.0044$ and $p < 0.0001$ respectively). The week-12 point was also significantly lower than the day-1 time point in the 12:1 group ($p = 0.0038$). For the 1:1 group, the day-1 measurement was significantly lower than the week-4 and 12 time points ($p = 0.0052$ and $p = 0.0110$ respectively).

Differential Scanning Calorimetry (DSC)

A representative DSC scan can be found in Chapter 6: Figure 6-8. A full compilation of figures with all of the individual DSC scans for both compositions and both time points can be found in Appendix C: Differential Scanning Calorimetry Measurements for DOPS and cholesterol coatings. These results have been tabulated below in Table 7-1.

Table 7-1 Compiled list of heat of enthalpies associated with specific peaks from DSC scans of the 12:1 and 1:1 DOPS:cholesterol groups. Heating scans are indicated by a light red background, and cooling scans with a light blue background. Exothermic peaks have a negative sign preceding the measurement.

		12:1 (DOPS:cholesterol)				1:1 (DOPS:cholesterol)		
		Day 1		Week 2		Day 1	Week 2	
		Peak 1	Peak 2	Peak 1	Peak 2	Peak 1	Peak 1	Peak 2
Cycle 1 (24-100°C)	Peak Temp (°C)	52.76	95.79	58.84	96.84	38.06	38.42	95.74
	Onset Temp (°C)	40.26	87.8	56.61	92.95	36.03	36.51	91.75
	Enthalpy (J/g)	5.362	0.9478	7.199	0.4474	0.3798	0.7604	0.618
Cycle 2 (100-24°C)	Peak Temp (°C)	NA		NA		NA	-20.19	
	Onset Temp (°C)	NA		NA		NA	-22.78	
	Enthalpy (J/g)	NA		NA		NA	-1.108	
Cycle 3 (24-100°C)	Peak Temp (°C)	96.36		96.74		94.98	33.32	96.2
	Onset Temp (°C)	92.66		92.15		92.2	31.37	61.68
	Enthalpy (J/g)	0.3152		0.3888		0.167	0.1394	0.4813
Cycle 4 (100-0°C)	Peak Temp (°C)	NA		-96.97		NA	-38.42	
	Onset Temp (°C)	NA		-92.88		NA	-36.51	
	Enthalpy (J/g)	NA		-0.172		NA	-0.7604	
Cycle 5 (0-100°C)	Peak Temp (°C)	96.29		96.97		33.73	34.51	96.35
	Onset Temp (°C)	89.77		92.88		29.66	31.64	90.69
	Enthalpy (J/g)	0.7671		0.172		1.033	1.159	0.5983
Cycle 6 (100-0°C)	Peak Temp (°C)	NA		NA		-19.01	-20.19	
	Onset Temp (°C)	NA		NA		-23.4	-22.78	
	Enthalpy (J/g)	NA		NA		-0.9037	-1.108	
Cycle 7 (0-100°C)	Peak Temp (°C)	96.26		48.91	96.87	33.43	34.19	96.17
	Onset Temp (°C)	90.47		41.48	91.33	29.18	31.51	90.89
	Enthalpy (J/g)	0.6867		0.107	0.5666	1.109	1.112	0.5181
Cycle 8 (100-0°C)	Peak Temp (°C)	NA		-43.61		-20.1	-33.32	
	Onset Temp (°C)	NA		-51.42		-24.15	-31.37	
	Enthalpy (J/g)	NA		-0.3548		-0.9746	-0.1394	

As seen in Table 7-1, all of the peaks for each run of the DSC scans are recorded. Results are discussed below, by treatment group.

12:1 Composition

At the day-1 measurement in the 12:1 group, the first heating scan had a large, endothermic broad peak at 52.8º C, and none of the cooling scans had any significant peaks. All of the heating cycles had small, broad endothermic peaks at about 96º C.

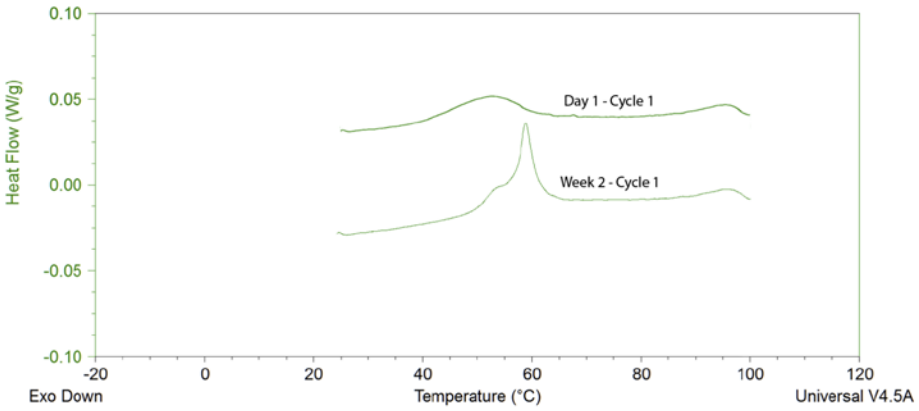

Figure 7-11 Cycle 1 heating scans from the DSC of the 12:1 group, at Day-1 and Week-2. Curves are displaced along the y-axis for presentation. Scan rate was 2ºC/min, exotherms point downward.

For the week-2 time point, the peak locations were at similar locations, except for the large peak at 52.8º C, which shifted to a higher temperature (as seen in Figure 7-11). There were also the additions of several more of the small, broad peaks at 96º C. The large broad endothermic peak that was at 52.8º C in the day-1 measurement shifted to the right (to a peak of 58.8º C), and sharpened considerably, while still maintaining a visible shoulder at the 52.8º C temperature.

1:1 Composition

In the 1:1 group at the day-one time point, all of the peaks were at one of two primary locations, endothermic peaks around 33º C during the heating cycles, and exothermic ones at 20º C during the cooling cycles. During the heating cycles there were endothermic peaks at 38º C (in cycle 1), and then at 33º C in cycles 5 and 6. During the 100-0º C cooling cycles (cycles 6 and 8) there were peaks at 20º C.

For the second weeks measurement, the peak locations were at similar locations overall, with the addition of several more of the small, broad peaks at 96º C. Additionally, the peak at 38º C during the first heating cycle increased slightly in size from week one to week-2 (from an enthalpy of 0.380 J/g to 0.760 J/g), while maintaining a similar shape.

Glancing Angle X-ray Diffraction (GAXRD) Results

The wide angle X-ray scattering results for DOPS, 12:1 and 1:1 groups aged in ambient conditions can be found in Figure 7-12. The small angle X-ray scattering results for the same groups can be found in Figure 7-13.

A background XRD spectrum of uncoated Ti_6Al_4V (that was polished, cleaned and passivated similar to the coated samples) was tested in both the small and wide angle regions. The background spectra did not exhibit any significant peaks, and can be found in Appendix E: Glancing Angle X-ray Diffraction Background.

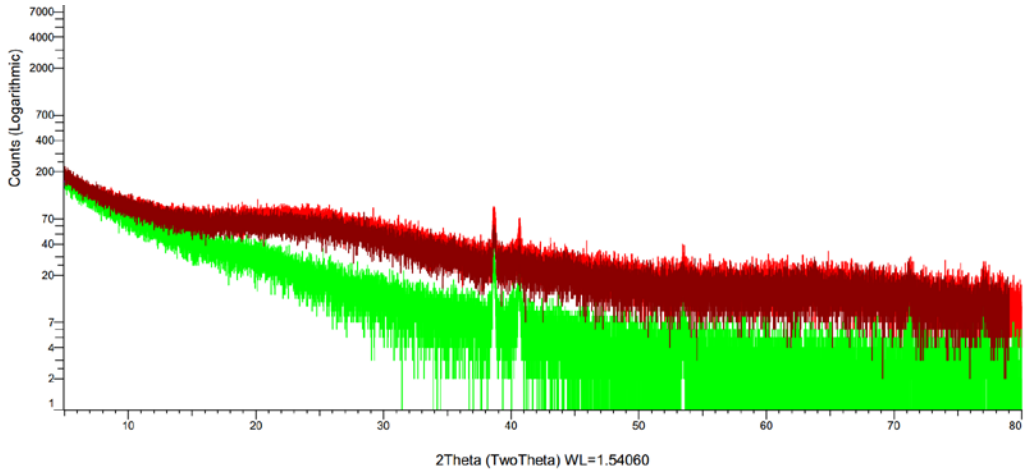

Figure 7-12 Stack of wide angle X-ray scattering profiles for DOPS, 12:1 and 1:1 samples aged in ambient conditions. Y-axis in arbitrary units of detector counts. The bright red line is DOPS, green line is 12:1, dark red line is the 1:1 group.

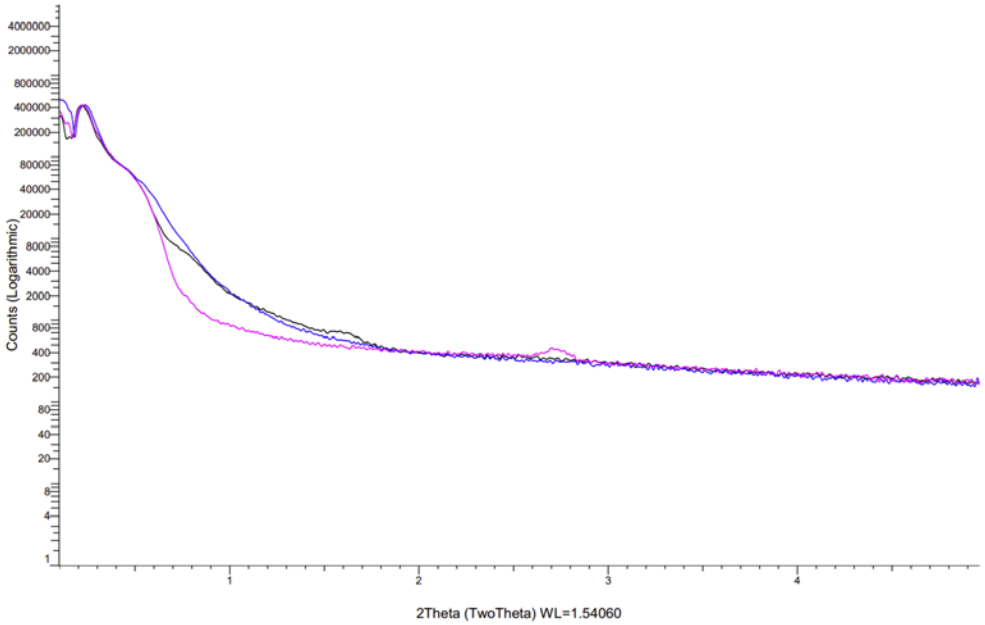

Figure 7-13 Stack of small angle X-ray scattering profiles for DOPS, 12:1 and 1:1 samples aged in ambient conditions. Y-axis in arbitrary units of detector counts. Blue line is DOPS, dark blue line is 12:1, magenta line is the 1:1 group.

As seen in the Figure 7-12, the wide angle X-ray spacing results are similar between the compositional groups, with peaks at about 38.8, 40.7 and 53.5 2theta. These correlate to a lattice spacing of 2.34 Å, 2.22 Å and 1.71 Å respectively. Peak matching did not indicate that the peaks

in either range matched with titanium, nor any other relevant/similar material to what was actually tested.

In the small angle region (Figure 7-13), the groups showed differences between treatments. The 12:1 group had a unique peak at 1.6 2theta, which correlates to a spacing of 55 Å. The 1:1 group had a unique peak at 2.7 2theta, which correlates to a spacing of 32.5 Å. The DOPS group was void of either of these peaks, but had a larger shoulder in the 0.6-1.2 2theta region (~14.7-7.4 nm spacing distance). The 1:1 group had the smallest shoulder in this region.

7.4.3 Discussion

Scanning White Light Interferometry

Coating Thickness

The coating thicknesses were not significantly influenced by the age of the samples in the ambient storage condition, though significant differences did exist between composition groups, similar to what was found in the desiccator storage location. This result of thicker coatings in the cholesterol groups is not surprising given the additional amount of material sprayed onto the substrates in the cholesterol containing treatments.

Coating Roughness

The coating roughness did have significant changes that were attributable to the passing of time, and for the effect of treatment with both the SRa and SRz roughness parameters. There was a significant composition by time interaction in both roughness parameters. Additionally, for the SRa measurements, there was a significant effect from the addition of calcium in the interaction between the composition and time.

The interpretation of the treatment by time interaction is similar as what was discussed for the desiccator storage location, that the time factor did not have a similar effect across all of the treatment groups. As seen in Figure 7-8 and Figure 7-10, the DOPS group stayed generally similar and slightly decreased in roughness over time. The 1:1 increased, and then plateaued in roughness after week-4. In contrast to those groups, the 12:1 composition had a fully significant trend reversal of first increasing, and then decreasing roughness from the day-1, to week-4, and then week-4 to week-12 time points.

These trends are interpreted as stemming from the 12:1 group undergoing a two or three state phase shift, with each state having different roughnesses associated with them. In other words, the initial, day-1 microstructure and mesophase is likely changing slowly over time into another, lower energy phase state which has as higher roughness, before it eventually transfers into a third state that has a much lower roughness (this would be a three phase explanation). Another possibility is that the system is undergoing a transition between two phases, and that the in-between (transitory) state happens to be more rough than either the beginning or end states (this is a two phase explanation).

It is interesting to note that calcium had a significant effect ($p=0.0115$) on the SRa roughness over time. It acted to increase the roughness of treatments, across all other factors. This result confirms the suspicions of Section 6.3, that calcium does indeed have an effect on the coatings, but needs time in order to diffuse through the coating and produce a significantly measurable effect.

Differential Scanning Calorimetry (DSC)

DSC was useful for determining the thermotropic behavior of the DOPS and cholesterol groups at different ages. For further background and discussion on the utility of DSC for determining crystalline cholesterol please reference Sections 2.3.2 and 6.4.2.

In the 1:1 group, there were distinct peaks associated with the anhydrous form of crystalline cholesterol (at 38º C) in the first heating scan that correlated to an initial amount of 13.4% [10.6-18.1% accounting for error] of phase separated anhydrous cholesterol crystals in the coating. After heating twice to 100º C from room temperature, any easily consolidated (e.g., oligomeric cholesterol that was easily convertible to an anhydrous form) and/or monohydrate crystalline cholesterol was converted to the anhydrous crystalline form, and subsequent full temperature cycles revealed that the total crystalline content of the coatings after conversion was approximately 39.2% [31.1-52.9%] of the total amount of cholesterol in the coating. In other words, the annealing effects of the DSC tests resulted in an increase in cholesterol crystallinity just as seen with desiccator storage.

At the week-2 time point, the 1:1 group's coatings maintained a similar peak distribution, with the primary difference being the enlargement of the cycle 1 peak at 38º C. The enthalpy increased 0.380 J/g to 0.760 J/g from day-1 to week-2 in this peak, while maintaining a similar shape. This is interpreted as an increase in the anhydrous crystalline cholesterol to a level of 26.9% [21.3-36.3%] at the week-2 time point. After the first two high temperature cycles (and associated conversion of any monohydrate cholesterol crystals to the anhydrous form), the total anhydrous crystalline content was similar to that of the day-1 measurement at 40.9% [32.5-55.25%]. This indicates that the total amount of easily formable anhydrous crystalline cholesterol in the sample stays fairly constant over the two weeks, but that the initial amount of anhydrous

crystalline cholesterol in the sample is slowly increasing with time. That is, at the time one measurement, only 13.4% of the cholesterol in the sample appeared in the first heating cycle's anhydrous peak, while in week-2 measurement this number increased to 26.9%.

For the 12:1 composition at day-1, there was a large and broad primary peak at 52.8º C (enthalpy of 5.36 J/g) that is attributed to a DOPS (with dispersed cholesterol) mesostructure. There were no peaks associated with any crystalline form of cholesterol in the 12:1 group, indicating that the cholesterol remained fully dispersed within the lipid matrix. This large 52º C peak only appeared during the first heating cycle (and not during subsequent cycles).

For the week-2 time point, the 12:1 group's coating maintained a similar looking set of peak locations, except that the large peak at 52.8º C shifted to a higher temperature (see Figure 7-11). The large and broad endothermic peak that was at 52.8º C in the day-1 measurement shifted to the right (to a peak of 58.8º C), and sharpened considerably, while still maintaining a visible shoulder at 52.8º C. This is interpreted as shift in the mesophase of the DOPS and dispersed cholesterol to a more consolidated and lower energy state. The broad shouldered initial peak at 52.8º C likely is the result of a range distribution of non-homogenous mesophases (likely a hexagonal packed structure), that gradually turns into a more uniform structure over time (to the sharp 58.8º C peak). This temperature region is similar to what has been seen in other lipid systems with a hexagonal packing structure [111].

X-ray Scattering Results (SAXS and XRD)

Ordered cholesterol structures and lipid mesophases can be studied with X-ray scattering techniques. Both the monohydrate and anhydrous forms of crystalline cholesterol have a bilayer type structure with a repeating space of about 34 Å [167], [168]. This spacing leads to X-ray

diffraction peaks in the small angle region of the spectrum. Because the spacing is the same for both the monohydrate and anhydrous forms of the crystalline cholesterol, XRD is only useful for determining the presence of crystalline cholesterol, and not the specific phase of the crystal.

The small angle X-ray diffraction region (Figure 7-13) was able to differentiate the treatment groups, with the 12:1 group having a unique peak at 1.6 2theta (correlating to a spacing of 55 Å). This spacing is presumed to be related to the DOPS with dispersed cholesterol mesophase that has been proposed (Section 6.4.2), as it is unique to the 12:1 group and is in the correct size scale range for hexagonal packing of DOPS systems [169].

The 1:1 group had a unique peak at 2.7 2theta (32.5 Å), which is in agreement with the spacing that has been associated in the literature with crystalline cholesterol (of approximately 34 Å) [100], [167], [168]. This result corroborates the results of the DSC tests, that the 1:1 does indeed contain phase separated cholesterol crystallites.

The DOPS group was void of both of these peaks, indicating a lack of cholesterol crystals or unique mesophase. It did however contain the largest shoulder in the 0.6-1.2 2theta region (~14.7-7.4 nm spacing region), which is likely due to a distribution of DOPS lamellar spacings. Typical bilayer spacing in a plasma membrane ranges from 5-10 nm [170]. Of note, the 1:1 treatment had the smallest shoulder in this (~14.7-7.4 nm spacing region, indicating that there may be a higher level of conformity of any lamellar spacing within this coating.

It is worth noting that the polishing procedure developed in Section 5.4 proved essential for the XRD measurements of the DOPS coatings. The measurements would not have been possible if the substrates had not been polished first, as the signal to noise ratio would have been too low due to excess beam scattering.

7.4.4 Conclusions

SWLI

It was found that there are indeed significant changes over time in surface morphology for coatings stored in ambient conditions. There were significant effects from time, composition, and calcium on the coatings' morphologies over time. Additionally, there was a treatment by time interaction, indicating that the ageing effect was not consistent across treatment groups. It is therefore concluded that the storage location and age of the sample is a critical consideration for the future development and analysis of DOPS and cholesterol coatings.

Differential Scanning Calorimetry Conclusions

DSC results were able to differentiate the coatings, and provided valuable insights to the different coating compositions and their microstructural states and crystalline cholesterol contents. Anhydrous cholesterol crystals were immediately observable in both of the 1:1 time points, and the initial amount increased from 13.4% of the total coating's cholesterol content at the day-1 point, to 26.9% in the week-2 measurement. The amount of easily consolidated anhydrous cholesterol crystal (cholesterol that converted to an anhydrous form after high temperature cycling) remained nearly constant at both measurements, at about 40% of the total coating cholesterol content.

The 12:1 group also demonstrated a change over time, with the large, broad peak at 52.8º C sharpening and shifting to a higher temperature of 58.8º C. This peak is associated with the mesophase of the DOPS and dispersed cholesterol consolidating to a more homogenous and ordered state. There were no peaks in the 12:1 group associated with cholesterol crystals, indicating that the cholesterol exists in a fully dispersed state within the DOPS structure.

Glancing Angle X-ray Diffraction

Glancing angle XRD also proved to provide useful insight into the DOPS and cholesterol coatings, and showed differences between the treatment groups, particularly in the small angle region. GAXRD served to elucidate and confirm results found with DSC. There were unique peaks in both of the cholesterol containing groups. In the 1:1 group, the peak at 2.7 2theta (32.5 Å) confirmed the existence of crystalline cholesterol in the 1:1 group. The 12:1 group had a unique peak at 1.6 2theta (correlating to a spacing of 55 Å), which is presumed to be associated the DOPS and fully dispersed cholesterol mesophase that was also found in the DSC results. The DOPS group was void of both of these peaks, but had a larger shoulder in the 0.6-1.2 2theta region (~14.7-7.4 nm spacing region), most likely indicating a distribution of similar lamellar bilayers.

7.5 Chapter Discussion

The day-1, week-4 and week-12 time points in this study were chosen due to limitations in the time required to manufacture and measure the samples. The first week of the study was consumed in the preparation and testing of the DOPS treatment group, the second week for the preparation and treatment of the 12:1 group, and the third week for the 1:1 group. This allowed for the immediate continuation of measurements on the DOPS group the following week, for that groups 4-week time point, and so on.

Within each treatment group, there were 24 samples (half with calcium, and half again split towards either the desiccator, or ambient storage location). On each sample, there were two measurement locations for SWLI, one for measuring the thickness (see Section 4.6), and one for

measuring the roughness (see Section 4.5). At each of the sample's two measurement locations, the thickness or roughness parameters were calculated within a 35-frame composite stitch area. That is, there were 70 individual capture frames for each of the 72 samples (5040 frames), all repeated at each of three time points.

Differences between Desiccator and Ambient Storage Conditions

The effects of ageing, while present in at both storage locations, were not similar in their effects for each treatment composition. The DOPS group in particular reacted differently over time when in the desiccator storage location compared to ambient storage, while the 1:1 group reacted similarly in both storage locations. In the statistical ANOVA model (detailed in Section 7.2.4), only 3 factors were included in the model (composition, calcium, and time). If the analysis is re-run including all 4 factors (composition, calcium, time, and location), the model shows a significant three-way interaction between the composition, time and storage location for both SRa and SRz roughness parameters ($p = 0.0007$ and $p = 0.0027$ for SRA and SRz respectively). This indicates statistically, that in addition to the time effect changing coatings differently over time, the location also plays a role in how the coatings age (and the effect is not similar across all the treatments).

Desiccator Storage Condition

A structure function interpretation for the reason for change over time for the treatment groups in the desiccator storage location is proposed as follows; the DOPS group may be continuing to undergo a consolidation into multilamellar vesicles, as it is a lower energy state than the more disordered, as-sprayed state. These multilamellar vesicles would appear rougher as

they continued to conglomerate and incorporate less ordered lipids from their surrounding environs.

The 1:1 group is likely consolidating anhydrous cholesterol crystals over time, that is, the initially supersaturated cholesterol crystals that formed during spraying continue to ‘grow’ over time because they are at a lower energy state than the nearby dispersed cholesterol molecules. As the cholesterol crystals consolidate and grow over time before reaching an equilibrium state, this results in an increase in coating roughness over the short term (due to the sharp anhydrous crystals growing) that then plateaus in the long term (as the crystals reach an equilibrium size).

Ambient Storage Condition

A proposed structure function interpretation for the cause of change over time for the treatment groups in the ambient storage location is as follows; the DOPS group is likely reordering to a lower energy state in the ambient environment as well, but as it has the ability to incorporate water from the atmosphere, it is likely that the lowest energy state would be a multilamellar structure that is more planar in configuration (as apposed to vesicle shaped). The water that would be incorporated in the coating would make it difficult for multilamellar structures to swell in a spherical (vesicle) configuration, and would instead drive the system to a stratified planar configuration. This would result in a minimal amount of change to the coating roughness, or a decrease in roughness, as observed in the data collected above.

The 1:1 group is likely undergoing a very similar process as in the desiccator location and consolidating cholesterol crystals over time. These cholesterol crystals would be at lower energy state than the nearby dispersed cholesterol molecules, driving a consolidation and growth over time before they reach an equilibrium state. This would result in an increase in coating roughness

over the short term that then plateaus in the long term (for similar reasons as in the desiccator storage location).

The 12:1 group is likely undergoing a two state transition over time, where the first state is a macroscopically disordered conglomeration of individual regions of a hexagonally packed phase. Over time, these un-aligned mesophases consolidate into a more tightly packed and repeating phase, which results in increased roughness in the short term, and an eventual decrease in roughness as the mesophase becomes more homogenous. This explanation coincides with what is seen in the initial, broad DSC peak at 52º C (numerous domains of the mesophase), followed a consolidation to a second state of a more consolidated and homogenized mesophase that results in a shift and sharpening of the DSC peak at 58º C (and associated 55 Å XRD spacing result).

7.6 Chapter Summary

The overarching goal of this chapter was to find out whether these coatings are stable, or change over time with storage. This goal was met, and it was conclusively answered that the coatings do indeed change over time, even when stored in a clean, dry environment (a vacuum desiccator). This result was counter to previous assumptions, and has profound implications to the future development and study of these DOPS and cholesterol coatings.

Additionally, it was found that the treatment compositions reacted differently to the ageing process, and to their storage location. Several of the cholesterol containing compositions increased, and then decreased in roughness over time, indicating multiple modes of action driving their morphological changes.

For the DSC studies, it was shown that the 1:1 cholesterol group has an initial quantity of phase-separated cholesterol crystals, which increase in mass over time in ambient storage conditions. XRD results confirmed this result, with a diffraction spacing of 33 Å, the same as reported for crystalline cholesterol [167], [168]. This composition tended to increase in roughness over the short-term in both storage locations, before reaching an equilibrium state.

In the 12:1 group, DSC results indicate a significant mesophase that is different from what is seen in either the DOPS or 1:1 groups. This mesophase gradually consolidates over time, as represented by the shift from a large broad peak in DSC at 52º C, to a sharper peak at 58º C. This result was further elucidated by XRD, which showed a an associated 55 Å XRD spacing result. In the ambient storage condition, the 12:1 composition tended to increase initially in roughness over in the short-term, before reaching an equilibrium state.

Additional knowledge was also gained about the effect of the calcium pretreatment on the coatings. While the calcium pretreatment did not contribute significantly in the short-term (confirming the results in Section 6.3), it was able to affect the coatings when given an adequate amount of time to diffuse through the coatings. Also of note, it was only in the ambient condition that the calcium effect was measurable, suggesting that the increased energy and availability of water in the ambient condition aided the diffusion of the calcium through the coating.

With the knowledge gained in this study, future efforts should take care to acknowledge and deal with the effect of ageing, and seek to optimize the microstructural mesophase state(s) of the coatings in order to address the relevant biological outcomes. At a minimum, it is recommended that the storage history of samples be recorded prior to their use and testing in order to be able to later attempt resolution of analysis discrepancies.

With the knowledge gained in this work, it is remarkably apparent that these lipid and cholesterol coatings are very dynamic systems. These coatings behave very differently than typically studied solid materials given their ability to rearrange significantly over relatively short time frames. While this ageing study uncovered many new questions for future exploration, and while it is interesting to note and analyze coating changes over time in *in vitro* conditions, the goal of the next phases of coating analysis and development should be on the functional optimization of the coatings. The relevant biological conditions for use, and the needed manufacture, transport, sterilization, storage, and implant procedures should all be kept in mind in the continued design and optimization of these coatings. The next steps of this process will be significantly aided with the newfound knowledge gained from this chapter's insight into the coating's time-dependent dynamics.

7.7 Limitations

It should be noted that the desiccator stored samples still had contact with environmental conditions while being measured. Given the now-known dynamic nature of the coatings, it is possible that these brief exposures to ambient conditions interfered with the results, and/or decreased the observable differences between groups due to any water that may have been absorbed during the SWLI measurement timeframe. In order to minimize any possible effects, samples were placed into a small desiccator next to the SWLI in between measurements

Due to the lack of access to a controlled environmental chamber, ambient conditions were not able to be maintained precisely and were subject to the changes in barometric pressure and humidity of the prevailing weather patterns. It is possible that any shifts in humidity over the

course of the study may have affected the sample groups unequally given the fact that the three treatment groups were offset by one week from each other.

XRD samples were aged longer than the longest time point in the other tests. The XRD samples were aged for 9 months prior to testing, and it is possible that they may have undergone a secondary transition(s) that was not associated with changes measured in the other techniques (DSC and SWLI). Ideally, the XRD samples should be measured at progressively longer time points in order to better determine any possible intermediate crystalline phase transitions.

Due to limited resources and time, only long-term stored samples were tested with XRD in this chapter. Ideally, an entire study of progressive time points with various compositions of DOPS and cholesterol would be analyzed. However, due to the resources required for testing numerous samples with XRD, it is advised that any future studies with XRD take place on samples that have already been approximately optimized in cholesterol concentration, in order to reduce the cost and time of analysis.

As mentioned previously (in Section 7.3.2), there was a lab incident that led to the loss of most of the 12:1 samples after the first (day-1) time point. Given the fact that this chapter's study took over 6 months to execute, it was not practical to restart for the sake of those samples. However, it may have been helpful to know how those samples could have possibly changed over time in the desiccator storage location.

7.8 Future Work

The discoveries in this chapter lay a solid foundation for issues to be aware of moving forward in the coating development and design process. There are several questions that have arisen with the knowledge gained of the coatings' change over time, such as confirming the exact

compositions of any mesophase(s) in the microstructure. It would be beneficial to study the biologically relevant factors for manufacture, storage, implantation and use, and then develop ways to test against those conditions in order to determine what mesophases are most relevant, all the while keeping in mind manufacture and storage effects.

Previous work had a difficult time gaining statistically significant results from the study of DOPS and cholesterol coatings [17], and the discoveries presented above go a long way towards explaining some of the reasons this took place. One contributing factor is substrate induced variability (see Section 5.4), where the rough substrate surface was found to be on the same size scale and order of the surface coatings. Another factor is the variance between samples within a given batch, and the variance between batches due to the e-spray process, which was not obvious using only SEM prior to the sensitive differentiating ability of the SWLI measurement methods developed in Section 4.5. Additionally, it was found in this chapter that ageing of the samples plays a dramatic role in coating morphology and structure. All of these parts of the picture combine to give a better view of how future efforts should be directed, with better awareness of the dynamics of the DOPS and cholesterol coatings, and with better tools to track and analyze the coatings.

It is suggested that future studies work backwards from a design perspective; that they seek to first and foremost determine the biologically relevant parameters around which to optimize the DOPS coatings. That is, the biologically relevant media, temperature, cell response, mechanical forces, etc., that the coating will need to address. Next, in controlled experiments, determine the coating composition and microstructure(s) that best meets the challenges of the environment in question. Finally, it would be advised to determine a way to store these coatings in the recently determined optimum configuration. This approach will decrease the amount of

wasted effort finding “ideal” storage conditions for coatings with structures that may end up being biologically suboptimal. Conversely, by keeping the end goal of the coatings at the forefront of the decision process, necessary compromises or design alterations can be made with a direct awareness of the influence of the biologically relevant parameters.

It may be beneficial to fill out all of the time points for the DSC study. Limits in time and resources allowed for the measurement of only three treatment compositions at day-one, and week-two time points each. Given the trend reversal (increasing, then decreasing roughness) that is now evident in several of the treatment groups, it would be interesting to continue DSC measurements at longer time points in order to try a bring further insight on this change. It may also prove insightful to reproduce the ambient storage conditions study with DSC in the desiccator storage location now that we know there are changes over time in both locations.

In regards to the confirmation and further exploration of the 12:1 groups unique mesophase(s), it is recommended that studies be pursued using ^{31}P and ^{2}H NMR techniques, combined with freeze fracture SEM and further XRD analysis [169]. Studies have shown that both cholesterol [69], [166], [169] and calcium cations [169] can induce a hexagonal phase transition in similar DOPS systems, and it is probable that more stable concentration ranges of DOPS and cholesterol can be found using these techniques.

Once biologically relevant parameters are determined, it may be helpful to utilize an environmentally controllable GAXRD instrument in order to test coatings in a partially and/or fully hydrated state. Difficulties may arise in getting a strong enough signal, and of maintaining coating integrity over the long XRD scan times (3-8 hours), but if these factors could be overcome, this method could provide valuable insight into any structural changes that the coatings undergo after hydration.

It is possible that an ageing step may actually be beneficial to the coatings, as it may act to consolidate the coating mesophase(s), as was found to already be taking place in the 12:1 treatment group (see DSC results in Section 7.4.2). If this annealing-type process proves to be a useful addition, it may help with the ageing problem by allowing the coatings to reach a lower energy state and equilibrium phase, making them more stable for future study, transport and storage.

Another area for future exploration is the development and use of an environmentally controlled, aseptic e-spray environment. This would serve two purposes, it would start the process of needed manufacturing changes required for making sterile implants for human use, and it would serve to reduce any variance in coatings due to changes in environmental conditions during the e-spray process. Additionally, it would be wise to start pursuing strategies for coating sterilization, in order to study the effects of the chosen sterilization process on the ageing and stability of the coatings as early in the process as possible.

References

[1] R. D. Crowninshield, A. G. Rosenberg, and S. M. Sporer, “Changing demographics of patients with total joint replacement,” *Clin. Orthop. Rel. Res.*, no. 443, pp. 266–272, 2006.

[2] P. Bills, L. Brown, X. Jiang, and L. Blunt, “A metrology solution for the orthopaedic industry,” *Journal of Physics: Conference Series*, vol. 13, pp. 316–319, Jan. 2005.

[3] S. Kurtz, K. Ong, E. Lau, F. Mowat, and M. Halpern, “Projections of primary and revision hip and knee arthroplasty in the United States from 2005 to 2030,” *The Journal of Bone and Joint Surgery*, vol. 89, no. 4, p. 780, 2007.

[4] J. B. Park and R. S. Lakes, *Biomaterials: an introduction*. Springer Verlag, 2007.

[5] M. Santin, W. Rhys-Williams, J. O’Reilly, M. C. Davies, K. Shakesheff, W. G. Love, A. W. Lloyd, and S. P. Denyer, “Calcium-binding phospholipids as a coating material for implant osteointegration,” *Journal of the Royal Society Interface*, vol. 3, no. 7, pp. 277–281, 2006.

[6] A. Merolli, M. Bosetti, L. Giannotta, A. W. Lloyd, S. P. Denyer, W. Rhys-Williams, W. G. Love, C. Gabbi, A. Cacchioli, P. T. Leali, M. Cannas, and M. Santin, “In vivo assessment of the osteointegrative potential of phosphatidylserine-based coatings,” *Journal of Materials Science-Materials in Medicine*, vol. 17, no. 9, pp. 789–794, 2006.

[7] R. Willumeit, M. Schossig, H. Clemens, and F. Feyerabend, “In-vitro interactions of human chondrocytes and mesenchymal stem cells, and of mouse macrophages with phospholipid-covered metallic implant materials,” *European Cells & Materials*, vol. 13, pp. 11–24, 2007.

[8] I. H. L. Hamelers, R. Staffhorst, J. Voortman, B. de Kruijff, J. Reedijk, P. Henegouwen, and A. de Kroon, “High Cytotoxicity of Cisplatin Nanocapsules in Ovarian Carcinoma Cells Depends on Uptake by Caveolae-Mediated Endocytosis,” *Clinical Cancer Research*, vol. 15, no. 4, pp. 1259–1268, 2009.

[9] I. H. L. Hamelers, E. van Loenen, R. Staffhorst, B. de Kruijff, and A. de Kroon, “Carboplatin nanocapsules: a highly cytotoxic, phospholipid-based formulation of carboplatin,” *Molecular Cancer Therapeutics*, vol. 5, no. 8, pp. 2007–2012, 2006.

[10] M. J. Velinova, R. Staffhorst, W. J. M. Mulder, A. S. Dries, B. A. J. Jansen, B. de Kruijff, and A. de Kroon, “Preparation and stability of lipid-coated nanocapsules of cisplatin: anionic phospholipid specificity,” *Biochimica Et Biophysica Acta-Biomembranes*, vol. 1663, no. 1–2, pp. 135–142, 2004.

[11] T. M. Allen, “Long-circulating (sterically stabilized) liposomes for targeted drug-delivery,” *Trends in Pharmacological Sciences*, vol. 15, no. 7, pp. 215–220, 1994.

[12] G. Gregoriadis, “Engineering liposomes for drug delivery: Progress and problems,” *Trends in Biotechnology*, vol. 13, no. 12, pp. 527–537, 1995.

[13] H. Pinto-Alphandary, A. Andremont, and P. Couvreur, “Targeted delivery of antibiotics using liposomes and nanoparticles: research and applications,” *International Journal of Antimicrobial Agents*, vol. 13, no. 3, pp. 155–168, Jan. 2000.

[14] J. C. Carmen, B. L. Roeder, J. L. Nelson, R. L. Robison Ogilvie, R. A. Robison, G. B. Schaalje, and W. G. Pitt, “Treatment of biofilm infections on implants with low-frequency ultrasound and antibiotics,” *AJIC: American Journal of Infection Control*, vol. 33, no. 2, pp. 78–82, 2005.

[15] S. G. Giulieri, P. Graber, P. E. Ochsner, and W. Zimmerli, “Management of infection associated with total hip arthroplasty according to a treatment algorithm,” *Infection*, vol. 32, no. 4, pp. 222–228, 2004.

[16] R. G. Richards, “Introduction: Implants and infection in fracture fixation ‘ten years on’,” *Injury*, vol. 37, no. 2S, pp. 1–2, 2006.

[17] D. Prawel, “A Drug Eluting, Osseointegrative Phospholipid Coating for Orthopedic Implants,” PhD Dissertation, Colorado State University, Fort Collins, CO, 2011.

[18] N. Sykaras, A. Iacopino, V. Marker, R. Triplett, and R. Woody, “Implant materials, designs, and surface topographies: their effect on osseointegration. A literature review,” *International Journal of Oral and Maxillofacial Implants*, vol. 15, no. 5, pp. 675–690, 2000.

[19] L. Jeys, A. Kulkarni, R. Grimer, S. Carter, R. Tillman, and A. Abudu, “Endoprosthetic reconstruction for the treatment of musculoskeletal tumors of the appendicular skeleton and pelvis,” *The Journal of Bone and Joint Surgery*, vol. 90, no. 6, p. 1265, 2008.

[20] S. Kurtz, F. Mowat, K. Ong, N. Chan, E. Lau, and M. Halpern, “Prevalence of primary and revision total hip and knee arthroplasty in the United States from 1990 through 2002,” *Journal of Bone and Joint Surgery-American Volume*, vol. 87A, no. 7, pp. 1487–1497, 2005.

[21] E. Karlson, L. Mandl, G. Aweh, O. Sangha, M. Liang, and F. Grodstein, “Total hip replacement due to osteoarthritis: the importance of age, obesity, and other modifiable risk factors* 1,” *The American journal of medicine*, vol. 114, no. 2, pp. 93–98, 2003.

[22] B. Stickles, L. Phillips, W. Brox, B. Owens, and W. Lanzer, “Defining the relationship between obesity and total joint arthroplasty,” *Obesity*, vol. 9, no. 3, pp. 219–223, 2001.

[23] R. J. Sierra, W. P. Cooney 4th, M. W. Pagnano, R. T. Trousdale, and J. A. Rand, “Reoperations after 3200 revision TKAs: rates, etiology, and lessons learned,” *Clin. Orthop. Relat. Res.*, no. 425, pp. 200–206, Aug. 2004.

[24] D. R. Sumner and J. O. Galante, “Determinants of stress shielding: design versus materials versus interface.,” *Clinical orthopaedics and related research*, no. 274, p. 202, 1992.

[25] J. D. Bobyn, E. S. Mortimer, A. H. Glassman, C. A. Engh, J. E. Miller, and C. E. Brooks, “Producing and avoiding stress shielding. Laboratory and clinical observations of noncemented total hip arthroplasty,” *Clin Orthop*, vol. 274, no. 1, pp. 79–96, 1992.

[26] R. Huiskes, H. H. Weinans, and B. Rietbergen, “The relationship between stress shielding and bone resorption around total hip stems and the effects of flexible materials,” *Clinical orthopaedics and related research*, pp. 124–134, 1992.

[27] J. Luetzner, F. Krummenauer, A. M. Lengel, J. Ziegler, and W. C. Witzleb, “Serum metal ion exposure after total knee arthroplasty,” *Clinical orthopaedics and related research*, vol. 461, p. 136, 2007.

[28] J. Daniel, H. Ziaee, C. Pradhan, P. B. Pynsent, and D. J. W. McMinn, “Blood and urine metal ion levels in young and active patients after Birmingham hip resurfacing arthroplasty FOUR-YEAR RESULTS OF A PROSPECTIVE LONGITUDINAL STUDY,” *Journal of Bone & Joint Surgery, British Volume*, vol. 89, no. 2, pp. 169–173, 2007.

[29] D. J. Langton, A. P. Sprowson, T. J. Joyce, M. Reed, I. Carluke, P. Partington, and A. V. F. Nargol, “Blood metal ion concentrations after hip resurfacing arthroplasty A COMPARATIVE STUDY OF ARTICULAR SURFACE REPLACEMENT AND BIRMINGHAM HIP RESURFACING ARTHROPLASTIES,” *Journal of Bone & Joint Surgery, British Volume*, vol. 91, no. 10, pp. 1287–1295, 2009.

[30] T. Kitsugi, T. Nakamura, M. Oka, Y. Senaha, T. Goto, and T. Shibuya, “Bone-bonding behavior of plasma-sprayed coatings of BioglassR, AW-glass ceramic, and tricalcium phosphate on titanium alloy,” *Journal of Biomedical Materials Research Part A*, vol. 30, no. 2, pp. 261–269, 1996.

[31] C. A. Homsy, “Bio-compatibility in selection of materials for implantation,” *Journal of Biomedical Materials Research*, vol. 4, no. 3, pp. 341–356, 1970.

[32] L. L. Hench and E. C. Ethridge, “An interfacial approach,” *Biomaterials*, 1982.

[33] W. Becker, C. Dahlin, B. E. Becker, U. Lekholm, D. Van Steenberghe, K. Higuchi, and C. Kultje, “The use of e-PTFE barrier membranes for bone promotion around titanium implants placed into extraction sockets: a prospective multicenter study,” *The International journal of oral & maxillofacial implants*, vol. 9, no. 1, p. 31.

[34] S. S. Haas, G. M. Brauer, and G. Dickson, “A characterization of polymethylmethacrylate bone cement,” *The Journal of Bone and Joint Surgery*, vol. 57, no. 3, p. 380, 1975.

[35] S. J. Hoshaw, J. B. Brunski, and G. V. B. Cochran, “Mechanical loading of Branemark implants affects interfacial bone modeling and remodeling,” *International Journal of Oral and Maxillofacial Implants*, vol. 9, no. 3, pp. 345–360, 1994.

[36] A. J. T. Clemow, A. M. Weinstein, J. J. Klawitter, J. Koeneman, and J. Anderson, “Interface mechanics of porous titanium implants,” *Journal of Biomedical Materials Research*, vol. 15, no. 1, pp. 73–82, 1981.

[37] “Noncemented Total Knee Arthroplasty : Clinical Orthopaedics and Related Research.” [Online]. Available: http://journals.lww.com/corr/Fulltext/1986/04000/Noncemented_Total_Knee_Arthroplasty.7.aspx. [Accessed: 05-Dec-2012].

[38] W. N. Capello, J. A. D’Antonio, M. T. Manley, and J. R. Feinberg, “Hydroxyapatite in total hip arthroplasty: clinical results and critical issues,” *Clinical orthopaedics and related research*, vol. 355, p. 200, 1998.

[39] K. Søballe, S. Overgaard, E. S. Hansen, H. Brokstedt-Rasmussen, M. Lind, and C. Bünger, “A review of ceramic coatings for implant fixation,” *Journal of long-term effects of medical implants*, vol. 9, no. 1–2, p. 131, 1999.

[40] R. J. Furlong and J. F. Osborn, “Fixation of hip prostheses by hydroxyapatite ceramic coatings,” *Journal of Bone & Joint Surgery, British Volume*, vol. 73, no. 5, p. 741, 1991.

[41] T. Geesink and G. Rudolph, “Hydroxyapatite-Coated Total Hip Prostheses Two-Year Clinical and Roentgenographic Results of 100 Cases,” *Clinical orthopaedics and related research*, vol. 261, p. 39, 1990.

[42] J. A. D’Antonio, W. N. Capello, M. T. Manley, and J. Feinberg, “Hydroxyapatite coated implants: total hip arthroplasty in the young patient and patients with avascular necrosis,” *Clinical orthopaedics and related research*, vol. 344, pp. 124–138, 1997.

[43] F. B. Bagambisa, U. Joos, and W. Schilli, “Mechanisms and structure of the bond between bone and hydroxyapatite ceramics,” *Journal of biomedical materials research*, vol. 27, no. 8, pp. 1047–1055, 2004.

[44] R. D. Bloebaum, D. Beeks, L. D. Dorr, C. G. Savory, J. A. Dupont, and A. A. Hofman, “Complications with hydroxyapatite particulate separation in total hip replacement,” *Clin Orthop*, vol. 298, pp. 19–26, 1994.

[45] F. R. DiMaio, “The science of bone cement: a historical review,” *ORTHOPEDICS-NEW JERSEY-*, vol. 25, no. 12, pp. 1399–1407, 2002.

[46] J. O. Galante, J. Lemons, M. Spector, P. D. Wilson, and T. M. Wright, “The biologic effects of implant materials,” *Journal of Orthopaedic Research*, vol. 9, no. 5, pp. 760–775, 1991.

[47] K. Kieswetter, Z. Schwartz, D. D. Dean, and B. D. Boyan, “The role of implant surface characteristics in the healing of bone,” *Critical Reviews in Oral Biology & Medicine*, vol. 7, no. 4, p. 329, 1996.

[48] Wikipedia contributors, “Lipid,” *Wikipedia, the free encyclopedia*. Wikimedia Foundation, Inc., 29-May-2012.

[49] Wikipedia contributors, “Phospholipid,” *Wikipedia, the free encyclopedia*. Wikimedia Foundation, Inc., 29-May-2012.

[50] M. M. Jensen, D. N. Wright, and R. A. Robison, *Microbiology for the health sciences*. Benjamin-Cummings Pub Co, 1997.

[51] L. B, *General structure of a phospholipid*. 2005.

[52] B. Derksen, *Phospholipid structure*. 2002.

[53] H. Ohvo-Rekilä, B. Ramstedt, P. Leppimäki, and J. Peter Slotte, “Cholesterol interactions with phospholipids in membranes,” *Progress in Lipid Research*, vol. 41, no. 1, pp. 66–97, Jan. 2002.

[54] G. Cevc, *Phospholipids Handbook*, 1st ed. CRC Press, 1993.

[55] G. Rouser, “Phospholipids and Blood Coagulation,” *Am J Clin Nutr*, vol. 6, no. 6, pp. 681–687, Nov. 1958.

[56] D. J. Hanahan and D. R. Nelson, “Phospholipids as Dynamic Participants in Biological Processes.,” *J. Lipid Res.*, vol. 25, no. 13, pp. 1528–1535, Dec. 1984.

[57] V. Prouzet-Mauléon, F. Lefebvre, D. Thoraval, M. Crouzet, and F. Doignon, “Phosphoinositides Affect both the Cellular Distribution and Activity of the F-BAR-containing RhoGAP Rgd1p in Yeast,” *The Journal of Biological Chemistry*, vol. 283, no. 48, pp. 33249–33257, 2008.

[58] L. E. Hokin, “Receptors and Phosphoinositide-Generated Second Messengers,” *Annual Review of Biochemistry*, vol. 54, no. 1, pp. 205–235, 1985.

[59] I. Avanti Polar Lipids, “18:1 PS (DOPS) 1,2-dioleoyl-sn-glycero-3-phospho-L-serine (sodium salt) 840035,” 20-Oct-2009. [Online]. Available: http://www.avantilipids.com/index.php?option=com_content&view=article&id=219&Itemid=206&catnumber=850365.

[60] en.wikipedia.org, “Phosphatidylserine,” 20-Oct-2009. [Online]. Available: http://en.wikipedia.org/wiki/Phosphatidylserine.

[61] D. J. Hanahan, *A guide to phospholipid chemistry*. Oxford University Press, USA, 1997.

[62] A. Blokland, W. Honig, F. Browns, and J. Jolles, “Cognition-enhancing properties of subchronic phosphatidylserine (PS) treatment in middle-aged rats: comparison of bovine cortex PS with egg PS and soybean PS,” *Nutrition*, vol. 15, no. 10, pp. 778–783, 1999.

[63] C. Gianotti, A. Porta, P. N. E. De Graan, A. B. Oestreicher, and M. G. Nunzi, “B-50/GAP-43 phosphorylation in hippocampal slices from aged rats: Effects of phosphatidylserine administration,” *Neurobiology of Aging*, vol. 14, no. 5, pp. 401–406.

[64] Y. Nishizuka, “Turnover of inositol phospholipids and signal transduction,” *Science*, vol. 225, no. 4668, p. 1365, 1984.

[65] F. Pedata, L. Giovannelli, G. Spignoli, M. G. Giovannini, and G. Pepeu, “Phosphatidylserine increases acetylcholine release from cortical slices in aged rats,” *Neurobiology of Aging*, vol. 6, no. 4, pp. 337–339, 1985.

[66] G. Toffano, A. Leon, S. Mazzari, G. Savoini, S. Teolato, and P. Orlando, “Modification of noradrenergic hypothalamic system in rat injected with phosphatidylserine liposomes,” *Life Sciences*, vol. 23, no. 10, pp. 1093–1101, 1978.

[67] M. G. Vannucchi and G. Pepeu, “Effect of phosphatidylserine on acetylcholine release and content in cortical slices from aging rats,” *Neurobiology of Aging*, vol. 8, no. 5, pp. 403–407.

[68] I. Vermes, C. Haanen, H. Steffens-Nakken, and C. Reutelingsperger, “A novel assay for apoptosis. Flow cytometric detection of phosphatidylserine expression on early apoptotic cells using fluorescein labelled Annexin V,” *J. Immunol. Methods*, vol. 184, no. 1, pp. 39–51, Jul. 1995.

[69] C. P. S. Tilcock, “Lipid polymorphism,” *Chemistry and Physics of Lipids*, vol. 40, no. 2–4, pp. 109–125, Jun. 1986.

[70] “Lipid bilayer,” *Wikipedia, the free encyclopedia*. 01-Dec-2012.

[71] R. Kumar and O. P. Katare, “Lecithin organogels as a potential phospholipid-structured system for topical drug delivery: a review,” *AAPS PharmSciTech*, vol. 6, no. 2, pp. E298–310, 2005.

[72] L. Zarif, “Elongated supramolecular assemblies in drug delivery,” *Journal of Controlled Release*, vol. 81, no. 1–2, pp. 7–23, May 2002.

[73] Y. . Shchipunov, “Lecithin organogel: A micellar system with unique properties,” *Colloids and Surfaces A: Physicochemical and Engineering Aspects*, vol. 183–185, no. 0, pp. 541–554, Jul. 2001.

[74] Wikipedia contributors, “Liquid crystal,” *Wikipedia, the free encyclopedia*. Wikimedia Foundation, Inc., 08-Sep-2012.

[75] A. . Lee, “Lipid–protein interactions in biological membranes: a structural perspective,” *Biochimica et Biophysica Acta (BBA) - Biomembranes*, vol. 1612, no. 1, pp. 1–40, May 2003.

[76] C. R. Loomis, G. G. Shipley, and D. M. Small, “The phase behavior of hydrated cholesterol.,” *J. Lipid Res.*, vol. 20, no. 4, pp. 525–535, May 1979.

[77] J. L. Browning and J. Seelig, “Bilayers of phosphatidylserine: a deuterium and phosphorus nuclear magnetic resonance study,” *Biochemistry*, vol. 19, no. 6, pp. 1262–1270, Mar. 1980.

[78] G. Ablon and A. M. Rotunda, “Treatment of lower eyelid fat pads using phosphatidylcholine: clinical trial and review,” *Dermatol Surg*, vol. 30, no. 3, pp. 422–427; discussion 428, Mar. 2004.

[79] P. J. Treacy and D. J. Goldberg, “Use of phosphatidylcholine for the correction of lower lid bulging due to prominent fat pads,” *J Cosmet Laser Ther*, vol. 8, no. 3, pp. 129–132, Sep. 2006.

[80] T. Cenacchi, T. Bertoldin, C. Farina, M. G. Fiori, and G. Crepaldi, “Cognitive decline in the elderly: a double-blind, placebo-controlled multicenter study on efficacy of phosphatidylserine administration,” *Aging (Milano)*, vol. 5, no. 2, pp. 123–133, Apr. 1993.

[81] M. Foldvari, A. Gesztes, and M. Mezei, “Dermal drug delivery by liposome encapsulation: Clinical and electron microscopic studies,” *Journal of Microencapsulation*, vol. 7, no. 4, pp. 479–489, Jan. 1990.

[82] A. Samad, Y. Sultana, and M. Aqil, “Liposomal Drug Delivery Systems: An Update Review,” *Current Drug Delivery*, vol. 4, no. 4, pp. 297–305, 2007.

[83] M. T. Hunley, M. G. McKee, and T. E. Long, “Submicron functional fibrous scaffolds based on electrospun phospholipids,” *Journal of Materials Chemistry*, vol. 17, no. 7, p. 605, 2007.

[84] J. Watanabe, T. Eriguchi, and K. Ishihara, “Stereocomplex Formation by Enantiomeric Poly(lactic acid) Graft-Type Phospholipid Polymers for Tissue Engineering,” *Biomacromolecules*, vol. 3, no. 5, pp. 1109–1114, 2002.

[85] V. P. Torchilin, “Micellar nanocarriers: pharmaceutical perspectives,” *Pharm. Res.*, vol. 24, no. 1, pp. 1–16, Jan. 2007.

[86] J. Sela, U. Gross, D. Kohavi, J. Shani, D. Dean, B. Boyan, and Z. Schwartz, “Primary mineralization at the surfaces of implants,” *CRITICAL REVIEWS IN ORAL BIOLOGY & MEDICINE*, vol. 11, no. 4, pp. 423–436, Nov. 2000.

[87] T. Kirsch and M. Pfäffle, “Selective binding of anchorin CII (annexin V) to type II and X collagen and to chondrocalcin (C-propeptide of type II collagen) Implications for

anchoring function between matrix vesicles and matrix proteins," *FEBS letters*, vol. 310, no. 2, pp. 143–147, 1992.

[88] D. Skrtic and E. Eanes, "Membrane-mediated precipitation of calcium phosphate in model liposomes with matrix vesicle-like lipid composition* 1," *Bone and mineral*, vol. 16, no. 2, pp. 109–119, 1992.

[89] M. Bosetti, A. W. Lloyd, M. Santin, S. P. Denyer, and M. Cannas, "Effects of phosphatidylserine coatings on titanium on inflammatory cells and cell-induced mineralisation in vitro," *Biomaterials*, vol. 26, no. 36, pp. 7572–7578, 2005.

[90] A. Satsangi, N. Satsangi, R. Glover, R. K. Satsangi, and J. L. Ong, "Osteoblast response to phospholipid modified titanium surface," *Biomaterials*, vol. 24, no. 25, pp. 4585–4589, 2003.

[91] N. Satsangi, A. Satsangi, R. Glover, J. L. Ong, and R. K. Satsangi, "Osteoblast response and calcium deposition on phospholipid modified surfaces," *Journal of Materials Science-Materials in Medicine*, vol. 15, no. 6, pp. 693–697, 2004.

[92] M. L. N. Huynh, V. A. Fadok, and P. M. Henson, "Phosphatidylserine-dependent ingestion of apoptotic cells promotes TGF-beta 1 secretion and the resolution of inflammation," *Journal of Clinical Investigation*, vol. 109, no. 1, pp. 41–50, 2002.

[93] J. D. de Bruijn, C. A. van Blitterswijk, and J. E. Davies, "Initial bone matrix formation at the hydroxyapatite interface in vivo," *Journal of Biomedical Materials Research*, vol. 29, no. 1, pp. 89–99, 1995.

[94] H. L. Casal, A. Martin, H. H. Mantsch, F. Paltauf, and H. Hauser, "Infrared studies of fully hydrated unsaturated phosphatidylserine bilayers. Effect of lithium and calcium," *Biochemistry*, vol. 26, no. 23, pp. 7395–7401, 1987.

[95] C. Pidgeon and R. J. Markovich, "Formation of the antiplanar-antiplanar phosphate conformation of dilauroylphosphatidylcholine bilayers," *Biochimica et Biophysica Acta (BBA) - Biomembranes*, vol. 1029, no. 1, pp. 173–184, Nov. 1990.

[96] R. Dluhy, D. G. Cameron, H. H. Mantsch, and R. Mendelsohn, "Fourier transform infrared spectroscopic studies of the effect of calcium ions on phosphatidylserine," *Biochemistry*, vol. 22, no. 26, pp. 6318–6325, 1983.

[97] J. J. Potoff, C. Manke, Z. Kas, and B. P. Jena, "Calcium Bridging Leading To The Dehydration Of Phospholipid Head-Groups," in *The 2007 Annual Meeting*, 2007.

[98] D. J. Peet, S. D. Turley, W. Ma, B. A. Janowski, J. M. A. Lobaccaro, R. E. Hammer, and D. J. Mangelsdorf, "Cholesterol and bile acid metabolism are impaired in mice lacking the nuclear oxysterol receptor LXRα," *Cell*, vol. 93, no. 5, pp. 693–704, 1998.

[99] Wikipedia contributors, “Cholesterol,” *Wikipedia, the free encyclopedia*. Wikimedia Foundation, Inc., 29-May-2012.

[100] D. Bach and E. Wachtel, “Phospholipid/cholesterol model membranes: formation of cholesterol crystallites,” *Biochimica et Biophysica Acta (BBA) - Biomembranes*, vol. 1610, no. 2, pp. 187–197, Mar. 2003.

[101] H. I. Petrache, D. Harries, and V. A. Parsegian, “Alteration of lipid membrane rigidity by cholesterol and its metabolic precursors,” in *Macromolecular Symposia*, 2005, vol. 219, pp. 39–50.

[102] D. Liu and L. Huang, “Role of cholesterol in the stability of pH-sensitive, large unilamellar liposomes prepared by the detergent-dialysis method,” *Biochimica et Biophysica Acta (BBA)-Biomembranes*, vol. 981, no. 2, pp. 254–260, 1989.

[103] M. S. Brown and J. L. Goldstein, “The SREBP Pathway: Regulation review of cholesterol metabolism by proteolysis of a membrane-bound transcription factor,” *Cell*, vol. 89, pp. 331–340, 1997.

[104] M. B. Sankaram and T. E. Thompson, “Modulation of phospholipid acyl chain order by cholesterol. A solid-state deuterium nuclear magnetic resonance study,” *Biochemistry*, vol. 29, no. 47, pp. 10676–10684, 1990.

[105] J. H. Ipsen, O. G. Mouritsen, and M. Bloom, “Relationships between lipid membrane area, hydrophobic thickness, and acyl-chain orientational order. The effects of cholesterol,” *Biophysical journal*, vol. 57, no. 3, pp. 405–412, 1990.

[106] K. Simons and E. Ikonen, “How Cells Handle Cholesterol,” *Science*, vol. 290, no. 5497, pp. 1721–1726, Dec. 2000.

[107] K. Simons and E. Ikonen, “Functional rafts in cell membranes,” *Nature*, vol. 387, no. 6633, pp. 569–572, Jun. 1997.

[108] D. L. Melchior, F. J. Scavitto, and J. M. Steim, “Dilatometry of dipalmitoyllecithin-cholesterol bilayers,” *Biochemistry*, vol. 19, no. 21, pp. 4828–4834, 1980.

[109] R. M. Epand, D. Bach, R. F. Epand, N. Borochov, and E. Wachtel, “A New High-Temperature Transition of Crystalline Cholesterol in Mixtures with Phosphatidylserine,” *Biophysical Journal*, vol. 81, no. 3, pp. 1511–1520, Sep. 2001.

[110] Y.-J. Geng, J. E. Phillips, R. P. Mason, and S. W. Casscells, “Cholesterol crystallization and macrophage apoptosis: implication for atherosclerotic plaque instability and rupture,” *Biochemical Pharmacology*, vol. 66, no. 8, pp. 1485–1492, Oct. 2003.

[111] R. M. Epand, D. W. Hughes, B. G. Sayer, N. Borochov, D. Bach, and E. Wachtel, “Novel properties of cholesterol–dioleoylphosphatidylcholine mixtures,” *Biochimica et Biophysica Acta (BBA) - Biomembranes*, vol. 1616, no. 2, pp. 196–208, Oct. 2003.

[112] S. Ramakrishna, *An Introduction to Electrospinning And Nanofibers*. World Scientific, 2005.

[113] J. Grace and J. Marijnissen, “A review of liquid atomization by electrical means,” *Journal of aerosol science*, vol. 25, no. 6, pp. 1005–1019, 1994.

[114] G. Höhne, W. F. Hemminger, and H.-J. Flammersheim, *Differential Scanning Calorimetry*. Springer, 2003.

[115] “Calorimeter,” *Wikipedia, the free encyclopedia*. 16-Nov-2012.

[116] M. Y. Efremov, E. A. Olson, M. Zhang, Z. Zhang, and L. H. Allen, “Probing glass transition of ultrathin polymer films at a time scale of seconds using fast differential scanning calorimetry,” *Macromolecules*, vol. 37, no. 12, pp. 4607–4616, 2004.

[117] I. Okazaki and B. Wunderlich, “Reversible melting in polymer crystals detected by temperature-modulated differential scanning calorimetry,” *Macromolecules*, vol. 30, no. 6, pp. 1758–1764, 1997.

[118] Y. Roos and M. Karel, “Differential scanning calorimetry study of phase transitions affecting the quality of dehydrated materials,” *Biotechnology Progress*, vol. 6, no. 2, pp. 159–163, 2008.

[119] S. D. Arnfield and E. D. Murray, “The influence of processing parameters on food protein functionality. I. Differential scanning calorimetry as an indicator of protein denaturation.,” *Journal-Canadian Institute of Food Science and Technology= Journal de l’Institut canadien de science et technologie alimentaire.*, vol. 14, no. 4, p. 289, 1981.

[120] C. G. Biliaderis, “Differential scanning calorimetry in food research—A review,” *Food Chemistry*, vol. 10, no. 4, pp. 239–265, Apr. 1983.

[121] R. N. McElhaney, “The use of differential scanning calorimetry and differential thermal analysis in studies of model and biological membranes,” *Chemistry and Physics of Lipids*, vol. 30, no. 2–3, pp. 229–259, May 1982.

[122] R. L. Biltonen and D. Lichtenberg, “The use of differential scanning calorimetry as a tool to characterize liposome preparations,” *Chemistry and physics of lipids*, vol. 64, no. 1, pp. 129–142, 1993.

[123] C. Huang and S. Li, “Calorimetric and molecular mechanics studies of the thermotropic phase behavior of membrane phospholipids.,” *Biochimica et biophysica acta*, vol. 1422, no. 3, p. 273, 1999.

[124] I. Kurganskaya, A. Luttge, and A. Barron, “The Application of VSI (Vertical Scanning Interferometry) to the Study of Crystal Surface Processes.” Connexions Web site, 13-Jul-2009.

[125] A. J. Howard, R. R. Rye, and J. E. Houston, “Nanomechanical basis for imaging soft materials with tapping mode atomic force microscopy,” *Journal of Applied Physics*, vol. 79, no. 4, pp. 1885 –1890, Feb. 1996.

[126] J. M. Huntley and M. Grédiac, “Editorial,” *Strain*, vol. 46, no. 1, pp. 1–2, Jan. 2010.

[127] X. Li, T. Yamauchi, H. Iwai, Y. Yamashita, H. Zhang, and T. Hiruma, “Full-field quantitative phase imaging by white-light interferometry with active phase stabilization and its application to biological samples,” *Opt. Lett.*, vol. 31, no. 12, pp. 1830–1832, Jun. 2006.

[128] D. Huang, E. A. Swanson, C. P. Lin, J. S. Schuman, W. G. Stinson, W. Chang, M. R. Hee, T. Flotte, K. Gregory, C. A. Puliafito, and A. Et, “Optical Coherence Tomography,” *Science*, vol. 254, no. 5035, pp. 1178–1181, Nov. 1991.

[129] G. Friedbacher and H. Bubert, *Surface and Thin Film Analysis*. John Wiley & Sons, 2011.

[130] C. Suryanarayana and M. G. Norton, *X-Ray Diffraction: A Practical Approach*. Springer, 1998.

[131] M. Dardo, *Nobel Laureates and Twentieth-Century Physics*. Cambridge University Press, 2004.

[132] B. E. Warren, *X-Ray Diffraction*. Courier Dover Publications, 1969.

[133] R. Guinebretière, *X-Ray Diffraction by Polycrystalline Materials*. John Wiley & Sons, 2010.

[134] M. F. Doerner and W. D. Nix, “A method for interpreting the data from depth-sensing indentation ins t rurnen ts,” *J. Mater. Res*, vol. 1, no. 4, 1986.

[135] W. C. Oliver and G. M. Pharr, “Improved technique for determining hardness and elastic modulus using load and displacement sensing indentation experiments,” *Journal of materials research*, vol. 7, no. 6, pp. 1564–1583, 1992.

[136] B. J. Briscoe, L. Fiori, and E. Pelillo, “Nano-indentation of polymeric surfaces,” *Journal of Physics D: Applied Physics*, vol. 31, no. 19, pp. 2395–2405, Oct. 1998.

[137] H. R. Wilde and A. WEHRSTEDT, “Introduction of martens Hardness HM: An internationally accepted designation for Hardness under test force,” *Materialprüfung*, vol. 42, no. 11–12, pp. 468–470, 2000.

[138] A. Wehrstedt, “Results of the revision of the ISO standards for Brinell, Vickers, Rockwell and Knoop Hardness Tests,” 2006.

[139] J. Malzbender, “Comment on hardness definitions,” *Journal of the European Ceramic Society*, vol. 23, no. 9, pp. 1355–1359, Aug. 2003.

[140] T. Triffo, “In vivo efficacy of antibiotic-eluting phospholipid coated implants,” COLORADO STATE UNIVERSITY, 2011.

[141] M. Morra, C. Cassinelli, G. Cascardo, P. Cahalan, L. Cahalan, M. Fini, and R. Giardino, “Surface engineering of titanium by collagen immobilization. Surface characterization and in vitro and in vivo studies,” *Biomaterials*, vol. 24, no. 25, pp. 4639–4654, Nov. 2003.

[142] J. L. Arias, M. B. Mayor, J. Pou, Y. Leng, B. León, and M. P.- Amor, “Micro- and nano-testing of calcium phosphate coatings produced by pulsed laser deposition,” *Biomaterials*, vol. 24, no. 20, pp. 3403–3408, Sep. 2003.

[143] I. Titanium Joe, “Titanium Joe, Inc.,” 06-Jun-2012. [Online]. Available: http://www.titaniumjoe.com/.

[144] Alfa Aesar, “Cholesterol, A11470,” 06-Jun-2012. [Online]. Available: http://www.alfa.com/en/GP100w.pgm?DSSTK=A11470&CAS=57-88-5.

[145] Zygo Corporation, “Film Analysis MetroPro Application (OMP-0506A).” Zygo Corporation, Jul-2005.

[146] M. Abramowitz and M. W. Davidson, “Numerical Aperture and Resolution.” Olympus Microscopy Resource Center, 2012.

[147] R. Leach, Ed., *Optical Measurement of Surface Topography*, 1st Edition. Springer, 2011.

[148] “Low Noise Interferometry Enables Characterization of Steep and Rough Surfaces.” Bruker Nano Surfaces - AFM and SPM.

[149] Agilent Technoligies, “Nanoindentation, Scratch, & Elevated Temperature Testing of Cellulose & PMMA films.” .

[150] C. N. Elias, Y. Oshida, J. H. C. Lima, and C. A. Muller, “Relationship between surface properties (roughness, wettability and morphology) of titanium and dental implant removal torque,” *Journal of the Mechanical Behavior of Biomedical Materials*, vol. 1, no. 3, pp. 234–242, Jul. 2008.

[151] V. Quaglini, P. Dubini, D. Ferroni, and C. Poggi, “Influence of counterface roughness on friction properties of engineering plastics for bearing applications,” *Materials & Design*, vol. 30, no. 5, pp. 1650–1658, May 2009.

[152] S. McLaughlin, N. Mulrine, T. Gresalfi, G. Vaio, and A. McLaughlin, “Adsorption of divalent cations to bilayer membranes containing phosphatidylserine.,” *The Journal of General Physiology*, vol. 77, no. 4, pp. 445 –473, Apr. 1981.

[153] S. Nir, C. Newton, and D. Papahadjopoulos, “Binding of Cations to Phosphatidylserine Vesicles,” *Bioelectrochemistry and Bioenergetics*, vol. 5, no. 1, pp. 116–133, 1978.

[154] W. W. Gerberich, W. Yu, D. Kramer, A. Strojny, D. Bahr, E. Lilleodden, and J. Nelson, “Elastic loading and elastoplastic unloading from nanometer level indentations for modulus determinations,” *Journal of materials research*, vol. 13, no. 2, pp. 421–439, 1998.

[155] R. J. Rodríguez, A. Medrano, J. A. García, G. G. Fuentes, R. Martínez, and J. A. Puertolas, “Improvement of surface mechanical properties of polymers by helium ion implantation,” *Surface and Coatings Technology*, vol. 201, no. 19–20, pp. 8146–8149, Aug. 2007.

[156] M. A. Meyers, P.-Y. Chen, A. Y.-M. Lin, and Y. Seki, “Biological materials: Structure and mechanical properties,” *Progress in Materials Science*, vol. 53, no. 1, pp. 1–206, Jan. 2008.

[157] J. G. Swadener, E. P. George, and G. M. Pharr, “The correlation of the indentation size effect measured with indenters of various shapes,” *Journal of the Mechanics and Physics of Solids*, vol. 50, no. 4, pp. 681–694, Apr. 2002.

[158] H. Gao, Y. Huang, W. D. Nix, and J. W. Hutchinson, “Mechanism-based strain gradient plasticity— I. Theory,” *Journal of the Mechanics and Physics of Solids*, vol. 47, no. 6, pp. 1239–1263, Apr. 1999.

[159] P. W. Van Dijck, B. De Kruijff, L. L. Van Deenen, J. De Gier, and R. A. Demel, “The preference of cholesterol for phosphatidylcholine in mixed phosphatidylcholine-phosphatidylethanolamine bilayers.,” *Biochimica et biophysica acta*, vol. 455, no. 2, p. 576, 1976.

[160] J. L. Rubenstein, B. A. Smith, and H. M. McConnell, “Lateral diffusion in binary mixtures of cholesterol and phosphatidylcholines,” *PNAS*, vol. 76, no. 1, pp. 15–18, Jan. 1979.

[161] T. N. Estep, D. B. Mountcastle, R. L. Biltonen, and T. E. Thompson, “Studies on the anomalous thermotropic behavior of aqueous dispersions of dipalmitoylphosphatidylcholine-cholesterol mixtures,” *Biochemistry*, vol. 17, no. 10, pp. 1984–1989, 1978.

[162] S. S. Cross, “How common is cholesterol embolism?,” *J Clin Pathol*, vol. 44, no. 10, pp. 859–861, Oct. 1991.

[163] W. Moolenaar and C. B. Lamers, “Cholesterol crystal embolisation to the alimentary tract.,” *Gut*, vol. 38, no. 2, pp. 196–200, Feb. 1996.

[164] F. Scolari, R. Tardanico, R. Zani, A. Pola, B. F. Viola, E. Movilli, and R. Maiorca, “Cholesterol crystal embolism: A recognizable cause of renal disease.,” *American journal of kidney diseases: the official journal of the National Kidney Foundation*, vol. 36, no. 6, p. 1089, 2000.

[165] A. Sedaghat and S. M. Grundy, “Cholesterol Crystals and the Formation of Cholesterol Gallstones,” *New England Journal of Medicine*, vol. 302, no. 23, pp. 1274–1277, Jun. 1980.

[166] P. L. Yeagle, “Cholesterol and the cell membrane,” *Biochimica et Biophysica Acta (BBA) - Reviews on Biomembranes*, vol. 822, no. 3–4, pp. 267–287, Dec. 1985.

[167] B. M. Craven, “Crystal structure of cholesterol monohydrate,” , *Published online: 22 April 1976; | doi:10.1038/260727a0*, vol. 260, no. 5553, pp. 727–729, Apr. 1976.

[168] H. S. Shieh, L. G. Hoard, and C. E. Nordman, “Crystal structure of anhydrous cholesterol,” , *Published online: 19 May 1977; | doi:10.1038/267287a0*, vol. 267, no. 5608, pp. 287–289, May 1977.

[169] C. P. S. Tilcock, M. B. Bally, S. B. Farren, P. R. Cullis, and S. M. Gruner, “Cation-dependent segregation phenomena and phase behavior in model membrane systems containing phosphatidylserine: influence of cholesterol and acyl chain composition,” *Biochemistry*, vol. 23, no. 12, pp. 2696–2703, 1984.

[170] F. S. Sjöstrand, “A comparison of plasma membrane, cytomembranes, and mitochondrial membrane elements with respect to ultrastructural features,” *Journal of Ultrastructure Research*, vol. 9, no. 5–6, pp. 561–580, Dec. 1963.

[171] “Harbor Freight Tools,” 22-Oct-2009. [Online]. Available: www.harborfreight.com.

[172] I. Avanti Polar Lipids, “18:0 PC (DSPC) 1,2-distearoyl-sn-glycero-3-phosphocholine 850365,” 20-Oct-2009. [Online]. Available: http://www.avantilipids.com/index.php?option=com_content&view=article&id=219&Itemid=206&catnumber=850365.

Appendix A: Protocols

Protocol A. Titanium Square Sample Preparation

Equipment and Materials Required:

- Foot actuated shear table
- Titanium sheet metal

1. Iteratively adjust the foot-actuated shearing table's stop plate by loosening the two adjustment bars until the table shears 7.5 mm strips.
    a. Adjust the table so that cut Ti strips are within 7.45-7.55mm (+/- 0.5mm).
    b. You can check the width that the shear table cuts by testing with a piece of scrap sheet metal until it is within specification.
2. Cut as many strips as desired in one direction.
3. Line up the cut strips together in groups of 5-10 perpendicular to the shear.
    a. It is helpful to place a spacer strip to the side of the strips to be cut so that all strips are held securely by the retention foot during shearing
4. Shear the strips so that small square samples are produced.
    a. Make sure that each strip individually rests against the shear stop plate in order to insure consistent dimensions.

Protocol B. Titanium Cleaning

Note: clean less than 20 samples at once (to prevent stacking in the beaker)

1.Sonicate for at least 15 minutes in 100 ml Acetone (stirring vigorously every 5 minutes)

2.Blow dry with lab air

3.Sonicate for at least 15 minutes in 100 ml Chloroform (stirring vigorously every 5 minutes)

4.Blow dry with lab air

5.Sonicate for at least 10 minutes in 100 ml 5% Liquinox (stirring vigorously every 5 minutes)

6.Rinse 3 times in Di water

7.Sonicate 15 minutes in 100 ml DI water (stirring vigorously every 5 minutes)

8.Rinse twice in pure ethanol

9.Blow dry with nitrogen

10. Store in closed container in a vacuum desiccator

Clean large samples (ultrasonic):

10min Acetone (rinse with tap)

10min Liquinox (rinse multiple with DI)

5min in DI

Acetone rinse/dry

>Stored in vacuum desiccator

Protocol C. Calcium Pretreatment of Titanium Samples

Overview

Calcium from calcium chloride applied to Ti samples at a 2.25 mM concentration.

Assumptions/Parameters for this Procedure

Samples are cleaned and prepared according to separate Ti Cleaning Protocol

Supplies/equipment

- Calcium source - calcium chloride (anhydrous)
- hot-plate/stirrer (temperature controlled)

Preparation

1. Weigh out $CaCl_2$
    a. 1 mole Ca in $CaCl_2$ weighs 109 grams; 2.25 mM = 0.245 mg/ml; 24.5 mg in 100 ml DIH_2O

Procedure

1. Place calcium chloride in 250 ml beaker
2. Add 100 ml DIH_2O to beaker and set on stirrer at 37°C, at 150 RPM.
3. Cover each with lab film and stir for 24 hours, occasionally mixing (manually) to prevent stacking effects. (note: an easy technique is to puncture a disposable LDPE pipette through the lab film cover and use it to jet the samples around as they stir. The pipette can be left in place until the samples are fully treated.
4. Rinse by replacing calcium solution with DIH_2O in each beaker, twice.

5. Vacuum dry and used immediately or vacuum pack in nitrogen and store at room temperature until use.

Ca pretreatment of large samples:

Modified as follows:

Only mix 25mL of salt solution

24.5/4=6.125 mg of CaCl2 into 25mL DI water

Mix on stir/hot plate at 37C with stir bar at 120 RPM

Started at ~2:45pm

Protocol D. Titanium Passivation

Clean surfaces: (no anhydrous methanol)

1. Note: clean less than 20 samples at once (to prevent stacking)
2. Sonicate 30 minutes in 100 ml **Acetone** (stirring vigorously every 5 minutes)
3. Blow dry with lab air
4. Sonicate 30 minutes in 100 ml **Chloroform** (stirring vigorously every 5 minutes)
5. Blow dry with lab air
6. Sonicate 15 minutes in 100 ml 5% **Liquinox** (stirring vigorously every 5 minutes)
7. Rinse 3 times in Di water
8. Sonicate 15 minutes in 100 ml **DI water** (stirring vigorously every 5 minutes)
9. Rinse twice in pure **ethanol**
10. Blow dry with **nitrogen**
11. Store in closed container in desiccator

- Alkaline cleaner if necessary (no cathodic/acidic cleaning for metals that pit or are susceptible to hydrogen contamination effects)
    - See Guide B 600 for Ti

Final surface treatment:

1. Immerse in 30% nitric acid solution for 40 minutes (at room temperature)
    a. Rinse thoroughly with DI water (3x times)
    b. Neutralize surface if porous
    c. Blow dry with lab air

Protocol E. Titanium Surface Polishing

Polishing Titanium with the OBRL Histology Grinders

Supplies needed:

Histology Grinder

Histology Slide - (located in right side of center island cabinet)

Ti samples - Already cut to desired size / shape

3M permenant double sided tape

240, 800, 1000, 1200 Grit sandpaper (in plastic containers on center island)

2500 grit sandpaper (these are the blue (or gray) sheets in the left side of the center island cabinet)

Polishing Paper (usually left out on the counter to the left of the two grinders)

Calibrator set: Custom Aluminum c-clamp and micron plunge gauge (in box in the right side of center island cabinet)

1. Mounting the Ti samples

- Use double sided tape to mount the Ti samples onto the histology slide

    - Press samples firmly into tape, it may help to warm tape or press samples after adhering to improve adhesion

    - You can line up multiple Ti samples onto one slide. You may want to start with a 2x3 grid, I have had good results with a full slide of samples (usually ~80% end up polished).

- Note: To improve results, grind the histology slide flat with the 800 grit paper for 1 minute before attaching samples.

2. Using the Histology Grinder (there are two, use the one on the right)

Equilibrate temperature of the grinding wheel

- Turn on histology grinder with power switch on backside of the control box on the right
- Start grinding wheel spinning: turn on power button (I) on lower right front of control box
- Turn on the water
- Turn cold water on at the faucet
- At faucet tip;
    - Turn off the valve that drains
    - Turn off the valve to the left grinder (the green tube)
    - Turn on the valve to the right grinder (the clear tube)
- Let cold water run at high flow rate over the spinning grinding wheel for 30 minutes

Check calibration of grinding wheel height

- Mount the custom Al c-clamp and plunge gauge onto the Aluminum side from on top of the grinder
- mount the plunge gauge so that it barely touches the grinding wheel
- Check the height of the copper grinding wheel at each of the three small adjustment screw locations
- The grinding wheel height next to all three screw heights should be at most within 1.5um
- If they are further apart than this, use the T-handled alan wrench (in drawer below grinder) to !SLOWLY! adjust height of the three set screws

Inserting the sandpaper sheets

- Starting with the lowest number (large) grit paper, wet disk front and back at other sink
- Roll paper Grit side outwards into a somewhat tight roll from one end of the disk to the other

- Unroll disk and repeat above step from ~30 deg different rotation

- Repeat above step until you have rolled the paper from ~6 different directions

- The paper disk should now have a downwards bend to the edges (this is so that it will 'stick' better when applying to the grinding wheel)

- With water running and the grinding wheel spinning, turn off just the spinning (The (O) button on lower right side of control panel).

- While the grinding wheel is slowing down, begin inserting the sandpaper disk onto the wheel.

- The paper should be adhered to the grinding wheel with a very thin and even film of water.

- Turn on spinning of the grinding wheel to check that the paper is adhered and centered

3. Sanding & Polishing the Samples

<u>Vacuum attachment of the histology slide in the grinder</u>

- Turn on the vacuum pump associated with the right grinder (vacuum pump is located under the control panel on the right side of the machine, and the on-off switch is on the top left of the pump).

- Twist the vacuum pump release valve clockwise to close the circuit

- Hold the histology slide with the previously attached Ti samples to the under side of the white polymer slide holder

- There are thin red guides at the back and right side of the holder that the histolgy slide should rest against (ie, push the slide back and to the right while holding it up in place)

- Wait for the pressure to reach ~400 before letting go of the slide

Initiating a grinding/polishing step

- When you are ready to start a grinding/polishing step, place both of the metal ring weights onto the center slide holder (there is a horizontal post facing you for attaching them) and gently allow the slide holder to descend into contact with the grinding wheel
- Turn on left-right ocsiclating motion of the slide holder (press the (I) button just left of the (I) button for turning on spinning of the grind wheel
- There is a timer on the center island counter for keeping track of time
- To stop grinding for a step, reverse the above directions. Make sure to stop the left right oscilation of the slide holder while it is at the center of its path

Polishing steps

- Use the following paper grits in this order:
- Optional: 240 or 320 Grit paper first for 5-40minutes (it is faster than the 800 grit)
- 800 grit for ~5-60 minutes (you will need to check to see if all of the samples are evenly worn)
- 1000 grit for 7 minutes
- 1200 grit for 7 minutes
- 2500 grit for 7 minutes
- Polishing paper for 8 minutes (these sheets can be reused many times, dont discard)

3. Tear down and clean up

- After removal of the histology slide and sanding paper, use the plant watering bucket located in the center island cabinet to rinse the copper grinder wheel
- Fill the bucket with hot water from the other sink and pour over the spinning grinding wheel
- Repeat above step twice (for a total of three rinses)
- Turn off water at faucet, turn off power to vacuum pump and turn off power to the grinder

control panel

- Depending on how long they were used, you can save the sandpaper disks for later use by rolling them and storing them in your chosen location

Additional Notes:

- **Record how many sheets of sandpaper you consume.**
- Sandpaper sheets can be reused. They should each last for around 20-25 minutes of polishing.
- The final polishing sheet can be reused longer, do not discard.
- Always check with the histologist (Bob or Cecily) if in doubt, these are their instruments.

Appendix B: Atomizing Nozzle Spray Deposition Methodology Development

An atomizing spray methodology was developed in order to deposit the DOPS and cholesterol coatings onto titanium and titanium alloy substrates. In brief, an air compressor was used for the high pressure air source and a digital airflow regulator was used to more finely control the air flow to an airbrush. The airbrush was then used to spray the phospholipid solutions onto 1 cm by 1 cm titanium (Ti) squares. The coated Ti squares were then dried in a vacuum to be later characterized using various microscopy techniques.

Equipment Used

A 2 hp, 8 gallon 115 maximum psi air compressor was acquired from Harbor Freight Tools (item 95386-1VGA) and used as the high pressure air source. A picture of the air compressor used in this study can be seen in Figure 8-1.

Figure 8-14 2 HP 8 gallon air compressor [171].

A hobbyists' airbrush kit was acquired from Harbor Freight Tools (item 47791-2VGA) and used for spraying the lipid mixtures. A picture of the airbrush kit used in this study can be seen in Figure 8-2.

Figure 8-15 Airbrush kit [171].

A digital air flow regulator was acquired from Harbor Freight Tools (item 98426-1VGA) and used for fine control of the air flow arriving at the airbrush. A picture of the digital air flow regulator used in this study can be seen in Figure 8-3.

Figure 8-16 Digital air flow regulator [171].

Additional equipment used includes standard pneumatic hoses and connections required to connect the air compressor, regulator, airbrush, etc. Ring stands, beakers, vials and various other equipment were also used from the lab as required.

Materials Used

All phospholipids used were obtained from Avanti Polar Lipids, Inc. The phosphatidylcholine used was 1,2-distearoyl-sn-glycero-3-phosphocholine (DSPC), catalog number 850356P and was ordered in powder form [172]. The phosphatidylserine used was 1,2-dioleoyl-sn-glycero-3-phospho-L-serine (DOPS), catalog number 840035P and was ordered in powder form [59]. The chloroform, methanol and DI water used were from standard chemistry stock.

The titanium used was acquired from Titanium Joe (1000 Parkland drive, Kingston, Ontario). The titanium is commercially pure grade 2 and was ordered as 0.016” thick sheets.

Sample Preparation Methods

To prepare the Ti squares, the sheet Ti was hand cut into 1 cm by 1cm squares using tin snips. If necessary, the squares were flattened with a hammer and then washed according to the procedure outlined in Table 8-1.

Table 8-2 Wash protocol for Ti squares

1	Note: clean less than 20 samples at once (to prevent stacking)
2	Sonicate 30 minutes in 100 ml Acetone (stirring vigorously every 5 minutes)
3	Blow dry with lab air
4	Sonicate 30 minutes in 100 ml Chloroform (stirring vigorously every 5 minutes)
5	Blow dry with lab air
6	Sonicate 15 minutes in 100 ml 5% Liquinox (stirring vigorously every 5 minutes)
7	Rinse 3 times in Di water
8	Sonicate 15 minutes in 100 ml DI water (stirring vigorously every 5 minutes)
9	Rinse twice in pure ethanol
10	Blow dry with nitrogen
11	Store in closed container in desiccator

For the phospholipid solutions, different molar concentration solutions were prepared by weighing the appropriate amount of phospholipid and then adding it and the appropriate amount of chloroform to a glass vial. The glass vials used had a Teflon cap liner added to the lid in order to withstand the chloroform. The prepared lipid solutions were stored in a -20 C freezer when not in use. Example phosphatidylserine weights and chloroform volumes for various concentration solutions are given in Table 8-2.

Table 8-3 Weight of phospholipid and volume of chloroform used for various concentrations of phospholipid solution.

Concentration (mM)	Phosphatidylserine Weight (grams)	Chloroform Volume (mL)
25	0.02025	1
50	0.04050	1
75	0.06075	1
100	0.08100	1

Atomizing Spray Methods Development

During spraying, the airbrush and Ti square being coated were kept inside a fume hood. A ring stand was used to support the holding mechanism for the Ti square being coated. One Ti square was sprayed at a time, with the airbrush tip typically being held between 1 and 2 inches away from the Ti surface.

The finely adjustable digital airflow regulator was placed directly upstream of the small airbrush hose. The main airflow regulator on the air compressor was used to roughly restrict the air pressure to less than 90 psi in order to protect the airbrush. The digital airflow regulator was then used to more finely adjust the airflow before it reached the airbrush. Given the airbrush handle has a simple on/off button to allow airflow, control of the airflow for coating purposes was therefore adjusted by means of the latter digital airflow regulator. The digital regulator's psi reading drops during spraying due to the increased drain in the line, so settings are given at a rest state (i.e. when the airbrush is not spraying). A typical resting setting of the digital regulator is 70 psi.

The nozzle coming from the spray solution on the tip of the airbrush can be opened or closed in order to adjust the volume of spray. In order to have a reference for later use, graduations on the nozzle were marked from 0-6. This is such that when the nozzle is twisted

fully shut, the marking will read 0, and conversely, when it is opened wide it will read 6. A typical set of spray parameters for the regulator and nozzle are 70 psi on the regulator and ‘2’ on the nozzle.

The airbrush kit used came with two large glass vials for the spray solution. These vials were significantly larger than needed for the small spray volumes used in this study. Modifications were therefore made to allow smaller glass vials to be attached to the airbrush. A small glass vial lid was drilled out to accommodate the airbrush intra-vial receptor tube. The small vial lid was then glued with cyanoacrylate to the inside of the airbrush’s built in threaded lid. In this way, both the larger, original glass vials, as well as the smaller glass sample vial are able to be attached to the airbrush. In addition, an adapter was made so that an even smaller glass vial could be attached to the airbrush. This adapter consists of a small glass sample vial’s threaded portion attached to the hollowed out portion of the regular sized sample vial’s lid. This allows the use of both a regular and small sample vial with the airbrush.

The intra-vial receptor tube built into the airbrush tended to swell during spraying with chloroform, so it was replaced with the fluorinated hose from an electro spraying setup (i.e. the hose between the syringe and the electrically charged spray needle). This replacement hose performed well, with minimal/negligible swelling.

Spray Methodology Development with Phosphatidylcholine

Initial practice with the airbrush was performed using only chloroform. The spray parameters were optimized such that a thin even film of chloroform was sprayed onto the surface of the Ti square. After the initial setup and practice with chloroform, a 100 mM phosphatidylcholine-chloroform solution was then added to the airbrush and sprayed with similar

settings. The spray behaved significantly different due to the addition of the phospholipid and the settings were adjusted again in order to mimic the chloroform only spray pattern. The phosphatidylcholine-chloroform spray parameters associated with an even thin wetting film across the Ti square's surface were 56 psi at the regulator and '3' at the nozzle.

Results

These setting produced an even wetting of the surface during spraying. However, after drying in a vacuum, the surfaces appeared splotched and splashed with large craters in the coating on the microscale. An SEM picture of a representative phosphatidylcholine surface coating at 25X and 200X are given in Figure 8-4 and Figure 8-5 respectively.

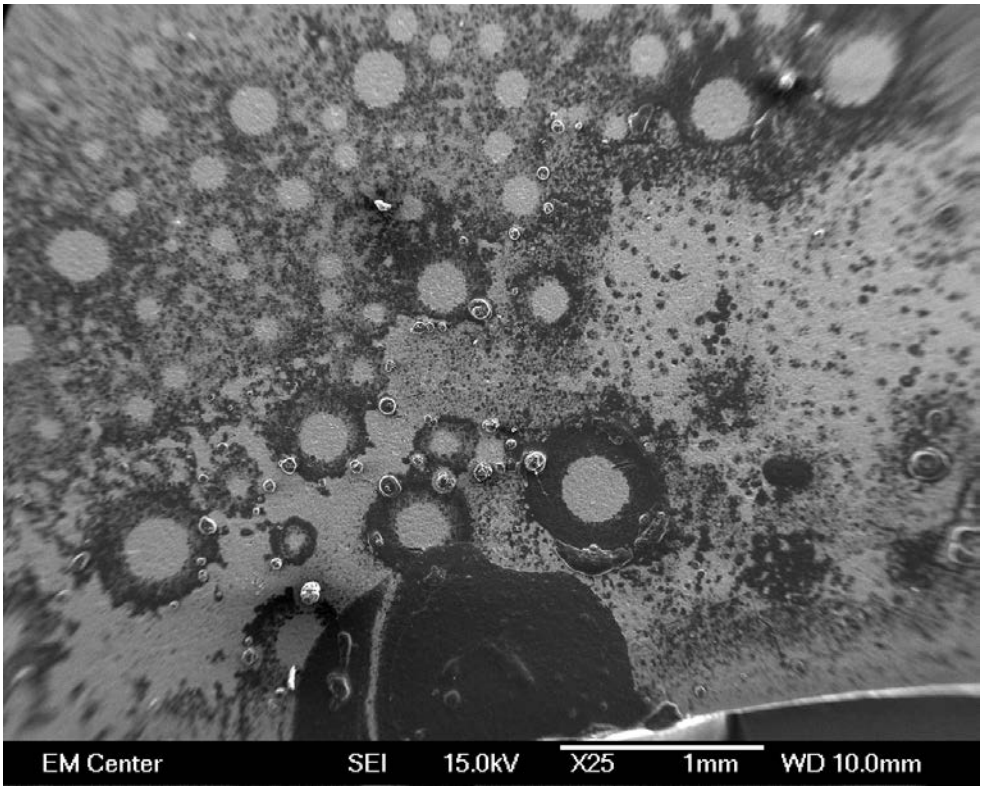

Figure 8-17 SEM of DSPC coated Ti at 25X.

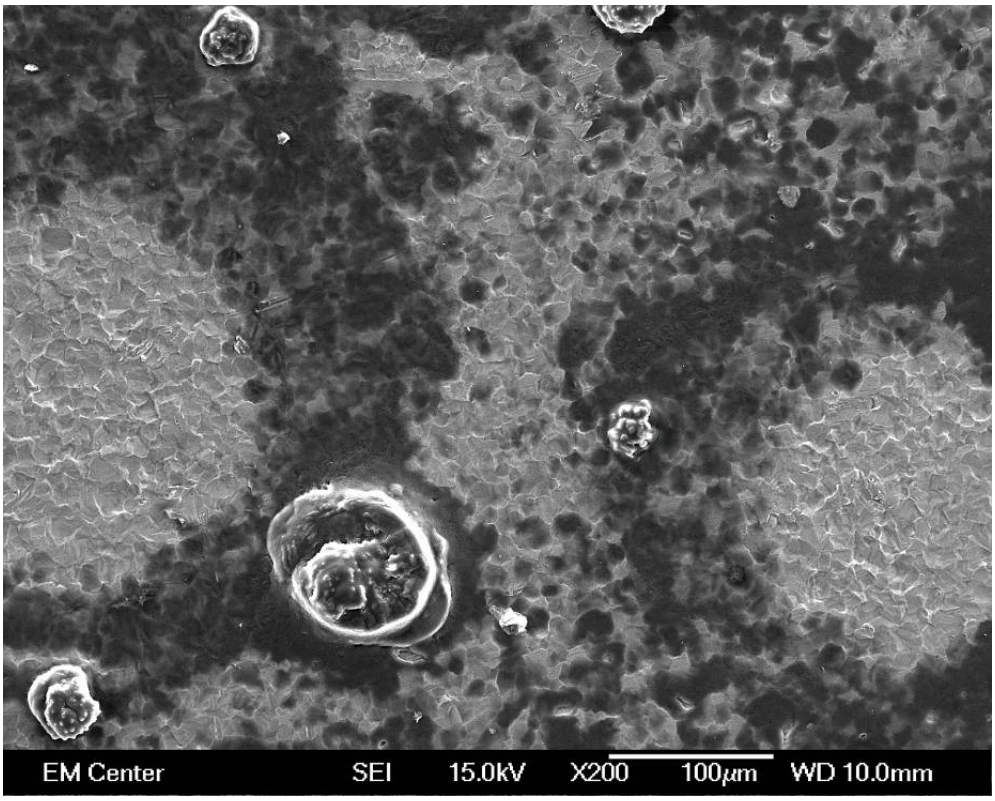

Figure 8-18 SEM picture of DSPC coated Ti at 200X.

As can be seen in Figure 8-4 and Figure 8-5, large splashes and globs can be seen across the surface of the Ti square. It can be noted that the 'splashes' tended to be larger closer to the edge of the Ti square. Upon very close inspection, the 'globs' on the surface (such as the one seen in the lower left middle of Figure 8-5) had repeating patterns typical of a dehydrated phospholipid structure. In addition, the coatings with this spray method were fairly inconsistent, with some samples being significantly blotchier than others at similar spray parameters

Conclusions

This spray method was concluded to be unacceptable due to the irregularities on the surface and inconsistency between samples. Further work was performed to optimize the spray parameters.

‘Dry’ Spray Method with Phosphatidylcholine

In order to improve the surface coatings, the spray parameters were adjusted so that the spray from the air brush was ‘dry’. In this way, the bulk of the chloroform was evaporated before reaching the surface. When spraying with these settings, the surface appears to fog, instead of having a wet film on it. The phosphatidylcholine-chloroform spray parameters associated with this ‘dry’ spraying method are 70 psi at the regulator and ‘1.3’ at the nozzle.

Results

These setting produced progressive fogging of the surface during spraying, which was easily controlled due to the relatively slow deposition rate. After drying, the surfaces appeared very even with negligible splotching/abnormalities across the surface. An SEM picture of a representative phosphatidylcholine surface coating using the ‘dry’ spray method at 50X and 500X are given in Figure 8-6 and Figure 8-7 respectively.

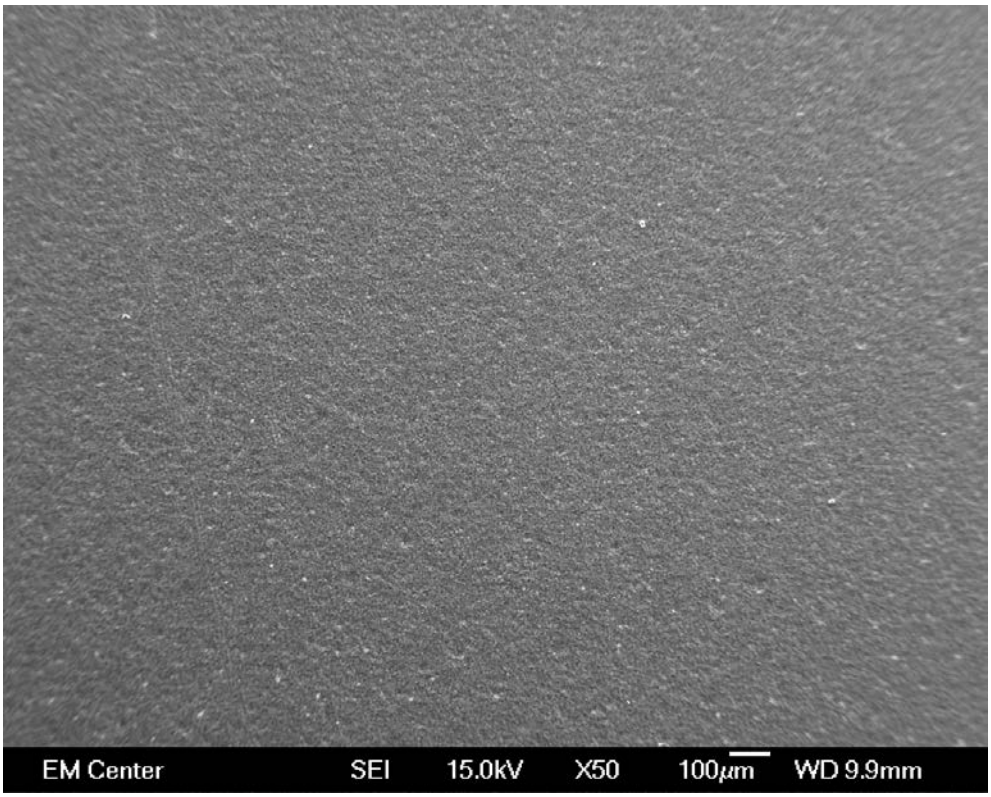

Figure 8-19 SEM picture of DSPC coated Ti with 'dry' settings at 50X.

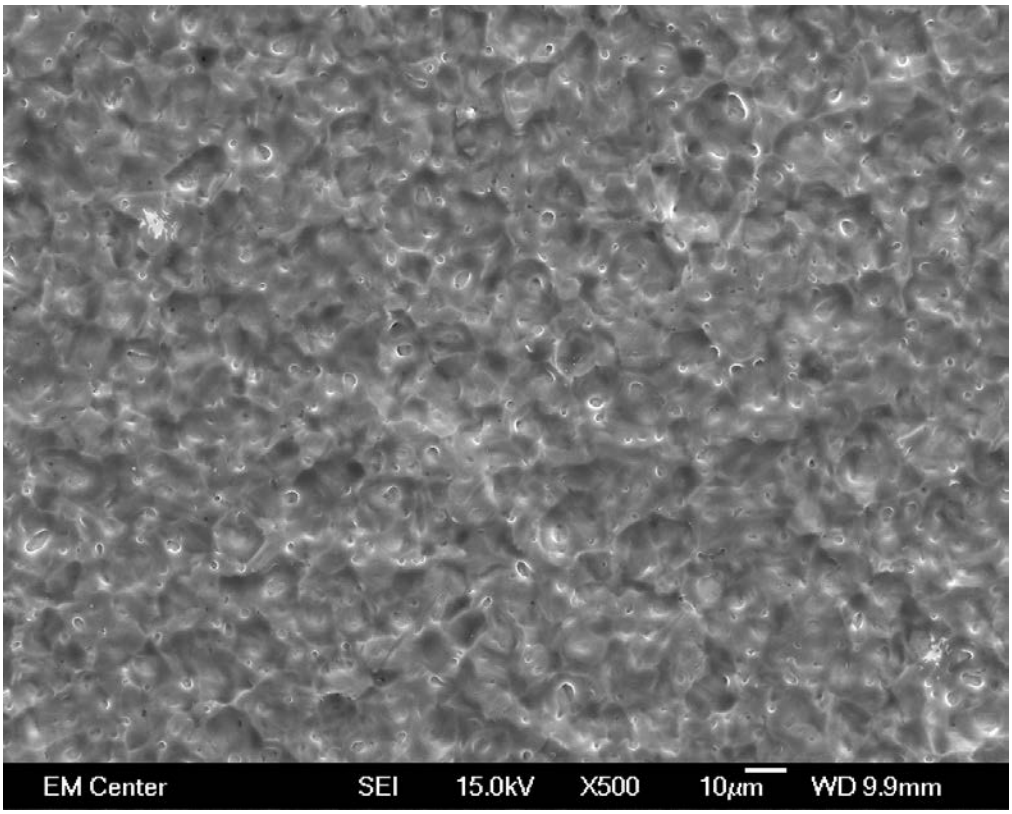

Figure 8-20 SEM picture of DSPC coated Ti with 'dry' settings at 500X.

As can be seen in Figure 8-6 and Figure 8-7, the surface is very even. A consistent coating of DSPC was seen across the whole Ti surface.

Discussion and Conclusions

This spray method was concluded to be acceptable due to the regular, even coatings. Similar surfaces to Figure 8-6 and Figure 8-7 were also obtained with lower concentration phosphatidylcholine-chloroform solutions. Therefore, further work was performed using this 'dry' spray method with the more expensive DOPS phospholipid.

It can be noted that this 'dry' method makes sense using the basic concepts during the spraying process. As the venturi effect during spraying creates a vacuum at the airbrush nozzle, the chloroform is for the large part evaporated while the lipid is propelled forward to the Ti

surface. It therefore makes sense that the more consistent surface is created when the chloroform is consistently evaporated to near completion at the airbrush nozzle. During a ‘wet’ spray, the phospholipid-chloroform solution would dry non-homogenously leading to splashes of lipid and inconsistent results.

Spray Methodology with Phosphatidylserine

Having optimized the general spray parameters with DSPC, DOPS was used next to coat Ti squares. The spraying process behaved very similarly with DOPS as it did with DSPC. Small adjustments were made to the spray parameters such that a typical parameter set is 70 psi at the regulator and ‘1.5-2’ at the nozzle depending on the phosphatidylserine-chloroform concentration.

Results

As with the ‘dry’ DSPC samples, this method also produced progressive fogging of the surface during spraying with an easily controllable deposition rate. After drying, the surfaces also appeared very even with minimal abnormalities across the surface. An SEM picture of a representative phosphatidylserine surface coating using the ‘dry’ spray method at 50X, 500X and 2,000X are given in Figure 8-8, Figure 8-9 and Figure 8-10 respectively.

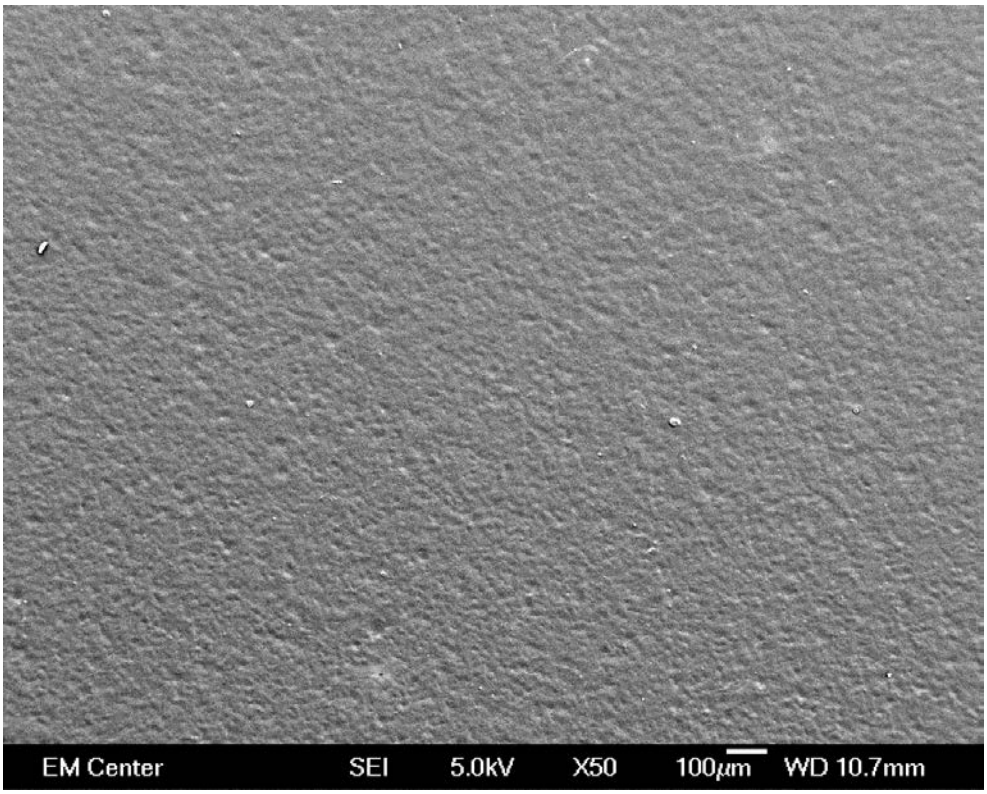

Figure 8-21 SEM picture of DOPS coated Ti at 50X.

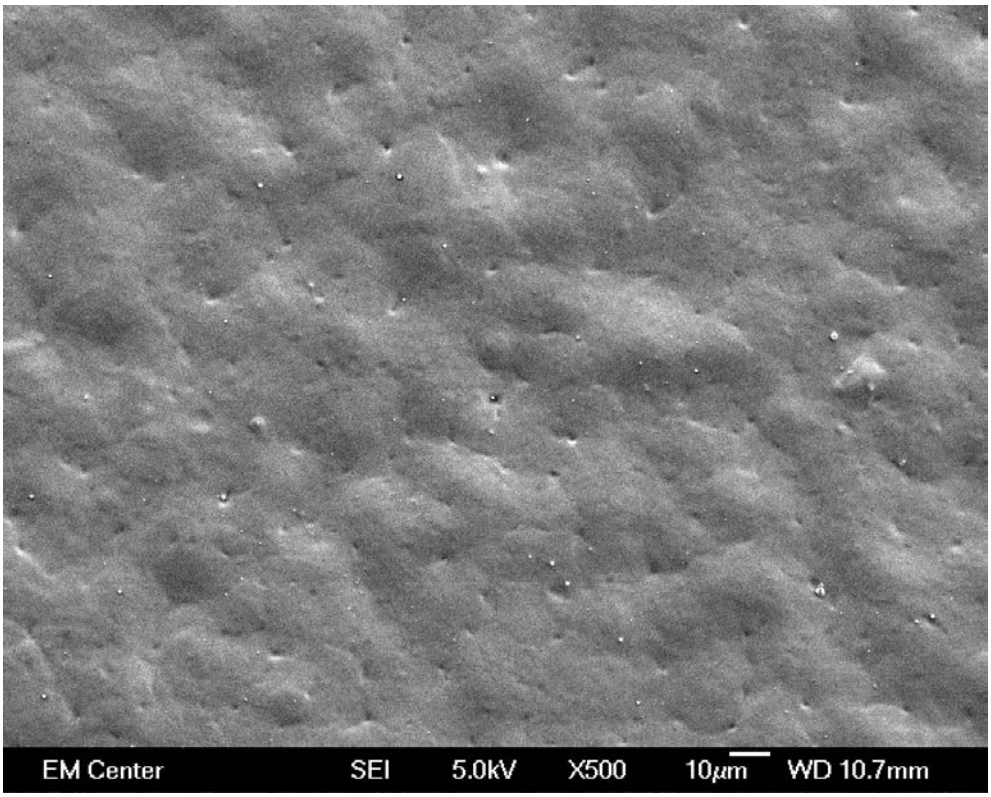

Figure 8-22 SEM picture of DOPS coated Ti at 500X.

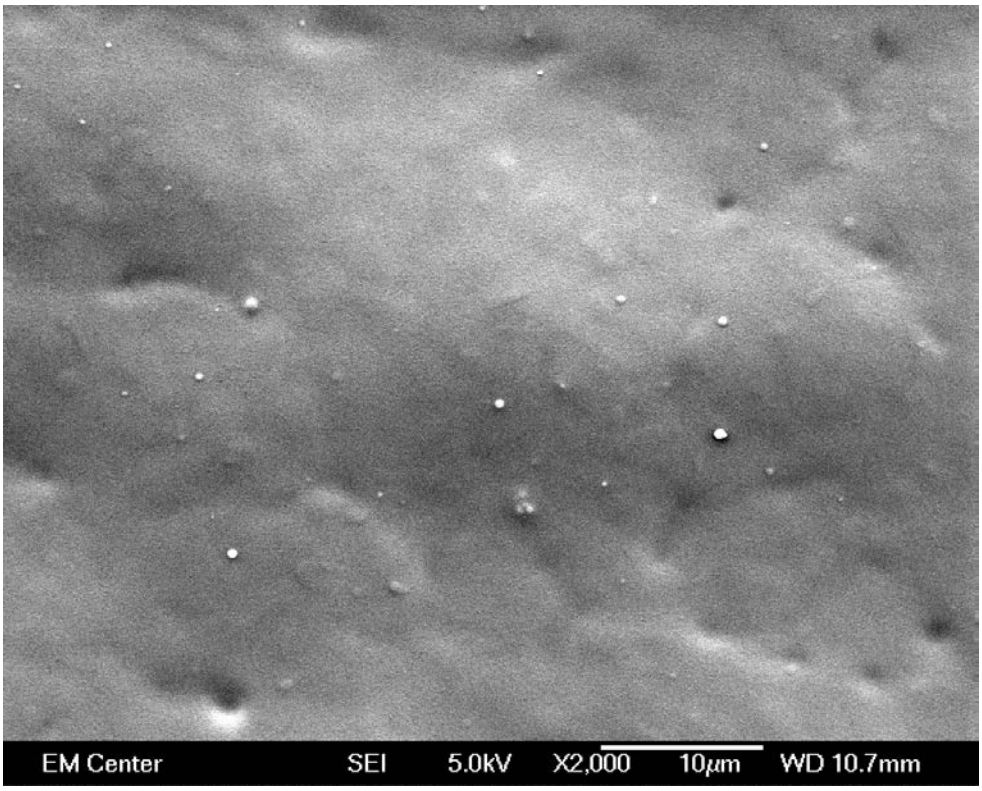

Figure 8-23 SEM picture of DOPS coated Ti at 2,000X.

As can be seen in Figure 8-8, Figure 8-9 and Figure 8-10 the surfaces produced with the 'dry' method are very even. A consistent coating of DSPC was seen across the whole Ti surface. It should be noted that unlike the DSPC surfaces, very small liposomes are apparent at high magnifications. These spheres are on the order of 300 nm to 1 μm in diameter.

Discussion and Conclusions

During the method development, it was found that multiple concentrations of DOPS-chloroform could be sprayed. 25, 50 and 100 mM concentrations were used, however, the highest concentration solution tended to be more difficult to work with and tended to clog the receptor hose more easily. Both the 25 and 50 mM concentrations spray relatively easily, so

future flexibility in deposition amounts can be achieved by using higher or lower concentrations in this range.

This spray method was also concluded to be acceptable due to the consistently regular, even coatings. Therefore, further work was continued using this ‘dry’ spray method with DOPS phospholipid.

Appendix C: Differential Scanning Calorimetry Measurements for DOPS and cholesterol coatings

Expiremental Methods

Differential Scanning Calorimetry (DSC) sample pans were coated using an aerosol spray deposition method (see Appendix B: Atomizing Nozzle Spray Deposition Methodology Development). Two DOPS:cholesterol treatment groups were tested. A 20mM DOPS in chloroform solution was used for both groups, with cholesterol being added at a 12:1 (DOPS:cholesterol) and 1:1 molecular ratio (resulting in 1.667 mM and 20 mM cholesterol concentrations, respectively). 2mL of solution was aerosol sprayed onto 3 DSC pans for the 1:1 group, and 2.66 mL of solution sprayed onto 2 pans for the 12:1 treatment group. The coated pans were then left to dry in a vacuum desiccator for at least 72 hours prior to testing with the DSC.

A DSC 2920 Modulated DSC (TA Instruments, New Castle, DE) was used to analyze the phase transition of the DOPS and cholesterol coatings between 0 and 100C. A 2º C/min ramp rate was used to cycle the DSC sample from room temperature (24º C) to 100º C and back twice (i.e., two heating and two cooling ramps). The sample was then cooled all the way to 0º C, after which it was cycled up to 100º C and down to 0º C twice (for a complete total of 4 heating cycles, and 4 cooling cycles).

The Tim points tested were as follows; both the 12:1 and 1:1 (DOPS:cholesterol) treatment groups were tested at immediately following vacuum drying (time 0 time point), and

after two weeks of ageing in atmospheric conditions (2 week time point). The DSC pans were sealed just prior to measurement with DSC in each case.

Measurement Results

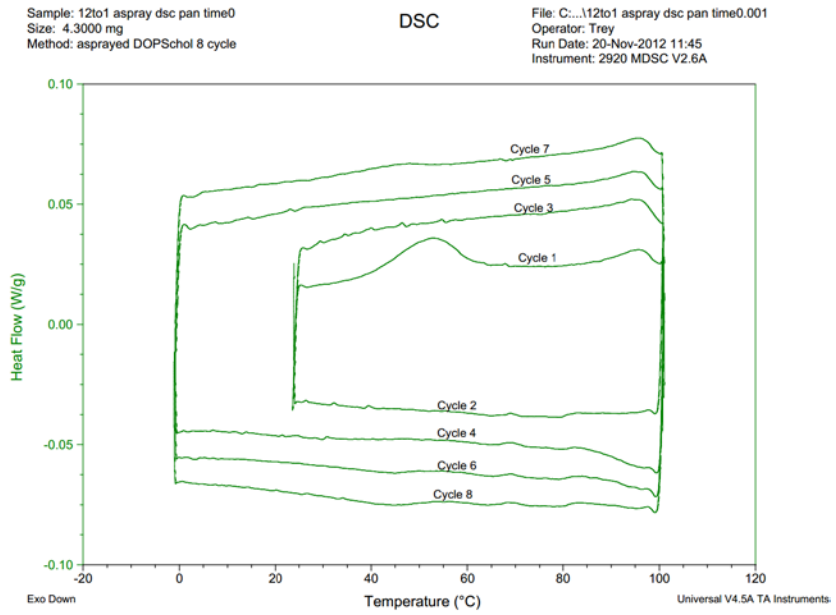

Figure 8-24 Day-1 DSC of 12:1 group. The top 4 curves are heating scans, and the bottom 4 are cooling scans. Curves are displaced along the y axis for presentation. Scan rate was 2ºC/min, exotherms face downward.

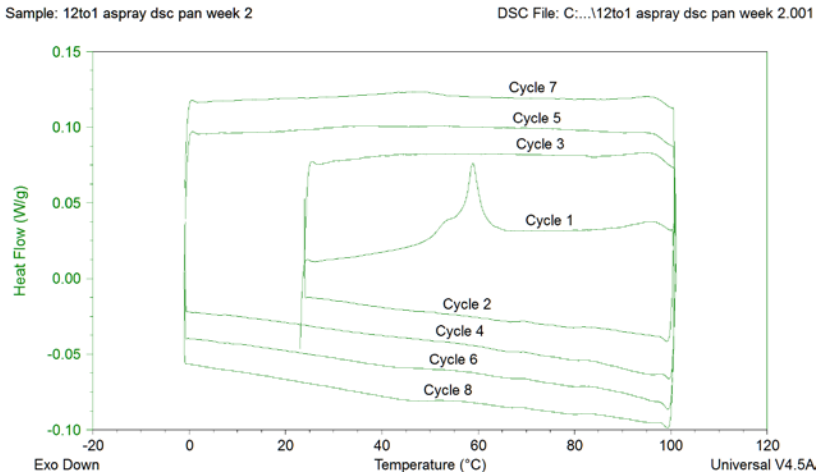

Figure 8-25 Week-2 DSC of 12:1 group. Curves are displaced along the y axis for presentation. Scan rate was 2ºC/min, exotherms face downward.

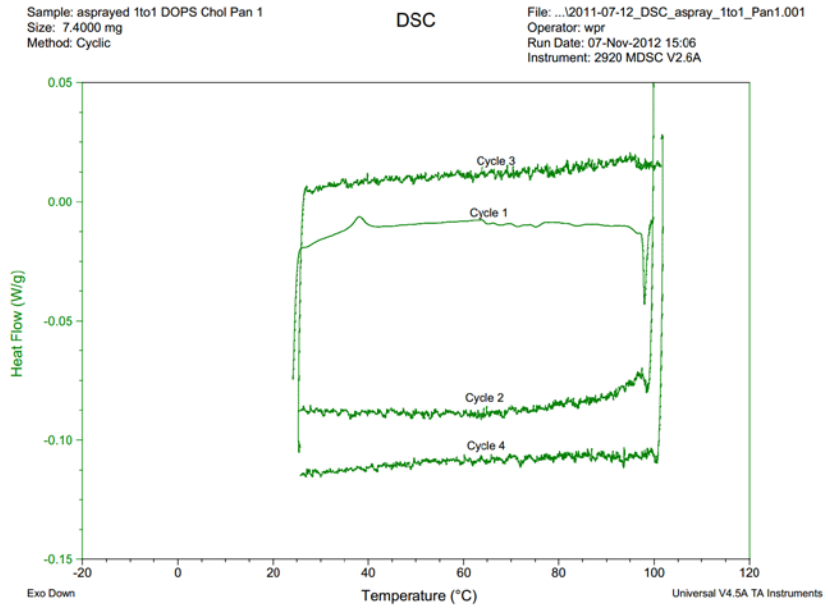

Figure 8-26 Day-1 DSC of 1:1 group, first run. Curves are displaced along the y axis for presentation. Scan rate was 2ºC/min, exotherms face downward.

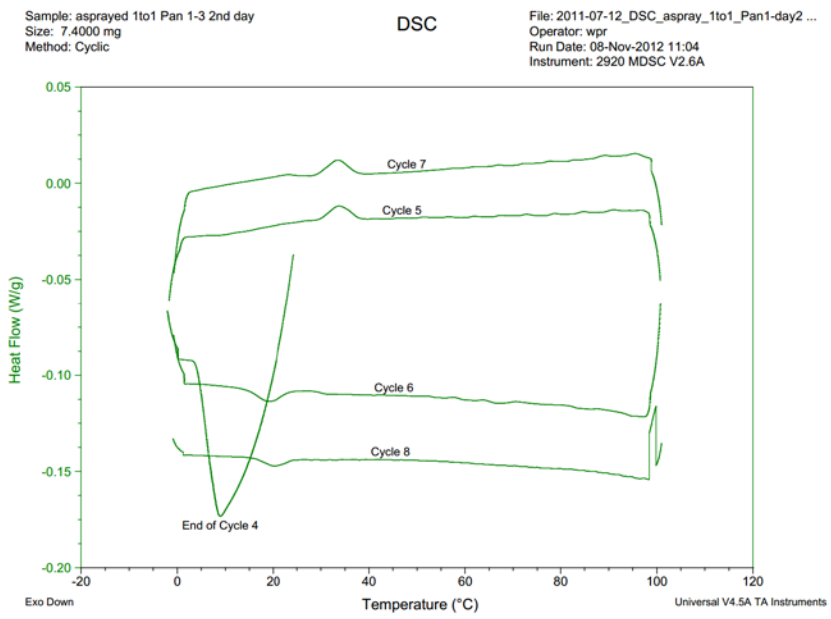

Figure 8-27 Day-1 DSC of 1:1 group, second run. Curves are displaced along the y axis for presentation. Scan rate was 2ºC/min, exotherms face downward.

Notes: The day-1 DSC measurements of the 1:1 group was run in two sessions. That is, the high temperature cycles between 24-100º C were run first (Figure 8-13), followed the next morning by the full 0-100º C cycles (Figure 8-14). The noisy curves (for cycles 2, 3 and 4) and the sharp exothermic peak at the end of cycle 1 (in Figure 8-13) is interpreted as an instrument control artifact due to an improperly controlled liquid nitrogen ballast.

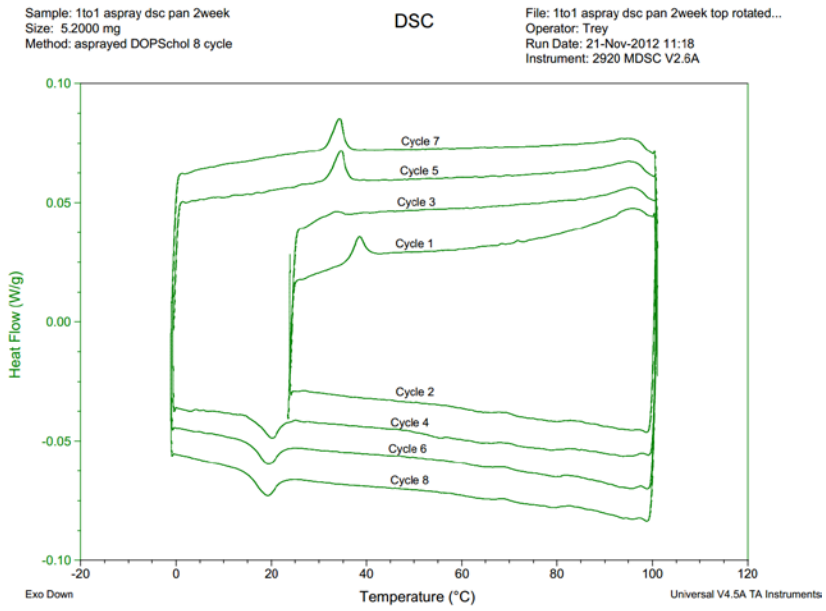

Figure 8-28 Week-2 DSC of 1:1 group. Curves are displaced along the y axis for presentation. Scan rate was 2ºC/min, exotherms face downward.

Appendix D: Scanning White Light Interferometry Ageing Study: Measurement Time Points Schedule and Weather Almanac Tables

SWLI Measurement Schedule for Ageing Study

	Task Name	Start	Finish
1	**E-Spray 1st round: DOPS & DOPS-no-Ca**	Mon 1/2/12	Tue 1/3/12
2	Day 1: SWLI DOPS Groups	Wed 1/4/12	Fri 1/6/12
3	SWLI measure controls	Mon 1/9/12	Mon 1/9/12
4	**E-Spray 2nd round: 12:1 & 12:1-no-Ca (w/ DOPS referrence)**	Mon 1/9/12	Tue 1/10/12
5	Day 1: SWLI 12:1 Groups	Wed 1/11/12	Fri 1/13/12
6	**E-Spray 3rd round: 1:1 & 1:1-no-Ca (w/ DOPS referrence)**	Mon 1/16/12	Tue 1/17/12
7	Day 1: SWLI 1:1 Groups	Wed 1/18/12	Fri 1/20/12
8			
9	4 Week: SWLI DOPS Groups	Wed 2/1/12	Thu 2/2/12
10	4 Week: SWLI 2nd round	Wed 2/8/12	Thu 2/9/12
11	4 Week: SWLI 1:1 Groups	Wed 2/15/12	Thu 2/16/12
12			
13	12 Week: SWLI DOPS Groups	Wed 3/28/12	Thu 3/29/12
14	12 Week: SWLI 12:1 Groups	Wed 4/4/12	Thu 4/5/12
15	12 Week: SWLI 1:1 Groups	Wed 4/11/12	Thu 4/12/12

SWLI Measurement Schedule for Ageing Study – Graphical Timeline

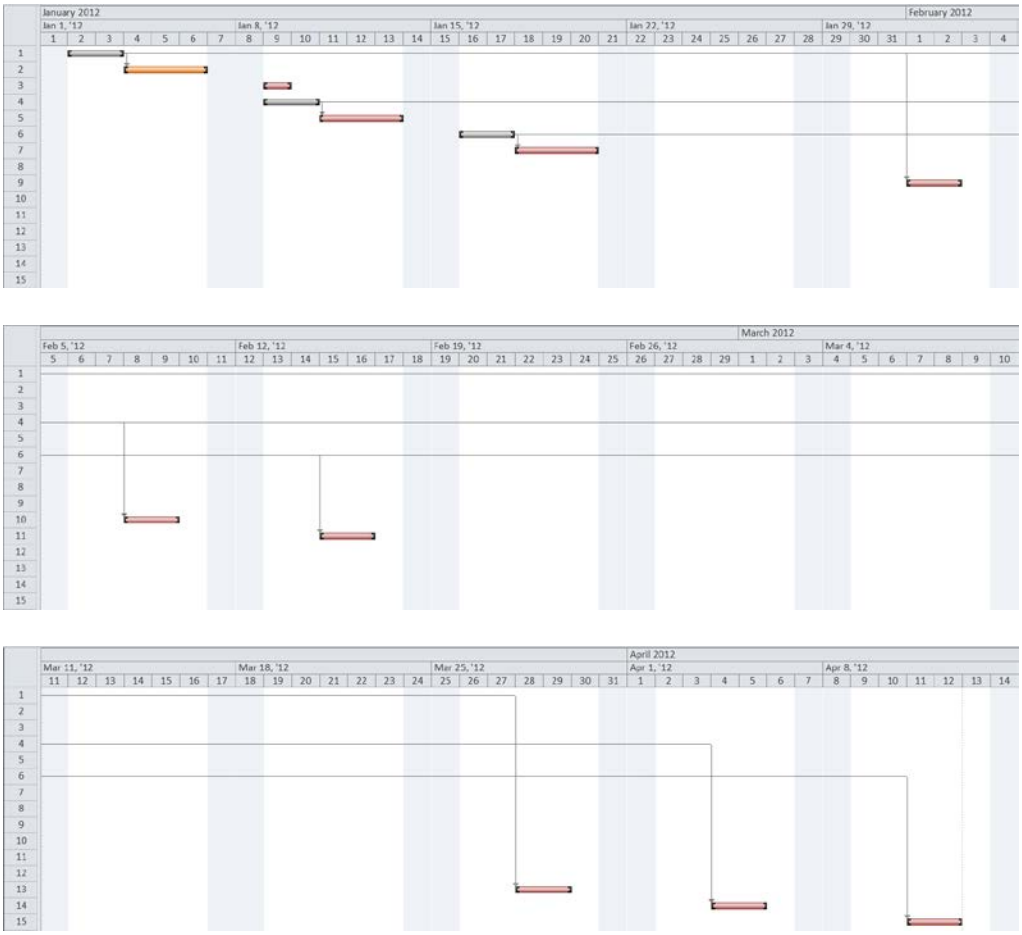

Weather Almanac Table Coinciding with SWLI Ageing Study – January

2012	Temp. (°F)			Dew Point (°F)			Humidity (%)			Sea Level Press. (in)			Visibility (mi)			Wind (mph)			Precip. (in)	Events
Jan	high	avg	low	high	avg	low	high	avg	low	high	avg	low	high	avg	low	high	avg	high	sum	
1	35	27	19	19	15	10	80	66	44	30.61	30.49	30.29	10	10	10	9	5	-	0.00	
2	44	30	15	27	21	10	86	66	46	30.61	30.42	30.24	10	10	10	8	3	-	0.00	
3	51	38	26	27	21	16	86	53	28	30.37	30.22	30.13	10	10	10	10	4	-	0.00	
4	51	37	23	28	22	14	74	58	35	30.39	30.34	30.28	10	10	10	10	4	-	0.00	
5	59	44	30	34	25	19	69	47	31	30.27	30.06	29.89	10	10	10	10	5	17	0.00	
6	50	38	24	27	24	18	80	57	30	30.11	30.02	29.89	10	10	10	15	5	17	0.00	
7	39	32	24	28	21	18	80	71	52	30.14	30.01	29.92	10	10	10	13	7	17	0.00	
8	39	29	19	21	18	14	93	69	45	30.20	30.15	30.12	10	10	10	10	3	-	0.00	
9	50	36	21	28	22	16	86	64	40	30.26	30.20	30.14	10	10	10	9	2	-	0.00	
10	55	40	24	34	25	18	86	59	34	30.12	29.92	29.79	10	10	10	13	3	-	0.00	
11	41	26	10	25	12	3	86	65	39	30.15	30.06	29.82	10	10	5	34	16	40	0.00	
12	42	24	6	18	9	1	85	52	25	30.10	30.05	29.98	10	10	10	20	6	-	0.00	
13	51	37	23	16	11	7	59	40	19	30.08	30.00	29.96	10	10	10	18	7	23	0.00	
14	55	38	21	21	14	7	63	40	23	30.13	30.03	29.88	10	10	10	17	9	18	0.00	
15	53	38	24	21	16	10	69	46	18	29.87	29.79	29.67	10	10	10	18	5	26	0.00	
16	42	27	10	23	16	7	93	69	27	30.03	29.75	29.61	10	9	0	16	7	21	0.00	
17	28	14	1	10	4	-2	100	69	31	30.16	30.06	29.99	10	9	1	10	5	-	0.00	
18	48	30	12	19	14	0	79	46	27	29.97	29.80	29.66	10	10	10	20	9	31	0.00	
19	60	51	42	28	25	21	43	35	29	29.78	29.70	29.60	10	10	10	33	18	43	0.00	
20	55	42	30	27	23	19	75	41	26	29.98	29.79	29.60	10	10	10	26	11	38	0.00	
21	51	36	21	28	23	18	86	67	41	29.89	29.55	29.29	10	10	10	18	4	24	0.00	
22	46	35	21	27	17	9	68	43	23	29.86	29.61	29.25	10	10	10	34	15	44	0.00	
23	44	30	17	19	16	10	80	60	36	29.90	29.84	29.80	10	10	10	15	6	-	0.00	
24	41	34	28	28	21	16	93	62	39	30.21	30.00	29.78	10	10	2	26	7	31	0.00	
25	64	40	17	27	18	12	93	59	15	30.15	30.04	29.91	10	10	10	26	6	37	0.00	
26	53	40	26	27	21	12	86	50	25	30.11	30.01	29.80	10	10	10	18	10	33	0.00	
27	44	34	23	25	20	12	86	60	34	30.28	30.05	29.78	10	9	1	26	10	33	0.00	
28	42	27	12	18	12	9	93	61	25	30.29	30.21	30.15	10	10	10	12	7	-	0.00	
29	60	40	21	21	16	10	64	39	20	30.18	30.11	30.00	10	10	10	14	5	18	0.00	
30	57	44	30	23	18	14	64	40	23	29.96	29.87	29.78	10	10	10	10	4	-	0.00	
31	46	36	26	21	16	12	69	44	29	30.06	29.99	29.90	10	10	10	15	6	-	0.00	

Comma Delimited File

Weather Almanac Table Coinciding with SWLI Ageing Study – February

2012	Temp. (°F)			Dew Point (°F)			Humidity (%)			Sea Level Press. (in)			Visibility (mi)			Wind (mph)			Precip. (in)	Events
Feb	high	avg	low	high	avg	low	high	avg	low	high	avg	low	high	avg	low	high	avg	high	sum	
1	48	34	21	21	16	12	80	48	27	30.17	30.12	30.08	10	10	10	14	4	18	0.00	
2	46	36	26	30	19	14	100	57	29	30.09	30.00	29.92	10	8	1	23	10	29	0.00	
3	30	29	28	27	25	21	93	85	69	30.34	30.24	30.12	10	4	1	24	18	29	0.00	
4	32	28	23	25	21	18	86	78	64	30.45	30.40	30.37	10	10	8	15	7	-	0.00	
5	30	22	15	21	18	14	100	82	64	30.39	30.30	30.21	10	8	1	7	1	-	0.00	
6	39	24	10	21	16	3	100	74	42	30.27	30.14	30.07	10	8	0	18	5	25	0.00	
7	26	22	17	21	18	12	93	83	69	30.39	30.34	30.29	10	9	2	10	5	-	0.00	
8	28	20	12	19	14	9	92	78	69	30.25	30.15	30.08	10	10	3	8	3	-	0.00	
9	39	29	19	25	20	14	93	69	52	30.16	30.12	30.10	10	10	5	24	6	-	0.00	
10	35	25	15	25	18	10	93	76	56	30.21	30.15	30.11	10	10	7	16	6	17	0.00	
11	19	12	6	14	8	3	92	80	63	30.36	30.30	30.21	10	9	2	15	7	-	0.04	
12	23	14	6	18	11	3	100	87	74	30.09	29.85	29.67	10	6	0	7	1	-	0.00	
13	39	29	19	30	24	16	93	80	70	29.76	29.69	29.61	10	8	4	9	4	-	0.00	
14	42	32	21	28	25	18	93	73	56	29.77	29.72	29.65	10	10	7	16	5	-	0.00	
15	33	28	24	27	23	19	93	80	70	30.08	29.94	29.79	10	10	9	14	6	16	0.00	
16	41	30	19	25	21	18	100	74	52	30.16	30.12	30.06	10	8	2	9	3	-	0.00	
17	33	26	19	27	22	14	100	84	65	30.18	30.09	30.01	10	8	0	10	4	-	0.00	
18	39	29	19	28	22	18	93	82	45	30.14	30.00	29.87	10	7	0	9	4	-	0.00	
19	42	32	23	28	22	18	86	68	45	29.85	29.70	29.56	10	10	10	10	3	-	0.00	
20	42	35	28	27	13	7	86	45	23	29.83	29.74	29.62	10	10	3	30	19	34	0.00	
21	51	38	24	25	18	10	69	44	26	29.85	29.78	29.71	10	10	10	20	8	26	0.00	
22	59	50	42	28	26	23	53	38	29	29.72	29.59	29.44	10	10	10	31	15	48	0.00	
23	46	36	26	34	18	9	86	58	38	30.02	29.78	29.45	10	9	1	34	21	50	0.00	
24	42	32	23	16	11	5	59	41	29	30.16	30.11	30.05	10	10	10	22	9	26	0.00	
25	62	40	19	27	14	9	80	48	17	30.09	29.76	29.56	10	10	9	36	11	46	0.00	
26	39	29	19	10	2	-2	58	30	17	30.20	30.01	29.82	10	10	10	37	20	44	0.00	
27	46	30	15	21	12	7	74	53	27	30.20	30.02	29.80	10	10	10	10	5	-	0.00	
28	42	32	23	28	24	19	87	77	42	29.77	29.58	29.49	10	10	4	18	8	25	0.00	
29	55	42	28	16	10	3	43	28	18	29.85	29.79	29.71	10	10	10	29	15	41	0.00	

Comma Delimited File

Weather Almanac Table Coinciding with SWLI Ageing Study – March

2012	Temp. (°F)			Dew Point (°F)			Humidity (%)			Sea Level Press. (in)			Visibility (mi)			Wind (mph)			Precip. (in)	Events
Mar	high	avg	low	high	avg	low	high	avg	low	high	avg	low	high	avg	low	high	avg	high	sum	
1	42	32	23	25	18	9	100	54	26	29.79	29.70	29.65	10	10	0	18	9	77	0.00	
2	33	25	17	21	11	1	93	56	34	30.01	29.91	29.79	10	10	7	22	6	29	0.00	
3	48	32	17	18	11	7	79	45	22	30.03	29.98	29.90	10	10	10	21	8	26	0.00	
4	62	45	28	25	19	16	69	39	16	30.13	30.06	29.92	10	10	10	10	6	-	0.00	
5	66	46	26	25	18	10	80	38	13	30.12	29.96	29.80	10	10	10	21	7	29	0.00	
6	71	50	30	21	12	3	48	23	10	29.78	29.58	29.41	10	10	10	32	11	44	0.00	
7	39	32	24	28	22	19	86	69	56	30.19	29.90	29.64	10	10	5	21	11	26	0.00	
8	50	36	21	19	14	9	86	48	22	30.49	30.41	30.25	10	10	10	12	4	-	0.00	
9	60	40	21	21	14	7	86	40	13	30.47	30.36	30.19	10	10	10	12	4	-	0.00	
10	69	48	26	36	20	9	81	39	15	30.14	29.98	29.84	10	10	10	16	5	23	0.00	
11	64	50	37	37	26	9	93	51	14	29.84	29.71	29.61	10	10	10	18	8	-	0.00	
12	66	52	39	23	17	12	42	28	15	29.94	29.83	29.67	10	10	10	15	6	24	0.00	
13	71	52	33	27	16	9	57	28	10	29.94	29.87	29.77	10	10	10	22	6	30	0.00	
14	73	56	39	18	12	7	39	18	10	30.02	29.93	29.84	10	10	10	21	10	24	0.00	
15	71	56	41	21	19	14	45	24	15	30.15	30.07	29.99	10	10	10	13	6	20	0.00	
16	73	53	33	28	23	16	75	35	13	30.00	29.89	29.76	10	10	10	18	6	-	0.00	
17	75	55	35	30	20	16	70	31	11	29.78	29.71	29.54	10	10	10	15	5	18	0.00	
18	71	52	33	28	21	16	60	32	14	29.58	29.44	29.25	10	10	3	38	9	46	0.00	
19	48	40	32	18	6	0	38	23	13	29.61	29.53	29.42	10	10	10	26	11	34	0.00	
20	55	44	32	21	12	5	60	33	15	30.01	29.89	29.68	10	10	10	17	10	23	0.00	
21	66	47	28	25	17	9	55	32	18	30.03	29.98	29.92	10	10	10	22	7	28	0.00	
22	71	52	33	30	23	19	60	38	14	30.02	29.96	29.86	10	10	10	22	7	28	0.00	
23	77	54	32	34	27	23	87	46	13	30.03	29.98	29.90	10	10	10	13	4	16	0.00	
24	75	57	39	32	26	19	57	32	18	30.10	30.06	30.00	10	10	9	18	8	28	0.00	
25	69	54	39	41	37	34	87	59	33	30.16	30.05	29.93	10	10	10	9	4	-	0.00	
26	80	60	41	45	33	12	82	55	10	29.90	29.71	29.45	10	10	3	33	9	45	0.00	
27	71	55	39	25	17	10	39	24	12	30.03	29.94	29.78	10	10	10	23	11	29	655.34	
28	75	55	35	30	24	19	61	37	12	30.03	29.96	29.81	10	10	10	14	7	21	0.00	
29	71	58	44	37	28	19	76	34	15	29.96	29.89	29.83	10	10	10	21	6	29	0.00	
30	77	60	42	28	23	16	50	26	17	29.93	29.88	29.79	10	10	10	15	7	18	0.00	
31	82	64	46	39	29	25	71	29	15	29.94	29.84	29.67	10	10	10	16	7	23	0.00	

Comma Delimited File

Weather Almanac Table Coinciding with SWLI Ageing Study – April

2012	Temp. (°F)			Dew Point (°F)			Humidity (%)			Sea Level Press. (in)			Visibility (mi)			Wind (mph)			Precip. (in)	Events
Apr	high	avg	low	high	avg	low	high	avg	low	high	avg	low	high	avg	low	high	avg	high	sum	
1	82	60	39	36	25	18	62	29	10	29.67	29.52	29.36	10	10	7	32	6	38	0.00	
2	57	48	39	30	28	25	61	50	33	30.16	29.88	29.52	10	10	7	38	27	44	0.00	
3	41	37	33	32	29	23	87	72	52	30.24	30.17	30.09	10	9	1	23	14	26	0.01	
4	64	50	35	37	33	27	81	58	37	30.09	29.95	29.83	10	10	10	13	5	-	0.00	
5	73	54	35	39	36	30	93	62	25	29.92	29.86	29.77	10	10	10	22	5	28	0.00	
6	77	58	39	45	30	7	93	54	10	29.83	29.72	29.58	10	8	2	31	10	44	0.00	
7	62	46	30	18	12	7	55	27	14	30.31	30.23	30.05	10	10	10	23	12	31	0.00	
8	71	50	30	21	18	12	64	34	10	30.30	30.24	30.14	10	10	10	12	6	18	0.00	
9	68	52	35	36	25	18	54	38	21	30.24	30.18	30.10	10	10	10	13	7	17	0.00	
10	78	58	39	45	36	25	87	53	16	30.19	30.08	29.97	10	10	10	16	6	-	0.00	
11	64	57	50	52	47	45	88	77	55	30.10	29.99	29.79	10	9	5	23	10	26	0.15	Thunderstorm
12	66	54	42	48	38	21	93	61	19	29.81	29.73	29.64	10	10	9	22	8	29	0.00	
13	64	50	37	36	27	18	87	43	18	29.82	29.76	29.70	10	10	10	21	10	30	0.00	
14	60	50	39	37	30	27	81	50	29	29.74	29.60	29.50	10	10	8	23	11	29	0.03	Thunderstorm
15	51	45	39	37	30	27	81	57	38	30.03	29.77	29.56	10	10	5	36	18	77	0.00	
16	60	46	33	34	28	21	93	52	23	30.14	30.10	30.03	10	10	7	10	6	16	0.00	
17	68	52	35	34	27	23	70	40	21	30.16	30.09	30.00	10	10	10	14	5	17	0.00	
18	71	54	37	39	33	28	75	49	22	30.13	29.99	29.84	10	9	0	26	5	31	0.00	
19	64	54	44	43	34	28	82	51	27	30.14	29.97	29.92	10	10	10	28	12	34	0.03	Thunderstorm
20	69	52	35	37	34	30	93	55	26	30.20	30.11	30.03	10	10	10	16	8	22	0.01	
21	75	60	46	37	35	28	71	39	25	30.30	30.12	30.03	10	10	10	15	6	20	0.00	
22	73	58	42	39	36	32	76	46	25	30.32	30.26	30.19	10	10	9	12	5	16	0.00	
23	82	63	44	39	34	30	76	40	15	30.23	30.12	30.00	10	10	10	16	6	22	0.00	
24	82	65	48	37	34	27	58	32	14	30.00	29.92	29.85	10	10	5	30	6	36	0.00	Thunderstorm
25	82	66	50	43	33	28	67	32	15	30.04	29.96	29.87	10	10	5	18	5	30	0.00	
26	78	66	53	48	41	36	67	42	23	30.03	29.88	29.69	10	10	8	20	6	32	0.00	
27	66	54	42	48	34	18	88	51	18	29.91	29.72	29.64	10	10	9	32	13	43	0.01	
28	62	50	39	30	15	7	57	25	14	30.01	29.94	29.88	10	10	10	24	14	26	0.00	
29	66	50	33	34	30	25	81	50	24	30.04	30.00	29.94	10	10	9	13	9	17	0.00	
30	78	58	39	34	25	16	61	31	11	30.05	29.90	29.73	10	10	10	21	6	30	0.00	

Comma Delimited File

Appendix E: Glancing Angle X-ray Diffraction Background

Background Spectra of Uncoated Polished and Passivated Ti_6Al_4V

Small Angle Results:

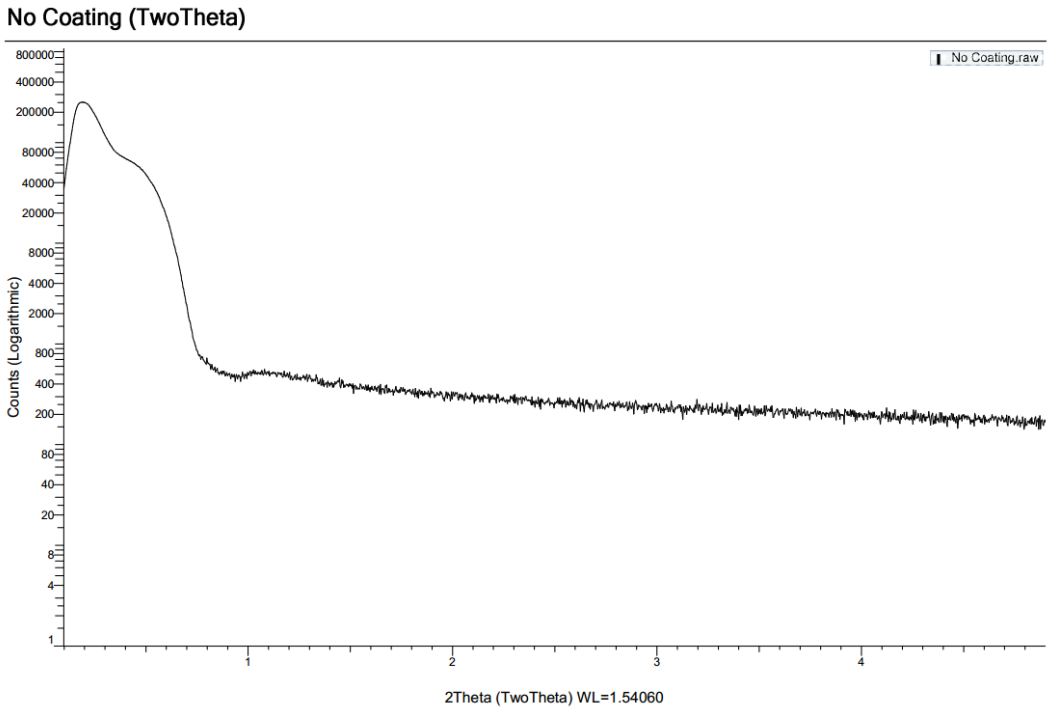

Wide Angle Results: